



PhD Thesis
Virginia Fernández Martínez

Role of miRNAs in early brain development

Programa de Doctorado en Neurociencias

Instituto de Neurociencias

Universidad Miguel Hernández-CSIC

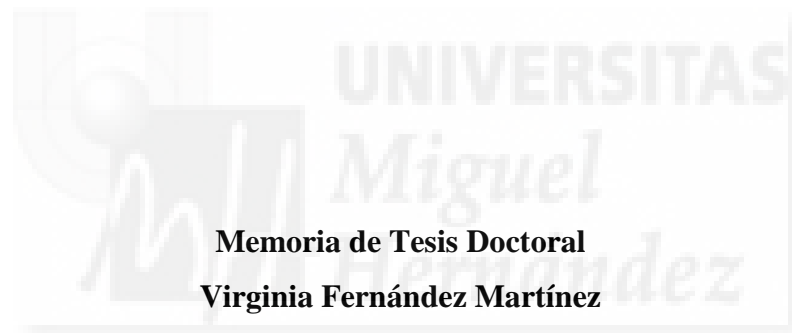
Thesis supervisor:

Víctor Borrell Franco



Instituto de Neurociencias
Universidad Miguel Hernández-CSIC

Role of miRNAs in early brain development



Director de Tesis
Víctor Borrell

San Juan de Alicante, 2018

Programa de Doctorado en Neurociencias



San Juan de Alicante, 15 of May 2018

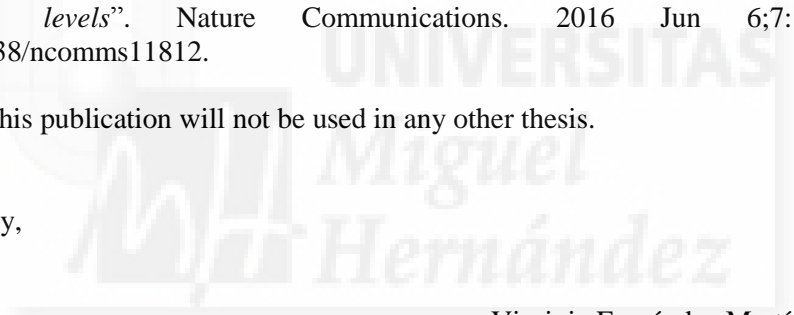
To whom it may concern:

The doctoral thesis developed by me, Virginia Fernández Martínez, with title: Role of miRNAs in early brain development, includes the following publication in which I am third author:

- Martínez-Martínez MÁ, De Juan Romero C, Fernández V, Cárdenas A, Götz M, Borrell V. “A restricted period for formation of outer subventricular zone defined by *Cdh1* and *Trnp1* levels”. *Nature Communications*. 2016 Jun 6;7:11812. doi: 10.1038/ncomms11812.

I declare that this publication will not be used in any other thesis.

Yours sincerely,



Virginia Fernández Martínez

A QUIEN CORRESPONDA:

Prof. Miguel Valdeolmillos López, Coordinador del Programa de Doctorado en Neurociencias del Instituto de Neurociencias, Centro Mixto de la Universidad Miguel Hernández-UMH y la Agencia Estatal Consejo Superior de Investigaciones Científicas-CSIC,

CERTIFICA:

Que la Tesis Doctoral “*Role of miRNAs in early brain development*” ha sido realizada por D.^a Virginia Fernández Martínez (DNI 74376487F) bajo la dirección del Dr. Víctor Borrell Franco y da su conformidad para que sea presentada a la Comisión de Doctorado de la Universidad Miguel Hernández.

Para que así conste a los efectos oportunos, firma el presente certificado en San Juan de Alicante a 18 de Mayo de 2018.

Fdo: Miguel Valdeolmillos

A QUIEN CORRESPONDA:

Dr. Víctor Borrell Franco, investigador científico del Consejo Superior de Investigaciones Científicas,

Autoriza la presentación de la Tesis Doctoral titulada “*Role of miRNAs in early brain development*”, realizada por D.^a Virginia Fernández Martínez (DNI 74376487F) bajo su inmediata dirección y supervisión en el Instituto de Neurociencias de Alicante, centro mixto CSIC-UMH, y que presenta para la obtención del grado de Doctor por la Universidad Miguel Hernández.

Y para que así así conste, y a los efectos oportunos, firma el presente Certificado en San Juan de Alicante, a 18 de Mayo de 2018.



Fdo: Víctor Borrell Franco

AKCNOWLEDGEMENTS

Saluts, honor e salvament.

Tengo la certeza de que este es el apartado que más gente va a leer (de hecho, la mayoría de personas que toquen este libro será lo ÚNICO que lean). Así que seré breve para no aburrir:

A los que me habéis ayudado de una forma u otra: Gracias. (Si tenéis más tiempo para leer, pasad a la siguiente página).

A los que no: ¿Por qué estáis leyendo este apartado de mi tesis?



Me gustaría aprovechar la oportunidad que da el escribir la tesis para dar las gracias a las personas que de una forma u otra me han ayudado a sobrevivir al doctorado.

En primer lugar, quisiera darle las gracias al mejor jefe que he tenido: Víctor. Muchísimas gracias por haber confiado en mí para formar parte de tu magnífico laboratorio, soy tremendamente afortunada por haber podido estar en él. Gracias por empujarme a pensar de manera crítica y por ayudarme a amar la investigación. Voy a echar mucho de menos las conversaciones contigo sobre cine, música y ciencia, los “Virginia, ¿estás ahí?” desde tu despacho, tus agasajos, tus ánimos en los peores momentos y tu entusiasmo en los mejores. Muchas gracias por haberme adoptado en tu familia científica durante tanto tiempo, estoy enamorada de este laboratorio y de la gente que lo conforma. Ojalá volviéramos a trabajar juntos.

Si he pasado por esta gran aventura que es el doctorado es gracias a un profesor que tuve en la Universidad, que revolucionó mis entrañas mentales y me hizo adorar la investigación. Juan Martínez-Pinna, esta tesis va dirigida a ti porque un día hace mucho, mucho tiempo (en una galaxia no muy lejana) te dije que si algún día conseguía algo medianamente importante científicamente hablando te lo debería a ti. Desearía poder dedicarte algo mejor y más grande, pero a esta tesis le he dedicado mucho esfuerzo y cariño así que espero que valga (por ahora). Gracias por hacer que flipara entendiendo cómo funcionamos, por encender en mí la llama de la pasión por la ciencia y por hacerme creer que si quería, podía investigar. Has cambiado mi vida y te estaré eternamente agradecida.

Cuando me paro a mirar todo lo que ha pasado en los últimos cuatro años me da vértigo, podría haber sido una tortura y si no lo ha sido es gracias a la cantidad de gente MARAVILLOSA que he conocido en el INA. Es lo que más voy a echar de menos, porque sois parte de mi familia.

Gracias a los compañeros que se fueron para seguir creciendo. Isa, gracias por servir de motivación con todo tu esfuerzo y dedicación. Marian, gracias por demostrarnos a todos que con un par de ovarios y con esfuerzo se pueden hacer cosas alucinantes y también por empezar con esta locura de proyecto que ocupa mi tesis. Hugo, italiani! se te ha echado de menos un montón por el labo... las cosas no son lo mismo sin tus “madre mía”, tus “eme ele” y tus limoncellos. Gracias por empezar con este proyecto suicida y por tu ayuda sobre supervivencia en el laboratorio. Espero seguir encontrándome contigo por congresos y poder disfrutar de tu compañía, siempre serás mi primer compañero de bancada☺. Sin duda, una de las personas a las que más se ha echado de menos en el labo es a Esther Picó. Eres un ejemplo en todos los sentidos, vales muchísimo y todo el mundo que ha tenido el placer de compartir tiempo contigo codo con codo no puede más que agradecer el haber tenido esa oportunidad. Es un topicazo pero te mereces lo mejor. Muchas gracias por haber dicho verdades como puños como solo tú sabes hacerlo, gracias por ser una borde adorable, por reírte de los problemas y por hacer que los demás nos riéramos contigo.

Ahora la que se va del laboratorio soy yo, y en él dejo a muchas personas que han hecho que quisiera ir a trabajar cada día. Sois de otro planeta y os quiero una pechá a todos. Camino, GRACIAS. Fuiste mi mentora y ahora eres de lo mejorcito que me llevo en la mochila: mi compañera y amiga. Gracias por apostar por mí (inexplicablemente jaja),

gracias por intentar persuadirme de la realidad de la ciencia al principio y por enseñarme después los mejores trucos de post-doc. Eres una persona espectacular a nivel científico pero eres todavía más increíble a nivel personal. Ojalá pudiera trabajar siempre contigo, allá donde vayas harás a la gente muy afortunada, y de donde te vayas dejarás un sitio irremplazable. Muchas gracias por las risas, por tu sinceridad, por ayudarme a tirar para adelante, por dejarme usar tu agua sigma ☺ y por haber leído y corregido este tostonazo de tesis. Y no puedo hablar de Camino sin nombrar a Pep, el desertor del labo. Aunque no haya conseguido que abandonaras a tu jefa para venirte conmigo, tengo que confesar que ha sido un verdadero placer haber disfrutado de tu compañía en el labo, pero sobre todo fuera de él. Eres un crack!

Hablando de cracks, tengo que reconocer que uno de los más notables que ha pisado este labo es Jorge. Te admiro, no sólo por trabajar en una habitación llena de drogas, si no por ser capaz de luchar por lo que realmente quieres hacer. Muchas gracias por romper los esquemas del laboratorio, por llevar siempre una sonrisa contigo y por contagiarla a los demás. Otra crack del labo a la que todos los que trabajamos en él le debemos la vida o, al menos, no haber acabado en la cárcel (por no haber justificado gastos o algo del estilo) es Bea. Eres absolutamente indispensable, muchísimas gracias por haberme ayudado siempre, sin ti no podría haber pasado por esta locura... Dudo que vuelva a encontrarme con alguien que me salve la vida una y otra vez con una sonrisa en la boca.

Estando en el laboratorio he podido disfrutar de las enseñanzas de una eminencia, un gran mentor que me enseñó con mucha paciencia (¬¬) a electroporar. Adri, ¿ahora quién me va a llamar novata? Trabajar contigo es como si tuviéramos media jornada, como si no fuéramos precarios y como si almorzáramos todos los días un pincho y una cerveza. Muchísimas gracias por tus pésimos chistes... no creo que vuelva a encontrar a nadie con ese sentido del humor y eso me rompe el corazón. Muchas gracias por enseñarme que hay cosas que nos deben de sudar la **** y que una cerveza es, a veces, la solución. Tienes un corazón que no entiendo cómo puede caberte en el pecho. Ahora nos despedimos pero yo voy a seguir poniéndote velas cada vez que tenga que electroporar algo chungo.

La verdad es que no sé cómo me he llegado a convertir en una especie de veterana, sin darme cuenta ha llegado sangre nueva al labo... y he de decir que no está tan mal el relevo. Lucía, eres la última en llegar y te deseo muchísima suerte en esta aventura. Alex, tienes todo lo que necesitas para llegar donde quieras. No dejes que nada te impida cumplir tus sueños. Muchas gracias por haberme aguantado en esta última etapa y ya sabes: May the Force be with you. Kaviya, gracias por tu sonrisa inquebrantable y por tu paciencia. Mucho ánimo en la recta final, tú puedes con todo! Espero que tu camino esté lleno de alegrías. También se queda en ésta nueva generación Ana, la pequeñita del labo!! Muchas gracias por mimarme, por ser como una inyección de cafeína, epinefrina y muchas más cosas acabadas en "ina", irradias una energía que contagia a todos los que te rodeamos. Gracias por estar ahí para un abrazo, un schoko-bon, un té o una cerveza. Vas a llegar muy lejos así que sólo espero que en ese viaje te pases por Génova a hacernos un vinito en el puerto. Después de Ana llegó mi compañera de mesa, mi wifie, Salma. Ojalá pudiera quedarme contigo hasta que acabes la tesis, pero estoy segura de que vas a sacarlo todo adelante como una campeona, porque "c'mon, you're egyptian". Confío al 100% en ti, espero que tú también lo hagas <3. Muchas gracias por estar a mi lado, por quererme

y entenderme, por dejarme conocerte, por apoyarme y por lo genial que me lo he pasado contigo. احد بك اذا. رائد مع اذت.

Dra. Mata, se me queda cortísimo todo lo que pudiera escribir para explicar lo agradecida que estoy de haberte conocido. Eres una mujer de las que marcan, no solo porque seas una enamorada de la ciencia, sino porque haces que la gente se enamore de ti; no hace falta quitapenas si tú estás cerca. Muchísimas gracias por toda tu ayuda, por enseñarme tantísimas cosas de dentro y de fuera del laboratorio. Eres brillante, y si alguien no es capaz de apreciarlo es porque tiene deficiencias cognitivas. Espero que nuestros caminos se vuelvan a cruzar, mientras tanto te estaré echando de menos.

Pero como en todas partes, no todo son cosas buenas. En este laboratorio me he encontrado con El Eje del Mal. Esther, muchas gracias por enseñarme a trabajar en un laboratorio, por forzar tu paciencia (sé que te sacamos de quicio), por cuidar de mí en los peores momentos y por hacer que al final me acabe riendo de todo. Eres increíble y te admiro mucho por coger los limones que te dan y tomártelos con tequila y sal. Este tiempo me has enseñado que aunque el viento sople en contra, si te propones algo y le hechas huevos: lo consigues. Muchas gracias por compartir tus maldades y por darle color a la vida. La otra pieza del Eje es muy pequeñita, pero ya se sabe que las mejores esencias se guardan en frascos pequeños...

Mon, cualquier cosa que escriba es demasiado exigua como para que te puedas imaginar lo agradecida que estoy de haber caminado contigo durante este viaje; aun así lo voy a intentar. Has sido un pilar sin el cual no habría sido capaz de aguantar ni un año, gracias por no dejarme caer y por empujarme a seguir hacia adelante. Gracias por haber estado a mi lado en las buenas, en las malas y en las peores. Gracias por vivir mis logros como tuyos y por sufrir mis penas. Eres tremendamente excepcional, capaz de hacer que un día horrible acabe siendo uno memorable. Todas las aventuras que hemos vivido juntas dan para escribir el guion de una serie con 11 temporadas y mirando todo lo que nos ha pasado volvería a empezar la tesis una y otra vez si es contigo a mi lado. Muchas gracias por haber estado pero sobre todo, gracias por quedarte. Te quiero mucho.

Kikita de mi corazón, hemos estado juntas en la carrera, en el máster y en el doctorado... y pese a ello te sigo queriendo un montón. Si eso no es amor verdadero que baje Dios y lo vea. Eres una crack de la ciencia pero a nivel personal parece que estés hecha de oro. Estoy tremendamente agradecida de que hayas aparecido en mi vida, y lo mejor es que sé que siempre vas a estar en ella. Muchas gracias por creer siempre en mí, por animarme cuando estaba dentro de un pozo y por entenderme en mis neurosis. No se puede explicar con palabras todo lo que me has ayudado en todos estos años, eres un pilar en mi vida y espero que lo sigas siendo por muchísimo tiempo más.

Alvarito, si la de arriba es una crack, tú ya eres la repanocha. Espero que seas consciente de que todos los que te rodeamos sentimos que tenemos una suerte inmensa. Te queda poquito para acabar así que: ¡mucho ánimo, que tú puedes con todo!

Dentro del trabajo mucha gente ha tenido que sufrirme haciendo la tesis... pero es que los que me sufrían fuera estaban todavía más indefensos! Si no llega a ser por las cantidades ingentes de cerveza que me he tomado con mis amigas, no hubiera salido viva de ésta. Gracias a Andro, Esthero, Mario, Sandru, Oso y Uva. Gracias por hacer que me

olvide (a veces literalmente) de todo lo que me trastornaba y por hacerme reír de lo malo cuando las cosas iban fatídicamente mal. Gracias por cuidarme tanto y por escuchar una y otra vez las movidas del labo. Teneros a vosotras, que habéis estado ayudándome durante diez años, vale más que cualquier título.

Los últimos serán los primeros. (Mateo 20:16-26)

Alejandro, ¿ves como sí que te iba a dejar mi tesis? ☺ Es absurdo intentar expresar en un par de frases lo sumamente feliz que me hace tenerte conmigo. Hace algo más de un año me tocó la lotería. Gracias por entrar en mi vida para traerme el amor y la poesía, y gracias por dejarme participar en la tuya. Haberte conocido me demuestra que haber hecho la tesis ha valido la pena con creces. La etapa del doctorado acaba, pero la nuestra no ha hecho más que comenzar.

Como veis, ha habido mucha gente que me ha ayudado a recorrer este camino, pero nada es comparable al tremendo esfuerzo que ha hecho mi familia.

Empezando por los dos hermanos que tengo, que son dos Soles: Samu, muchas gracias por inspirarme a crecer, por creer en mí, por incitarme a apuntar a las estrellas, por todo tu amor y por apoyarme siempre. Gracias por enseñarme que, con amor, no hay distancia. Gracias por traer a Angélica a mi vida. Cuñis, eres una mujer extraordinaria, te admiro muchísimo y agradezco tremendamente que formes parte de esta familia. Gracias a los dos por haberme dado la oportunidad de ser tía y por descubrir que personitas muy pequeñas (Valentina y Daniela) me pueden robar el corazón. Germán, ay mi hermano el mediano! Gracias por preocuparte por mí y por cuidarme pase lo que pase, por ser un apoyo para todos y por hacer que en casa siempre gane la alegría. Desi, gracias por haber traído las risas a la familia, por ser tan tremenda y por hacerte querer tantísimo. Gracias por habernos traído a Lucía, ese bichito que nos trae locos de amor.

Y por último, lo más importante: Mamá, Papá, muchísimas gracias por quererme tantísimo. Gracias por apoyarme en cada decisión (buena o mala) que he tomado en mi vida, gracias por animarme a conseguir todo lo que me propongo, gracias por alegraros en cada logro que consigo y por ayudarme a superar los malos tragos. Gracias por las toneladas de besos y abrazos y por los “tú sí que vales”. Esta tesis es casi más vuestra que mía, porque sin todo vuestro apoyo y cariño no hubiera acabado ni el bachillerato. Sois un ejemplo de valor, de esfuerzo y de amor y espero (algún día) ser la mitad de genial de lo que lo sois vosotros. No os hacéis una idea de lo muchísimo que os quiero.

A Juan Martínez-Pinna



1. Abbreviations	22
2. Summary/Resumen	30
3. Introduction	38
3.1 Mammalian Central Nervous System	38
<i>3.1.1 General organization</i>	38
<i>3.1.2 Regional Identity</i>	38
<i>3.1.3 Antero-posterior Axis</i>	39
<i>3.1.4 Dorsal-ventral Axis</i>	41
3.2 Development of the telencephalic neuroepithelium	45
<i>3.2.1 Cellular mechanisms controlling telencephalic development</i>	48
<i>3.2.2 Molecular mechanisms controlling telencephalic development</i> ..	52
<i>3.2.3 Progenitor cell lineage</i>	54
<i>3.2.4 Progenitor cell heterogeneity</i>	55
3.3 microRNAs as molecular regulators of progenitor's behaviour	56
<i>3.3.1 miRNAs in the nervous system</i>	56
<i>3.3.2 miRNAs Overview</i>	57
<i>3.3.3 Biogenesis (canonical VS non canonical).</i>	57
<i>3.3.4 Target recognition</i>	61
<i>3.3.5 Silencing</i>	62
<i>3.3.6 Regulation of miRNA pathway</i>	65
<i>3.3.7 miRNAs as genetic tools for gene silencing</i>	67
3.4 Human alterations of miRNAs	70
<i>3.4.1 Cancer</i>	70
<i>3.4.2 Let-7 family in human cancer</i>	72
3.5 Mouse models for the study of miRNAs	74
4. Objectives	82
5. Materials and Methods	86
6. Results	104
Part1. Early ablation of functional <i>Dicer</i> leads to brain malformations. 106	
<i>Characterization of <i>Rx-Cre; Dicer^{F/F}</i> mouse. Cortical phenotype</i>	108

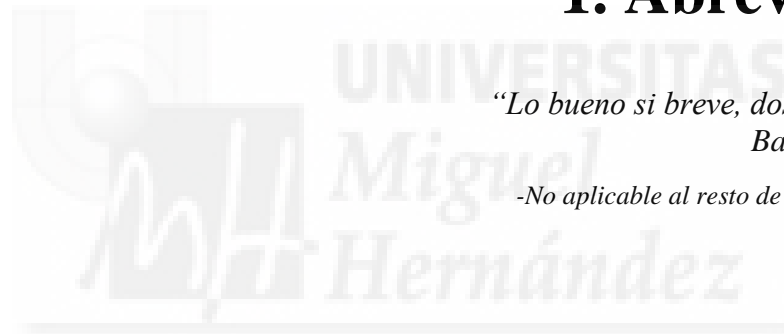
<i>Disorganization of rostro-ventral telencephalon and presence of rosettes</i>	112
<i>Rosette types and their distribution across time and space</i>	116
<i>miRNA depletion causes alterations in proliferation and apoptosis</i> ...	118
<i>Loss of miRNA leads to apical junction belt disruption and neuronal delocalization</i>	121
<i>Differentially expressed genes in miRNA-depleted animals</i>	123
Part2. Role of <i>let-7/p53/Irs-2</i> axis during brain development	128
<i>p53 is required for rosette formation in Dicer ablated embryos</i>	130
<i>Overexpression of Irs-2 promotes rosette formation</i>	132
<i>Function of IRS-2 in iPSC-derived cerebral organoids</i>	135
7. Discussion	142
8. Conclusions/Conclusiones	156
9. Annex 1. Author's published scientific contribution	160
10. References	180



1. Abreviations

“Lo bueno si breve, dos veces bueno”
Baltasar Gracián

-No aplicable al resto de la presente Tesis-



1. Abbreviations

2' OH	2' hydroxyl group
5'cap	five-prime cap
Ago2	Argonaute 2
AMOs	Anti-miRNA antisense inhibitors
Amp	Ampicilin
AP	Anteropeduncular area
aRGC	apical Radial Glia Cell
Arl13b	ADP-ribosylation factor-like protein 13B
BCIP	5-bromo-4-chloro-3-indolyl phosphate
B-CLL	B-cell Chronic Lymphocytic Leukemia
bRGC	basal Radial Glia Cell
<i>C. elegans</i>	<i>Caenorhabditis elegans</i>
CaMKII	Calcium/Calmodulin dependent protein Kinase II
Ccng1	Cyclin G1
CD133	Prominin- 1
Cdk	Cyclin- dependent kinase
ceRNAs	competing endogenous RNAs
CFSs	Common Fragile Sites
Cnot6l	CR4-NOT Transcription Complex Subunit 6 Like
CNS	Central Nervous System
Col18a1	Collagen Type XVIII Alpha 1 Chain
CoupTF1	COUP Transcription Factor 1
Csf1r	Colony Stimulating Factor 1 Receptor
Ctgf	Connective Tissue Growth Factor
Ctrl	Control
DAPI	4',6-diamidino-2-phenylindole
DCP1/2	mRNA-Decapping Enzyme 1/2
Ddx3x	DEAD-Box Helicase 3, X-Linked
DFGs	Differentially Expressed Genes
DGCR8	DiGeorge syndrome Critical Region 8 protein
Dl1	Delta 1
dLGE	dorsal LGE

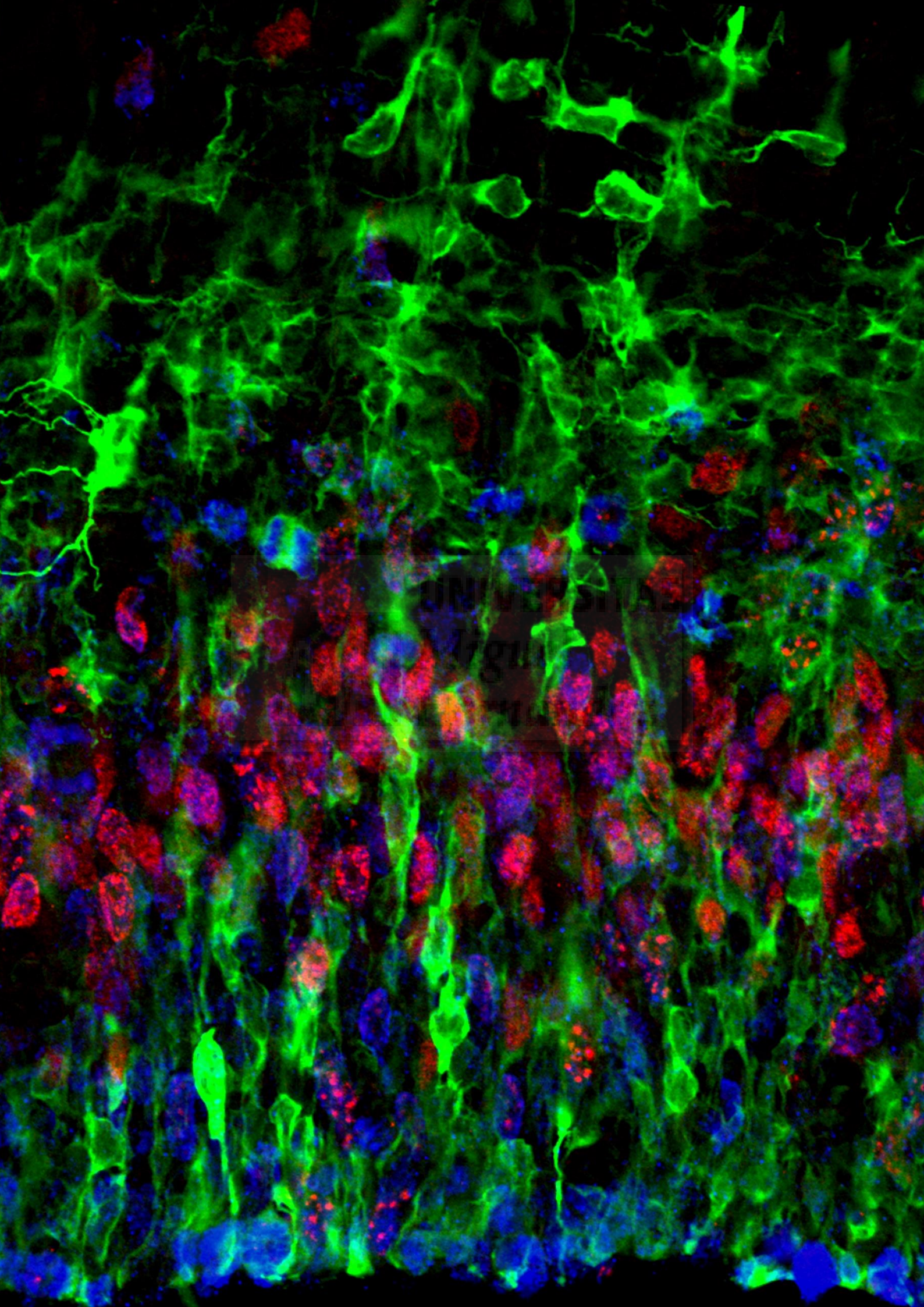
Dlx2	Distal-Less Homeobox 2
Dlx5	Distal-Less Homeobox 5
DNA	Deoxyribonucleic Acid
ds RBD	Double-stranded RNA-binding domain
ds	Double strand
DV	Dorso-Ventral
eIF4G	eukaryotic Translation Initiation Factor 4 Gamma
eIFs	eukaryotic initiation factors
ETANTR	Embryonal Tumor with Abundant Neuropili and True Rosettes
ETMR	Embryonal Tumours with Multi-layered Rosettes
EXP5	Exportin 5
F/F	Flox/flox
FACS	Fluorescence-Activated Cell Sorting
FMR1	Fragile X Mental Retardation 1
Foxg1	Forkhead box protein G1
FS	Fast Spiking
Fw	Forward
FXR1	Fragile X-Related Protein 1
GFAP	Glial Fibrillary Acidic Protein
GFP	Green Fluorescent Protein
GLAST	Astrocyte-Specific Glutamate Transporters
Grm1	Glutamate Metabotropic Receptor 1
GS	Glutamine Synthase
Gsx2	GS Homeobox 2
Hcls1	Hematopoietic Cell-Specific Lyn Substrate 1
HSURs	Herpesvirus Saimiri U-Sich RNAs
Igfr2r	Insulin Like Growth Factor 2 Receptor
INM	Interkinetic Nuclear Migration
IPC	Intermediate Progenitor Cells
IRES	internal ribosome entry site
Irs-2	Insulin Receptor Substrate-2
Itgb1	Integrin Subunit Beta 1
IUE	In Utero Electroporation
Kif23	Kinesin Family Member 23

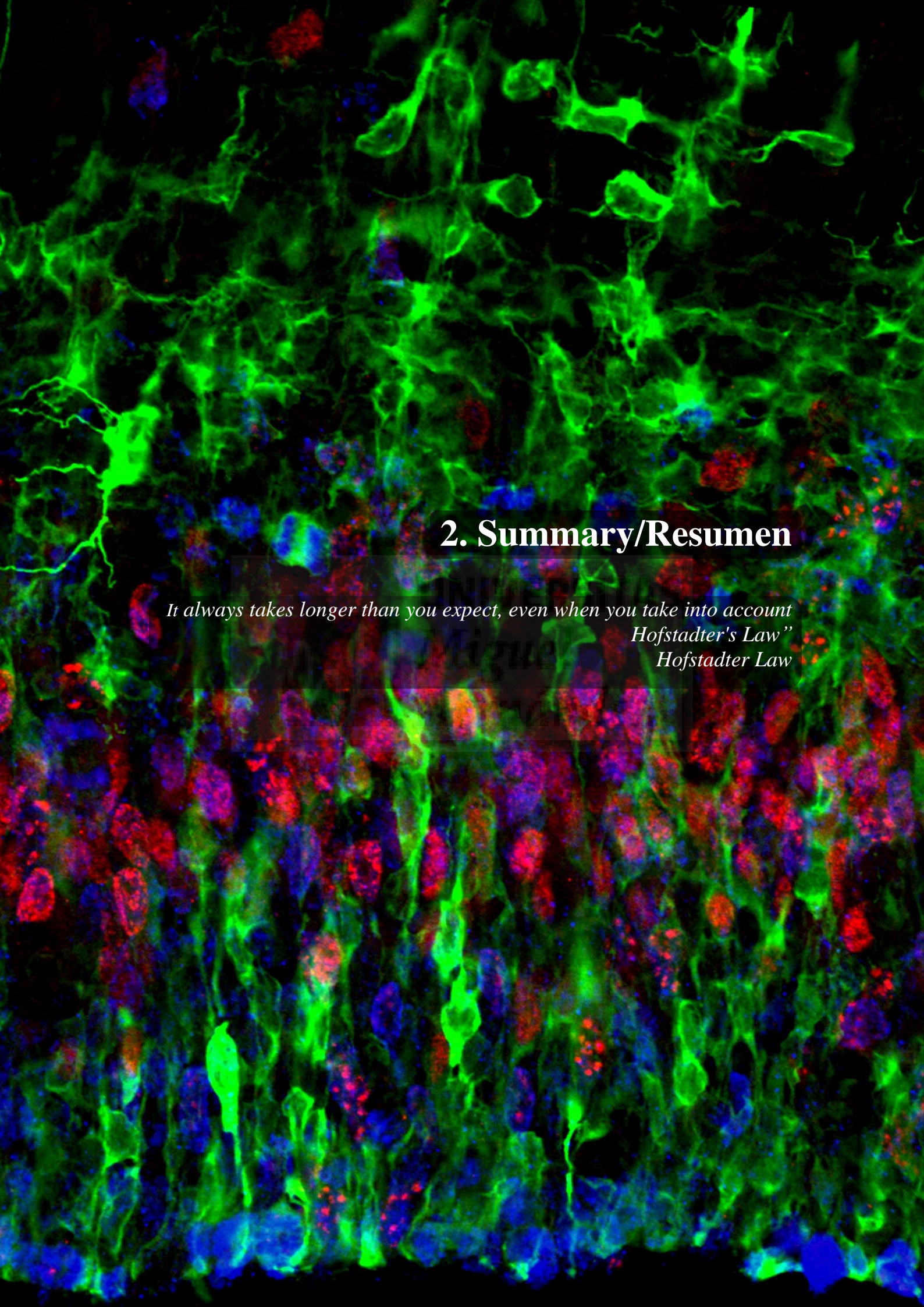
Klhl42	Kelch-like protein 42
KO	Knock Out
L4	fourth Larval stage
LB	Luria-Bertani
Let-7	Lethal-7
LGE	Lateral Ganglionic Eminence
lin 41	cell lineage 41
loxP	locus of X-over P1
Lrp2	Low Density Lipoprotein-Related Protein 2
Lyn	Lck/Yes novel tyrosine kinase
MBS	miRNA Binding Sites
MGE	Medial Ganglionic Eminence
miARN	micro ácidoribonucleico
miR	microRNA
miRISC	miRNA-induced silencing complex
miRNA	microRNA
mRNA	messenger RNA
MZ	Marginal Zone
NBT	Nitroblue Tetrazolium
NCx	Neocortex
NECs	Neuro Epithelial Cells
ng	nanograms
Ngn2	Neurogenin 2
Nkx2.1	NK2 Homeobox 1
NL	Neuronal layer
OB	Olfactory Bulb
OE	Overexpression
Onecut2	Onecut homeobox 2 transcription factor
ORF	Open Reading Frame
oSVZ	outer Sub-Ventricular Zone
P	Pallium
PABP	Poly-A Binding Protein
PACT	Kinase R-Activating Protein
Par3	Partitioning defective 3

PARN	Poly(A)-Specific Ribonuclease
Pax6	Paired box 6
PAZ	Piwi Argonaut and Zwillie
p-bodies	Processing-Bodies
pCAG	CAG promote
PH3	Phospho-Histone 3
PIK3	Phosphatidylinositol-4,5-bisphosphate 3-kinase
pNCx	primordium of the Neocortex
PNPT1	Polynucleotide Phosphorylase PNPase old-35
POA	Preoptic Area
pOB	primordium of the Olfactory Bulb
POH	Preoptic–Hypothalamic Area
Pten	Phosphatase and tensin homolog
PTENP1	Phosphatase and Tensin Homolog Pseudogene 1
Purb	Purine Rich Element Binding Protein B
PV+	Parvalbumin-positive
RA	Retinoic Acid
Rest	RE1 Silencing Transcription Factor
RISC	RNA-Induced Silencing Complex
RNA PolII/III	RNA Polymerase II/III
RNA	Ribonucleic Acid
Rv	Reverse
Rx3	Retinal homeobox gene 3
SD	ssRNA-dsRNA junction
Shh	Sonic hedgehog
siRNA	small interfering RNA
snoRNAs	Small Nucleolar RNAs
SOM+	Somatostatin-positive
SP	Subpallium
ss	Single strand
St	Septum
SVZ	Subventricular Zone
Tbr1	T-Box, Brain 1
Tnfrsf1b	TNF Receptor Superfamily Member 1B

TNFα	Tumor Necrosis Factor Alpha
TRBP	TAR RNA binding protein
Trp53	Transformation-Related Protein 53
TuD	Tough Decoy
Tuj1	Neuron-specific class III beta-tubulin
Tut4	Terminal uridylyltransferase 4
um	Micrometres
VZ	Ventricular Zone
WT	Wild-Type
XRN-1/2	5'-3' Exoribonuclease 1/2
Zfyve26	Zinc Finger FYVE-Type Containing 26
Zmat3	Zinc Finger Matrin-Type 3
Z-score	Standard Score
βCat	Catenin beta-1





A fluorescence microscopy image of a tissue section. The image shows a complex network of cells and fibers. The green signal highlights a dense network of fibers, likely collagen or elastin, forming a mesh-like structure. The blue signal, likely DAPI, stains the nuclei of various cells, including fibroblasts and epithelial cells. The red signal, likely a specific marker, highlights certain cells or structures, possibly indicating areas of inflammation or specific cell types. The overall appearance is that of a highly organized and interconnected tissue structure.

2. Summary/Resumen

*It always takes longer than you expect, even when you take into account
Hofstadter's Law”
Hofstadter Law*

2. Summary/Resumen

The brain is the most complex biological structure, from which our conscience emerges. During evolution, the increase in size and complexity of brains (especially the cortex) paved the way to a spectacular development of cognitive and mental abilities. This expansion facilitated the addition of microcircuits with a similar basic structure, which increased brain complexity and contributed to its uniqueness. Given that the final size and shape of an adult brain are determined by the behaviour of progenitor cells during early development, understanding the cellular and molecular mechanisms regulating these actions is fundamental to unravel of how the brain behaves in healthy and pathological conditions. Cellular mechanisms regulating brain formation have been widely studied; however, many of the molecules that control these mechanisms remain unknown. One of the most important mechanisms controlling the molecular program of progenitor cells involves miRNAs. These are molecules that bind specifically messenger RNA molecules, controlling their expression and abundance, and consequently controlling cellular fate. In this thesis we have investigated how microRNAs control brain development at early embryonic stages. Firstly, we studied how the absence of Dicer (enzyme required for miRNA maturation) impacts brain size and organization. We found that loss of miRNAs produces changes in cell proliferation and cell death, inducing the formation of proliferative rosettes. Next, we investigated which miRNAs were responsible for the defects observed after loss of Dicer, finding that *let-7* is the family of miRNAs most affected. To understand which protein coding genes are responsible for the formation of rosettes and the other phenotypes found in Dicer mutants, we searched for differentially expressed genes in this condition that may be influenced by *let-7* miRNAs. We found an increase in the expression of genes involved in signalling pathways regulating proliferation and cell death including *Irs-2* and *p53* respectively. Previous studies demonstrated that *Irs-2* and *p53* are regulated by *let-7* and that stress signals upregulate *Irs-2*. We then found that in Dicer mutants an increase p53 activation (presumably increasing cell death) is necessary for producing rosettes. However, in wild-type animals rosettes can be generated overexpressing *Irs-2* (which increases proliferation but not cell death) and this is rescued just by overexpressing *let-7*. These results suggest that high *Irs-2* (direct or indirectly- through an increase in stress signals or a decrease in *let-7*) is sufficient to produce rosettes. We have identified a signalling pathway through which two antagonistic processes (cell death and proliferation) are linked by *let-7* and whose

deregulation leads to the disruption of brain germinal layers and the appearance of rosettes.

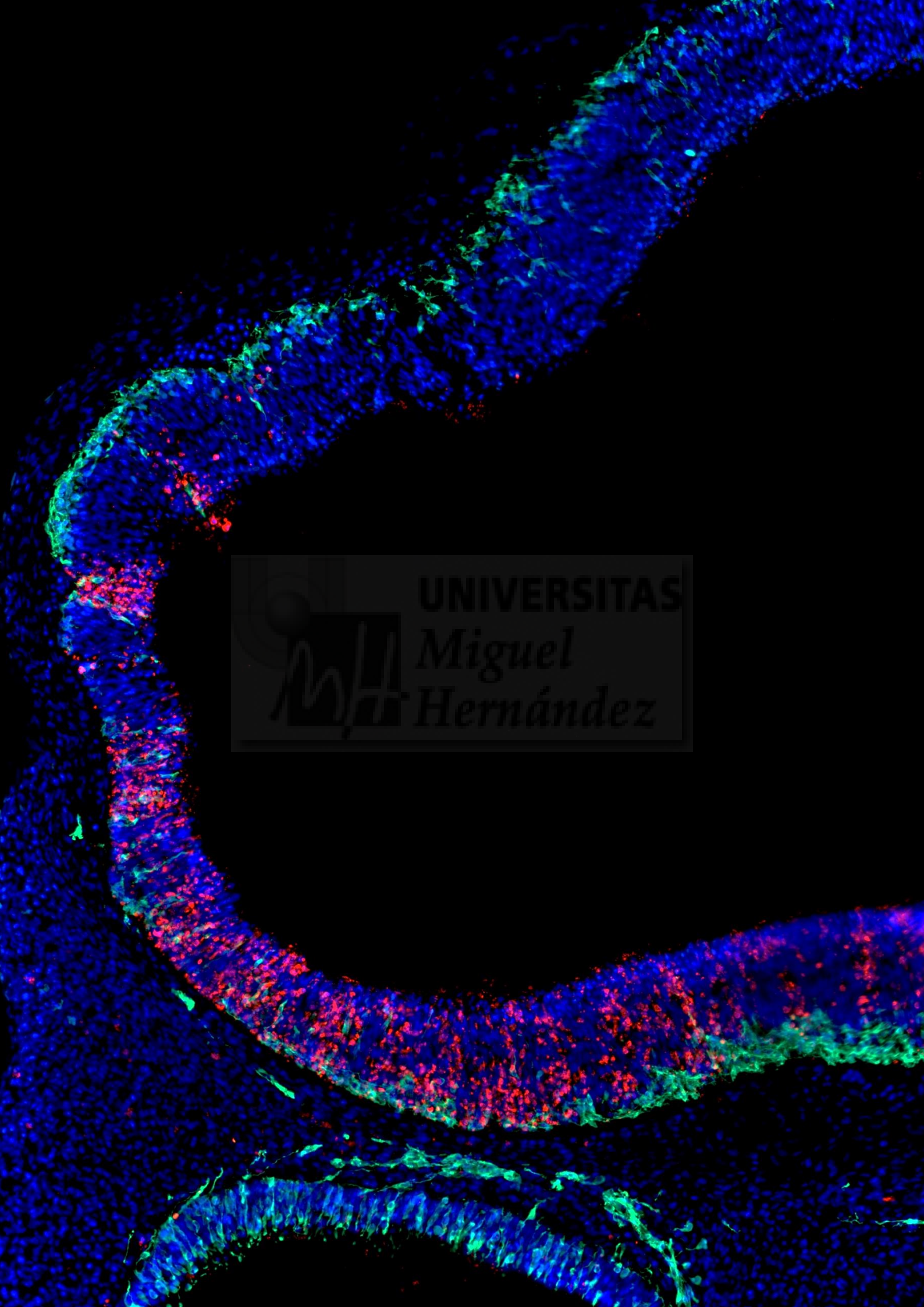


2. Summary/Resumen

El cerebro es la estructura más compleja de la que somos conscientes (y la que nos permite tener conciencia). Durante la evolución, el aumento en el tamaño y la complejidad de los cerebros (especialmente la corteza) abrió el camino hacia un desarrollo espectacular en las habilidades cognitivas y mentales. Esta expansión facilitó la adición de microcircuitos con una estructura básica similar, lo que aumentó la complejidad y contribuyó a su singularidad. Dado que el tamaño y la forma final de un cerebro adulto son determinadas por acciones que ocurren durante el desarrollo temprano del telencéfalo, comprender los mecanismos celulares y moleculares que regulan estas acciones es fundamental para aumentar nuestro conocimiento sobre cómo se comporta el cerebro tanto en condiciones saludables como patológicas. Los mecanismos celulares que regulan la formación del cerebro han sido ampliamente estudiados; sin embargo, muchas de las moléculas que están tras estos mecanismos siguen sin ser identificadas. Una de las maquinarias más importantes para controlar el programa celular es la de los miARNs. Los miARNs son moléculas que se unen de forma específica al ARN mensajero, pudiendo controlar su expresión y la cantidad de los mismos, controlando así el destino celular. En esta Tesis hemos investigado cómo los microARNs controlan el desarrollo del cerebro a edades tempranas durante el desarrollo embrionario. En primer lugar hemos estudiado cómo la ausencia de Dicer (enzima necesaria para la maduración de miARNs) afecta al tamaño y a la organización del cerebro. Encontramos que la pérdida de miARNs produce cambios en proliferación y muerte celular así como la formación de rosetas proliferativas. A continuación, comprobamos qué miARNs eran responsables de los defectos observados tras la pérdida de Dicer, viendo que la familia más afectada era la de *let-7*. Seguidamente y para comprender qué genes son los responsables de la formación de rosetas y del resto de fenotipos encontrados en mutantes de Dicer, buscamos genes significativamente expresados en esta condición. Así descubrimos un aumento tanto en la expresión de genes implicados en vías de señalización que regulan proliferación y muerte celular, incluyendo *Irs-2* y *p53* respectivamente. Estudios previos han demostrado que *Irs-2* y *p53* están regulados por *let-7*. A continuación vimos que en los mutantes para Dicer es necesario un aumento en la muerte celular (a través de la activación de p53) para producir rosetas. Sin embargo, en animales silvestres se pueden generar rosetas sobreexpresando únicamente *Irs-2* (que aumenta la proliferación pero no la muerte celular) y esto se rescata simplemente sobreexpresando *let-7*. Estos resultados sugieren que aumentando *Irs-2*

(directa o indirectamente a través de un aumento en las señales de estrés o a través de una disminución en *let-7*) es suficiente para producir rosetas. Hemos identificado una vía de señalización a través de la cual dos procesos antagónicos (muerte celular y proliferación) están vinculados por *let-7* y cuya desregulación conduce a la alteración de las capas germinales del cerebro y la aparición de roseta





 UNIVERSITAS
Miguel
Hernández



Introduction

UNIVERSITAT

"I am so small and the literature... so vast"

Miguel

Vicent LoLordo

Hernández

3. Introduction

3.1 Mammalian Central Nervous System

3.1.1 General organization

The mammalian nervous system is one of the most complex biological systems. During embryogenesis is one of the earliest systems to begin its formation and the last to be completed after birth. With regard to the diversity of cell types, cytoarchitecture and neural circuitry, the complexity is greatest in the neocortex: the seat of higher cognitive functions, the captain Spok of the hole body. It is in charge of processing all our experiences. Its dramatic expansion during mammalian evolution is thought to be responsible of the, sometimes exceptional, cognitive abilities of modern humans (DeFelipe 2011) .

The nervous system is divided in two major components: central and peripheral. The Central Nervous System (CNS) is divided from front to back into forebrain, midbrain, and hindbrain (Gurtan, Lu et al. 2012). During development, the nervous system derives from the ectoderm (one of the three germ layers of vertebrate embryos) during a process called neural induction where the neural plate is specified. Subsequently, the neural plate closes onto itself forming the neural tube, which extends rostro-caudally in a process called neurulation. While neurulation progresses, the rostral end of the neural tube starts expanding in a process called cephalization which initiates the eventual emergence of the cerebrum.

3.1.2 Regional Identity

To understand how a simple closed tube in a developing embryo will give rise to a brain, we should understand how cells start differentiating and producing more specialized structures. That is one of the major challenges in neurobiology due to the enormous complexity of the telencephalon. Considering the entire nervous system, the brain is where the neuronal diversity achieves its maximum.

The primordium of the brain and the spinal cord is the neural tube. The process by which the neural tube is formed is called neurulation. In this process, the neural groove gradually deepens as the neural folds become elevated. At the end of this process, the folds converge and fuse in the middle line, converting the groove into the closed neural tube. During this type of neurulation, the original ectoderm is divided into three sets of

cells: the neural tube which is internally positioned and will form the brain and spinal cord, in the external part the epidermis of the skin, and the neural crest cells (Figure 1A).

The cerebrum arises from a series of vesicles at the cephalic end of the neural tube. The differentiation of the neural tube into the different regions of the central nervous system is produced in three different ways at the same time. First, anatomically, the neural tube and its lumen constrict to form the chambers of the brain and the spinal cord. Then, in a tissue level, cell populations in the neural tube rearrange themselves to form the different functional areas of the brain and the spinal cord. At the cellular level, progenitor cells populating the neural tube (neuroepithelial cells, NECs) differentiate in order to give rise to different progenitor population such as apical radial glia cells (aRGCs) and subsequently, to different kinds of neurons and glia (Bayraktar and Doe 2013).

3.1.3 Antero-posterior Axis

The most anterior portion of the neural tube will undergo drastic changes. In this region, the neural tube vesicles will differentiate into three primary vesicles: forebrain (prosencephalon), midbrain (mesencephalon), and hindbrain (rhombencephalon). By the time the posterior end of the neural tube closes, secondary bulges—the optic vesicles—have extended laterally from each side of the developing forebrain (Figure 1B) (SF 2000).

Even before the posterior portion of the tube has formed, the prosencephalon becomes subdivided into the anterior telencephalon and the more caudal diencephalon. The telencephalon will eventually form the two symmetric cerebral hemispheres, and the diencephalon will form the thalamic and hypothalamic brain regions that receive neural input from the retina, which is a derivative of the diencephalon (SF, 2000).

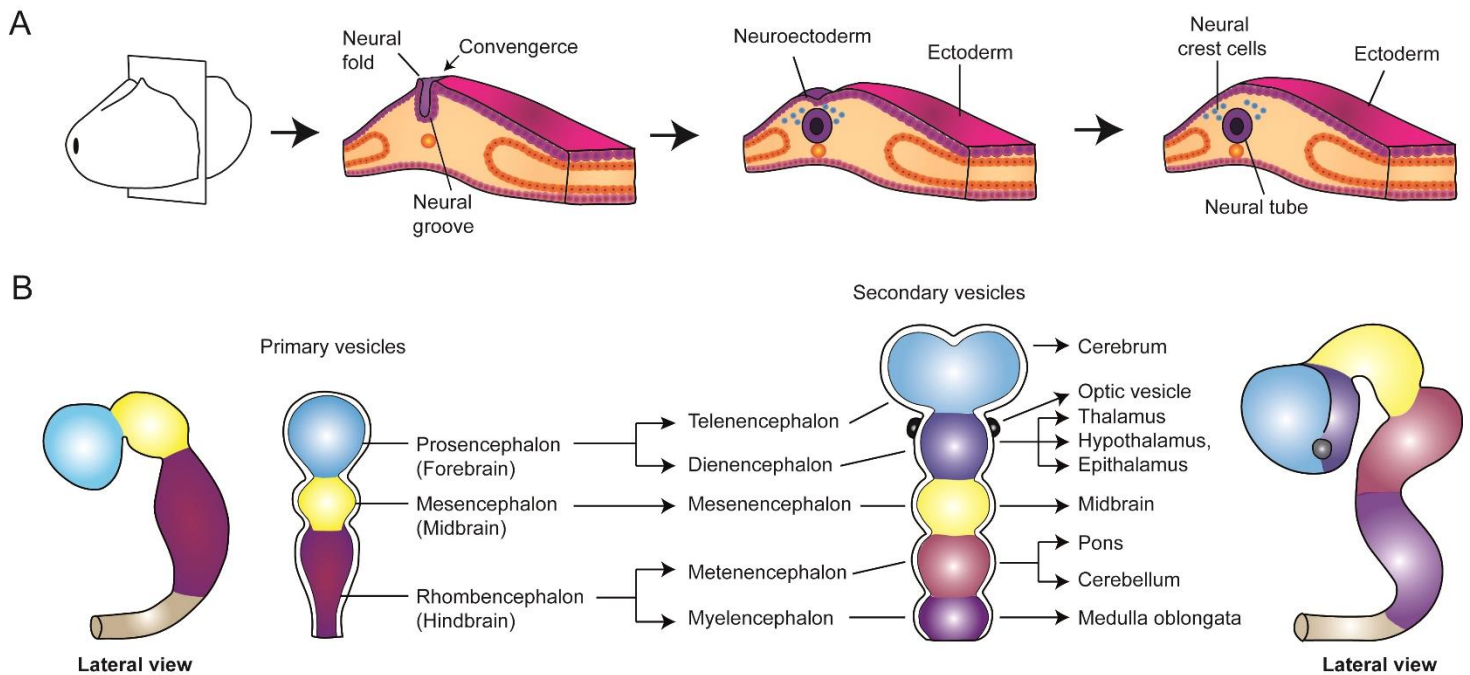


Figure 1. Early Embryonic Development of Nervous System. (A) The neuroectoderm folds inward to start forming the neural groove. The two sides of the neural groove converge forming the neural tube, which lies below the ectoderm. The anterior end of the neural tube will form the brain, while the posterior part will become the spinal cord. The neural crest will form the peripheral structures. (B) Regionalization of the mouse embryonic CNS at E8.5 (left) and E12.5 (right). The embryonic neural tube increases in complexity through enlargements called vesicles; (left) the primary vesicle stage has three regions, and (right) the secondary vesicle stage, which has five regions. (Modified from (Gordon Betts 2017)).

The first stage in the specification of the telencephalic territory is the acquisition of anterior identity within the prosencephalic vesicle (Kanellopoulou, Muljo et al. 2005). The neuroectoderm adopts the anterior identity during neuralization, and in a subsequent steps, the prospective caudal regions are posteriorized due to a gradient of secreted factors such as members of the Wnt family. Anterior areas of the forebrain prevent posterior identity acquisition by the secretion of Wnt antagonists from the anterior patterning center (Durstion, Timmermans et al. 1989). Two of these antagonists secreted are *Hesx1* and *Six3*, which repress the expression of Wnt signalling components like *Axin2* and *Wnt1*; anterior identity is also actively determined by the expression of *Fgf* signaling (mostly through *Fgf8*) secreted by the anterior neural ridge (Braun et al, 2003; Andoniadou & Martinez-Barbera, 2013). Altogether, the coordinated activity of morphogen gradients initiates and maintains the expression of transcription factors that define discrete domains inside the CNS.

3.1.4 Dorsal-ventral Axis

Simultaneous to the antero-posterior specification of the brain, the telencephalon is also compartmentalized in dorsal and ventral territories: pallium and subpallium respectively, which are separated by the pallial-subpallial boundary (PSB). The pallium will give rise to the Hippocampus (Hp), cerebral Cortex (Cx) and Olfactory Bulb (OB), whereas the subpallium will give rise to the striatum and the pallidum (both are part of Basal Ganglia (BG)), the basal forebrain area and the preoptic area (SF 2000). The dorso-ventral polarity of the neural tube is produced due to signals coming from adjacent structures. The roof (dorsal) part receives both Bmp4 and Bmp7 signals from the epidermis, and the floor (ventral) receives Sonic hedgehog signalling from the notochord (Figure 2B).

The pallium and the subpallium are called dorsal and ventral areas respectively, but their true topological relationship is anteroposterior (Cocas, Georgala et al. 2011). During embryogenesis, the telencephalon is divided by the pallial-subpallial boundary. Caudally to this line there is the pallium, which gives rise to the cortex (the major source of excitatory neurons), and rostrally there is the subpallium, the major source of inhibitory neurons (Cocas, Georgala et al. 2011). But during development the pallium will grow in such a manner that will give the impression to be dorsal to the subpallium. The subpallium gives rise to the lateral ganglionic eminence (LGE), the ventral-most part produces the medial ganglionic eminence (MGE) and the central part, the central ganglionic eminence (CGE). The future telencephalic territories can be defined early in development by the expression of Nkx2.1 in the ventral MGE and Gsh1, Gsh2 in the intermediate LGE. Pax6 is expressed in the dorsal telencephalon, being involved in the specification of pallial identity (Moreno and González 2011). Thus, in the telencephalon, Nkx2.1, Gsh2 and Pax6 are complementary expressed, providing some of the earliest markers for the respective territories and being key regulators for their normal development.

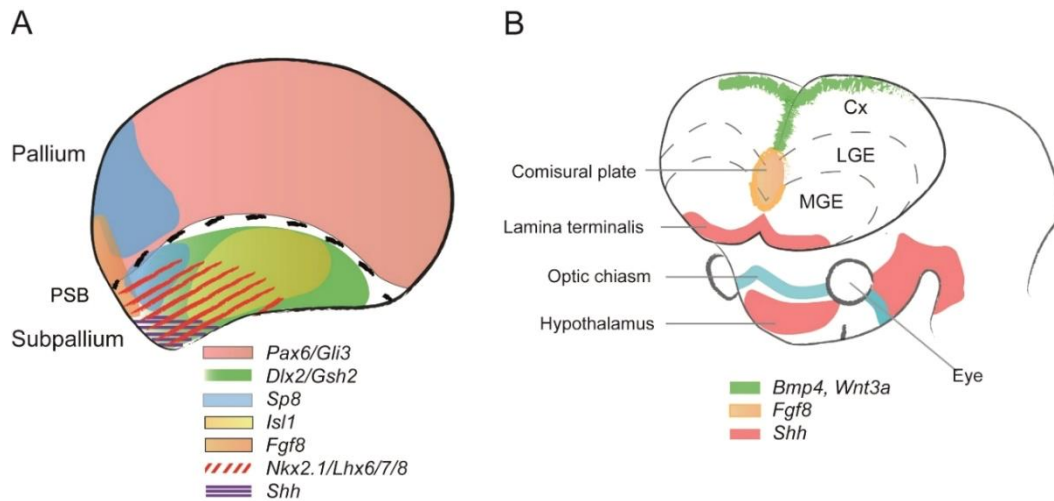


Figure 2. CNS regionalization in mouse embryos (A) Diagram of developmental plan of mouse telencephalon PSB. Showing the expression of the genes indicated pallium-subpallium boundary. **(B)** Schema of a frontolateral view of the mouse telencephalon showing the patterning centers as marked by expression of the genes indicated. (Modified from (Storm, Garel et al. 2006, Sugahara, Aota et al. 2011)).

3.1.4.1 Structures generated from the pallium

The main parts of the mammalian pallium are the named as medial, dorsal, lateral and ventral pallial sectors (Figure 3). The medial pallium forms hippocampal and parahippocampal structures (in addition to the pallial septum), the dorsal pallium forms the neocortex, the lateral pallium forms the insula and claustrum and the ventral pallium gives rise to all the olfactory bulb, the anterior olfactory nucleus, the anterior piriform cortex and the ventral part of intermediate archistriatum cortical structures (Kaas 2016). In mammals, the pallium is a relatively simple structure, with a laminar organization in the major part of its areas. Nevertheless, the ventral pallial components present a structure formed by nuclei, contributing to the amygdalar complex. Then, the lateral (olfactory cortex) and the medial (hippocampal region) pallial derivatives present a three layer organization, whereas the isocortex is characterized by its conspicuous six-layered structure (Montiel and Aboitiz 2015). In addition, the isocortex is organized into radial columns that derive embryologically from cells following the same radial glial trajectory, and in most cases are clonally-related (Kaas 2016). During mammalian brain development, laminated areas undergo a greater expansion compared with the nucleated areas.

The pallium is separated from the subpallium based on its differential molecular identity, which leads to the general rule that pallial neurons are glutamatergic and subpallial neurons are GABAergic. However, this separation is blurred at later stages by tangential migrations from subpallium to pallium and from pallium to subpallium. Subpallial inhibitory neurons migrate into the pallium, such that by the end of development, the pallium will contain around 20% subpallial cells; particularly, the olfactory bulb is invaded via the rostral migratory stream by subpallial cells and processes.

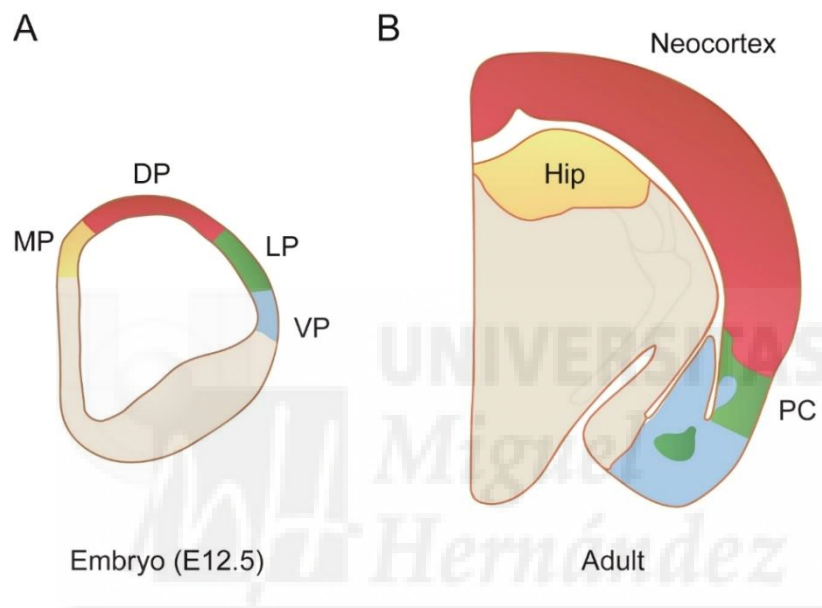


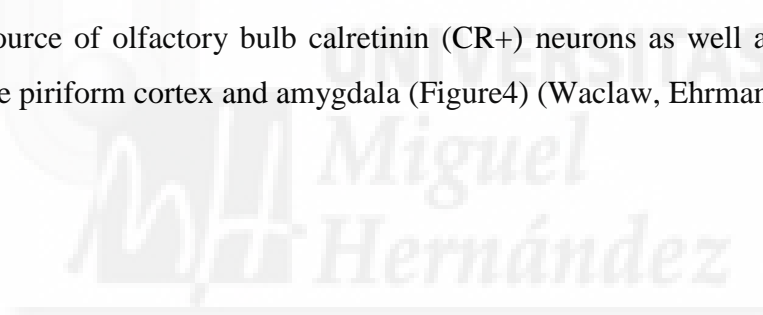
Figure 3. Spatial patterning of pallial progenitors. In mammals, the embryonic pallium (A) is spatially subdivided in at least four progenitor domains: Medial pallium (MP, yellow), dorsal pallium (DP, red), lateral pallium (LP, purple) and ventral pallium (VP, blue). The adult brain regions generated by each domain are shown (B) with the same colour code. Hippocampus (Hip), PC (Piriform Cortex). Modified from (Luzzati 2015).

3.1.4.2 Structures generated from the subpallium

The subpallium has been subdivided into four major domains: striatum, pallidum, diagonal area and preoptic area (POA). The striatal domain largely corresponds to the LGE, whereas the MGE encompasses the pallidal domain, the diagonal area, and part of the POA (Puelles, Harrison et al. 2013). In the developing subpallium, a rapid burst in proliferation produces the formation of the lateral and medial ganglionic eminences. These two structures together with the subpallial septum will express *Dlx5* at E12.5,

whereas the expression of Nkx2.1 and Lhx6 is restricted to the medial eminence, the subpallial septum and the POA (Figure 4) (Medina, Abellan et al. 2014, Kaas 2016).

The subpallium is the source of all the interneurons found in the pallium at mature stages. The medial ganglionic eminence is the major source of interneurons, giving rise to the morphologically-heterogeneous non-fast spiking somatostatin-positive (SOM+) interneurons and fast spiking (FS) parvalbumin-positive (PV+) subsets of cortical interneurons (Butt, Fuccillo et al. 2005, Fogarty, Grist et al. 2007). In contrast to the MGE, the CGE appears to provide a more restricted subset of interneurons, giving rise only to the calretinin-positive (CR+) bipolar interneurons and double bouquet cells, this area is marked with Er81 and Zcchc12. The lateral ganglionic eminence is marked with Er81 and its ventricular zone is marked with Gsx2 (with a high dorsal to low ventral gradient). The LGE can be subdivided into two different areas that will generate different types of interneurons: dorsal (dLGE) and ventral (vLGE) (Stenman, Toresson et al. 2003). The vLGE appears to be a major source of striatal GABA projection neurons while the dLGE is a source of olfactory bulb calretinin (CR+) neurons as well as subclasses of neurons in the piriform cortex and amygdala (Figure4) (Waclaw, Ehrman et al. 2010).



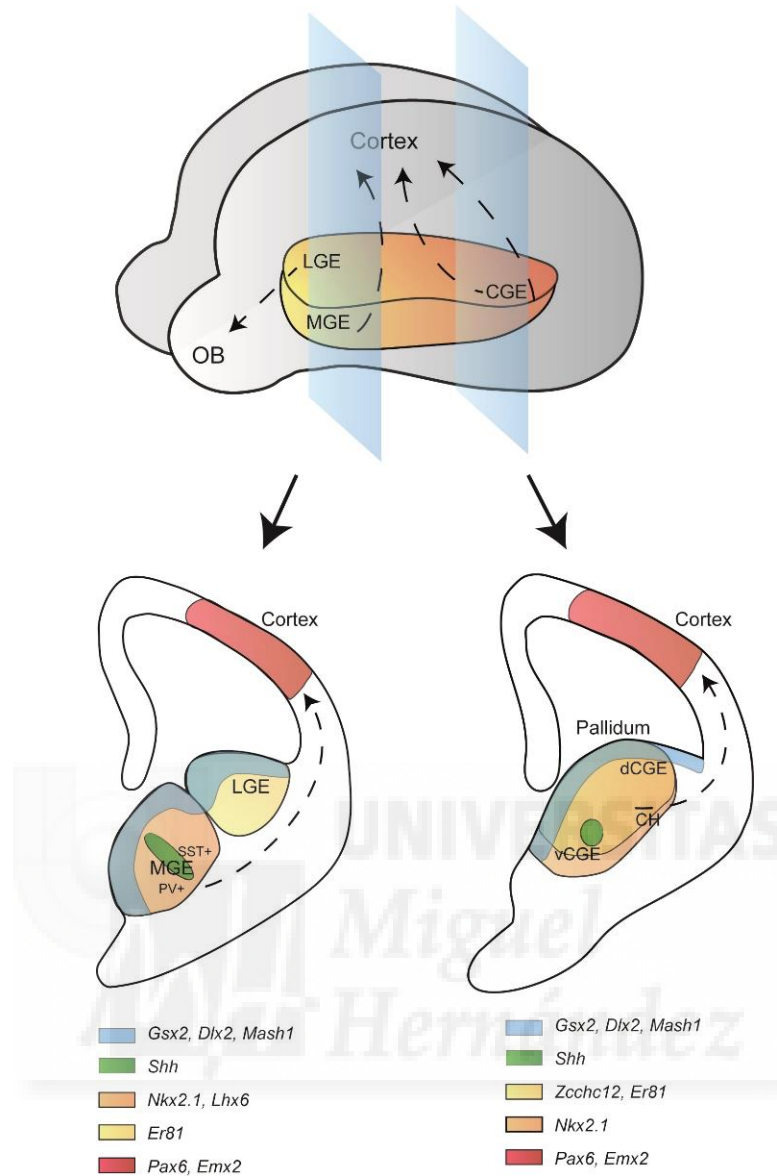


Figure 4. Description of interneuron birth place and relevant gene expression profile. Top shows ganglionic eminence distribution in a mouse brain and the major interneurons migration streams, CGE is a caudal extension of the more anterior tissues. Bottom shows anterior (left) and posterior (right) coronal sections through the telencephalon of an E13.5 mouse. Pertinent marker gene expression profiles are depicted of the proliferative niches of the ganglionic eminences. Relative origin of interneuron subtypes are shown in RED. Note the Shh expression domains. Abbreviations; LGE, lateral ganglionic eminence; MGE, medial ganglionic eminence; CGE, caudal ganglionic eminence (v ventral and d dorsal); OB, olfactory bulb; PV, Parvalbumin; SST, Somatostatin; CR, Calretinin. (Extracted from (Arber and Li 2013)).

3.2 Development of the telencephalic neuroepithelium

At the onset of neurogenesis, the telencephalon is composed of a monolayer of neural stem neuroepithelial cells (Bayer & Altman, 1991). NECs are highly polarized and attached to each other by adherents and tight junctions at the level of the apical domain (inner surface of the telencephalic vesicle) (Figure 5A). They move their cell nucleus

between the apical and basal sides of the neuroepithelium in coordination with the cell cycle: basal-directed movement during G1, basal position during S-phase, apical-directed movement during G2, and mitosis at the apical surface. This cyclic movement is known as interkinetic nuclear migration and is completely asynchronous between NECs, conferring the neuroepithelium a pseudostratified appearance.

The fact that all telencephalic structures share a common origin, and are formed by the same multipotent type of cells (Figure 5B), suggests that different telencephalic areas may develop following similar strategies. (Urbach R 2000-2013).

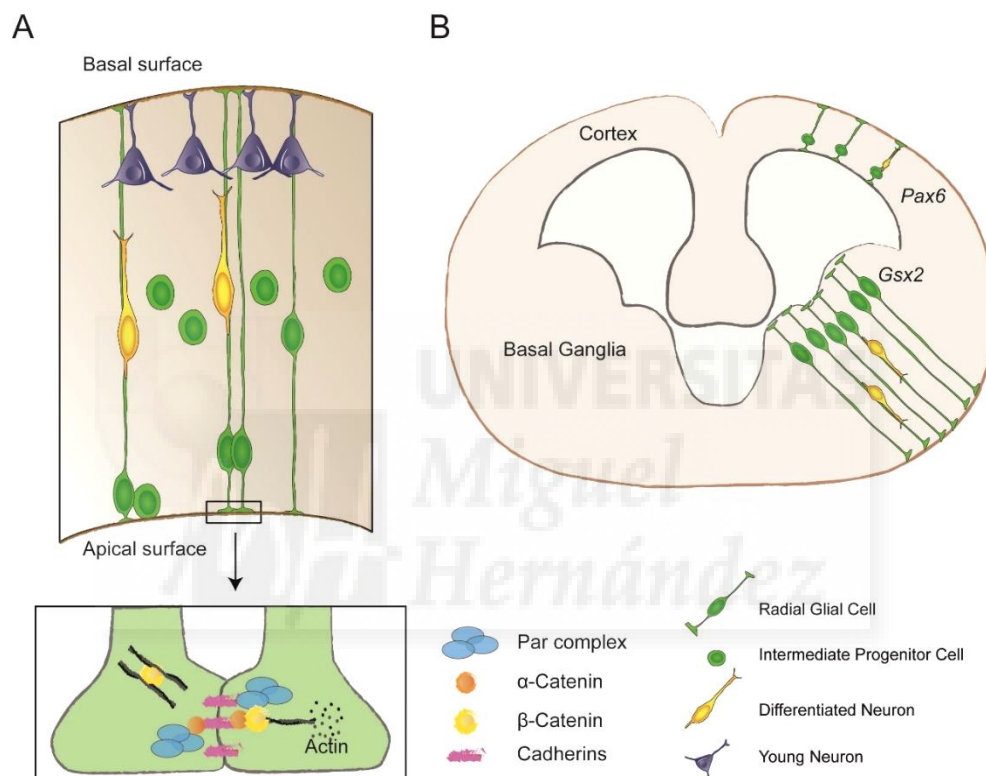


Figure 5. Glial cells as stem and progenitor cells in the developing brain. (A) Schema of the developing brain showing different progenitor types: aRGCs and IPC (green). aRGCs have an apico-basal polarity with an apical membrane delineated by junctional complexes containing tight and adhesion junction proteins like cadherins (pink), α - and β -catenin (orange and yellow respectively), and proteins of the Par complex (blue). (B) Schema showing how RGCs are disposed in different areas of the developing brain. Modified from (Dimou and Gotz 2014).

In vertebrates, immediately prior to the onset of neurogenesis, NECs start losing tight junctions and begin acquiring features typical of glial cells including the expression of brain lipid-binding protein (BLBP), vimentin, and Pax6, thus becoming apical radial glial cells (Taverna, Gotz et al. 2014). This new type of progenitor cell maintains some neuroepithelial features, including: a) expression of the intermediate-filament protein Nestin (Wonders and Anderson 2006); b) apical-located centrosomes; c) adherent

junctions in the apical side of the plasma membrane formed by proteins as Par3 (partitioning defective protein-3) (Figure 5A) and Par6/aPKC (atypical protein kinase C) (Wonders and Anderson 2006); and d) contact with the basal lamina.

In mice, the transition from NECs to aRGCs takes place between embryonic day 10 (E10) and E12 (Wonders and Anderson 2006). Like NECs, aRGCs undergo interkinetic nuclear migration, divide at the apical surface of the developing cortex and undergo self-amplifying divisions. aRGCs gradually start dividing asymmetrically to generate one aRGC plus a different cell. These new cells accumulate at the basal side of the cortical primordium, while the cell bodies of aRGCs remain in the apical side, forming the Ventricular Zone (VZ). With the accumulation of cells above the VZ, the basal process of aRGCs (known as radial glial fibre) elongates while remaining attached to the basal lamina. Asymmetric aRGC divisions may generate one aRGC plus either one neuron or one Intermediate Progenitor Cell (IPC) (Malatesta et al, 2000; Noctor et al, 2001, 2004; Haubensaket al, 2004; Miyata et al, 2004). IPCs are secondary progenitor cells without apical–basal polarity, they don't undergo interkinetic nuclear migration, reside and divide in a location immediately basal to the VZ, the subventricular zone (SVZ), a proliferative cell layer that is located basally to the ventricular zone. Contrary to aRGCs, IPCs express the transcription factor Tbr2 (Englund, Fink et al. 2005). In mouse, the vast majority of IPCs divide once to produce 2 neurons (neurogenic, self-consuming divisions), and hence, they are viewed as a strategy to amplify the production of cortical neurons (Figure 6). However, because each IPC self-consumes at mitosis, their relative abundance compared to aRGCs is quite low (Kowalczyk, Pontious et al. 2009). Populating the SVZ we also find basal Radial Glia Cells (bRGCs), which present many similarities with aRGCs including a basal process extended radially and contacting the basal lamina of the telencephalon, and expression of the transcription factor Pax6, but the cell body of bRGCs is located and divides at basal positions in the SVZ. In mouse, bRGCs do not self-amplify nor produce IPCs, but are essentially neurogenic. In contrast to mouse, studies in higher mammals like ferret and humans demonstrate that bRGCs are highly amplificative in these species (Reillo, de Juan Romero et al. 2011, Pilz, Shitamukai et al. 2013, Martinez-Martinez, De Juan Romero et al. 2016). They appear to be mostly self-amplifying at early stages (generating more bRGCs) and then astrocytogenic at later stages. This category of progenitors is especially abundant in the cortex of gyrencephalic species, thought to be critical for the formation of gyri and sulci (Nonaka-Kinoshita,

Reillo et al. 2013, Pilz, Shitamukai et al. 2013). Moreover, human and ferret (both gyrencephalic species) bRGCs are morphologically and molecularly very similar, but human bRGCs have been reported to self-amplify only occasionally. Instead, they may mostly self-renew and generate multipolar daughter cells, presumably neurogenic IPCs, which would continue dividing for a limited number of cycles (Hansen, Lui et al. 2010). However, conflicting data from non-human primates challenges this interpretation, suggesting that bRGCs undergo several rounds of self-amplifying divisions (Betizeau et al., 2013).

The size and the shape of an adult brain is defined by processes occurring during the development of the telencephalon. These processes are regulated through different strategies such as modifying the final number, the shape and the position of progenitor cells. The molecular program of those progenitors is different between species and areas, leading to a high variety of mature brains.

3.2.1 Cellular mechanisms controlling telencephalic development

3.2.1.1 Proliferation and neurogenesis

As NECs and RGCs produce by them are the progenitor cells that will give rise to neurons populating the whole telencephalon, their pool size determines the number of their derived neurogenic progenitor cells and eventually the final number of cortical neurons. Thus, the pool size of progenitors has a fundamental impact on the size of the mature brain (Dimou and Gotz 2014). NEC abundance may be increased by extending the time period of their self-amplification and delaying the onset of neurogenesis. The importance of their amplification on the final brain size has been experimentally demonstrated in mouse, where progenitor abundance in the embryonic cortex may be increased by either promoting their re-entry into cell cycle or preventing programmed cell death (Chenn and Walsh 2002, Kingsbury, Rehen et al. 2003). In both cases, the increase in the number of progenitors lead to expansion in surface area and folding of the neuroepithelium.

As previously pointed out, immediately prior to the onset of neurogenesis NECs will give rise to aRGCs. As a consequence, most of the neurons in the brain are derived directly or indirectly from aRGCs (Wonders and Anderson 2006). This type of progenitor is more fate-restricted than neuroepithelial cells (Wonders & Anderson, 2006). In terms of potential of generation different cell types, some authors affirm that aRGCs are

restricted to the generation of a single cell type, either astrocytes, oligodendrocytes or -as in most cases in neurogenesis- neurons (Grove, Williams et al. 1993, Malatesta, Hartfuss et al. 2000, Noctor, Flint et al. 2001, Malatesta, Hack et al. 2003). Despite they are more fate-restricted than NECs, aRGCs produce different cell types: initially they undergo symmetric divisions giving raise to two daughter aRGCs, but they lose their proliferative potential predictably and progressively as development proceeds. This evidence showed by Susan McConnell and others (McConnell 1988, Desai and McConnell 2000, Gao, Postiglione M et al. 2014) suggested that the proliferative potential of aRGCs may be controlled by a molecular clock that counts the rounds of cell division, as also suggested for neurogenesis of cerebellar granule cells (Espinosa and Luo 2008).

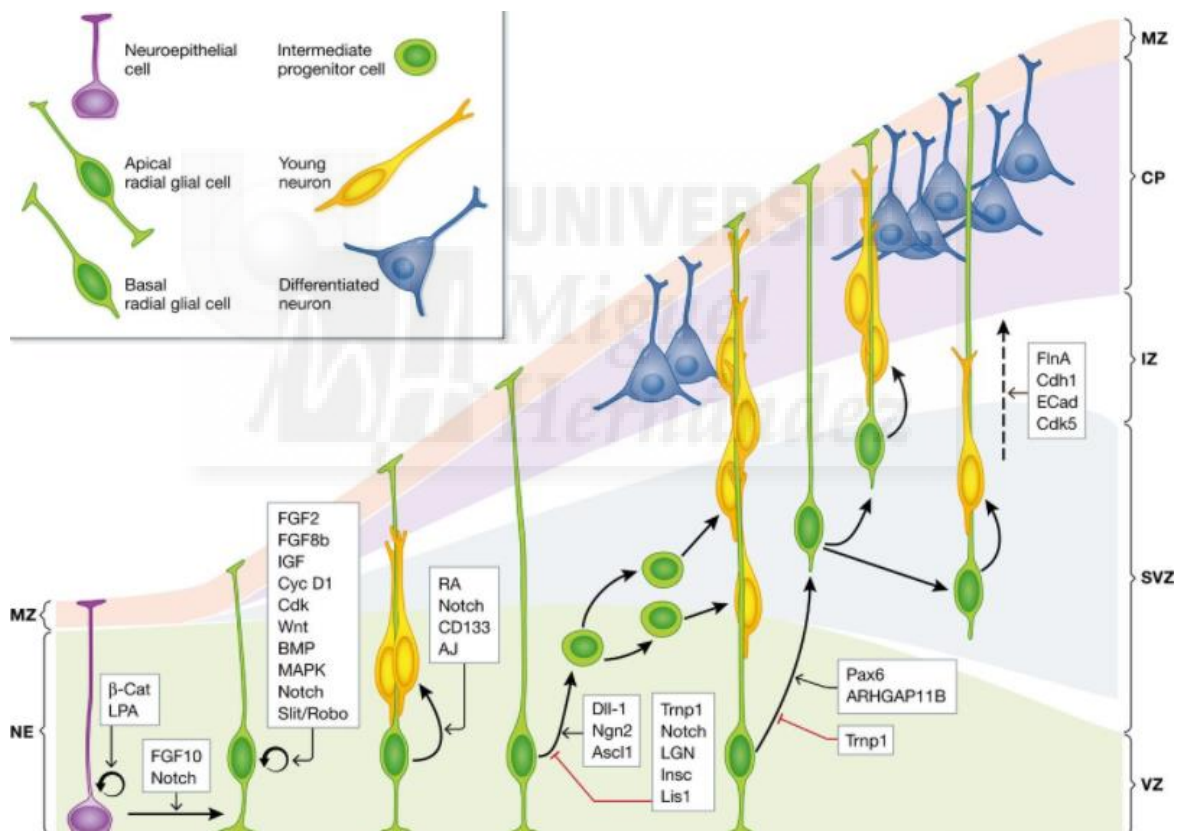


Figure 6. Stem cells in the developing cerebral cortex of gyrencephalic brains and their molecular regulation. Schema depicting the main types of progenitor cells and their lineage relationships in the developing cerebral cortex. Arrows indicate lineage relationships demonstrated by time- lapse imaging and/or by retroviral lineage tracing. During the expansion phase, most neuroepithelial cells divide symmetrically to self- amplify to generate apical radial glial cells. During the neurogenic phase, most aRGCs divide asymmetrically to generate neurons, either directly or indirectly through intermediate progenitor cells or basal radial glial cells. Molecules or pathways regulating some of these steps are indicated. MZ, marginal zone; CP, cortical plate; IZ, intermediate zone; SVZ, subventricular zone; VZ, ventricular zone. Extracted from (Fernández, Llinares- Benadero et al. 2016)

As neurogenesis progresses, there is a lower requirement for aRGC expansion/renewal and a greater need for neuron production, so there is a gradual predominance of asymmetric aRGC divisions producing IPCs (Figure6) (Noctor, Martinez-Cerdeno et al. 2004, Kowalczyk, Pontious et al. 2009).

The expansion of the SVZ is a strategy to allow the expansion of the brain. This needs initially generation of large amounts of SVZ progenitors from the VZ, but at some point this secondary germinal layer will follow a lineage totally independent from the VZ, and its neurogenic potential will be exponentially increased (Martinez and Cols, 2016). In gyrencephalic species, the seeding of progenitors in the SVZ (especially in the oSVZ) is produced in a short time window during which there is a decrease in the production of aRGCs and an increase in the production of bRGCs finally located in the oSVZ (Martinez-Martinez, De Juan Romero et al. 2016). The subpallium is the region of the murine brain with the largest SVZ and subsequent neuronal progeny. This may be explained by differences between the behaviour of progenitors in pallium and in subpallium. It has been described that in the SVZ of both, the pallium and the subpallium of gyrencephalic species there are the same type of progenitors (bipolar radial glia cells –bpRGs-) (Pilz, Shitamukai et al. 2013). This suggests that, in addition to coming from the same kind of primordial progenitors, both pallium and subpallium present similar strategies for increasing the final size of a particular area and this strategy can be adjusted more or less depending on the species and brain area.

3.2.1.2 Radial/tangential migration

Newborn cortical excitatory neurons migrate from their layer of birth to the vicinity of the cortical surface, where they will coalesce into nascent neuronal layers. This process is named radial migration (Rakic 1972). The scaffold of radial glial fibres (the basal processes of RGCs that spans perpendicular between the ventricular and the pial surface of the cortex), provides the necessary physical substrate and guide for these neurons during their radial migration. The physical interaction between RGC and neuron is under a tight molecular regulation, and if the interaction is disrupted, it can affect to the final position of neurons and to the layering in the cortex (Rakic, Stensas et al. 1974, Elias, Wang et al. 2007). Due to this dependence of radially migrating neurons on radial glial fibres, the trajectory of these fibres could determine the migratory route and influence the

final location of new neurons along the cortical surface (Rakic 1995). Consequently, in lissencephalic species, sibling neurons born from one progenitor normally occupy neighbouring positions in the mature cerebral cortex (O'Leary and Borngasser 2006).

Newborn interneurons migrate first radially and then tangentially from the ventral territories to occupy the different layers of neocortex (Anderson, Marin et al. 2001, Magalhães 2016). Interneurons born in the dorsal LGE (dLGE) migrate tangentially along the rostral migratory stream to the OB, while interneurons born in other ventral regions migrate tangentially to the neocortex (Marin and Rubenstein 2001, Marin 2013). Several waves of migrating interneurons enter the neocortex through distinct migratory pathways: first, following a superficial pathway within the MZ, and later following a deep pathway within the lower part of the IZ and the SVZ (Anderson, Marin et al. 2001, Magalhães 2016).

It has been described that cortical interneurons differentiate during radial migration. Performing clonal analysis of progenitors in the MGE Brown et al. (Brown, Chen et al. 2011) found several cell types forming a unique labelled clone, in which there were apical radial glia cells; then, basally to the VZ they found multipolar progenitor cells; and in the most apical positions, differentiating interneurons.

3.2.1.3 Specification and differentiation

The fact that interneurons are postmitotic on the initiation of migration, and that there are subgroups of interneurons differentiated by their spatial origin and their birthdate has important implications regarding to the process of interneuron specification. Clearly, the progenitors of the MGE- and CGE-derived interneuron subgroups have molecular differences at the time that they exit the cell cycle. A comparison of two MGE progenitor fate-mapping experiments suggests that key aspects of interneuron subgroup fate are likely to be specified as the progenitors leave the cell cycle, and not by factors encountered during migration (Brown, Chen et al. 2011).

Once neurons finish the process of migration, they begin terminal differentiation. This process has a fundamental impact in the final size of the brain, essentially by increasing the size of cell somas and the volume of the neuropile: growth and branching of apical and basal dendrites; extension and branching of the axon; formation of spines and boutons for synaptic connectivity. The density of cortical neurons, cell body size, and extent of their dendritic and axonal arbors are remarkably different between mammals,

correlating with brain size (Herculano-Houzel, Manger et al. 2014, Fernández, Llinares-Benadero et al. 2016) and also contributing to cortical expansion (Reillo, de Juan Romero et al. 2011, Dimou and Gotz 2014).

3.2.2 Molecular mechanisms controlling telencephalic development

3.2.2.1 Progenitor amplification

Understanding the molecular control of progenitor amplification is a beautiful and complex part of the developmental knowledge. There are thousands of molecules controlling the cell cycle of progenitor cells, but here I will try to summarize some of the molecules implicated in controlling the pool of progenitors of the developing telencephalon.

Fibroblast Growth Factors (FGFs) pathways

FGFs block the maturation of cortical progenitors (inhibit neurogenesis) and, promote their proliferation by regulating the duration of the cell cycle. The role of FGF signalling is critical for cortical growth, as its loss at early stages accelerates neuron production and loss of RGCs, resulting in reduced cortical surface area (Rash, Lim et al. 2011). Conversely, overactivation of FGF signalling by infusion of FGF2 or FGF8b causes the overproliferation of cortical progenitors and cortical expansion in surface area. FGFs influence cortical progenitors via regulation of cell cycle proteins. FGF2 and insulin-like growth factor (IGF) 1 upregulate the expression of cyclin D1 and downregulate the expression of p27(kip1), a cyclin- dependent kinase (Cdk) inhibitor, thereby shortening the G1 phase of the cell cycle and promoting self- amplificative divisions (Raballo, Rhee et al. 2000, Mairet-Coello, Tury et al. 2009). Activation of this FGF signalling cascade drives cortical expansion, which is accompanied by the incipient folding of the otherwise smooth mouse cortex (Rash, Lim et al. 2011), and in the already gyrencephalic ferret cortex, it causes extra folding (Masuda, Toda et al. 2015). Not surprisingly, cortical progenitor populations may be expanded directly by overexpressing Cdk4 and cyclin D1 (Lange, Huttner et al. 2009). In the mouse cortex, this promotes cortical growth and megalencephaly, but not folding (Nonaka-Kinoshita, Reillo et al. 2013), which highlights the molecular and cellular complexity of the process of cortical folding (Borrell and Calegari 2014, Fernández, Llinares- Benadero et al. 2016).

Notch pathway

Other important signalling pathway regulating cortical progenitor proliferation and self-renewal include the Notch pathway. In addition of promoting the transition from NECs to aRGCs at early developmental stages (Gaiano, Nye et al. 2000, Martynoga, Drechsel et al. 2012), activation of the Notch pathway at later stages inhibits the generation of IPCs from aRGCs (Mizutani, Yoon et al. 2007, Martynoga, Drechsel et al. 2012). Conversely, the onset of Dll1 expression (the main ligand of Notch1) coincides with the expression of the pro- neural proteins Ngn2 and Ascl1, major transcriptional regulators of neurogenesis and direct regulators of Dll1 expression (Castro, Skowronska-Krawczyk et al. 2006, Martynoga, Drechsel et al. 2012).

The Notch pathway can be additionally activated by Slit/Robo signalling, with similar consequences: impairment of neurogenesis at early stages by promoting the self-renewal of aRGCs (Borrell, Cardenas et al. 2012). Importantly, Notch signalling seems to be required for the self-renewal of oSVZ progenitors in the human cerebral cortex (Hansen, Lui et al. 2010).

Wnt, BMP, MAPK, IGF, RA pathways

Activation of Wnt pathway promotes proliferation and self-renewal of aRGCs at early developmental stages (Machon, van den Bout et al. 2003, Woodhead, Mutch et al. 2006), while at later stages it promotes the maturation of aRGCs into IPCs (Viti, Gulacsi et al. 2003, Hirabayashi, Itoh et al. 2004) and it may even promote neurogenesis (Munji, Choe et al. 2011). Thus, the effects of Wnt signalling in cortical development are complex and time-regulated during development. The BMP pathway has similarly elusive and complex inputs into the regulation of cortical neurogenesis. At early developmental stages, BMP signals induce neurogenesis (Li, Cogswell et al. 1998, Mabie, Mehler et al. 1999), while at later stages, they block neurogenesis to promote astrocyte differentiation (Gross, Mehler et al. 1996). The Ras- MAPK- ERK pathway controls the mitogen-stimulated proliferation of cortical progenitors and its negative regulators, thus ensuring progenitor self-renewal and preventing premature differentiation (Phoenix and Temple 2010). Then, IGF- 2 secreted into the cerebrospinal fluid by the choroid plexus is another potent mitogen promoting proliferation of VZ cortical progenitors (Lehtinen and Walsh 2011). Retinoic acid (RA) signalling has also been identified as important in regulating the balance between cortical progenitor self-renewal and neurogenesis, where RA

secreted by the meningeal membranes promotes neurogenesis while limiting aRGC amplification (Siegenthaler, Ashique et al. 2009). Contrary to the classical signalling pathways mentioned above, the RA pathway holds promise as an important regulator of cortical expansion and folding, as its genetic blockade induces remarkable folding of the mouse cortex (Siegenthaler, Ashique et al. 2009). The downstream transducers of RA signalling in this context are not known, but the orphan nuclear hormone receptor CoupTF1 and the pro- neural transcription factors Ngn1 and 2 may be involved (Ribes, Stutzmann et al. 2008, Harrison-Uy, Siegenthaler et al. 2013, Fernández, Llinares-Benadero et al. 2016).

3.2.3 Progenitor cell lineage

Lineage regulation of the different types of progenitor cells, including their production and maintenance, is a critical determinant of telencephalic size (Borrell and Gotz 2014).

In the cerebral cortex of mouse, ferret, and humans, bRGCs and IPCs are generated from aRGCs in the VZ (Reillo, de Juan Romero et al. 2011, Wang, Tsai et al. 2011). This process is seemingly associated with, and controlled by, the mitotic spindle orientation of aRGCs (Shitamukai, Konno et al. 2011), which is known to have a significant influence on the acquisition of asymmetric cell fates by cortical progenitors (Postiglione, Juschke et al. 2011, Xie, Juschke et al. 2013). When progenitors in the early neuroepithelium self-amplify, they divide mostly in perpendicular orientations, while oblique cleavage planes augment as neurogenesis becomes predominant. Disruption of these orientations at early stages leads to depletion of the progenitor pool. Orientation of the mitotic spindle in the mammalian cerebral cortex is regulated by a number of factors, including LGN, Insc, and Lis1 (Postiglione, Juschke et al. 2011, Shitamukai, Konno et al. 2011, Xie, Juschke et al. 2013).

In addition to the cleavage plane orientation, there are other cellular mechanisms regulating cortical progenitor cell fate, particularly symmetric versus asymmetric fates, which include the maintenance of the apico-basal polarity by Notch signaling, Par3, Par6, prominin- 1 (CD133), and other proteins related to the apical adherents junctions (Gotz and Huttner 2005). A decrease in apical junction proteins like Par3 or Par6 switch the mode of aRGC division from self- renewing to neurogenic, while their overexpression promotes aRGC self- renewal (Costa, Wen et al. 2008).

Regarding the subpallial telencephalon, neural progenitor cells generates interneurons and oligodendrocytes (Yung, Gokhan et al. 2002). The generation of these different cell types depends on transcription factors expressed within the subpallium. For example, *Dlx2* and *Olig2* are known to be essential for the differential formation of neurons or oligodendrocytes in this area. *Dlx2* is a homeobox transcription factor which expression will determine the formation of neurons instead of oligodendrocytes. Overexpressing *Dlx1/2* inhibits the expression of *Olig2* (marker of precursor cells that will give rise to oligodendrocytes) (Eisenstat, Liu et al. 1999).

3.2.4 Progenitor cell heterogeneity

The advent of single- cell transcriptomics has revolutionized the neurodevelopmental field by allowing uncovering an extraordinary molecular heterogeneity of progenitor cell types in the developing cerebral cortex (Pollen, Nowakowski et al. 2014). This technology has revealed that aRGCs and bRGCs are molecularly more heterogeneous in the developing folded cortex of humans and other gyrencephalic species (3 classes of aRGC, 2 classes of bRGC) than in the smooth cortex of mouse (2 classes of aRGC, 1 class of bRGC) (Pollen, Nowakowski et al. 2014, Camp, Badsha et al. 2015, Fernández, Llinares- Benadero et al. 2016).

Single- cell transcriptomics is already highlighting the potential relevance of specific signalling cascades and molecular programs in the formation and maintenance of different progenitor types in different brain areas. Taking into account the wide variety of progenitor types (aRGC, bRGC, SAP, SNPs...) and their specie-specificity and area-specificity, it makes sense to consider their role in producing different neuronal progeny (in terms of neural type or in clonal size). Accordingly, driving MGE progenitors towards apical or basal progenitors can alter their cell fate (Gotz and Huttner 2005).

Finally, another factor that can alter progenitor's behaviour in agreement with previous population- wide transcriptomic analyses and functional manipulations is the extracellular matrix and its components, which are recently highlighted as central in stimulating cortical progenitor proliferation and self- renewal (Pollen, Nowakowski et al. 2014).

3.3 microRNAs as molecular regulators of progenitor's behaviour

MicroRNAs are a family of 19–25 nucleotide small RNAs that negatively regulate gene expression (with some exceptions as during cell quiescence (Vasudevan, Tong et al. 2007)). They are involved in a large number of cellular and biological events. As their expression pattern is different at different time points and in different areas, they are ideal candidates for the regulation of developmentally timed events, including the proper regionalization of the telencephalon (Magalhães 2016).

MicroRNAs (miRNAs) are highly conserved, single-stranded, small non-coding RNA molecules that bind to the target mRNA and reduce, through different mechanisms (from translational inhibition to mRNA degradation), the final levels of protein production (Sugahara, Aota et al. 2011) in a tissue-specific and developmental-stage specific manner. Levels of mature miRNA are controlled by transcriptional regulation, enzymatic processing, and stability of the miRNA. A single miRNA specie can target different messenger RNAs (mRNAs) and a single mRNA can be regulated by different miRNAs. There are several steps in which miRNAs can be regulated. Taking all this into account, we can figure out the enormous complexity of the system's regulation that allows miRNAs to control in a very precise way the quantity of mRNA that will be translated (Fiore, Siegel et al. 2008).

3.3.1 miRNAs in the nervous system

Combining the ability of miRNAs to effectively modify the expression pattern of many target mRNAs, with the tight control of their expression suggests that miRNAs may play important roles modulating cellular states that take place during development. Some authors (Heimberg, Sempere et al. 2008) propose that miRNAs may be one of the contributors to changes in brain morphology in recent evolutionary time. Focussing in the onset of neurogenesis, it has been shown that some miRNAs, like *miR-134* and *miR-184* regulate neural progenitor maintenance and proliferation, while *let-7* family miRNAs (*let-7a/let-7b*), *miR-9*, *miR-137* and *miR-124* have been implicated in promoting neuronal differentiation (Bian, Xu et al. 2013, Cao, Li et al. 2016). Among them, the most abundant miRNAs in the brain are *miR-9* and *miR-124* which role regulating neuronal differentiation and controlling proliferation (targeting several components of the Notch signalling pathway) have been extensively studied (Stappert, Roese-Koerner et al. 2015, Cao, Li et al. 2016).

3.3.2 miRNAs Overview

Similar to protein coding genes, the vast majority of miRNA genes are transcribed by RNA Polymerase II (RNA PolII) (Cai, Hagedorn et al. 2004, Lee, Kim et al. 2004, Fiore, Siegel et al. 2008). It has been postulated that lineage specific and temporal transcription of miRNAs is regulated by the expression of specific transcription factors together with posttranslational chromatin modifications. miRNAs sequences are distributed all along the genome and they can be localized both in exonic and intronic regions, as well as intergenic locations (Fiore, Siegel et al. 2008). miRNAs that are located in the same cluster (0.1-50 kb from each other) have similar expression patterns (Baskerville and Bartel 2005, Fiore, Siegel et al. 2008), as is the case of *miR-17-92* and *miR-23-27a-24* clusters. They have a similar expression pattern because they are generated from one polycistronic transcript which is PolII-dependent (Lee, Kim et al. 2004, Fiore, Siegel et al. 2008). Otherwise, miRNAs which genes are separated by more than 50 kb are usually expressed in a non-coordinated manner (Baskerville and Bartel 2005).

3.3.3 Biogenesis (canonical VS non canonical).

The vast majority of miRNAs biogenesis starts with the transcription by RNA polymerase II (Lee, Kim et al. 2004), despite the fact that some of the miRNAs are transcribed by RNA polymerase III (Borchert, Lanier et al. 2006). This process produces a primary transcript known as primary miRNA (pri-miRNA). The structure of pri-miRNAs can be divided into four major parts: a terminal loop, the upper stem which contain the mature miRNA duplex (ds), the lower stem (ds), and the basal segments, which are ss flanking sequences. Both the lower and upper stems make up the 33bp long stem. The junction between the basal segment and the stem is named as the ssRNA-dsRNA junction (SD). The major part of pri-miRNAs show a five-prime cap (5'cap) and a polyadenylated 3' end (Figure7).

After transcription, inside the nucleus, the RNaseIII endonuclease Drosha cleaves the pri-miRNA. Which is then processed by Drosha 11bp away from the hairpin stem (in the SD junction) (Lee, Ahn et al. 2003). Drosha binds to the DiGeorge syndrome Critical Region 8 protein (DGCR8) and creates a complex known as microprocessor, which processes pri-miRNAs (Han, Lee et al. 2006). The cleavage of pri-miRNAs performed by microprocessor gives as a result a RNA molecule named pre-miRNA. It is important to point that pri-mRNAs can be processed in a Drosha-independent manner, which is one

of the non-canonical pathways of pre-miRNA production, and finally generates “miRtrons” (Westholm and Lai 2011).

After microprocessor processing, pre-miRNAs are actively exported into the cytoplasm in order to complete their maturation. The exportin 5 (EXP5) forms a transport complex with the GTP-binding nuclear protein RAN-GTP and one pre-miRNA. Once in the cytoplasm, the pre-miRNA processing complex digests the 70 bp pre-miRNA into a mature miRNA duplex of ~ 19-25 bp (Figure 7). This complex is formed mainly by three enzymes: the endoribonuclease Dicer (RNase III), the TAR RNA binding protein (TRBP) and the kinase R-activating protein (PACT). They bind together to increase the stability and the processing activity of the complex. In mammals, the presence of Dicer is essential, as Dicer-deficient mouse embryos die at early stages (see later). The mouse homolog of Dicer protein contains several conserved domains: two RNaseIII domains at the C-term followed by a double stranded RNA binding domain, the N term includes a DEX/ATPase, RNA Helicase, the DUF283 domain and a PAZ domain (Du, Lee et al. 2008, Doyle, Badertscher et al. 2013).

The RNase III domains of *Dicer* are located in tandem and form an intramolecular dimer that creates a catalytic centre. The N-terminal helicase domain of *Dicer* enhances the recognition of the pre-miRNAs by interacting with the terminal loop. The PAZ (PIWI-AGO-ZWILLE) domain binds to the termini of pre-miRNA (MacFarlane and Murphy 2010).

After generation of the mature miRNA duplex, the strands are unwound in an ATP-independent process. One of the resulting strands (miRNA-guide strand) associates with the RNA-induced silencing complex (RISC) giving as a result miRISC complex. After this process, miRISC can bind to mRNA transcripts and repress their translation or destabilize mRNAs by deadenylation or degrade them. The miRISC complex is formed by the association of Dicer, TRBP, PACT, the Argonaute 2 protein (Ago2) and GW182 (Yang and Lai 2010). TRBP recruits Dicer to Ago2; Ago2 has cleavage activity and degrades target mRNAs that are strongly complementary to the guiding miRNAs. However, if the miRISC/mRNA complex is partial complementary, Ago2 inhibits the translation of the target mRNA without cleaving it (Figure 7) (Rana 2007). It has been previously suggested that, in mammals, the guide strand is selected due to its thermodynamic stability, the less stable strand will be incorporated into the RISC with higher probability whereas the passenger strand (miRNA*-passenger strand) is generally

degraded (Yang and Lai 2010, O'Carroll and Schaefer 2013). However, miRNA sequencing data, indicate that some miRNA-passenger strand are not degraded and are expressed in similar concentrations to their corresponding guide strand (Huang, Nguyen et al. 2014). Taking this into account, one pre-miRNA can produce 2 different mature miRNAs, each one having different targets and, maybe, different biological functions (He and Hannon 2004, O'Carroll and Schaefer 2013).

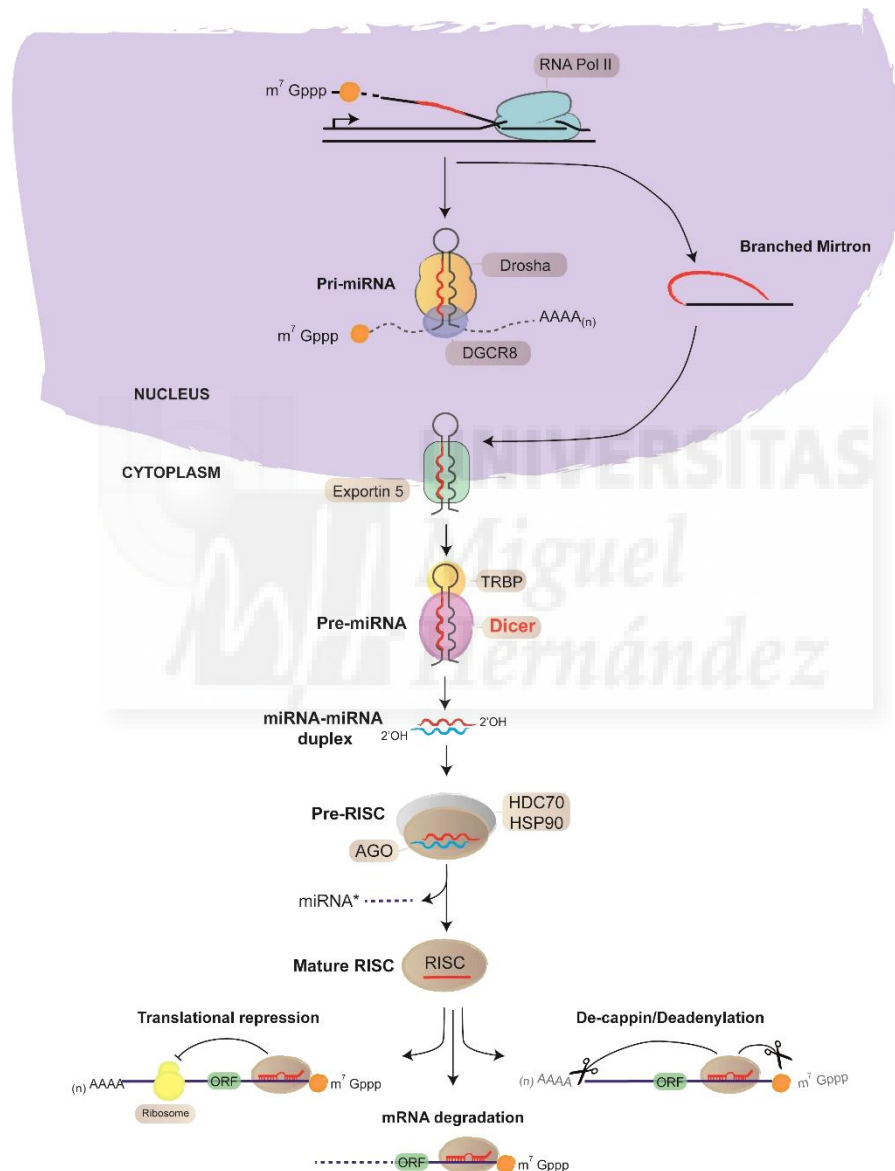


Figure 7 MicroRNA biogenesis. In the canonical miRNA biogenesis pathway, the pri-miRNA is transcribed by RNA polymerase II (Pol II), it begins with a 7-methylguanosine cap (m⁷Gppp) and ends with a 3' poly(A) tail. The pri-miRNA contains a stem-loop structure that is processed by Drosha (in orange) and DGCR8 (blue) in the nucleus, resulting the pre-miRNA that will be actively exported to the cytoplasm by the Exportin 5 (green) where Dicer (purple) together with TRBP (yellow) will cleave to liberate a miRNA-miRNA* duplex. This duplex will be loaded into an Argonaute (Ago) protein with the help of the HSC70-HSP90 chaperone machinery. Then, the

miRNA* will be extracted from the complex, producing a mature RNA-induced silencing complex (RISC). Alternative pathways (right) replace individual steps of miRNA precursor processing. Sometimes the pri-miRNA is generated from a branched mirtron structure that undergoes debranching and then enters in the pathway exiting the nucleus. After the formation of the mature RISC, this can bind to the target mRNA and promote the repression of the translation, its de-capping or deadenylation or the direct degradation of the mRNA). Modified from (van Rooij and Olson 2012) and (Ameres and Zamore 2013).

Non-canonical pathways

miRNAs that need both, microprocessor and the pre-miRNA processing complex to be mature are generated using the “canonical pathway”, but there are also non-canonical pathways that are Drosha/DGCR8 and *Dicer* independent ways for processing of pri- and pre-miR, called as “noncanonical pathways”. The first one is the miRtron pathway, it was identified for first time in *Drosophila melanogaster* (it is conserved in vertebrates but occurs less frequently) (Berezikov, Chung et al. 2007, Babiarz, Hsu et al. 2011), where the splicing and debranching of short hairpin introns of mRNA coding genes generate pre-miRNAs independent of the processing of Drosha/DGCR8 (Figure 8). These introns are directly exported and processed by Dicer (Okamura, Hagen et al. 2007). In addition to miRtrons, some small RNAs may be originated from other non-coding RNAs. For instance tRNAs, tRNA-like precursors, small nucleolar RNAs (snoRNAs) and small nuclear RNA-like viral RNAs have been shown to participate in the RISC complex independently of Drosha/DGCR8 but in a Dicer-dependent manner (Babiarz, Hsu et al. 2011). Moreover, there is a Drosha-dependent but Dicer-independent noncanonical pathway for the generation of miRNAs. This pathway relies on Ago2 and specifically on its endonuclease activity required for the cleavage of the pre-miRNA (Figure 8) (Havens, Reich et al. 2012). There is only one miRNA processed using the Dicer-independent pathway: miR-451, but the total contribution of the Ago2- dependent pathway needs to be deeply investigated (Cheloufi, Dos Santos et al. 2010). Unlike prototypical pre-miRNAs that have a two-nucleotide- long 3' overhang (group I pre-miRNAs), some pre-miRNAs (group II pre-miRNAs, including the major part of the let- 7 family in vertebrates) present a 1- nucleotide long 3' overhang, this group of pre-miRNAs are extended by 1 nucleotide through monouridylation mediated by terminal uridylyl transferases (including TUT2, TUT4 and TUT7) and to be able to be processed by Dicer in an efficient manner is required the monouridylation (Figure 8) (MacFarlane and Murphy 2010).

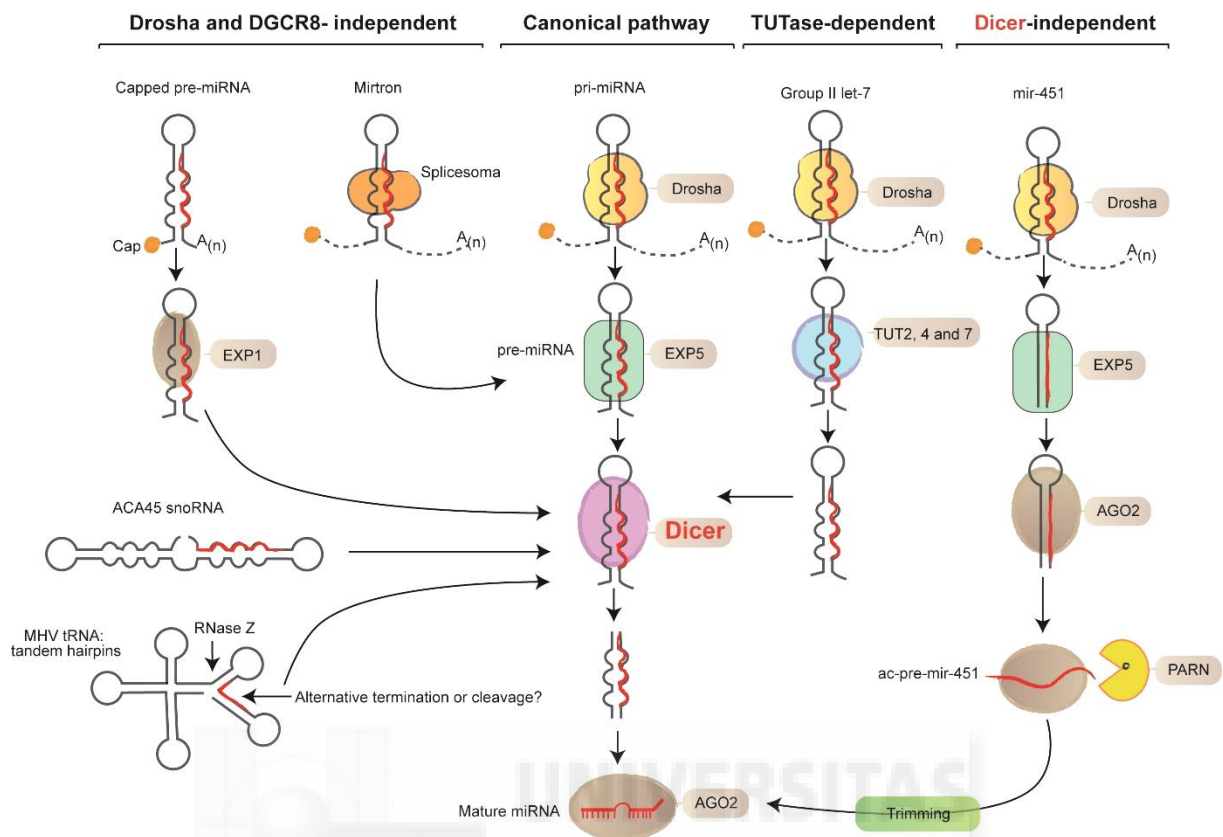


Figure 8. Non-canonical pathways of miRNA biogenesis. The 7-methylguanosine (m^7G)-capped pre-miRNA is generated through transcription, without the processing of Droscha, to be then exported to the cytoplasm by Exportin 1 (EXP1). Mirtrons produce pre-miRNAs directly through splicing and posterior debranching. Some mirtrons contain 5' or 3' single-stranded RNA tails that require being trimmed before *Dicer* processing. Some small nucleolar RNAs (snoRNAs), and tRNAs (or even tRNA-like RNAs) also can be cleaved and produce pre-miRNAs. The group II of pri-miRNAs that are dependent of Terminal uridylyl transferase (TUTase) give rise to pre-miRNAs with a shorter 3' overhang that is suboptimal for *Dicer* processing, so they require being monouridylated in order to be processed by *Dicer*. Finally, in the *Dicer*-independent pathway, the pre-mir-451 is produced by Droscha, exported to the cytoplasm by EXP5 and then loaded on Argonaute 2 (Ago2) without *Dicer* processing. Ago2 cleaves the stem of pre-mir-451, generating Ago-cleaved pre-mir-451 (ac-pre-mir-451), which is then trimmed by the 3'-5' exonuclease poly (A)-specific ribonuclease (PARN). Modified from (Ha and Kim 2014).

3.3.4 Target recognition

The small size of miRNAs makes it difficult to have a high specificity inside the transcriptome, because the shorter the sequence the higher is the probability of being repeated. Taking into account this and the fact that sometimes a partial complementarity between the miRNA and its target site is sufficient, there is a considerable number of genes that may be regulated by a single mRNA. This property increases the complexity of predicting miRNA targets.

In plants, the major part of target sites are present in both coding exons and in 3' untranslated regions (UTRs). Thus, target sites which are located in the middle region of the mRNA are susceptible to be paired with miRNAs but experimental data with miRNA target sites located inside coding regions suggest a less effective regulation as compared with the ones located in the 3'UTR (Easow, Teleman et al. 2007, Gu, Jin et al. 2009). In animals, most of the target mRNAs analysed are regulated in their 3'UTR and the major part of miRNAs only form partial duplexes with their targets (Ha and Kim 2014). The most common motif is perfect pairing between nucleotides 2 and 7 at the 5' end of the miRNA (named "seed region"), and the target site of the mRNA. The pairing between the seed region and the target site is necessary and sufficient for regulate the mRNA by the miRNA pathway. Sometimes, the imperfect pairing of the seed to a target site is compensated by a high number of 3' end interactions which enhance the level and effectiveness of mRNA silencing (Ha and Kim 2014). Due to the short size of seed sequence the miRNA machinery has low specificity; solving this problem, other factors may influence the target selection in vivo, as the presence of AU-riches areas and unstructured ones which enhances the accessibility to the miRNA complex (Ha and Kim 2014).

In animals, the complementarity between miRNA and mRNA target region is mainly partial, with mismatches in the miRNA/mRNA duplex (the major part of the mismatches are located in the central region) and these mismatches avoid Ago2-dependent cleavage (Hutvagner and Zamore 2002). Despite the total complementarity between miRNA and mRNA barely occurs, it is important to point that there are some bases that must be totally complementary, these are the first bases of the miRNA sequence (2–7) or seed sequence, which are responsible for the definition of target specificity (Doench and Sharp 2004).

3.3.5 Silencing

Once the seed sequence is bound to the target site, the silencing of the mRNA begins. The greater is the complementarity between seed sequence and mRNA, the greater will be the degree of mRNA silencing. If there is a 100% complementarity between seed sequence and its target, the mRNA will be degraded, being the first step an Ago2-mediated cleavage (Figure 9) (Hutvagner and Zamore 2002). But as total complementarity rarely occurs in animals, miRNA-mediated mRNA degradation rarely occurs (Yekta, Shih et al. 2004, Hornstein, Mansfield et al. 2005). When the mRNA is

bound to the miRNA/RISC complex, different scenarios can occur. These scenarios predominantly include mRNA destabilization (and posterior degradation) and translational repression (Fabian, Sonenberg et al. 2010). It is also important to point that sometimes, the association of the miRNA with the 3' or 5' UTR causes target mRNA translational activation (Vasudevan, Tong et al. 2007, Henke, Goergen et al. 2008). This was shown by Vasudevan and colleagues, they showed that miRNAs repress translation in proliferating cells but upregulate translation in quiescent cells arrested in G0/G1 phases. This activation is produced when the complex formed by Ago2 and miR369-3 binds to the 3' UTR of TNF α mRNA and this union promotes the recruitment of the fragile X-related protein 1 (FXR1) leading to the enhance of mRNA translation (Figure 9). Despite this activation can occur in some concrete conditions; usually, the union between a mRNA and miRISC results in a small repression of mRNA expression being the maximal repression between 1.5 and 2-folds (Selbach, Schwanhausser et al. 2008, Guo, Ingolia et al. 2010).

The degradation of mRNAs takes place in discrete cytoplasmic complexes named processing-bodies (p-bodies) and in stress granules which are dynamic complexes whose assembly is dependent on the quantity of non-translating mRNAs (Franks and Lykke-Andersen 2008). These specialized granules contain a fraction of Ago proteins and are sites of RNA storage and catabolism. They are conformed by mRNAs and proteins that are involved in mRNA degradation as decapping (DCP1/2) and deadenylating enzymes (Franks and Lykke-Andersen 2008). In p-bodies (also known as GW bodies) we can also find some members of the GW182 protein family (Eystathioy, Chan et al. 2002), this proteins are involved in the repression of mRNAs due to miRNAs because the interaction of Ago2 with GW182 plays an important role in the miRNA silencing of mRNA and if this interaction is abolished, Ago2 is not able to cleavage mRNAs (Figure 9) (Rehwinkel, Letunic et al. 2005, Behm-Ansmant, Rehwinkel et al. 2006, Jakymiw, Pauley et al. 2007, Eulalio, Huntzinger et al. 2009).

As has being previously pointed, the mRNA degradation due to miRNA binding is not the major way of miRNA silencing. When there is no perfect match between seed sequence and target site, one of the mechanisms of silencing is translational repression. In this mechanism it is also implicated GW182, it directly interacts with the poly-A binding protein (PABP) and, by preventing the formation of the closed loop between PABP and eIF4G interrupt the initiation of the translation (Figure 9) (Fabian, Sonenberg

et al. 2010). However, the observation that mRNAs without poly-A tails (to which PABP does not specifically bind) are still under the effect of miRNA-mediated translational repression indicates that although PABP is one of the targets for miRNAs, its function can explain only a part of the overall miRNA-mediated translational repression. (Figure 9) (Humphreys, Westman et al. 2005). Moreover, miRNAs have been demonstrated to interfere with ribosome elongation, inducing ribosome drop-off or facilitation proteolysis of the nascent polypeptides, this last option comes from studies from Nottrott et al. (Nottrott, Simard et al. 2006) in which they proposed that the miRNA machinery recruits proteolytic enzymes to polysomes, which leads to the degradation of nascent polypeptides (Figure 9) (Fabian, Sonenberg et al. 2010, Pasquinelli 2012).

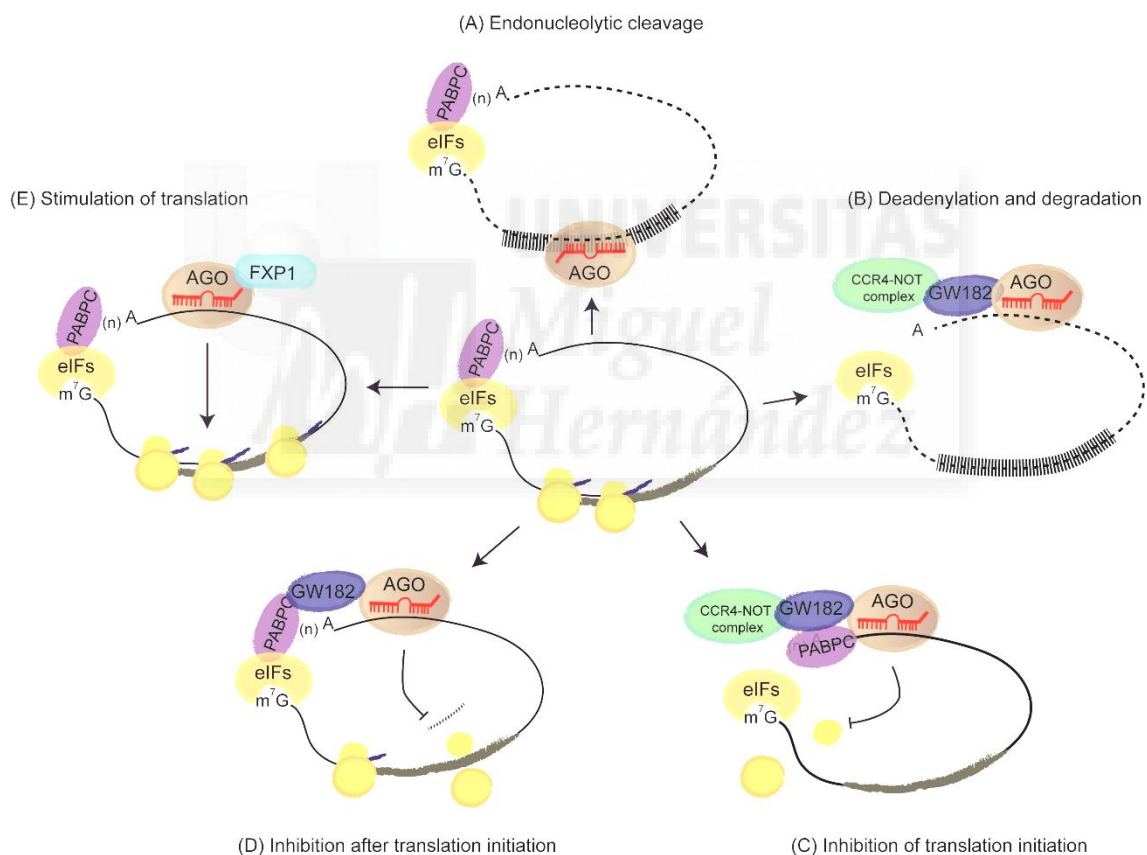


Figure 9. Mechanisms of target regulation by miRNAs. Scheme showing different pathways through which miRNAs regulate gene expression. A complex of eukaryotic initiation factors (eIFs) binds the 5' cap (m^7G) and the poly (A)-binding protein (PABPC) which is bound to the poly A tail of the mRNA. Thus, the 5' and 3' ends of mRNA are connected, stimulating the translation by the ribosome (shown in yellow). From this central scenario, miRNAs can act through different mechanisms: **(A)** Binding between a miRNA and its target site promotes the mRNA cleavage by Ago, which leads to the degradation of the mRNA. **(B)** If the pairing between miRNA and the mRNA is partial, the result will be the deadenylation of the mRNA. mRISC recruits GW182 and the CCR4-NOT complex causing the loss of the poly(A) tail, which produces the dissociation of PABPC, degrading the mRNA. **(C, D)** mRISC can also induce

translational repression by inhibiting a step after initiation, promoting the ribosome drop-off or also stimulating proteolysis of the incipient peptide. (E) It has been described that miRNAs can also upregulate the target expression through a mechanism involving Ago2 and FXR1. Modified from (Pasquinelli 2012).

3.3.6 Regulation of miRNA pathway

The pathway through which miRNAs act as transcriptional regulators is itself under transcriptional, posttranscriptional, and posttranslational regulation. These regulations affect the protein and RNA components of the pathway. As there are miRNA genes located inside introns of protein-coding genes, these miRNAs share the promoter of the host gene but, additionally, they have different transcription start sites (Lee, Jeon et al. 2002) and, also, the promoters of intronic miRNAs can be different from the ones of their host genes. Then, as miRNA transcription is performed by RNA PolII, it is regulated by RNA PolII-associated transcription factors together with epigenetic mechanisms as, for instance, DNA methylation or histone modifications (Lee, Jeon et al. 2002).

The regulation of miRNA transcription allows regulating at a posttranscriptional level certain miRNA inside a transcription unit. This is what occurs with the cluster formed by *miR-100/let-7/miR-125*. This cluster plays an important role during development of bilateral animals and, interestingly, only *let-7*, but not the other miRNAs belonging to the same cluster, is suppressed post-transcriptionally in embryonic stem cells and, also in certain cancer types in mammals (Lee, Jeon et al. 2002).

Apart from the production, the regulation of miRNA turnover is an equally important and highly regulated event. It is well known that miRNAs are around ten times more stable than mRNAs (Ha and Kim 2014) and for example, *miR-208* persists for 3 weeks after transcription of its host gene is blocked (Zhang, Qin et al. 2012). Due to their half-life and their wide action field, turnover of mature miRNAs is a very important mechanism of miRNA regulation.

The half-life can be very different among miRNAs, and two of the features that determine the half-life of an RNA molecule are 5' cap structures and 3' polyA tails. These are added to the major part of protein-coding Pol II transcripts in order to protect them from degradation, avoiding the exonucleolytic decay pathways. pri-miRNAs are both capped and polyadenylated, but mature miRNAs lack any 3' poly A or 5' cap structures. In plants, 3' methylation protects the major part of miRNAs from degradation, this

methylation is also found to be important for some *Drosophila* miRNAs (Ha and Kim 2014).

Several nucleases have been proposed to cleave and degrade miRNAs. In *C.elegans*, the 5'–3' exoribonucleases XRN-1 and XRN-2 were shown to degrade mature miRNAs (Ha and Kim 2014). In humans, the human polynucleotide phosphorylase PNPase old-35 (also known as PNPT1), which is a 3'–5' exonuclease, degrades some mature miRNAs in melanoma cells (Lee, Jeon et al. 2002). In order to avoid miRNA destruction, there are some ways to increase their stability. For example, Ago proteins protect and stabilize miRNAs from degradation both in plants and in animals (Ha and Kim 2014) protecting both ends of miRNAs from degradation by making them inaccessible to nucleases.

There are also some specific ways of miRNA regulation that had been described, for example regarding *let-7* and *Lin-28/Tut4*. It has been shown that Lin-28 together with Tut4 promote the downregulation of *let-7* miRNA in different organisms (Hagan, Piskounova et al. 2009, Heo, Joo et al. 2009, Yang and Lai 2010). Lin-28 recognizes a conserved motif inside the hairpin of some *let-7* pre-miRNAs (Heo, Joo et al. 2009) and recruits Tut4, that will target the *let-7* pre-miR for degradation, giving as a result the reduction of the mature *let-7* (Hagan, Piskounova et al. 2009, Heo, Joo et al. 2009, Yang and Lai 2010).

Another way of regulating miRNAs is modifying their activity, instead of promoting or preventing their degradation. This mechanism is thought to play an important role in neurons. The molecules driving this type of regulation are endogenous sponges, which are RNA sequences containing binding sites for one specific miRNA that can act as high-affinity decoy targets. Endogenous sponges are present in different organisms: In plants there is the TPSI family of noncoding RNAs (Franco-Zorrilla, Valli et al. 2007), in viruses there are the Herpesvirus saimiri U-rich RNAs (HSURs) (Cazalla, Yario et al. 2010), and in mammals there is the PTENP1 pseudogene (Poliseno, Salmena et al. 2010). There is also a particular class of long noncoding RNAs that may act as miRNA sponges, the competing endogenous RNAs (ceRNAs), which play an important role in muscle differentiation and in tumour suppression (Cesana, Cacchiarelli et al. 2011, Karreth, Tay et al. 2011). It has been proposed (Ebert and Sharp 2010) that miRNA-target genes might also act as endogenous sponges, especially the ones that have multiple and consecutive miRNA-binding sites. For example, the 3' UTR of the onecut homeobox 2

transcription factor (Onecut2) has 13 individual *miR-9*- binding sites within its sequence so when the mRNA of Onecut2 is in the cell, the pool of *miR-9* will massively binds to it, which will decrease the amount of free *miR-9* (Lewis, Burge et al. 2005).

3.3.7 miRNAs as genetic tools for gene silencing

While biological functions of miRNAs machinery are still being investigated, it seems clear that the miRNA pathway is an important mechanism of gene expression regulation to maintain the correct cellular homeostasis of tissues, and which disruption can lead to several alterations including cancers, neurodegenerative disorders and cardiovascular diseases (van Rooij, Sutherland et al. 2007).

Likewise, it seems clear that miRNAs are promising molecules for therapeutic application. Around 2,000 human miRNAs have been recorded in the miRBase and since more than 60% of the human protein-coding genes contain at least one conserved miRNA-binding site, plus numerous non-conserved sites, the vast majority of protein-coding genes are virtually under the control of miRNAs (Kim, Kim et al. 2016).

As there are many diseases that come from the expression of mutated genes, or from the overexpression of particular normal genes, the finding of miRNA machinery opens a new tool for treating diseases by targeting the genes responsible of them, and also for generating models (animals or *in vitro*) that mimic the pathological scenario to then investigate processes altered in the disease. The overexpression of natural miRNAs can be achieved for investigation's models by, for example the expression of the genomic region encoding the primary miRNA transcript, or directly introducing the custom designed miRNAs (which are commercially available) (Figure 10). If instead of the downregulation of a certain gene what is needed is its upregulation, this can be achieved by decreasing the quantity of free miRNAs using as a tool miRNAs inhibitors (previously named as anti-miRs, antagomiRs, AMOs -Anti-miRNA antisense inhibitors-, sponges, or decoys) (Stenvang, Petri et al. 2012, Li and Rana 2014). These are antisense molecules with high complementarity with a particular miRNA, which act by binding and sequestering the miRNA, inhibiting it from binding to its natural targets (Figure 10).

There are basically two different ways of miRNA inhibitors delivery; direct cellular delivery of chemically synthesized inhibitors; or delivery of a genomic vector containing the genetic information for producing the inhibitor, such that once in the cytoplasm, the inhibitor will be transcribed (Figure 10) (Bak, Hollensen et al. 2013, Chen,

Gao et al. 2015). Using the first option, RNA molecules will contain target sequences for the miRNA that is wanted to be downregulated, this is the most employed way of miRNA inhibition. Inhibitors can also attract the silencing complex including the miRNA in a way that will reduce the formation of miRNA-mRNA complexes. Nevertheless, chemically synthesized sequences need the use of a high-efficient delivery method and also a repeated administration in order to achieve long-lasting miRNA inhibition. This is not the case for miRNA inhibitors expressed directly from DNA, as they present the advantage of being compatible with viral vectors for highly efficient delivery. One of the most used miRNA inhibitors expressed from DNA are Tough Decoys (TuDs) inhibitors. TuD miRNA inhibitors, have a hairpin-like structure sustaining an internal loop which contains two miRNA-binding sites (MBS) with complementary sequences to the miRNA of interest. Stem structures flank laterally MBS with linkers (Figure 11). TuD act when MBS bind to the miRNA, creating a bulge that prevents the action of the miRNA upon the target mRNA (Haraguchi, Ozaki et al. 2009, Yoo, Hajjar et al. 2017) (Figure 11).



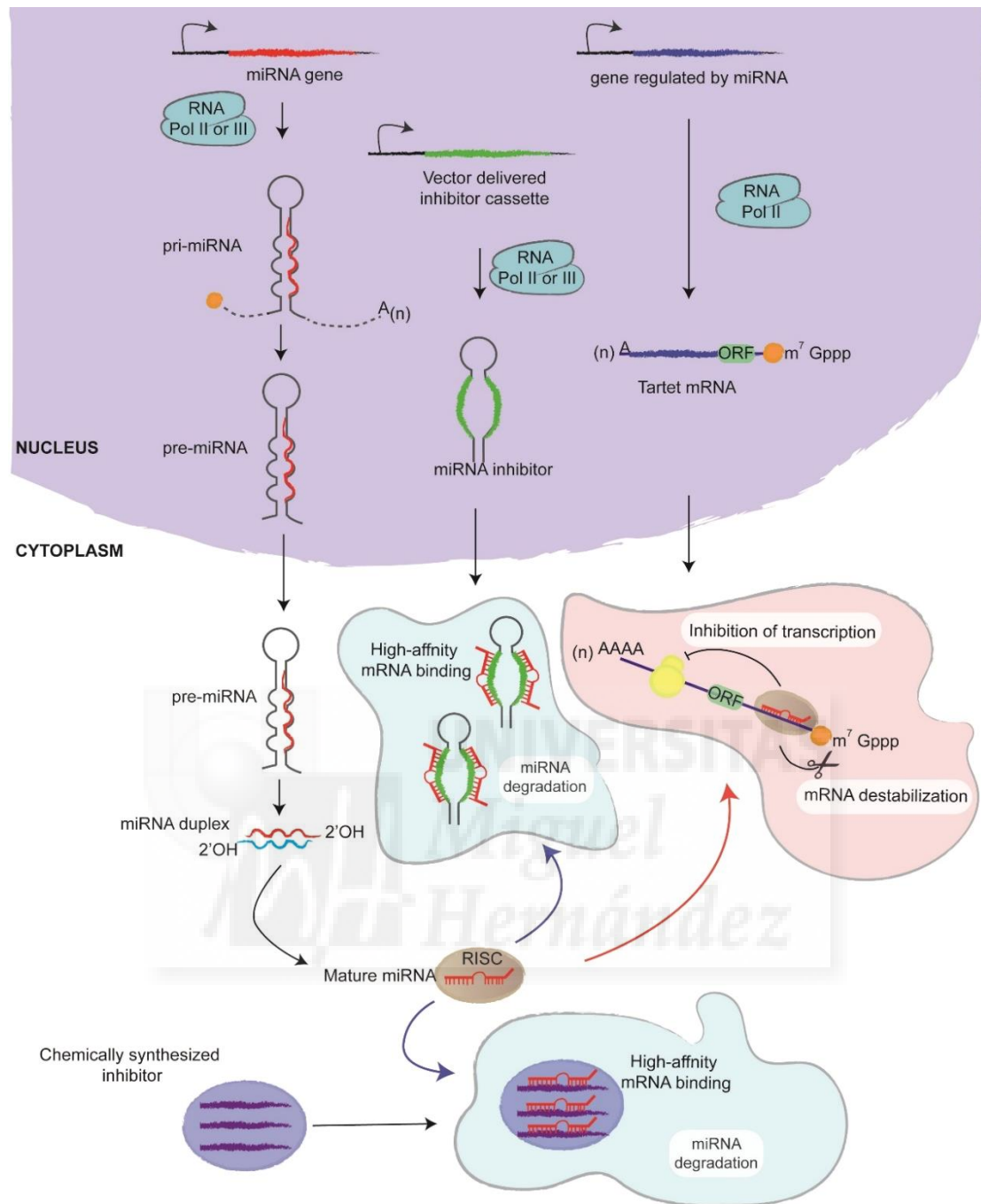


Figure 10. Schematic view of the anti-miRNA function of vector-encoded and Chemically synthesized miRNA inhibitors. Overview of miRNA biogenesis, miRNA regulation of mRNAs expression, and miRNA inhibition by both vector-encoded and chemically synthesized inhibitors. Long primary miRNA transcripts (red) are transcribed from the genome, processed and sequentially transported to the cytoplasm, where they will be matured so they will be able to repress their target genes through the RNA-induced silencing complex (RISC). A Tough Decoy-type miRNA inhibitor carrying miRNA binding sites (green) is intracellularly transcribed and interferes with natural miRNA regulation by attracting and binding miRNAs, promoting the degradation of the miRNA, as well as when miRNAs bind the Chemically synthesized miRNA inhibitors, located in the cytoplasm. Modified from (Bak, Hollensen et al. 2013).

a great amount of evidence demonstrating the importance of miRNAs in cancer (Zhang, Pan et al. 2007). Changes in miRNA expression and function may contribute to the processes of initiation and maintenance of tumours. miRNAs which are involved in those processes have been named as “oncomirs,” and they may act as either tumour suppressors or oncogenes (Lim, Lau et al. 2005).

In cancer, miRNA transcription is regulated by a high number of transcription factors, some of them characterized as tumour suppressors or oncogenes. Some analyses conclude that differences in the amount of transcription factors could promote or inhibit the transcription of specific miRNAs, some of these transcription factors are directly involved in cancer like Myc and p53 (Fiore, Siegel et al. 2008). The *miR-17-92* cluster is one of the first oncogenic miRNA clusters found which expression is promoted by the transcription factor Myc upon binding to the E-box in the *miR-17-92* coding sequence (Ji, Rao et al. 2011). The *miR-17-92* cluster is frequently over-expressed in different tumours like B-cell lymphomas, breast, colon, lung, pancreas, prostate, and stomach cancers (Mogilyansky and Rigoutsos 2013). Myc can regulate the expression of miRNAs in two different points, first affecting the transcription, and then blocking the maturation of certain miRNAs (Fiore, Siegel et al. 2008). In order to block miRNA maturation is frequently necessary the cooperation with other binding proteins like, for instance Lin28, which acts as a negative regulator of *let-7* (Fiore, Siegel et al. 2008, Viswanathan, Daley et al. 2008, Barh, Malhotra et al. 2010).

The mechanisms of miRNA deregulation in human cancer are not completely understood, but recent findings indicate that multiple processes could be involved (Reddy 2015). It has been well documented that most pri-miRNAs are transcribed from promoters that are regulated by transcription factors (Megraw, Baev et al. 2006, Schanen and Li 2011, Wang, Li et al. 2011, Catalanotto, Cogoni et al. 2016), and several examples of miRNA deregulation in cancer due to transcriptional deregulation have been reported (Palmero, de Campos et al. 2011, Rupaimoole, Calin et al. 2016), like the one related with Myc, lin28 and *let-7*. Some studies also suggest that epigenetic alterations play an important role in the dysregulation of miRNAs taking place in human cancers (Suzuki, Maruyama et al. 2013, Saito, Saito et al. 2014) and also that genomic mutations may contribute to the downregulation of mature miRNAs. In addition, different groups have demonstrated that abnormalities in the DNA copy number are also involved in miRNA deregulation (He, Thomson et al. 2005, Zhang, Huang et al. 2006). Finally, in cancer, an

alteration in the functionality of proteins required for miRNA synthesis could occur, promoting tumorigenesis (Kumar, Lu et al. 2007). Thus, the deregulation of miRNAs in human cancer may be promoted by different mechanisms acting separately or in concert, including: transcriptional deregulation, epigenetic alterations, mutations, DNA copy number abnormalities, and defects in the miRNA biogenesis machinery (Esquela-Kerscher and Slack 2006, Deng, Calin et al. 2008).

3.4.2 *Let-7* family in human cancer

Let-7 was the second miRNA discovered, just after *lin-4* in *Caenorhabditis elegans*. It was first identified as a heterochronic gene (Reinhart, Slack et al. 2000). Heterochronic genes act in a sequential and stage-specific manner, regulating cell fate during the different larval transitions in *C. elegans* (Moss 2007, Lee, Han et al. 2016). *let-7* regulates the transition from the fourth larval stage (L4) to adult (Reinhart, Slack et al. 2000). During the development of *C. elegans*, hypodermal seam cells display asymmetric cell divisions, similar to cortical progenitor cells (for instance aRGCs). This results in one daughter cell that will differentiate, plus one that will continue being a progenitor at each larval stage. In the last step of development (from L4 to adult), all progenitor cells undergo terminal differentiation, giving rise to the adult alae (longitudinal ridges that are present during specific stages of development). Interestingly, cells with a mutation in *let-7* don't perform the final differentiation, but undergo extra cell divisions, without giving rise to the adult alae (Reinhart, Slack et al. 2000). This overgrowth causes that the majority of *let-7* mutants die prematurely, giving the name to *let-7*: lethal-7. These studies together support the idea that *let-7* acts as a key regulator of correct developmental timing (Reinhart, Slack et al. 2000, Boyerinas, Park et al. 2010).

It has been shown that the *let-7* family of miRNAs is highly conserved across different animal species from *C. elegans* to humans (Pasquinelli 2012). Due to its important role controlling the switch between cellular programs during development from proliferation to differentiation, it is not surprising that changes in the normal expression of this miRNA could lead to many types of cancer (Boyerinas, Park et al. 2010). Thirteen members of the *let-7* family have been identified to date (*let-7a-1*, *let-7a-2*, *let-7a-3*, *let-7b*, *let-7c*, *let-7d*, *let-7e*, *let-7f-1*, *let-7f-2*, *let-7g*, *let-7i*, *miR-98*, and *miR-202*) (Table 1). They have similar sequences and target a wide spectrum of different genes (Roush and Slack 2008).

Table 1. Sequence of *let-7* family members. The seed sequence is indicated in yellow. Consensus mature sequences are placed at the top of the box, where only perfectly aligned sequences are capitalized. Consensus sequences of the mature human *let-7* family members, as assessed by MEME (<http://meme-suite.org>, bottom panel).

Consensus	u	G	A	G	G	U	A	G	u	A	g	g	U	U	G	u	a	u	a	G	U	U
	1	2	3	4	5	6	7	8	9	10	11	12	13	14	15	16	17	18	19	20	21	22
has-let-7a-1	U	G	A	G	G	U	A	G	U	A	G	G	U	U	G	U	A	U	A	G	U	U
has-let-7a-2	U	G	A	G	G	U	A	G	U	A	G	G	U	U	G	U	A	U	A	G	U	U
has-let-7a-3	U	G	A	G	G	U	A	G	U	A	G	G	U	U	G	U	A	U	A	G	U	U
has-let-7b	U	G	A	G	G	U	A	G	U	A	G	G	U	U	G	U	G	U	G	G	U	U
has-let-7c	U	G	A	G	G	U	A	G	U	A	G	G	U	U	G	U	A	U	G	G	U	U
has-let-7d	A	G	A	G	G	U	A	G	U	A	G	G	U	U	G	C	A	U	A	G	U	U
has-let-7e	U	G	A	G	G	U	A	G	G	A	G	G	U	U	G	U	A	U	A	G	U	U
has-let-7f-1	U	G	A	G	G	U	A	G	U	A	G	A	U	U	G	U	A	U	A	G	U	U
has-let-7f-2	U	G	A	G	G	U	A	G	U	A	G	A	U	U	G	U	A	U	A	G	U	U
has-let-7g	U	G	A	G	G	U	A	G	U	A	G	A	U	U	G	U	A	C	A	G	U	U
has-let-7i	U	G	A	G	G	U	A	G	U	A	G	A	U	U	G	U	G	C	U	G	U	U
has-miR-98	U	G	A	G	G	U	A	G	U	A	A	G	U	U	G	U	A	U	U	G	U	U

Let-7 is widely considered as a tumour suppressor miRNA, due to its targeting of multiple oncogenes (for instance RAS, c-Myc and HMGA2). One of the most important mechanisms through which *let-7* acts as a tumour suppressor is downregulating the translation of these three RAS proteins, which were the first oncogenes discovered in human tumours (Johnson, Grosshans et al. 2005). The expression of *let-7* family members is downregulated in many cancer types when compared to normal tissue, it is also known that this downregulation contributes also to tumour progression (Boyerinas, Park et al. 2010). In some types of cancer, most of *let-7* family members appear to be downregulated (Takamizawa et al. 2004, Dahiya et al. 2008, O'Hara et al. 2009); however, sometimes there are specific members of the family downregulated in particular cancer types. For example, low expression of *let-7d* was found in head and neck squamous cell carcinoma patients, and a downregulation of *let-7* was indicative of poor survival in ovarian cancer (Shell, Park et al. 2007, Shields, Emmett et al. 2007).

The expression of this tumour suppressor miRNA is regulated by Lin28/Lin28B, RNA binding proteins that suppress the function of *let-7* (Viswanathan, Powers et al. 2009). Interestingly, Lin28 has been identified as one of the *let-7* targets (Boyerinas, Park et al. 2008, Rybak, Fuchs et al. 2008), so *let-7* and Lin28 are part of a double negative feedback loop regulating expression of both participants, a loop which is conserved from *C. elegans* to humans (Rybak, Fuchs et al. 2008). Moreover, the expression of Lin28/Lin28B is upregulated in various types of cancer in which has been shown a downregulation of *let-7* (Viswanathan, Powers et al. 2009).

Studies by Zhu and colleagues (Zhu, Shyh-Chang et al. 2011) show that the *let-7*/Lin28 axis controls glucose uptake regulating insulin-PI3K-mTOR signalling. An increase in Lin28 expression leads to a decrease in *let-7* expression, in turn increasing the expression of multiple direct *let-7* targets which include Irs-2, PIK3, Akt2 and RICTOR. It is well known that mTOR signalling is activated in conditions of dysregulated proliferation including many cancer types, so it has been reported the alteration in the expression of different elements of the mTOR pathway (PI3K, PTEN, Akt...) in many cancer types, including breast, ovarian, renal, colon and head and neck cancers (Pópulo, Lopes et al. 2012).

3.5 Mouse models for the study of miRNAs

In order to understand the function of particular miRNAs, these have been deleted individually in *C. elegans* (Lai 2015) and *D. melanogaster* (Sandmann and Cohen 2007). Similarly, there is a library of mouse miRNA knockouts (Park, Choi et al. 2010). Just few of the initial mutants in *C. elegans* (*let-7*) and *D. melanogaster* (*bantam* miRNA) were lethal, and the number of miRNA-mutants lethality is even lower in mouse models, presenting only some of them developmental issues (Park, Choi et al. 2010).

As many miRNAs share their target genes, the deletion of one of the members from a family may not significantly modify the expression of its target genes sufficiently in order to overstep the threshold required to produce phenotypic changes. Thus, it may be necessary to generate more complicated knockouts to totally ablate an entire miRNA family *in vivo*. Then, in order to understand the function of tissue specific miRNAs in a certain time point, Cre-dependent knockouts of members from the miRNAs biogenesis machinery have been used.

3.4.2.1 Deletion of functional *Dicer*

Given that the vast majority of miRNAs are *Dicer* dependent, one of the most frequently used tools to study their function is the generation of *Dicer*-deficient organisms. This was first done in mammals in 2003, when Bernstein et al (Bernstein, Kim et al. 2003) showed that *Dicer*-deficient mice are not viable and that the development of *Dicer* mutants was arrested before the body plan was configured during gastrulation. Interestingly, Bernstein and colleagues postulated that, given that *Dicer* is maternally contributed in mice this may affect the timing of the lethality observed in *Dicer* mutant mouse embryos. This study demonstrates that *Dicer* and, by extension, the mRNA machinery, are required for embryonic vertebrate development. Another example of this *Dicer*-deficient strategy was performed with zebrafish (Giraldez, Cinalli et al. 2005, Schier and Giraldez 2006). In this model, the lack of mature miRNAs caused severe malformations in the central nervous system and other organs and these phenotypes were rescued injecting selected miRNAs (Giraldez, Cinalli et al. 2005).

3.4.2.1.1 Brain-specific *Dicer*-deficient models

Over the last few years, our understanding of miRNA contribution to nervous system development has improved dramatically due to the effort of several groups which add up to a developmental series of *Dicer* depletions in neural tissue (De Pietri Tonelli, Pulvers et al. 2008, Kawase-Koga, Otaegi et al. 2009, Li, Bian et al. 2011, Nowakowski, Mysiak et al. 2011). Together, the data support the hypothesis that miRNAs regulate cell differentiation and cell cycling in the developing nervous system. In these *Dicer* deficient lines, the recombination driven by Cre was under the control of a specific promoter: *Emx1* (expressed from E9.5 and restricted primarily to cortical subdivisions of the telencephalon (Gorski, Talley et al. 2002)); Nestin (expressed from E10.5 but with a low rate of recombination (Kawase-Koga, Otaegi, & Sun, 2009)); *CamKII* (recombination starts at E15.5 and takes place all over the forebrain (Davis et al, 2008)), *Foxg1* -forkhead box protein G1 (recombination at E8.0 in the telencephalon (Radhakrishnan and Alwin Prem Anand 2016)) and *hGFAP* (expressed in the developing dorsal forebrain from E 13.5 (Zhang, Ge et al. 2015)) (Figure 12 A, 12B).

Emx1-Cre Dicer conditional KO

This mutant mouse line shows a strong reduction in the olfactory bulb and in the cortex, where embryos also present a reduction on the cortical thickness. This was thought to be

due to thinner neuronal layers but not progenitor layers. De Pietri et al. found that, between E12.5 and E14.5, there is a massive increase in apoptosis in the cortex of these mutants, and this cell death is concomitant with a reduction in phospho-histone 3 mitotic cells (PH3+). *Dicer* elimination further resulted in a defective cortical layering, with a dramatic loss of upper-layer neurons. The loss of miRNAs in these mutants also affected some aspects of neuronal differentiation, such as the expression of *Foxp2*, important in neuronal differentiation, suggesting deficient or altered neuronal subtype specification. (De Pietri Tonelli, Pulvers et al. 2008).

Nestin-Cre Dicer conditional KO

Kawase-Koga et al. showed that these animals die only after birth, but at embryonic stages they already present a reduction in the thickness of the dorsal and lateral cortex, while the telencephalic ventricles are enlarged. VZ, SVZ and CP are reduced, whereas the IZ is expanded by E18.5. These *Dicer* mutants don't fail producing early-born neurons (*Tbr1*+), but late-born neurons (*Map2*+) are dramatically decreased. The basal ganglia present an increase in apoptotic cells, giving as a result a decrease in cortical interneurons. The vast majority of the phenotypes described in this mutant line became obvious only between E 15.5 and E18.5, while *Nestin* is expressed already at E10.5. This difference was explained by the authors arguing that *Nestin-Cre* mice present a weak *Cre* activity, which is translated in a delayed ablation of *Dicer* proteins in the cortex (Kawase-Koga, Otaegi et al. 2009).

CaMkII-Cre Dicer conditional KO

Using this mouse line, Tigwua et al. discovered that loss of miRNAs by E15.5 in the cortex, hippocampus and striatum is lethal during early postnatal development. These mutant mice had microcephaly (50% of reduction in brain mass) together with enlargement of the ventricles (hydrocephaly), and a reduction axonal tracts (Davis, Cuellar et al. 2008).

Foxg1-Cre Dicer conditional KO

In this mutant, markers of RGCs in the VZ (such as *Nestin*) are reduced in the dorsal telencephalon at early embryonic stages (around E12.5). Neurons and basal progenitors are dislocated and there is an increase in apoptosis from E11.5 onwards. The authors concluded that *Dicer* deficient neuroepithelium does not establish the appropriate

molecular signature of RGCs at E11.5, which may alter the behaviour of progenitors, leading to an increase in *Tbr2*⁺ cells and a disorganization of the laminar architecture of both basal progenitors and neurons (Nowakowski, Mysiak et al. 2011).

hGFAP-Cre Dicer conditional KO

Studies by Zhang et al. revealed that in the absence of miRNA in RGCs there is a prolongation of the RGC identity due to an increase in Notch signalling. They also showed that, postnatally, the cell soma translocation of RGCs and the retraction of their radial processes are delayed in the cerebral cortex of *Dicer* mutants. The retraction of the radial process is reduced in the postnatal cerebral cortex. (Zhang, Ge et al. 2015)

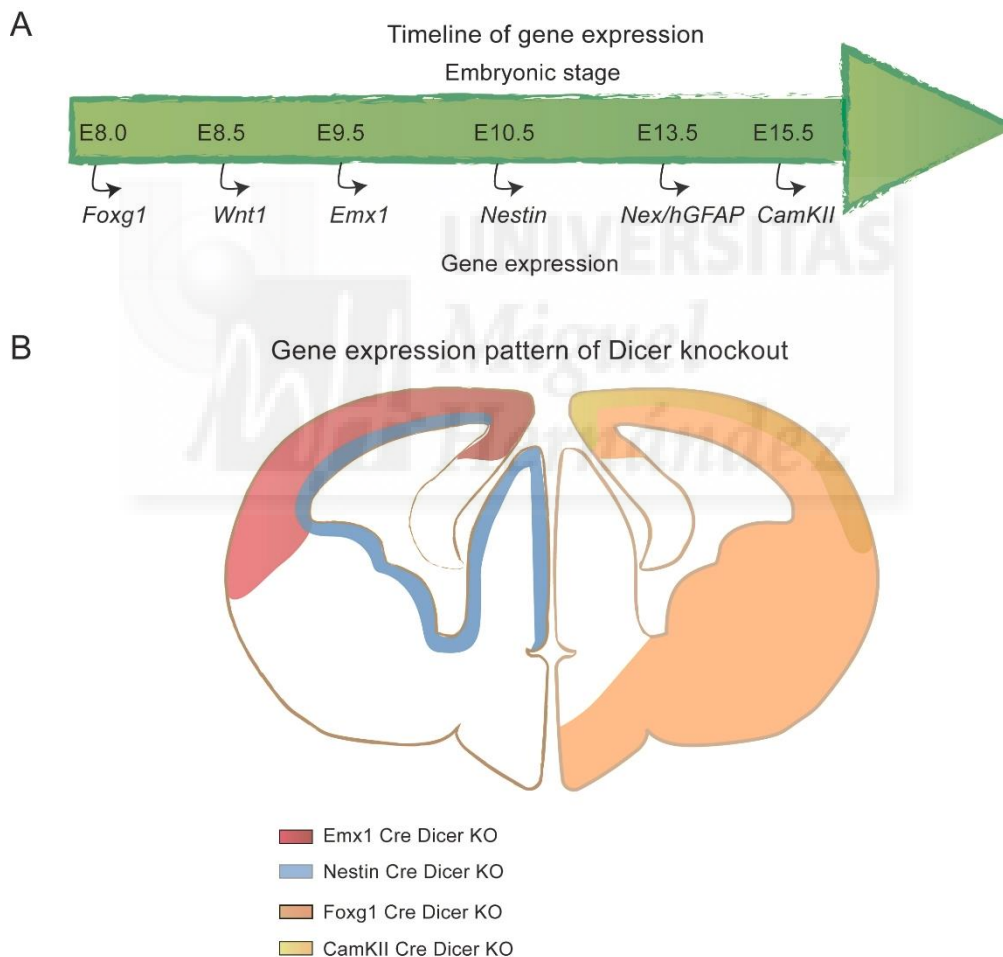


Figure 12. Time line of gene expression and gene expression pattern in the developing mouse brain. (A) Time line showing when the expression of different genes starts in the developing mouse brain. (B) Schema of a coronal section showing the area affected under the effect of different Cre-dependent *Dicer*. Modified from (Radhakrishnan and Alwin Prem Anand 2016)

UNIVERSITAS
Miguel
Hernández



4. Objectives

"Veo mi camino, pero no sé hacia dónde conduce. No saber hacia dónde voy es lo que me inspira a recorrer el camino"

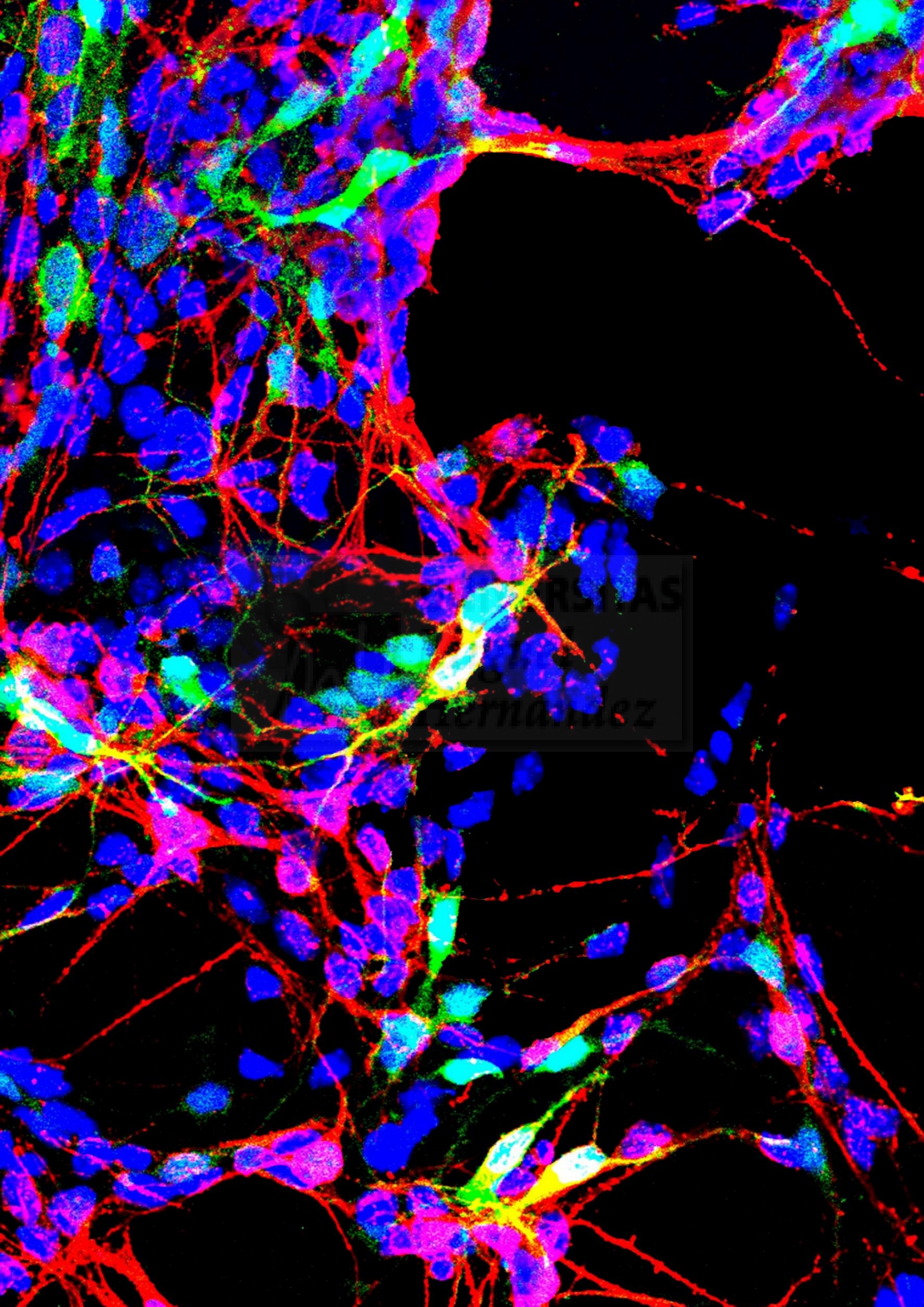
Rosalía de Castro

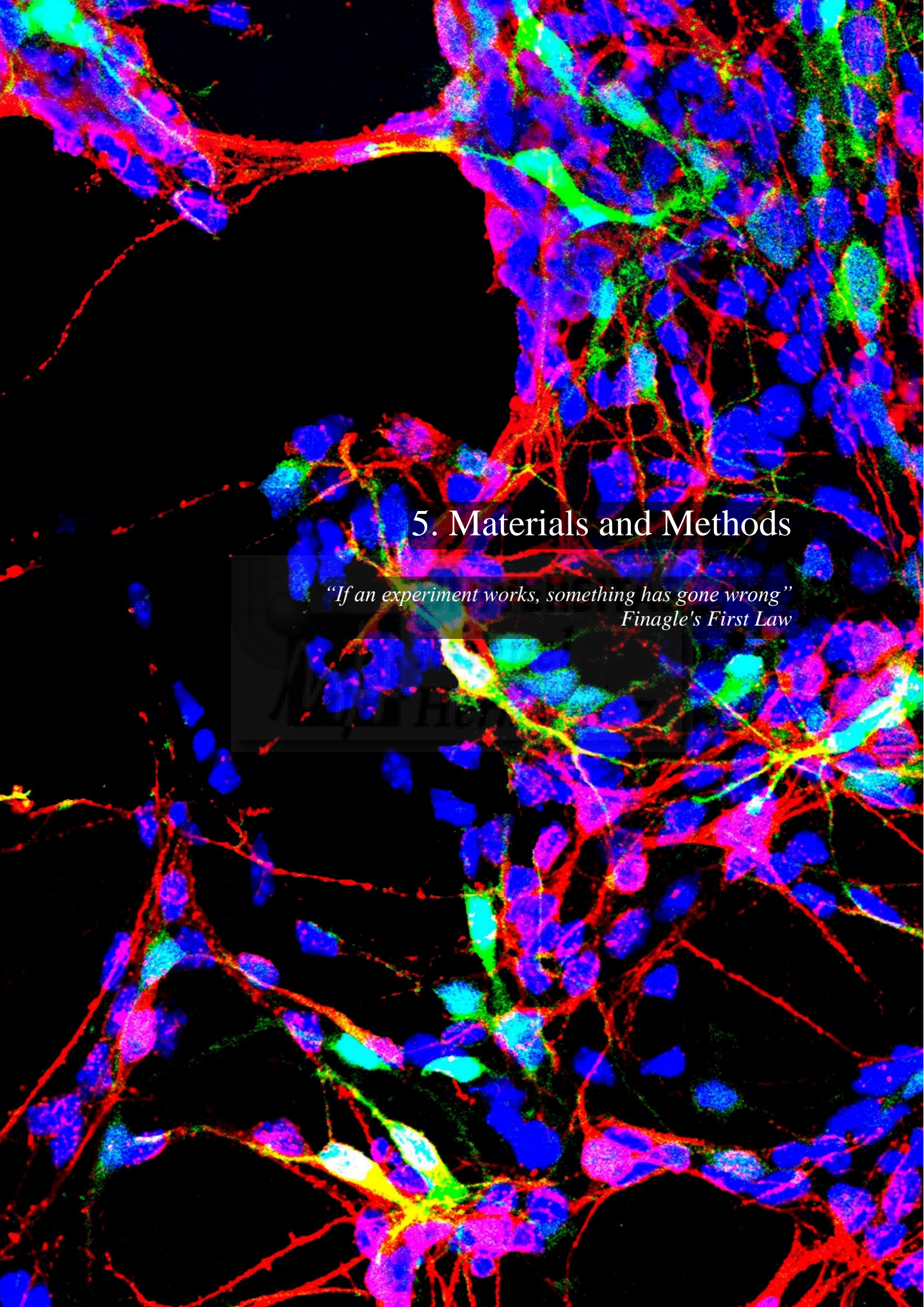


4. Objectives

The main goal of this work is to understand the role of miRNAs in the development of the telencephalon. In particular, we would like to understand how miRNAs regulate the behaviour of neural progenitors. To this end, I have focused my research on the cellular and molecular mechanisms affected after Dicer ablation and aimed to the following specific goals:

1. To determine if the loss of Dicer causes changes in the early development of the telencephalon.
2. To determine which miRNAs and protein-coding genes are transcriptionally changed upon Dicer ablation, and to assess possible candidates responsible for the phenotype observed in Dicer mutant embryos.
3. To identify miRNAs and their target genes responsible of the major phenotype in the absence of Dicer.



A complex fluorescence microscopy image of a neural network. The image shows a dense web of neurons with cell bodies and branching processes. The neurons are stained with multiple fluorescent dyes, resulting in a vibrant display of colors: blue for nuclei, red for cytoplasm or membranes, and green for specific organelles or markers. The background is black, making the brightly colored structures stand out. The overall appearance is that of a highly interconnected and intricate biological system.

5. Materials and Methods

*“If an experiment works, something has gone wrong”
Finagle's First Law*

5. Materials and Methods

Mice

Wild-type mice and mice carrying Cre transgene were maintained in a CD1 background. *Dicer*^{F/F} and tdTomato mice were maintained in C57BL/6 background.

We generated *Rx-Cre; Dicer*^{F/F} mice by breeding *Rx3-Cre* mice (obtained from Robert Hindges laboratory) (Swindell, Bailey et al. 2006) with mice carrying loxP-flanked *Dicer1* alleles (*Dicer1*^{tm1Bdh/J}) (Harfe, McManus et al. 2005) in order to generate conditionals mutants in which *Dicer1* is deleted from the telencephalon.

DicerFw1 and *DicerRv* were used to detect the wild-type allele of *Dicer*. *DicerDel* and *Dicer Rv* primers were used to detect the knockout allele of *Dicer*. MeRxgenoF and MeRxgenoR were used to detect the presence of Cre transgene.

Rx-Cre; tdTomato mice were generated by breeding *Rx-Cre* mice (Swindell, Bailey et al. 2006) with the tdTomato reporter line (B6;129S6-Gt(ROSA)26Sortm9(CAG-tdTomato)Hze/J) (obtained from O. Marín laboratory)(Madisen, Zwingman et al. 2010). *Rx-Cre; Dicer*^{F/F}; p53^{F/F} mice were generated by breeding *Rx-Cre; Dicer*^{F/F} mice with p53^{F/F} mice.

To genotype these mice, we used the following primer sequences:

DicerFw1: 5'-CCTGACAGTGACGGTCCACCG-3'

DicerRv: 5'-CATGACTCTTCAACTCAAAC-3'

DicerDel: 5'-CCTGACCAAGGCAAGTCATTC-3'

MeRxgenoF: 5'-GTTGGGAGAATGCTCCGTAA-3'

MeRxgenoR: 5'-GTATCCCACAATTCCTTGCG-3'

TdTomato WT Fw: 5'-AAGGGAGCTGCAGTGGAGTA-3'

TdTomato WT Rv: 5'-CCGAAAATCTGTGGGAAGTC-3'

TdTomato Mut Fw: 5'-CTGTTCTGTACGGCATGG-3'

TdTomato Mut Rv: 5'-GGCATTAAAGCAGCGTATCC-3'

Trp53^{tm1Bm} Fw: 5'-GGTTAAACCCAGCTTGACCA-3'

Trp53^{tm1Bm} Rv: 5'-GGAGGCAGAGACAGTTGGAG-3'

For all PCR reactions performed in this thesis, thermocycling conditions were as follow: 32 cycles of 30 s at 94 °C, 30 s at 58 °C, and 50 s at 72 °C. All genotyping reactions contained approximately 200 ng of template DNA, 100 µM dNTPs, 0.5 µM primers, 2.5 mM MgCl₂, 2.5 U of Taq DNA polymerase and 1 × PCR buffer in a 20-µl volume. The day of vaginal plug was consider to be embryonic day (E) 0.5. Mice were kept at the Instituto of Neurociencias de Alicante in accordance with Spanish and European regulations.

Constructs

For GFP expression for both *in vivo* and *in utero* assays, we used an enhanced green fluorescent protein (EGFP) expression vector pCAG-EGFP (generous gift of F.H. Gage). In order to perform functional assays overexpressing IRS-2 we used a pBS mouse IRS-2 (originated by Ronald Kahn (Addgene plasmid # 11372) (Tsuruzoe, Emkey et al. 2001).

For ISH probe synthesis, the next plasmids we used: mouse *Ngn2* (Borrell, Cardenas et al. 2012), *Pax6* (de Juan Romero, Bruder et al. 2015), *Dicer* exons 22-23, IRS-2. And five different plasmids kindly provided by Oscar Marín: *Dlx2*, *Nkx2.1*, *Dlx5*, *Gsx2* and *Lhx6*,

Ngn2 forward: TTTCCGAGACTGTGTTGCTG and reverse: CTGACTATGGGGAGGTGAGG. *Pax6*, forward: AGCATGCAGAACAGTCACAGC and reverse: AGCATGCAGAACAGTCACAGC. *Dicer* exons 22-23, forward: CCAAGCCCAGCAATGAATGT and reverse: CCAAATCGCATCTCCCAGG. *IRS-2*, forward: TTCATGTCCCTTGACGAGTATG and reverse: GGTCTGGGTTCTCCATAGACAG.

In order to achieve the downregulation of miRNAs we designed specific Tough Decoys for let-7 as described in (Haraguchi, Ozaki et al. 2009, Yoo, Hajjar et al. 2017). Two stem structures with a single miRNA binding sites (MBS) linked by linkers were designed. MBS in the will contain a central mismatch in the centre. The oligonucleotide can contain two of the same or different MBS sequences, in our case we are going to use two sequences of the same miRNA. The bulge will produce a non-complementation between the central nucleotides. We then inserted three nucleotide linkers between the stem sequence and MBS. In order to have a proper “control plasmid” for the experiments, we designed also a Scramble Tough Decoy that will bind no miRNA.

Let-7 Tough Decoy:

5' **GATCCGACGGCGCTAGGATCATC** **AAGTGAGGTAGTAGG** **ATCTTTGTATA**
 GTTGAAGTATTCTGGTCACAGAATACAAGTGAGGTAGTAGG **ATCTTTGTAT**
 AGTT**GAA** **GATGATCCTAGCGCCGCTTTTTTGGAAA** 3'

Scramble Tough Decoy:

5' **GATCCGACGGCGCTAGGATCATC** **AACTGGGCGTATAGAC** **ATCTGTGTTCCG**
 TTCCAAGTATTCTGGTCACAGAATACAAGTGGGCGTATAGAC **ATCTGTGTT**
 CGTT**CAAGATGATCCTAGCGCCGCTTTTTTGGAAA** 3'

Stem; **Linker**; MBS; **Bulge**; **Stem-loop**

Then we inserted this cassette into the BamHI-HindIII sites of pSilencer2.1-U6 puro vector (Ambion) to generate TuD RNA expression plasmids. The ligation products were transformed into competent *Escherichia coli* and the cells were plated in X-Gal/IPTG LB agar for blue/white colony screen. White colonies (also with no central blue coloration) were picked and replated on LB./Amp (Luria Broth/Ampicilin) plates to ensure that pure clones are obtained before performing plasmid preps. Plasmid DNA were purified with a NucleoBond Xtra Midi kit (Cultech, ref: 22740410.50), and resuspended in 10 mM Tris-HCl (pH 8.0).

In situ hybridization and immunohistochemistry

Brain were fixed at 4% paraformaldehyde (PFA, Sigma, ref: 441244-1KG) in phosphate buffer (PB) pH 7.3 at 4°C for 30 minutes to 2 hours. Brains used for in situ hybridization (ISH) were post-fixed overnight. Then, brains were cryoprotected with 15%, 20% and 30% sequential sucrose (Sigma, ref: S7903-1KG) solution, immersed in Cryo-medium Neg-50 (Thermo Scientific, ref: 6502), frozen and sectioned at 20 um using a cryostat.

For immunohistochemistry, sections were sections were incubated in blocking solution (Normal Horse Serum 10% (GIBCO, ref: 16050-122), TritonX-100 (Sigma, ref: T8787-250ML) 0.25%, BSA (Sigma, ref: A9576-50ML) 2%, PB 0.1M) for two hours and incubated in primary antibodies overnight at 4 °C, after washing them, sections were incubated with appropriate fluorescently conjugated secondary antibodies and counterstained with 4',6-diamidino-2-phenylindole (DAPI) (Sigma, ref: D9542). Primary antibodies used were: anti- Arl13b (1:500, rabbit polyclonal, Abcam, ref: ab83879), anti- β -Catenin (1:2000, rabbit polyclonal, Sigma, ref: C2206), anti-BrdU (1:500, rat monoclonal, Abcam, ref: ab6326), anti-cleaved Caspase 3 (1:150, rabbit polyclonal, Werfen, ref: 9661), anti-Ctip2 (1:500, Abcam, ref: ab18465), anti-dsRed (1:1000, rabbit polyclonal, Clontech, ref: 632496), anti-GFP (1:1000, chicken polyclonal, Aves Lab, ref: GFP-1020), anti-Ki67 (1:500, rabbit polyclonal, Abcam, ref: ab15580), anti-Nestin (1:500, mouse polyclonal, anti-phosphohistone H3 (1:1000, rabbit polyclonal, Upstate, ref:06-570), anti-Tbr1 (1:500, rabbit polyclonal, Abcam, ref: ab31940), anti-Tbr2 (1:500, rabbit polyclonal, Millipore, ref: ab31940), anti- β III tubulin (1:1000, mouse monoclonal, Covance, ref: MMS-435P), anti- p53 phospho S15 (1:500, rabbit polyclonal, Abcam, ref: ab1431), anti-Par3 (1:500, rabbit polyclonal, Millipore, ref: MABF28), anti-Pax6 (1:500, rabbit polyclonal, Millipore, ref: AB2237).

Secondary antibodies used were: biotinylated anti-Rabbit IgG (1:200, goat polyclonal, Vector Lab, ref: BA-1000), biotinylated Fab anti-Rabbit IgG (1:200, goat polyclonal, Jackson ImmunoResearch, ref: 711-067-003), Alexa488 anti-mouse IgG (1:200, donkey polyclonal, Invitrogen, ref: A-21202), Alexa488 anti-rabbit IgG (1:200, donkey polyclonal, Invitrogen, ref: A-21206), Alexa555 anti-mouse IgG (1:200, donkey polyclonal, Invitrogen, ref: A-31570), Alexa555 anti-rabbit IgG (1:200, donkey polyclonal, Invitrogen, ref: A-31572), Alexa488 anti-chicken IgY (1:200, Jackson ImmunoResearch, ref: 703-545-155), Cy2 Streptavidin (1:200, goat polyclonal, Jackson ImmunoResearch, ref: 016-220-084), Cy5 Streptavidin (1:200, goat polyclonal, Jackson ImmunoResearch, ref: 016-170-084).

For *in situ* hybridization, of coding genes sense and anti-sense cRNA probes were synthesized and labelled with digoxigenin using the DIG RNA Labeling Kit (SP6/T7) (Roche, ref: 11175025910) according to the manufacturer's instructions. *In situ* hybridization (ISH) was performed as described elsewhere (Reillo, de Juan Romero et al. 2011). Briefly, 20- μ m-thick frozen brain sections were hybridized with DIG-labelled cRNA probes overnight in hybridization solution [50% formamide (Ambion, ref: AM9342), 10% dextran sulphate (Sigma, ref: D8906-100G), 0.2% yeast tRNA (Invitrogen, ref: 15401-011), 1 \times Denhardt's solution (from a 50 \times stock; Sigma, ref: D2532), 1 \times salt solution (containing 0.2 M NaCl (Sigma, ref: S9888-2.5KG), 0.01 M Tris-HCl (Sigma, ref: T3254-1KG), 5 mM NaH₂PO₄ (Sigma, ref: 71505-250G), 5 mM Na₂HPO₄ (Sigma, ref: S3264-500G), 5 mM EDTA, pH 7.5)]. After sections were washed, alkaline phosphatase-coupled anti-digoxigenin Fab fragments were applied. For visualization of the labelled cRNAs, sections were incubated in nitroblue tetrazolium (NBT, Sigma, N6639-1G) /5-bromo-4-chloro-3-indolyl phosphate (BCIP; Roche, ref: 11585002001) solution [3.4 μ l/ml from NBT stock and 3.5 μ l/ml from BCIP stock in reaction buffer (100 mg/ml NBT stock in 70% dimethylformamide; 50 mg/ml BCIP stock in 100% dimethylformamide; Roche, ref: D4551-250ML)].

For *in situ* hybridization of mature miRNAs, miRCURY™ LNA™ microRNA ISH Detection Probes (Qiagen) using locked-nucleic-acid-modified (LNA) probes, an approach previously shown to reveal the presence of mature miRNAs but not their precursors. We used the protocol described in Kloosterman et al work (Kloosterman, Wienholds et al. 2006).

Bromodeoxyuridine labelling experiments

BrdU was diluted at 10mg/ml in 0.9% NaCl and always administrated at 50mg/kg body weight. For S-phase progenitor determination, a single dose of BrdU was injected at E17.5, embryos were fixed 30 min later and the percentage of Ki67+ cells labelled with BrdU was calculated. For cell cycle re-entry calculation, a single intraperitoneal injection of BrdU was administrated at E16.5, embryos were fixed 24 hr later and the percentage of BrdU+ cells labelled with Ki67 was calculated. In this cell-cycling experiments three cell populations are identifiable:

1. Ki67+cells corresponding the whole pool of cycling cells (proliferating progenitor cells) at the time of fixation.
2. Ki67+ BrdU+: progenitor cells that performed self-renewal cell divisions.
3. BrdU+: cells that were in S phase at the time of BrdU injection.

Tissue microdissection and RNA sequencing analysis

For RNA extraction, E11.5 brains of wild-type animals and *Dicer* KOs were dissected in cold RNase free medium and tissue blocks were vibrotome cut at 250 um. Living telencephalic slices were further microdissected with microscalpels in ice-cold RNase free medium to isolate the primordium of the olfactory bulb. Tissue pieces were immediately frozen in dry ice and sent to Dr. Federico Calegari's Laboratory in Dresden, where Martina Dori performed the extraction of RNA and the RNA sequencing analysis.

For the RNA extraction, tissue was dissociated using the Neural Tissue Dissociation Kit with Papain (Miltenyi Biotech, ref: 130-092-628) according to the manufacturer protocol. RNA was extracted using Quick RNA Mini Prep (Zymo Research, ref: R1055) according to the product protocol. For the sequencing, 1µg of total RNA was delivered to DeepSeq Facility (CRTD/Biotec) for library preparation and sequencing. Libraries were prepared with the NEB Next Small RNA Library Prep Kit and sequenced on Illumina HiSeq 2500.

The RNA-sequencing output was in FASTQ format. Wild-type and *Dicer* KO RNA-seq datasets are from three biological replicates each. After a quality check using FASTQC v2.6.14, the output was aligned to the mouse genome (mm9) with UCSC's annotations using TopHat v2.0.8 (Trapnell et al, 2009). Only uniquely mapped reads were

retained for further analysis. SAMTOOLS v0.1.19 (Li et al, 2009) was used to convert the BAM output to SAM format and to sort the BAM file. The read counts per gene were calculated using the HTSeq program, v0.5.4p1 (Anders et al, 2015). The DESeq package (Oshlack et al, 2010) was used to generate normalized read counts and for differential gene expression analysis. DESeq called differentially expressed genes with FDR cutoff of 0.05 and $\text{abs}(\text{FC}) > 1.5$ were considered as significant differentially expressed genes. GO term analysis was performed using GenePattern GSEAPreranked (Subramanian et al, 2007) and ToppGene (Chen et al, 2009). Gene lists derived from RNA-seq analysis of wildtype and *Dicer* KO primordium of the OB are supplied in Methods, **Table 1**. MiRNAs list derived from RNA-seq analysis of wildtype and *Dicer* KO primordium of the OB are supplied in Methods, **Table 2**.

Quantitative real-time PCR (qRT-PCR)

qRT-PCR of both cell culture and brain tissue was performed. For brain tissue of E11.5: brains of wild-type animals and *Dicer* KO were dissected in cold RNase free medium and tissue blocks were vibratome cut at 250 μm . Living slices of telencephalic vesicles were further microdissected with microscalpels in ice-cold RNase free medium to isolate the primordium of the olfactory bulb. Tissue pieces were immediately frozen in dry ice for RNA extraction. In the other hand, cultured cells transfected with plasmids of interest were collected and rapidly putted on ice for RNA extraction.

For miRNA qRT-PCR: small RNA was extracted using mirVana™ miRNA Isolation Kit (Ambion, ref: AM1560) and then a 2-steps qRT-PCR was performed. 1st: cDNA synthesis of each miRNA with stem-loop specific primers using TaqMan™ MicroRNA Reverse Transcription Kit (Applied Biosystems; ref: 4366596) together with the primer from TaqMan™ MicroRNA Assay (for mature let-7, we used RT-hsa-let-7a; Thermo Fisher, ref: 4427975), and 2nd: real time quantification using PCR because of the chain elongation produced by the stem-loop primer unfolding, this allows the binding of 2 primers and 1 probe needed for the quantification, this second step was performed using TaqMan™ MicroRNA Assay (TM-hsa-let-7a; Thermo Fisher, ref: 4427975) together with the TaqMan™ Gene Expression Master Mix (Applied Biosystems, ref: 4369016).

The RT-PCR reaction was made with:

-7 μ l/reaction of qRT-PCR Master Mix: 0.15 μ l of 100mM dNTPs (with dTTP); 1 μ l of MultiScribe™ Reverse Transcriptase (50 U/ μ L), 1.5 μ l of 10 \times Reverse Transcription Buffer, 0.19 μ l of RNase Inhibitor, 20U/ μ L and 4.16 μ l of Nuclease-free water (TaqMan™ MicroRNA Reverse Transcription Kit (Applied Biosystems; ref: 4366596)).

-5 μ l/reaction of RNA sample, the total amount of sRNA in each reaction is 50ng.

-3 μ l/reaction of RT stem-loop primer (Thermo Fisher, ref: 4427975).

This reactions of 15 μ l final volume were incubated in a C1000 Thermal cycler (Bio-Rad) with the next program: 30 min at 16°C, 30 min at 42°C, 5 min at 85°C, and ∞ at 4 ° C.

Then, the quantitative PCR amplification was loaded with: 1 μ l of TaqMan MicroRNA Assay (20 \times), 1.33 μ l of product from RT reaction, 10 μ l of TaqMan 2 \times Universal PCR Master Mix, 7.67 μ l of Nuclease-free water. For running the reaction, we used a StepOne™ Real-Time PCR System (Applied Biosystems, Life Technologies). The reactions were amplified for 15 s at 95 °C and 1 min at 60 °C for 40 cycles. The thermal denaturation protocol was run at the end of the PCR to determine the number of products that were present in the reaction. Reactions were run in triplicate. The cycle number at which the reaction crossed an arbitrarily-placed threshold (CT) was determined for each miRNA to a scramble miRNA (U6), this was described using the equation $2^{-\Delta CT}$ where $\Delta CT = (CT_{miRNA} - CT_{U6})$.

For long RNA qRT-PCR: Total RNA was extracted using RNeasy Mini Kit (Quiagen, ref: 74104) followed by treatment with RNase-free DNase Set (Quiagen, ref: 1101177). Then, we used Maxima First Strand cDNA Synthesis Kit for quantitative real-time PCR (qRT-PCR) (Thermo Fisher, ref: K1671). And the quantitative RT-PCR was performed using the Step One Plus sequence detection system and the TaqMan™ Gene Expression Master Mix (Applied Biosystems, ref: 4369016), with each point examined in triplicate. Transcript levels were calculated using the comparative C_t method normalized using S18. Each independent sample was processed in triplicate. Real-time quantitative PCR was performed using standard protocols on an Applied Biosystems 7900HT Sequence Detection System equipped with a 384-well reaction plate. The reactions were amplified for 15 s at 95 °C and 1 min at 60 °C for 40 cycles. The thermal

denaturation protocol was run at the end of the PCR to determine the number of products that were present in the reaction. Reactions are run in triplicate. The cycle number at which the reaction crossed an arbitrarily-placed threshold (CT) was determined for each gene 18S rRNA was described using the equation $2^{-\Delta CT}$ where $\Delta CT = (CT_{miRNA} - CT_{18S rRNA})$.

In utero Electroporation

Mouse embryos were electroporated in utero in the OB at E12.5. Briefly, pregnant females were deeply anesthetized with isoflurane and the uterine horns exposed. 2 μ l of plasmid solution was injected into the lateral ventricle using pulled glass needles (WPI; ref: 1B120F-4), and square electric pulses of 30V and 50ms were passed through the uterus five times, spaced 950ms using a square pulse electroporator (Cuy21EDIT Bex C.,LTD) using round electrodes (CUY650P5,Nepa Gene). Then, the uterine horns were placed back in the abdominal cavity, which was then suture closed and the female was allowed to recover. Plasmid concentrations were as follows: GFP= 0.7 μ g/ μ l, IRS-2= 1 μ g/ μ l, Scramble TuD: 1 μ g/ μ l, let-7 TuD= 1 μ g/ μ l, MISSION let-7a, let-7b, let-7c mimic (Sigma; ref: HMI0002, HMI0007 and HMI0009) = 20 nM. Combinations of these plasmids were done maintaining the same final concentrations.

Image analysis and quantification

Images were acquired using a fluorescence microscope (Zeiss Axio Imager Z2) with Apotome.2 and coupled to two different digital cameras (AxioCam MRm and AxioCam ICc) or an inverted confocal microscope (Olympus FluoView FV1000). All images were analysed with ImageJ (Fiji). The total thickness of the cerebral cortex, or thickness of the Tuj1+ and VZ layer, were measured from DAPI-stained or immunostained coronal sections using ImageJ software. In the cerebral cortex, cells were counted from the mediolateral to the dorso-parietal neocortex and at medial rostrocaudal levels, identical between controls and mutants. For each section, the total count of cells was normalized to the length of the apical VZ surface. For cleaved Caspase-3, all positive nuclei were counted.

For studies of colocalization, single plane images were obtained using a confocal microscope (Olympus FluoView FV1000) and analysed with ImageJ (Fiji).

Quantification of total volume of rosettes was performed analysing all rostro-caudal slices from each brain and drawing rosettes perimeter in a Neurolucida station.

3D images of clarified brains were taken using an inverted confocal microscope (Olympus FluoView FV1000). A chamber was built with the help of Victor (Instituto de Neurociencias) to confine the DBE and protect the microscope. We built a 3D printed imaging chamber, with the Visijet M3 Clear resin, which is resistant to DBE. We secure the chamber to the microscope slide with Kwik-sil epoxy (VWR). This epoxy is compatible with DBE, cures instantaneously and has no permanent bond, so the sample and spacers can be recovered after imaging. We putted the sample in the chamber then placed the grating in the top of the sample to lock up it then filled the chamber with DBE through the filling inlet with a pipet and closed the chamber with its cover. Then, acquired images were analysed and mounted using the software Imaris 8.

Immunolabeling and clearing of whole brains

E17.5 WT and *Dicer* KO embryos were perfused and their brains were post-fixed in 1xPBS/4%PFA at 4°C 2h with shaking, then they were washed in PBS with shaking at room temperature (RT) 1h x 3times. After this first step, samples were pre-treated with methanol as follows:

Sample pre-treatment with methanol:

1. Dehydrate in methanol (JTBaker; ref: 8405)/PBS series (freshly prepared): 50%, 80%, 100%; 1h each at RT.
2. Wash further with 100% methanol for 1h.
3. Chill the sample over ice; bleach in 5% H_2O_2 (Sigma, ref: H1009) in 20%DMSO (Sigma, ref: D2650) /methanol o/n at 4°C (1 volume 30% H_2O_2 /1 volume DMSO/4 volume methanol, ice cold).
4. Wash in 100% methanol, RT 1h x3.
5. Incubate in 20%DMSO/methanol, RT 2h.
6. Rehydrate in methanol/PBS series (fresh prepared): 80%, 50%, 0%; 1h each at RT.
7. Wash in 1xPBS/0.2% TritonX-100 (Sigma, ref: T8787-250ML), RT 1h x2.

Immunolabeling: Then, treated samples are ready for the immunolabeling, this protocol is a variation of the regular one used for immunohistochemistry:

1. Incubate pre-treated samples in 1xPBS/0.2% TritonX-100/ 20% DMSO/ 0.3M glycine (Panreac Sintesis, ref: 151340.1609), 37°C o/n.
2. Block in 1xPBS/ 0.2% TritonX-100/ 10%DMSO/ 6% Normal Donkey Serum (Jackson ImmunoResearch, ref: 017-000-121) at 37°C during 4 days.
3. Wash in 1xPBS/ 0.2%Tween-20 with 10µg/ml heparin (Sigma, ref: H3149) (PTwH) at RT 1h x 2.
4. Incubate with primary antibody (anti-Pax6 (1:500, rabbit polyclonal, Millipore, ref: AB2237)) in PTwH/ 5%DMSO/ 3% Normal Donkey Serum, at 37°C during 4 days.
5. Wash in PTwH 10min x 1, 15min x 1, 30min x 1, 1h x 1 and then 2h x 1.
6. Incubate with secondary antibody (Alexa555 anti-rabbit IgG (1:200, donkey polyclonal, Invitrogen, ref: A-31572)) in PTwH/ 3% Normal Donkey Serum at 37°C during 4 days.
7. Wash in PTwH 10min x 1, 15min x 1, 30min x 1, 1h x 1 and then 2h x 1.

Clearing: adapted from the 3DISCO protocol (Ertürk, Becker et al. 2012):

1. Incubate the sample overnight in 50% Tetrahydrofuran/H₂O (THF, Sigma, ref: 186562-12X100ML) in a glass vial with a silicon coated cap (Thermo Scientific, ref: C326-0020). For each step, use between 5 and 10mL per tube. The steps must be gradual to avoid excessive contraction of the tissue and must be performed in darkness.

2. Incubate during 1h in 80% THF

3. Incubate 2x1h in 100% THF

4. Incubate in Dichloromethane (DCM; Sigma, ref: 270997-12X100ML) until the sample sinks at the bottom during 5 min. The sample may not sink if air bubbles are trapped inside. DCM increases the shrinkage of soft tissues in embryos (such as the brain), so short incubations for embryos and early post-natal brains are recommended (less than 10min).

5. Incubate in DiBenzyl Ether (Sigma, ref: 108014-1KG) until the sample is clear (20min for E17.5 brains). The vial containing DBE should be filled almost completely with DBE to prevent the air inside the vial from oxidizing the sample. Then, change the DBE and store samples in darkness at RT.

DBE, which is used for storage and imaging, is a skin irritant exhibiting toxicity class II (moderate toxicity) according to the material safety data sheets (MSDSs), so was

handled with care, including wearing gloves, with those precautions can be used on an open bench for slide mounting and for microscopy.

Cerebral organoids

We followed a variation of Lancaster et al protocol (Lancaster, Renner et al. 2013). We used BJ (ATCC® CRL-2522™) human iPS cells kindly provided by Dr Silvia Cappello, this line was established from skin taken from normal foreskin from a newborn human male is commercially available (ATCC, ref: CRL-2522), this human pluripotent stem cell line was regularly checked and confirmed negative for mycoplasma. On day 0 of organoid culture, iPS cells at less than passage 50 were dissociated by Accutase (Sigma, ref: A6964) treatment and iPS cells were removed by gravity separation of stem cell colonies to generate single cells. In total, 9000 cells were then plated in each well of an ultra-low-binding 96-well plate (Corning, ref: 7007) in human ES media with low concentration basic fibroblast growth factor (bFGF; Peprotech, ref: 100-18B) (4 ng/ml) and 50 μ M Rho-associated protein kinase (ROCK) inhibitor (VWR, ref: 688000-5). Medium was changed after 3 days leaving out low bFGF and Rock inhibitor.

When Embryoid bodies (EBs) begin to brighten and have smooth edges (day 6 or 7), transfer EBs to 500 μ l neural induction media (containing Dulbecco's modified eagle medium (DMEM; Fisher, ref: 11330-032)/F12, 1:100 N2 supplement (Fisher, ref: 17502048), Glutamax (Fisher, ref: 35050-038), minimum essential media-nonessential amino acids (MEM-NEAA; Sigma, ref: M7145-100ML) and 1 μ g ml/1 heparin (Sigma, ref: H3149)) in a low-adhesion 24-well plate (Sigma, ref: CLS3473-24EA) (1-2 per well) using a cut P200 tip to carefully transfer without disrupting. Aggregates should become brighter around the outside with visible neuroepithelia after a few days in the neural induction media (after 4-5 days); healthy cell aggregates should have smooth edges.

When neuroepithelia were evident (day 10 or 11), they were transferred to Matrigel (BD Biosciences, ref: 356230) droplets using a cut P200 tip, transfer aggregates one by one to dimpled Parafilm (Polysciences, ref: 24364) (dimpled Parafilm was made covering a tip holder with a sheet of parafilm and pushing parafilm into holes to create dimples). The excess of media was removed and droplets of Matrigel were added to each aggregate. Each aggregate was positioned in the centre of the droplet using a pipette tip. In order for the Matrigel to polymerize, we placed the parafilm sheet in a 6 cm dish inside

the incubator. Then Matrigel droplets were removed from the Parafilm and grown in neural induction media.

When tissues begin to show more complex neuroepithelia with some budding outgrowth (after 2-3days) change media to Improved differentiation media without vit.A containing 1:1 mixture of DMEM/F12 and Neurobasal (Gibco, ref: 21103-049) with 1:200 N2 supplement, 1:100 B27 supplement without vitamin A (Fisher, ref: 12587010), 3.5 μ l l-1 2-mercaptoethanol (Sigma, ref: M3148-25ML) , 1:4,000 insulin (Sigma ref: I9278-5ML), 1:100 Glutamax (Fisher, ref: 35050-038), 1:200 MEM-NEAA (Sigma, ref: M7145-100ML) and Penicillin/streptomycin (P/S; Sigma, ref: P0781). Wnt activator CHIR (Tocris (BIOGEN), ref: 4423) was added at a final concentration of 3 μ M per dish for 3 days. Since CHIR is stable for 2 days, the media was changed once within the 3 days.

Between day 18 and day 20, in order to improve the diffusion of nutrients and oxygen, dishes with cerebral organoids were putted in a shaker inside the incubator. Then, on day 25 the media was changed to Improved differentiated media with vit.A (IDM+A) and feed twice a week. IDM+A contained 1:1 mixture of DMEM/F12 and Neurobasal (Gibco, ref: 21103-049) with 1:200 N2 supplement, 1:100 B27 supplement with vitamin A (Fisher, ref: 17504044), 3.5 μ l l-1 2-mercaptoethanol (Sigma, ref: M3148-25ML) , 1:4,000 insulin (Sigma ref: I9278-5ML), 1:100 Glutamax (Fisher, ref: 35050-038), 1:200 MEM-NEAA (Sigma, ref: M7145-100ML) and Penicillin/streptomycin (P/S; Sigma, ref: P0781), 10mM HEPES (Sigma, ref: H4034-25G), 0.4 mM vitamin C (Sigma, A4544).

Finally, on day 40 we added Matrigel (100ul Matrigel/ 5 ml dish) to Improved differentiation media with vit.A and fed twice a week the cerebral organoids until the time of analysis, when tissues were fixed in 4% paraformaldehyde for 20 min at 4 °C followed by washing in PBS three times for 10 min. Then, they were cryoprotected with 15%, 20% and 30% sequential sucrose (Sigma, ref: S7903-1KG) solution, immersed in Cryo-medium Neg-50 (Thermo Scientific, ref: 6502), frozen and sectioned at 20 μ m using a cryostat.

Cerebral organoids electroporation

Electroporation was performed under aseptic conditions using a Petri dish, a square pulse electroporator (TSS20 OVODYNE ELECTROPORATOR, MCI) and round electrodes (CUY650P5, Nepa Gene). A total of 3 μ l of 1.7 μ g/ μ l total plasmid (GFP= 0.7 μ g/ μ l, IRS-

2= 1 μ g/ μ l, Scramble TuD: 1 μ g/ μ l, let-7 TuD= 1 μ g/ μ l, MISSION let-7a, let-7b, let-7c mimic= 20 nM. Combinations of these plasmids were done maintaining the same final concentrations) was injected in 4–5 locations within the organoid and electroporation was performed in differentiation media without antibiotics at 10 pulses, 80 V, 100 ms duration, 2 s interval.

Target prediction

The prediction of genes regulated by let-7 was performed using miRWalk2.0 (<http://zmf.umm.uni-heidelberg.de/mirwalk2>). It is an online tool that was developed to generate possible miRNA interactions with all the regions of genes by gathering 13 prediction data sets from another existing miRNA-target resources. Interestingly, miRWalk2.0 offers a framework to obtain statistically significant miRNA interactions on genes associated with pathways, ontologies and classes of gene and proteins (Dweep and Gretz 2015).

Statistical analyses

Statistical analysis was carried out in GraphPad Software. P values below 0.05 were considered statically significant. Data are presented as mean \pm standard error of the mean (SEM) throughout the Thesis. Normality and variance tests were fort applied to all experimental data. When data follows a normal distribution, paired comparisons were analysed with t-test, while multiple comparisons were analysed using either ANOVA with post-hoc Bonferroni correction (equal variances) or the Welch test with post-hoc Games-Howell (different variances). A X²-test was applied to analyse the distribution of cells in bins.

Tables 1-2. Results.

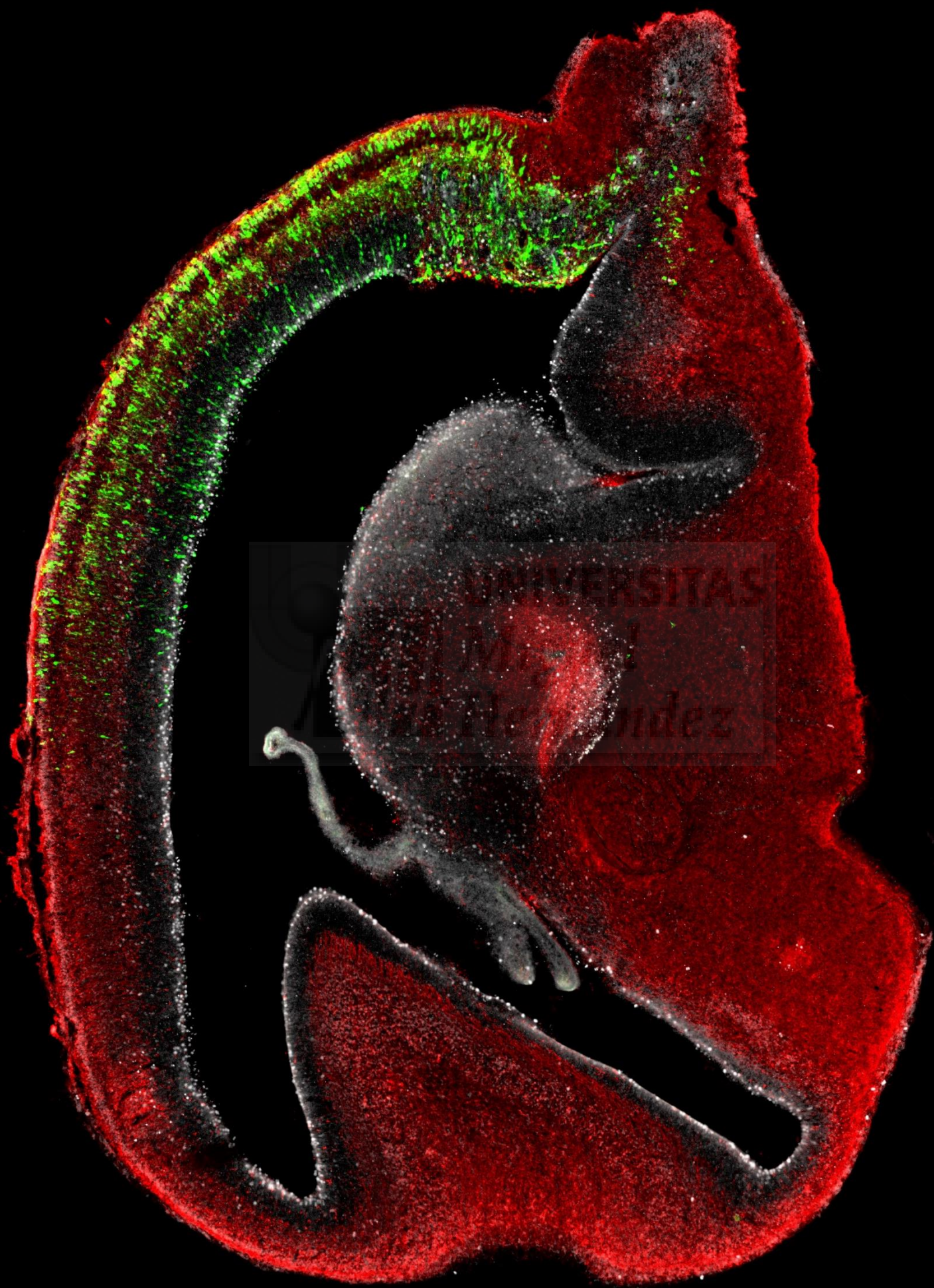
Table 1. Genes obtained with RNA-seq analyse. A total of 325 genes were found overexpressed in *Dicer* KO animals compared with the WT (the list of all genes attached in Annexed file 1). Here there are genes related with cell death and proliferation, as well as the ones with a higher Log₂Fold Change (Log₂FC). In the table there are reported the gene name (Gene), Q value (adjusted P value), the mean of read counts for 9 WT embryos (mean WT) and the mean of read counts for 9 *Dicer* KO embryos (mean KO).

Gene	log2FC	Q value	mean WT	mean KO
<i>Prtg</i>	1.904465359	1.06E-30	669.9	3695.2
<i>Lin28a</i>	1.931912739	1.87E-28	624.3	3898.4
<i>Greb1</i>	1.346471814	9.52E-25	502	1458.3
<i>Spon1</i>	1.287211577	3.08E-13	191.2	609.8
<i>Acpp</i>	1.485943566	1.87E-12	14.6	119.3
<i>Onecut2</i>	1.443880583	6.99E-12	168.6	1051.7
<i>Ccng1</i>	1.181379149	6.47E-11	1823.3	5318.7
<i>Trim71</i>	1.247619175	3.80E-10	671.3	2374.3
<i>Igdcc3</i>	1.017298453	4.57E-10	3467.5	8150.5
<i>Nr6a1</i>	1.188587624	2.24E-09	227.4	741.5
<i>Slc19a2</i>	1.044794365	4.23E-09	528.4	1324.5
<i>Nr1d2</i>	0.956664845	4.23E-09	318.1	705.8
<i>Ano3</i>	1.275972454	4.36E-09	54.9	347.3
<i>Zfp568</i>	0.870860633	5.71E-09	1900.3	3825.9
<i>Irf1</i>	1.01046725	1.28E-08	174.4	423.8
<i>Rab11fip1</i>	0.913454973	4.09E-08	444.6	954
<i>Fndc1</i>	1.156332107	8.70E-08	8.1	90.5
<i>Rtl1</i>	1.107439947	1.00E-06	27.6	122.9
<i>Ret</i>	0.995571177	5.64E-06	12.1	130.6
<i>Six3</i>	0.923655969	1.03E-05	1110.1	2706.4
<i>Polr3g</i>	0.809590325	1.20E-05	725.5	1456.7
<i>Dll1</i>	0.891225499	2.08E-05	5029.1	11772.2
<i>Gm16551</i>	0.938279776	2.52E-05	10.5	97.6
<i>Gylt1b</i>	0.901758852	2.84E-05	472.9	1149.3
<i>Magel2</i>	0.965722752	2.95E-05	257.7	793.6
<i>Galnt12</i>	0.915255736	5.16E-05	619.5	1626.7
<i>Purb</i>	0.556384903	5.82E-05	5190.5	7941
<i>Lrp2</i>	0.903534897	8.74E-05	208.5	1380.3
<i>Nefl</i>	0.921403537	8.74E-05	384.5	1120

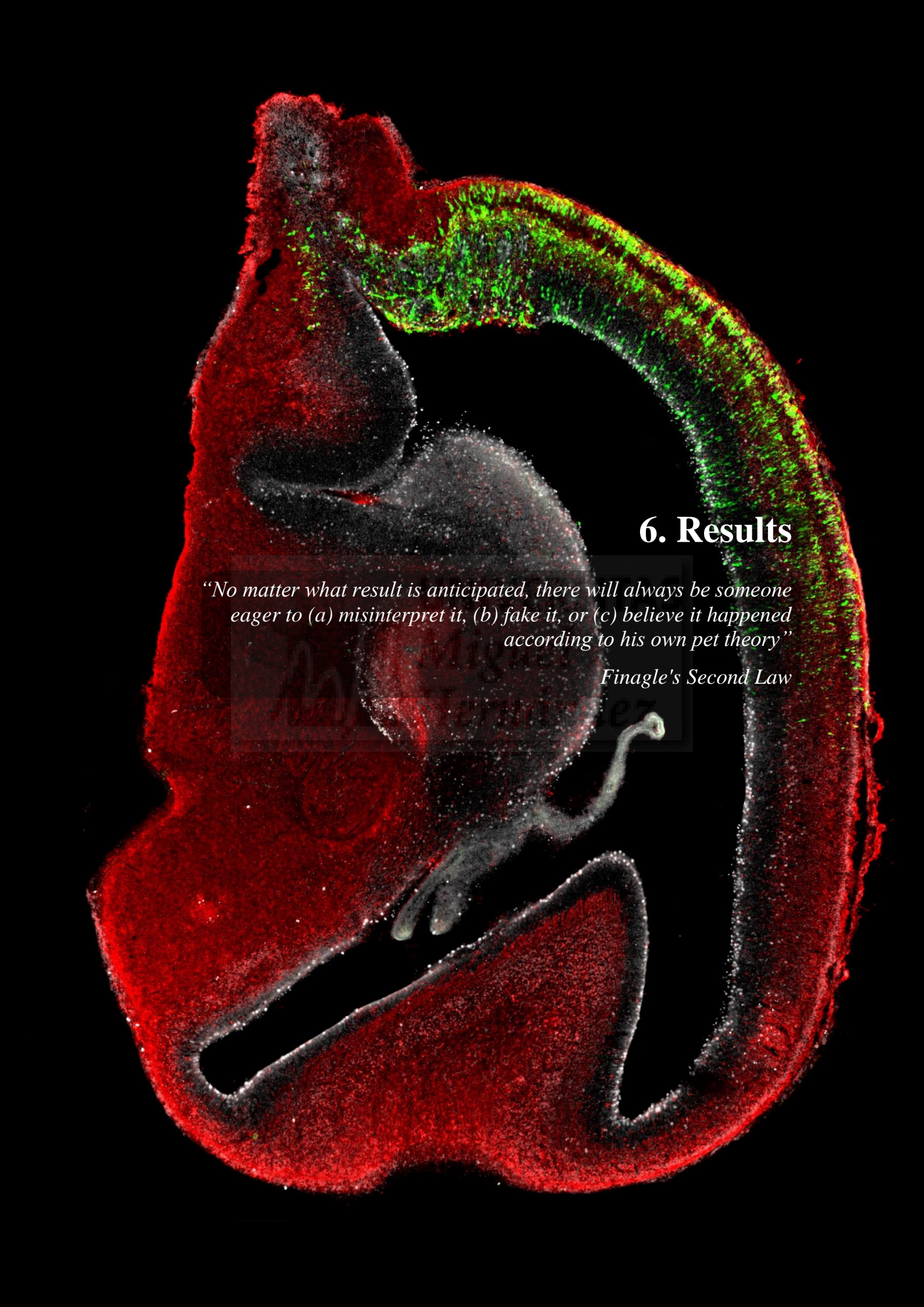
Lrp2	0.903534897	8.74E-05	208.5	1380.3
Fzd5	0.894757633	9.52E-05	334.9	875.9
Lhx8	0.875269643	0.00020405	21.6	128.9
Mpeg1	0.874351534	0.00039213	133.1	419
Zbtb16	0.703556723	0.0004867	467.9	867
Trp53inp1	0.576838089	0.00206492	2230.5	3581.8
Rest	0.450597955	0.00380292	3230.3	4567.5
Cnot6l	0.419512981	0.00411692	2009.2	2760.6
Col18a1	0.498399805	0.00465502	8266.2	12282.2
Irs2	0.590678207	0.00649148	961.3	1614.3
Klhl42	0.512692029	0.00686601	953.2	1445.9
Igf2r	0.367129975	0.00805741	7039.2	9259.2
Pten	0.391143961	0.00907925	4076.3	5479
Lyn	0.469044594	0.02499361	304.8	449.3
Tnfrsf1b	0.531238611	0.02702386	146.1	236.6
Hcls1	0.554890235	0.02844491	138.8	235
Kif23	0.376755841	0.02883298	4241.2	5674.4
Zfyve26	0.378636481	0.02883298	1294.1	1735.5
Csf1r	0.60317625	0.02903086	334.7	660.2
Csf1r	0.60317625	0.02903086	334.7	660.2
Shh	0.479710097	0.03003613	34	305.2
Map3k5	0.592453936	0.03477182	82.7	165.2
Zmat3	0.4234907	0.03555014	3596.6	5068.3
Ctgf	0.543347066	0.03562793	439.9	746.4
Ddx3x	0.381765321	0.04137523	35667.2	48167.1
Itgb1	0.334834527	0.04192489	10702.2	13806.9
Itgb1	0.334834527	0.04192489	10702.2	13806.9
Cyr61	0.538795029	0.04322586	744.3	1275.8

Table 2. miRNAs obtained with RNA-seq analyse. A total of 11 known miRNAs were found to be significantly (adjusted p value < 0,01) reduced in *Dicer* KO embryos compared to WT animals (note that miR-9 has a p value of 0,0103). Three novel differentially expressed miRNAs were found: *mmu-mir-n-140-5p*, *mmu-mir-n-152-5p* and *mmu-mir-n-44-5p* (in blue) In the table there are reported the miRNA name (miRNA), Log₂ Fold Change (log₂FC), Q value (adjusted P value), the mean of read counts for 6 WT embryos (mean WT) and the mean of read counts for 6 *Dicer* KO embryos (mean KO). * Note that the value showed in the Q value/ p value cell for *mmu-mir-n-194-5p* is the p value. Due to that the low number of total reads for that particular miRNA made impossible to perform the Q value.

miRNA	log ₂ FC	Q value / p value*	mean WT	mean KO
<i>mmu-mir-n-140-5p</i>	-6.955900593	6.70E-65	1083.2	0
<i>mmu-mir-n-152-5p</i>	-6.957632225	6.70E-65	1083.9	0
<i>mmu-mir-n-44-5p</i>	-5.462684366	1.30E-30	796.7	0
<i>mmu-let-7i-5p</i>	-1.711051288	1.73E-12	9043.7	2585.4
<i>mmu-miR-99a-5p</i>	-0.989481913	1.81E-09	26852.4	13309.5
<i>mmu-let-7g-5p</i>	-1.227423397	4.54E-08	7993.7	3288.6
<i>mmu-let-7f-5p</i>	-1.253712098	1.87E-07	10490.1	4207.7
<i>mmu-let-7f-5p</i>	-1.256079342	1.87E-07	10366	4149.7
<i>mmu-let-7b-5p</i>	-2.256055558	1.76E-06	581.2	76.3
<i>mmu-miR-98-5p</i>	-1.602558825	2.70E-05	465.9	131
<i>mmu-let-7c-5p</i>	-1.666425243	4.23E-05	15938	4121.1
<i>mmu-let-7c-5p</i>	-1.668306596	4.23E-05	15858	4091.3
<i>mmu-miR-139-5p</i>	-1.056182472	0.00031234	886.9	404.8
<i>mmu-let-7d-5p</i>	-1.439482754	0.00074703	1864.6	578.1
<i>mmu-let-7a-5p</i>	-1.041266634	0.00091544	13295.5	6097.2
<i>mmu-let-7a-5p</i>	-1.041651981	0.00091544	13319	6106
<i>mmu-miR-149-5p</i>	-0.748643163	0.00811699	2194.8	1270.9
<i>mmu-miR-9-5p</i>	-0.756879654	0.01032753	355137.1	203647.7
<i>mmu-mir-n-194-5p</i>	5.023544012	1.08E-27*	0	232.1



UNIVERSITAS
INDONESIA
Indones



6. Results

“No matter what result is anticipated, there will always be someone eager to (a) misinterpret it, (b) fake it, or (c) believe it happened according to his own pet theory”

Finagle's Second Law

Part1. Early ablation of functional Dicer leads to brain malformations



Characterization of Rx-Cre; Dicer^{F/F} mouse. Cortical phenotype

In order to understand the role of miRNAs during early telencephalic development, we ablated functional *Dicer* from neuroepithelial cells of the telencephalon at E7.5 (two days before neurogenesis starts). To achieve such an early recombination, we used as a genetic tool an *Rx3-Cre* (named *Rx-Cre* in this thesis) knock-in mouse line, in which Cre recombinase is expressed under the control of *Rx3* promoter. *Rx3* is specifically expressed in the anterior neural plate starting at embryonic day 7.5, later in the development it is strongly expressed in the optic vesicles and the ventral forebrain (there is also expression in other parts of the body like the developing heart) (Figure 1A) (Klimova, Lachova et al. 2013). To confirm the spatial specificity of *Rx-Cre* mediated recombination, we crossed *Rx-Cre* mice with a *tdTomato* reporter line (Madisen, Zwingman et al. 2010). Using this reporter line, we confirmed that in the developing brain: Td tomato was visible in the rostro-ventral telencephalon from E10.5 to P1 (Figure 1A) in the VZ derived from previously recombined neuroepithelial cells, and also in the neurons derived from them.

We crossed this mouse line with one carrying a conditional allele for *Dicer1* (*Dicer^{F/F}*) in which exons 22 and 23 (encoding two RNaseIII domains) are flanked by loxP sites (Murchison, Partridge et al. 2005). The result of this cross is an *Rx-Cre; Dicer^{F/F}* mouse line, referred to as *Dicer* mutant or *Dicer* KO in this thesis (Figure 1B).

To confirm that Cre-mediated recombination eliminated *Dicer*'s 22 and 23 exons, we performed *in situ* hybridization of these *Dicer1* exons in control and *Dicer* mutant animals (Figure 1C). We used as a control, for this and all the following experiments, homozygous mice with floxed *Dicer* without *Rx-Cre* transgene (*Rx^{wt/wt}; Dicer^{F/F}*). In agreement with the TdTomato expression, we found that recombination of the *Dicer* locus occurred mainly in the rostro-ventral part of the telencephalon, especially in the rostral part of the neocortex (NCx), the primordium of the OB (pOB) (Figure 1D), the septum (Stm) and the basal ganglia (BG).

To confirm the loss of miRNAs upon *Rx-Cre* mediated ablation of functional *Dicer*, we tested the expression of the mature *miR-9* in *Rx-Cre; Dicer^{F/F}* mice at E12.5, as this is one of the highly expressed miRNAs in the developing vertebrate brain (Radhakrishnan and Alwin Prem Anand 2016). For this purpose, we performed *in situ* hybridization using locked-nucleic-acid-modified (LNA) probes commercially available.

Analysis of *miR-9* expression at E12.5 in the rostral telencephalon of WT embryos revealed the presence of this mature miRNA throughout the cortical wall (including VZ, SVZ and cortical plate) and in the primordium of the olfactory bulb (pOB) (Figure 1D). Consistent with the loss of *Dicer* upon *Cre* recombination that takes place especially in the rostro-ventral part of the telencephalon (Figure 1A), we found a reduction in the expression of *miR-9* in the primordium of the NCx (pNCx), together with a particularly dramatic reduction in the pOB (Figure 1D) and the BG. As *miR-9* is one of the most abundant miRNAs in the mouse brain, the reduction in its expression confirmed the reduction of functional *Dicer* in *Dicer* KO embryos.

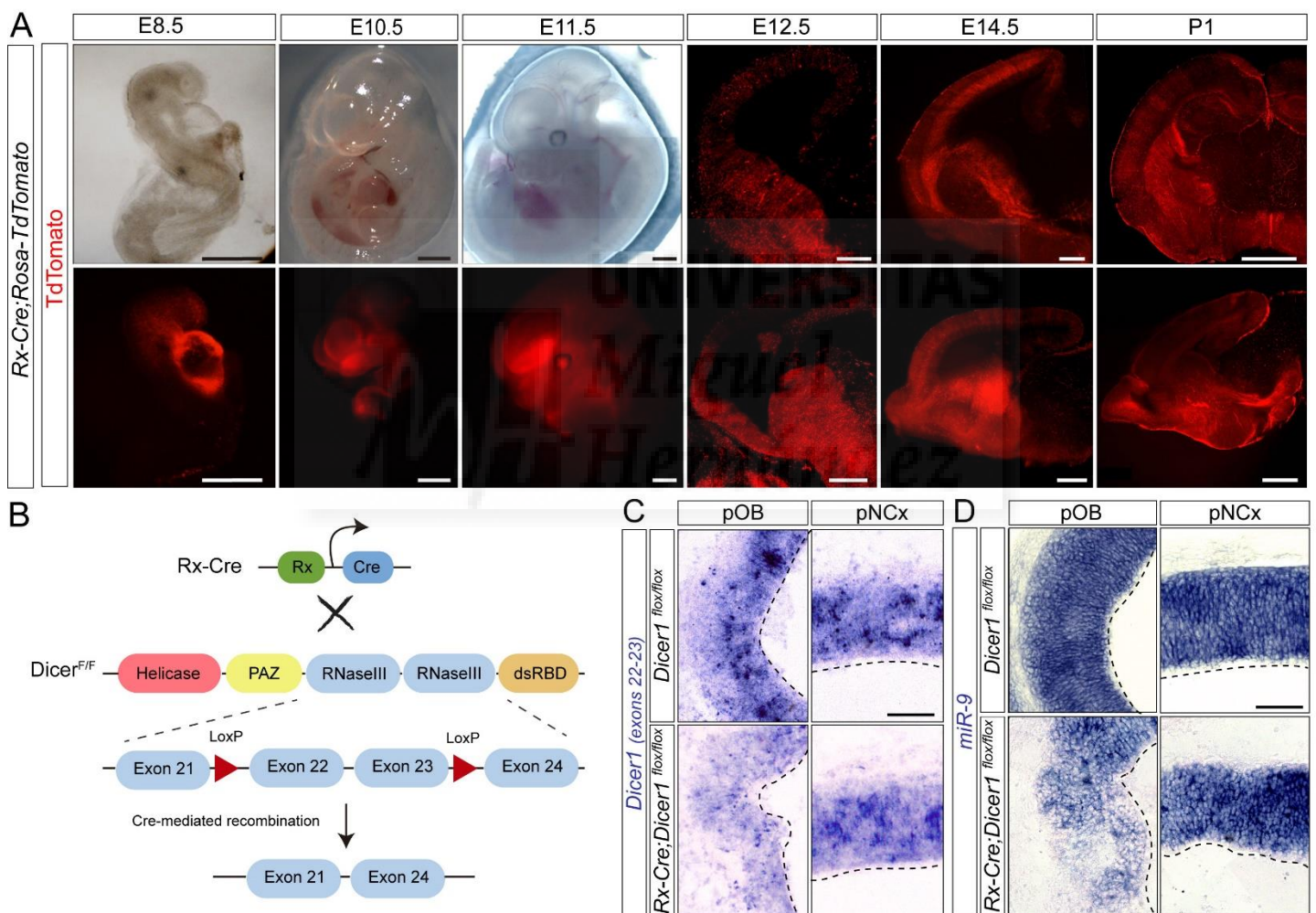


Figure 1. Generation and recombination of *Dicer* mutant mice. (A) Whole mount (E8.5-E11.5), coronal (E12.5-P1, upper panels) or sagittal sections ((E12.5-P1, bottom panels) showing tdTomato expression (in red) under the promoter of *Rx3*. (B) Schema showing the generation of the *Dicer* mutant mice. *Rx-Cre* mouse line with a 4-kb DNA fragment upstream of the *Rx3* gene driving *Cre* expression was crossed with *Dicer*^{F/F} line, in which the exons 22 and 23, the RNase III domains, are flanked by loxP sites. (C) Sagittal sections of WT and *Dicer* mutant animals at E12.5 showing the expression of *Dicer* exons 22-23, the ones ablated in our *Dicer* mutant. (D) Sagittal sections showing *in situ* hybridization of control and conditional *Dicer* knockout (*Rx-*

Cre; Dicer^{F/F}) embryos, using LNA antisense probes for *miR-9*, notice the dramatic reduction of *miR9* expression in the pOB of mutants. Scale bars, 500 μ m (E8.5-E11.5, **A**), 300 μ m (E12.5-E14.5, **A**), 1mm (P1, **A**); 100 μ m (**C**, **D**).

To investigate the necessity of miRNAs in the development of the telencephalon, we started analysing *Dicer* mutant brains at E17.5, just before they prematurely die at embryonic day 18.5. At E17.5 we found a reduction of the telencephalic volume in *Dicer*-ablated animals (Figure 2A, 2B) without changes in the lamination (Figure 2C). To determine the cause, we quantified the thickness of the whole cortical wall both including and excluding the cortical plate (Figure 2G). The result of this analysis showed that the reduction in the thickness of *Dicer* mutant's cortex is due to a reduction in the cortical plate but not in germinal layers. Accordingly, this reduction comes with a decrease in the thickness of the neuronal layer labelled with Tuj1 (Figure 2D). Despite of this, the lamination of the cortex was not altered at E17.5 (Figure 2C).

To understand the origin of this deficient abundance of neurons, we next investigated the amount of dividing progenitor cells. We didn't find differences in apical Radial Glia (aRG) mitoses (apical mitoses) at any age except at E12.5, where there is a slight reduction (Figure 2I). This decrease in apical mitoses temporally coincides with an increase in apoptosis (Figure 2J) which takes place between E11.5 and E13.5. After this period, levels of cell death decrease down to control and basal mitoses increase above WT levels (Figure 2H, 2J, 2M). Regarding the number of basal mitosis (defined as cells undergoing mitoses located 11 cell bodies away from the ventricular surface (Pilz, Shitamukai et al. 2013), we found a reduction on them at E13.5. Accordingly, we also found a slight reduction in the quantity of Tbr2 positive cells from E11.5 to E13.5 (Figure 2K, 2L), suggesting that, there is a reduction of IPCs at this stage. The increase in basal mitoses that we have observed, one day after (at E14.5) could be indicative of a compensatory mechanism in order to recover the number loss of progenitors.

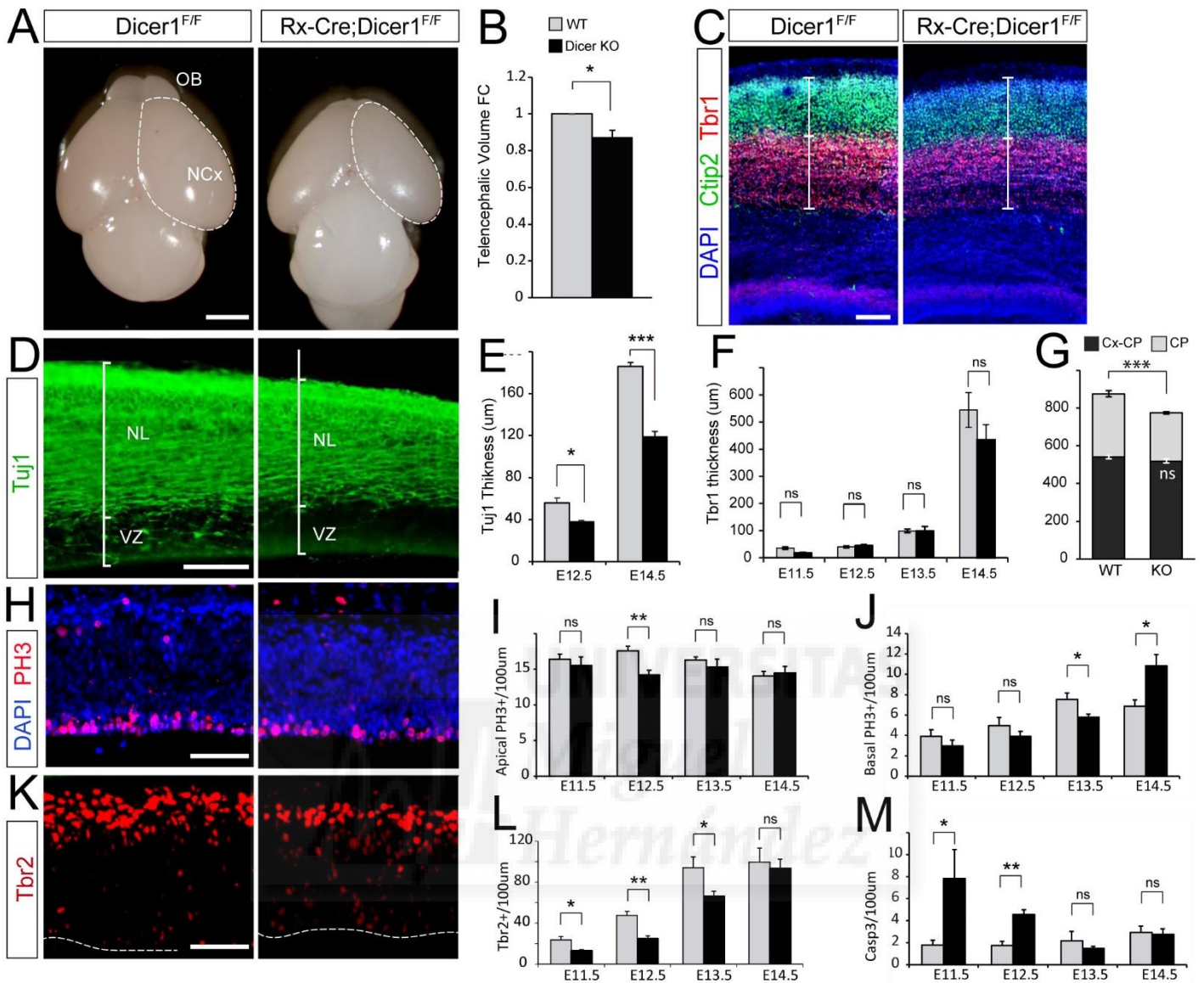


Figure 2. Cortical phenotype in *Dicer* mutant embryos. (A) Comparison of E17.5 brains of WT (left) and *Dicer* mutants (*Rx-Cre; Dicer^{F/F}*, right) littermate mice. Note the reduction of cerebral cortex (Cx) size and the virtual loss of olfactory bulbs (OB) in *Dicer* mutants. (B) Quantification of telencephalic volume in WT and in *Dicer* mutants showing a reduction of 15%. (C) Layer-specific markers of layer VI (*Tbr1*) and layer V (*Cux1*) at E17.5. (D) High magnification image of cerebral cortex from E14.5 WT and *Dicer* mutant embryos. (E) *Tuj1* thickness at the labelled age. (F) Quantification of the *Tbr1* positive cells layer. (G) Graphical representation of the whole cortical thickness with (white bars) or without (black bars) including the cortical plate. (H) High magnification of E12.5 cerebral cortex from both WT and *Dicer* mutant embryos, with labelled phospho-histone 3 (PH3, in red). (I) Quantification of apical PH3 positive cells. (J) Quantification of basal PH3 positive cells. (K) Immunolabeling of *Tbr2* positive cells at E12.5. (L) Quantification of *Tbr2* positive cells at indicated ages. (M) Quantification of Activated Caspase-3 at the indicated ages. All histograms show average \pm SEM. For all the quantifications: $n \geq 3$, t-test * $p < 0.05$, ** $p < 0.01$, *** $p < 0.001$. Scale bars, 1mm (A), 100 μ m (C, D, H, K).

Disorganization of rostro-ventral telencephalon and presence of rosettes

In addition to the reduction in cortical thickness and neurogenesis, at E17.5 we also found that *Dicer* KO embryos showed a strong reduction in the size of the olfactory bulb (Figure 3A-C), as revealed by DAPI staining of sagittal sections, consistent with previous observations (De Pietri Tonelli et al., 2008). To determine if the OB of *Dicer* mutants was properly structured, we performed *in situ* hybridization of *Grm1*, a marker of mitral cells, in E17.5 embryos (Figure 3B). We found that *Dicer* mutants had a smaller (Figure 3C) but well organised OB, in which mitral cells were located conforming a single layer like in a wild-type situation (Figure 3B).

Interestingly, in *Dicer* ablated embryos we found a dramatic structural disorganization of the rostro ventral part of the telencephalon: OB, septum and BG (Figure 3A, 3D, 3I). Moreover, we found an increase in the amount of progenitor cells identified by Ki67 immunoreactivity in the rostro-ventral telencephalon (Figure 3D). These progenitors were arranged forming rosette structures, composed by a ventricular-like cavity (sometimes collapsed by neurons) surrounded by progenitors that displayed apical and basal mitoses and basally to this progenitor layer there was a band of neurons (Figure 3E). *Dicer* mutants only had rosettes in the OB, the septum and basal ganglia, coincident with higher levels of *Cre*-mediated recombination (Figure 1A). These rosettes showed the same structure that those originated in three different scenarios: in *Lgl1*^{-/-} mice (Klezovitch et.al; 2003); in human primitive neuroectodermal tumours (neuroblastic rosettes) (Burger and Scheithauer 1994; Sanguenza et al. 1994; Graham and Lantos 2002) and in Embryonal Tumours with Multi-layered Rosettes (ETMR; (Phillips, Tihan et al. 2015).

In order to understand the 3D structure of *Dicer* KOs' rosettes, we then clarified whole E17.5 brains after Pax6 labelling (See Methods) (Figure 3F). At this developmental stage, the major part of rosettes were spheres located in the rostro-ventral part of the telencephalon, but we also found tubular rosettes with horizontal and vertical orientations. We further investigated whether *Dicer* ablation, in addition to increase the total number of progenitors, also affected the quantity of cycling-progenitors (Turrero García, Chang et al. 2016). In order to elucidate whether progenitor cells in rosettes were progressing through the cell cycle (synthesizing DNA) or they were arrested in other phase, we injected a single pulse of BrdU intraperitoneally to pregnant females 30 minutes before

fixation of the tissue, when embryos were E17.5. Then, the fraction of progenitor cells in S phase was determined by calculating the percentage of BrdU positive and Ki67 positive cells out of total Ki67 positive cells ($\text{BrdU}^+/\text{Ki67}^+$, Figure 3G). We found a significant increase in the percentage of neural progenitors that were cycling were in rosettes from *Dicer* KO animals compared with control cortical progenitors, indicating that upon the loss of miRNAs there is an increase in cycling progenitors (Figure 3H).

Then, we wanted to elucidate if progenitors from rosettes are undergoing self-amplifying divisions than control progenitors and thus, increasing the population of progenitors in detriment of neuronal production. For this purpose, we analysed the index of cell cycle re-entry ($\text{Ki67}^+ \text{BrdU}^+/\text{BrdU}^+$) in progenitors of control NCx and *Dicer* KO rosettes. The result of this experiment revealed a significant increase in the percentage of neural progenitors that re-entered the cell cycle in rosettes compared to controls, indicating that loss of miRNAs led to an increased progenitor self-amplification (Figure 3H). Together, these results suggest that functional *Dicer*, and therefore miRNAs, are important for controlling cell cycle progression of neural progenitors in the murine embryonic brain.

Dicer KO rosettes had a lumen in their centre. In order to determine whether this cavity exhibits features reassembling those of a telencephalic ventricle, we immunostained E14.5 rosettes for apical complex proteins like partitioning defective 3 (Par3; Figure 3J), and adherents junction proteins like β -Catenin (Figure 3L). We observed that *Dicer* rosettes fulfilled these features, including the presence of ciliated neuroepithelial cells surrounding the central lumen (Figure 3K), resembling multifocal ependymal rosettes found in human brain malformations (Saugier-Veber, Marguet et al. 2017). To investigate the regional identity of clustered progenitors forming rosettes, we analysed the expression of progenitor markers Pax6 and Tbr2 by immunolabeling. Pax6 is highest expressed in the pallium and in the pallial-subpallial boundary (Yun, Potter et al. 2001, Hébert and Fishell 2008). Tbr2 is a typical marker of intermediate progenitor cells in the telencephalic pallium (Bulfone, Martinez et al. 1999), but it is also expressed transiently in excitatory newborn neurons and in the glia-to intermediate progenitor transition (Englund, Fink et al. 2005). We found that pallial rosettes were positive for both Pax6 and Tbr2 and those in the subpallium were negative for both markers (Figure 3M). Moreover, trying to understand if rosettes maintained the identity of the specific area in which they are located, we analysed the expression of marker genes using *in situ*

hybridization (Figure 3N). Rosettes located in pallial regions exhibited pallial identity as confirmed by labelling for *Ngn2* (Cocas, Georgala et al. 2011) and *Pax6*. Regarding rosettes found in the subpallial area, all of them were positive for *Dlx2* (a pan-ventral marker), whereas negative for *Dlx5* (a ventral marker that is not found in the VZ of BG), indicating that these rosettes had ventral VZ identity. As expected, rosettes located in the MGE expressed its specific marker *Nkx2.1* (Waclaw, Wang et al. 2009). Surprisingly, when we studied the pattern of expression of *Gsx2* (a marker of ventricular and subventricular progenitors in the dLGE) we found that rosettes located in the putative SVZ of the dLGE were negative for *Gsx2*. At this stage in a control situation, progenitors from the most ventral part of the LGE will be *Gsx2* negative, forming the vLGE, and the ones placed in the dorsal LGE will highly express *Gsx2* promoting the production of dLGE fates, including olfactory bulb interneurons (Waclaw, Wang et al. 2009). Taken together, those results suggest that rosettes are not produced from progenitors derived from the dLGE.



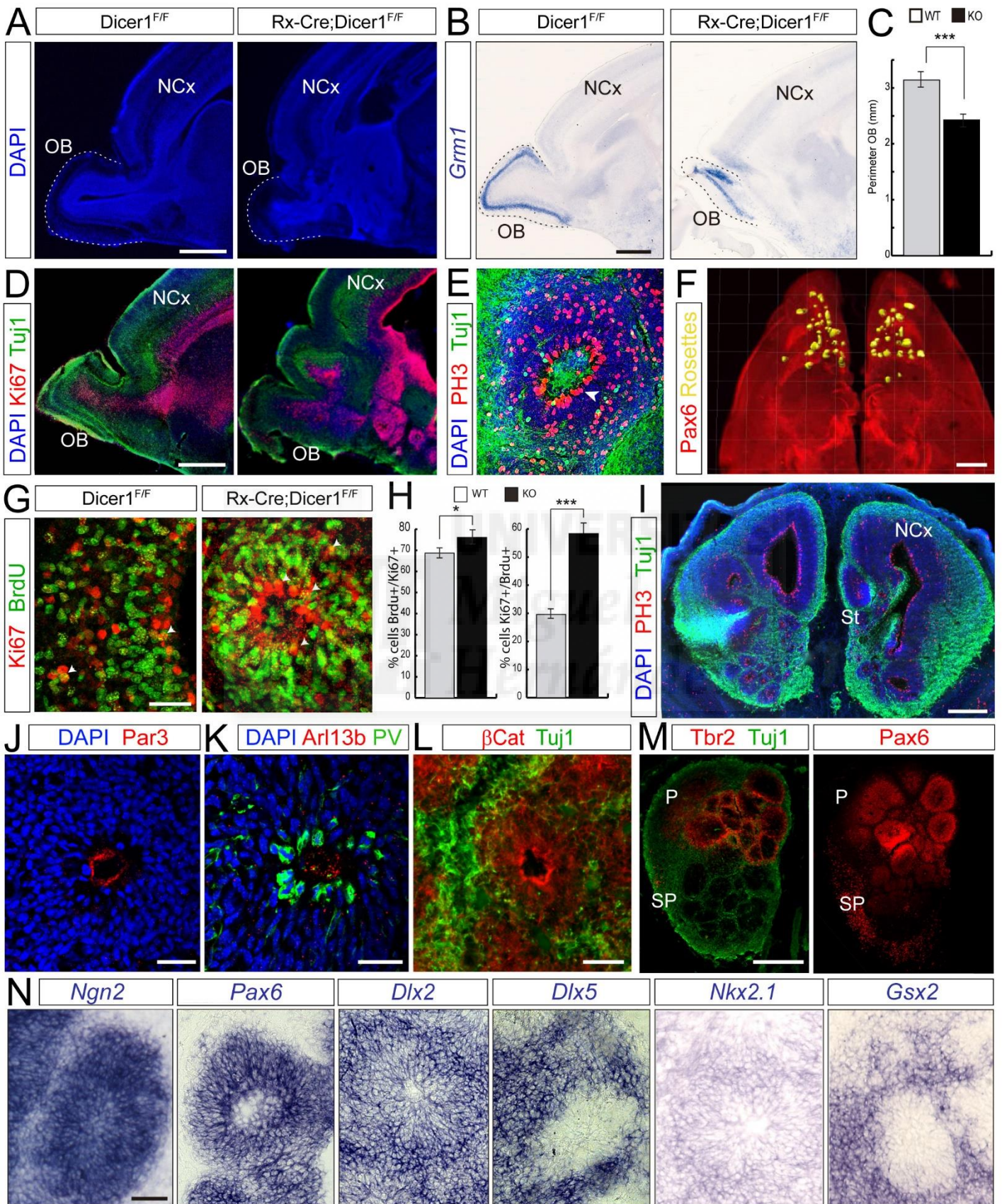


Figure 3. Rostral phenotype of *Dicer* mutants. Rosette characterization. (A) Comparison of E17.5 brains of control (left) and *Dicer* knockout (right) littermate mice using DAPI staining (blue) in a 40- μ m sagittal section, (B) In situ hybridization of *Grm1* in E17.5 control and *Dicer* KO embryos showing the perimeter of the OB (black dashed line) quantified in (C). (D) E17.5 brains of control (left) and *Dicer* KO (right) mice showing immunostaining for Ki67 (red), Tuj1 (green) and DAPI (blue). (E) Rosette from an E17.5 *Dicer* KO embryo, presenting both apical (white arrowheads) and basal (black arrowheads) mitoses labelled with PH3 (red) and neurons, as shown by Tuj1 immunostaining (green). (F) E17.5 brain from a *Dicer* KO immunostained for Pax6 (red) and clarified using iDISCO protocol. Yellow structures correspond to reconstructed rosettes. (G) E17.5 sections showing immunostaining for Ki67 (red) and BrdU (green). Analysis of % of S-phase progenitors comparing progenitors of rosettes with progenitors from the OB of WT E17.5 embryos (H, left). Cell cycle re-entry comparing progenitors of rosettes with progenitors from the OB of WT E17.5 embryos (H, right). (I) Coronal section from an E14.5 *Dicer* KO embryo showing immunostaining for PH3 (red), Tuj1 (green) and DAPI (blue). (J) Rosette from E14.5 *Dicer* KO embryo with apical junction proteins in its centre (Par3, in red). (K) Evidence of RGC (labelled with PV in green) forming rosettes with cilia (Arl13b in red) in an E14.5 *Dicer* KO embryo. (L) High magnification of an immunostaining for β -catenin (red) and Tuj1 (green) in an E14.5 *Dicer* mutant. (M) Low magnification of coronal sections from E14.5 *Dicer* KO rostral part of the brain showing immunostaining for: In the left: Tbr2 (red) and Tuj1 (green) and in the right: Pax6 (red). (N) High magnifications of rosettes from E14.5 *Dicer* KO mice, showing ISH of the indicated genes. All histograms show average \pm SEM. For all the quantifications: $n \geq 3$, t-test * $p < 0.05$, ** $p < 0.01$, *** $p < 0.001$. Scale bars, 500 μ m (A-F), 25 μ m (G, J, K, L, N), 200 μ m (I, M).

Rosette types and their distribution across time and space

Dicer mutants showed three different types of rosettes at E14.5 (Figure 4A, 4B), that we have characterized as: Type 1 rosettes, small invaginations of the ventricular surface, frequently surrounded by neurons going through the thickness of the tissue and ending in the line of the ventricle; Type 2 rosettes, the invagination became more pronounced but the lumen of the ventricle was still connected to the lumen of the rosette. In this type of rosette, the neuronal surrounding was much more obvious. Type 3 rosettes, closed structures without a connexion with the ventricle. (Figure 4B). These three different types of rosettes exhibited different temporal distribution along development. For instance, at E17.5 *Dicer* KO embryos mainly showed Type 3 rosettes (Figure 4C). When we analysed the presence of rosettes earlier in development (E14.5), we noticed that the prevalence of Type 3 was lower, at the same time that we began identifying more Type 2 and Type 1 rosettes. Curiously, going even earlier in development (E12.5) we found a high prevalence of Type 1, a small proportion of Type 2 rosettes and a total absence of Type 3 rosettes (Figure 4C). The differential distribution along development suggested that these three different types of rosettes were three phases of maturation. Type 1 is in fact Phase 1 rosette, the first sign of rosette formation. This develops into a more invaginated

rosette (Type/Phase 2) until finally detach from the ventricle producing a mature Type/Phase 3 rosette (Figure 4B).

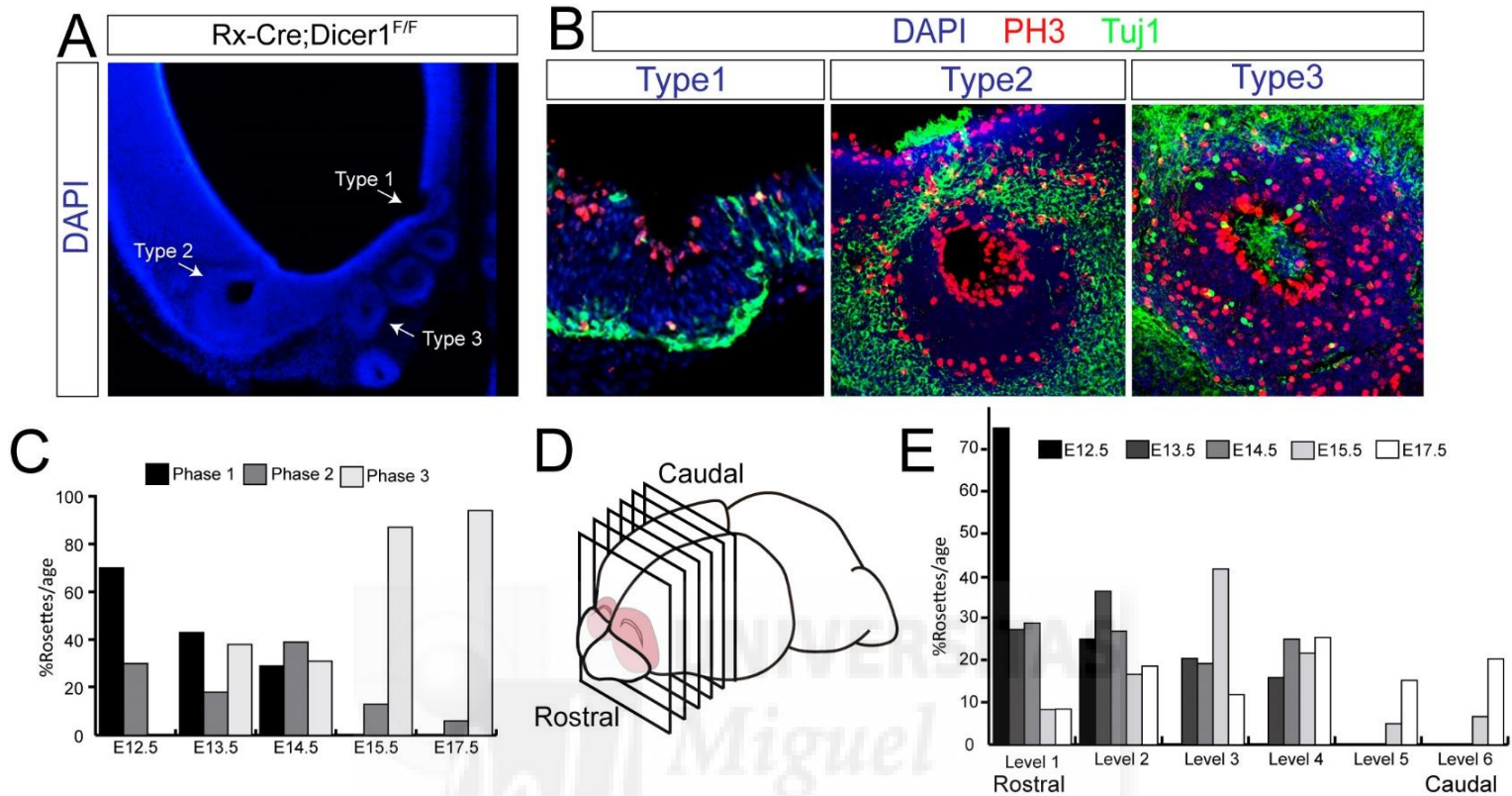


Figure 4. Rosette formation and their differential temporal and physical distribution. (A) DAPI staining of 40 μm coronal section of E14.5 *Dicer* KO. Note the presence of Type1, 2 and 3 rosettes in the ventral telencephalon. (B) Immunofluorescence microscopy of 20 μm coronal cryosections of the ventral telencephalon from *Dicer* KO animals (E12.5, left; E14.5, centre; E17.5 right) showing DAPI (blue), PH3 (red) and Tuj1 (green) immunostaining. (C) Differential distribution of different rosette phases through the development. (D) Sampling strategy for *Dicer* KO analyses. Brains were divided into six equidistant bins, and the percentages of rosettes appearing in each bin was determined. (E) Percentage of rosettes found in each level for a given age. Data is shown as the mean of the percentage of rosettes in each level and/or age. At least 2 complete brains were analysed for each age.

The fact that the formation of rosettes takes place following a rostro-caudal gradient, prompt us to quantify the spatial distribution of rosettes. We divided the rostro-caudal axis of the rostral half of the brain in consecutive levels, being level 1 the most rostral and level 6 the most caudal (Figure 4D) and then quantified the different phases of rosette in each level. We performed this measurement at different times during development and found that Phase 1 rosettes appeared first at E12.5 in the most rostral levels, but later in the development we could find Phase 1 rosettes progressively more

caudally. This result suggests that the first place in which rosettes are formed is the rostral part of the telencephalon. Interestingly, at later stages (E15.5 and E17.5) we found Phase 3 rosettes in the most caudal levels (5 and 6), where we had never observed phase 1 rosettes at previous stages of development, suggesting that some of the rosettes that were generated rostrally, were able to grow in the horizontal plane, and end in more caudal positions.

miRNA depletion causes alterations in proliferation and apoptosis

As *Dicer* ablation resulted in the formation of rosettes and a reduction in the OB perimeter, we first decided to investigate whether this phenotype was related to a defect in proliferation or neurogenesis at early stages during development. In order to address that question, we quantified mitotic figures as identified by immunostaining for phosphohistone H3 (Figure 5A, 5B). This showed that the relative abundance of mitotic apical progenitors was unaltered in the primordium of the OB from *Dicer* KO embryos between E10.5 and E13.5 (Figure 5B, top graph). Interestingly, analysis of the relative abundance of basal mitosis showed that at E12.5 there is an increase in basal proliferation (Figure 5B, lower graph). As we didn't find a decrease in the total number of cells undergoing mitoses, but a slight increase in density of basal mitoses, we concluded that the reduction in the perimeter of the OB (Figure 3C) is not due to a reduction in neurogenesis.

Thus, we hypothesized that the rostral phenotype may be caused by increased apoptosis. Supporting this idea, several *in vitro* and *in vivo* studies have demonstrated the role of miRNAs as both proapoptotic and antiapoptotic factors (Mott, Kobayashi et al. 2007, Raver-Shapira, Marciano et al. 2007, Davis, Cuellar et al. 2008). In order to address that question, we performed analysis of the rostro-ventral telencephalon by immunofluorescence for activated Caspase 3 (Figure 5C-G). These results showed that miRNA ablation produced a dramatic increase in apoptosis, observed in a short time window from E11.5 until its maximum at E12.5, when the whole thickness of the tissue was full of cells undergoing apoptosis (Figure 5D), this has been previously reported in other *Dicer* KO models (Swahari, Nakamura et al. 2016, Chmielarz, Konovalova et al. 2017). Interestingly, the occurrence of apoptotic events always started at E11.5 following

a columnar pattern. Between these columns of cells dying, non-apoptotic cells started forming ventricular invaginations (Figure 5C).

Given the massive increase in cell death in *Dicer* KO embryos, and that at E11.5 the vast majority of cells populating the telencephalic wall are progenitors, we wanted to investigate if progenitors were undergoing apoptosis after *Dicer* ablation. To confirm that, we examined in one hand the coexpression of activated Caspase 3 and Pax6, in order to know how many apoptotic cells were progenitors; in the other, we studied the coexpression of activated Caspase 3 and Tbr1, to see if they were also neurons undergoing apoptosis (Figure 5E, 5F). We found that, at E11.5, the majority of apoptotic cells were progenitors (68.33 ± 9.34 % Caspase3 positive cells), but there was also a fraction of dying neurons (8.71 ± 4.53 % Caspase3 positive cells; Figure 5G).

Taken together the analyses of both apoptosis and proliferation, these results suggested that despite we only found a slight increase in the relative number of proliferative cells, as the major part of the OB cells at E12.5 are undergoing apoptosis, the cells that remain alive must be proliferating more in order to maintain the number of mitoses at WT levels; otherwise, the proportion of dividing cells would be reduced in a tissue with such a dramatic increase in cell death. Thus, loss of miRNAs at early stages produced an increase in cell death both in progenitors and in neurons, being this effect more pronounced in progenitors. Then, the increase in cell death was followed by an increase in proliferation that finally maintained the number of proliferating cells.

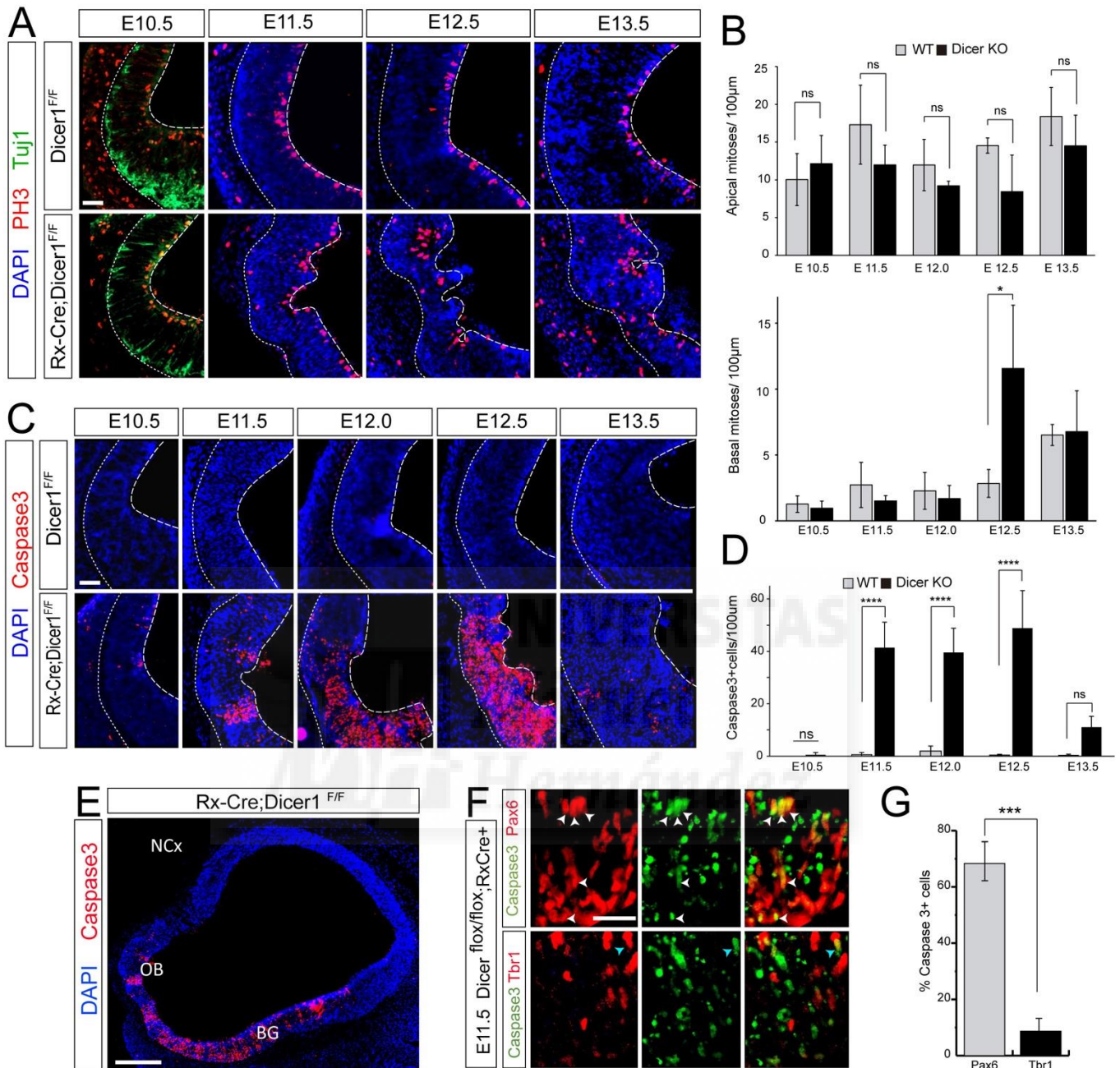


Figure 5. Loss of miRNAs results in increased apoptosis and proliferation. (A,C) High magnification images of the OB in control and Dicer KO embryos at the indicated ages immunostained for the indicated markers, and (B,D) quantifications. Mitoses (PH3+ cells) were distinguished as apical (top graph) and basal (bottom graph). (E) Low magnification from an E11.5 Dicer KO embryo immunostained for activated Caspase 3 (red) and DAPI (blue). Note the columnar pattern in which apoptosis appears. (F) Confocal microscopy (images of single optical sections) of sagittal sections of the OB stained for activated Caspase 3 (green) and Pax6 (red, top panels) or Tbr1 (red, bottom panels). (G) Quantification of double stained cells. Data are the mean \pm SE from 3 or more embryos, bars indicate S.E. *P<0.05, **P<0.01, ***P<0.005, ****P<0.001 Scale bars, 25µm (A, C), 200µm (E), 20µm (F).

Loss of miRNA leads to apical junction belt disruption and neuronal delocalization

We then investigated whether *Dicer* ablation affected neuronal migration. For this purpose, we analysed the distribution of Tuj1 positive cells through the thickness of the developing OB (Figure 6A). We found that in *Dicer* KO animals neurons were delocalized at E11.5, and then (E12.0 and E12.5) the delocalization began to be much more dramatic (Figure 6A). Interestingly, at E12.0 there were groups of neurons that were localized in the ventricular lining or even inside the ventricle (Figure 6A), forming heterotopias. These heterotopias grew during development, suggesting that the degree of disorganization increases during development in the absence of miRNAs.

The appearance of neuronal heterotopias in *Dicer* KO embryos coincided with the maximum of apoptosis in the OB, thus, we wanted to investigate whether cell death could lead to altered apical junctions, promoting neuronal delocalization. Comparison of apical junction proteins of control and *Dicer* mutant embryos identified by immunostaining for Par3 (Figure 6B) revealed that neuronal intrusions in the ventricle were coincident with areas with disrupted apical junction complex. Considering these observations, in the absence of miRNAs at early stages of neurogenesis (E11.5–12.5), an increase in cell death occurred concomitant with a loss in apical junction proteins in areas where neurons were misslocalized forming neuronal heterotopias. Intriguingly, these alterations took place without decreasing apical proliferation and with an increase in basal mitoses. Taking together, these results we postulated that in a tissue with high rate of proliferation, heterotopias could act as physical barriers preventing the lateral expansion of the ventricle and promoting the formation of rosettes.

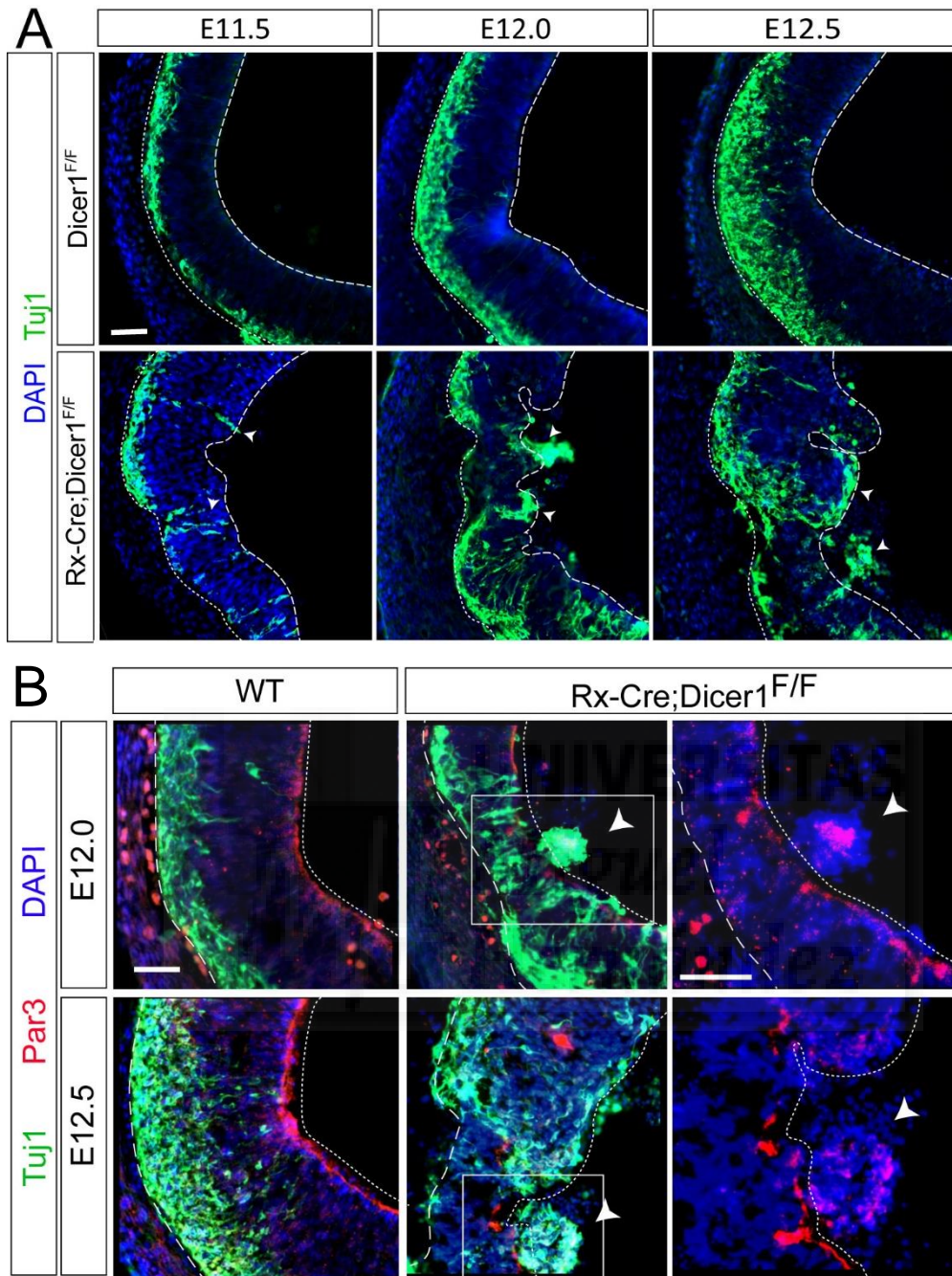


Figure 6. *Dicer* ablation causes neuronal delocalization and disruption of the apical junction belt. (A) Immunofluorescence microscopy of 20- μ m sagittal cryosections showing a high magnification of the OB of control and conditional *Dicer* KO at indicated age showing Tuj1 (green) and DAPI (blue). Note the presence of neurons close to the ventricle in *Dicer* mutant embryos. (B) Immunofluorescence microscopy of 20- μ m sagittal cryosections showing a high magnification of the OB of control and conditional *Dicer* KO at E12.0 and E12.5 showing Tuj1 (green), Par3 (red) and DAPI (blue), right images are high magnifications of the boxes from *Dicer* KO. Note neuronal intrusions inside of the ventricle (white arrowhead).

Differentially expressed genes in miRNA-depleted animals

Next, we studied the transcriptional mechanisms underlying rosette formation in the rostro-caudal part Dicer KO telencephalon. Given that *Dicer* mutants started showing neuronal, apical junction and apoptotic alterations at E11.5, we decided to analyse changes in the transcriptome of the OB at this stage. We dissected the primordium of the OB from control and *Dicer* KO animals in order to perform then RNA-Seq analysis of both protein coding and protein non-coding genes.

RNA-Seq results of protein-coding genes showed that 230 genes were differentially expressed (DEGs) in *Dicer* KO as compared to control and OBs (Figure 7A). In order to identify the main biological processes affected by these DEGs, we performed a gene ontology analysis using the web-based DAVID v6.7 software. The categories most highly affected were cell migration, regulation of apoptosis, homeobox, metabolic processes and increase of apoptosis (Figure 7B). Among these, we found several DEGs that were related to p53 (also known as Trp53inp). Under normal conditions, p53 is expressed at an extremely low level but upon DNA damage, post-translational modifications as acetylation and phosphorylation convert p53 from a latent to an active form promoting its accumulation in the cell nucleus (Siliciano, Canman et al. 1997). Activated p53 transactivates a set of target genes that lead to cell cycle arrest and/or apoptosis, depending on the severity of DNA damage. Some of the DEGs related with the p53 pathway were: *Trp53inp*, *Itgb1*, *Igfr2r*, *Pten*, *Ddx3x*, *Zmat3* and *Rest* (Okamura, Arakawa et al. 2001, Iwamoto 2002, Freeman, Li et al. 2003, Sun, Zhou et al. 2013, Bersani, Xu et al. 2014, Nechiporuk, McGann et al. 2016, Laudato, Patil et al. 2017) (Figure 7C).

Due to the proliferative nature of rosettes found in *Dicer* KO embryos, we also focused in DEGs that positively regulate cell proliferation: *Shh*, *Tnfrsf1b*, *Irs2*, *Polr3g*, *Csf1r*, *Purb*, *Lrp2*, *Ccng1*, *Klhl42*, *Kif23*, *Zfyve26*, *Cnot6l*, *Lyn*, *Col18a1*, *Itgb1*, *Hcls1* and *Ctgf* (Erickson, de Sauvage et al. 1994, Shimo, Nakanishi et al. 1999, O'Laughlin-Bunner, Radosevic et al. 2001, Gritli-Linde, Bei et al. 2002, Aslam, Mittal et al. 2009, Sipola, Seppinen et al. 2009, Mercier, Bachvarova et al. 2011, Wong, Pollan et al. 2011, Takahashi, Fusaki et al. 2012, Dhanoa, Cogliati et al. 2013, Habif, Grasset et al. 2013, Liu, Gao et al. 2013, Andersen, Hammer et al. 2015, Cheng, Jutooru et al. 2015, Olmos-Alonso, Schetters et al. 2016, Stamateris, Sharma et al. 2016, Peuhu, Salomaa et al. 2017) (Figure 7D).

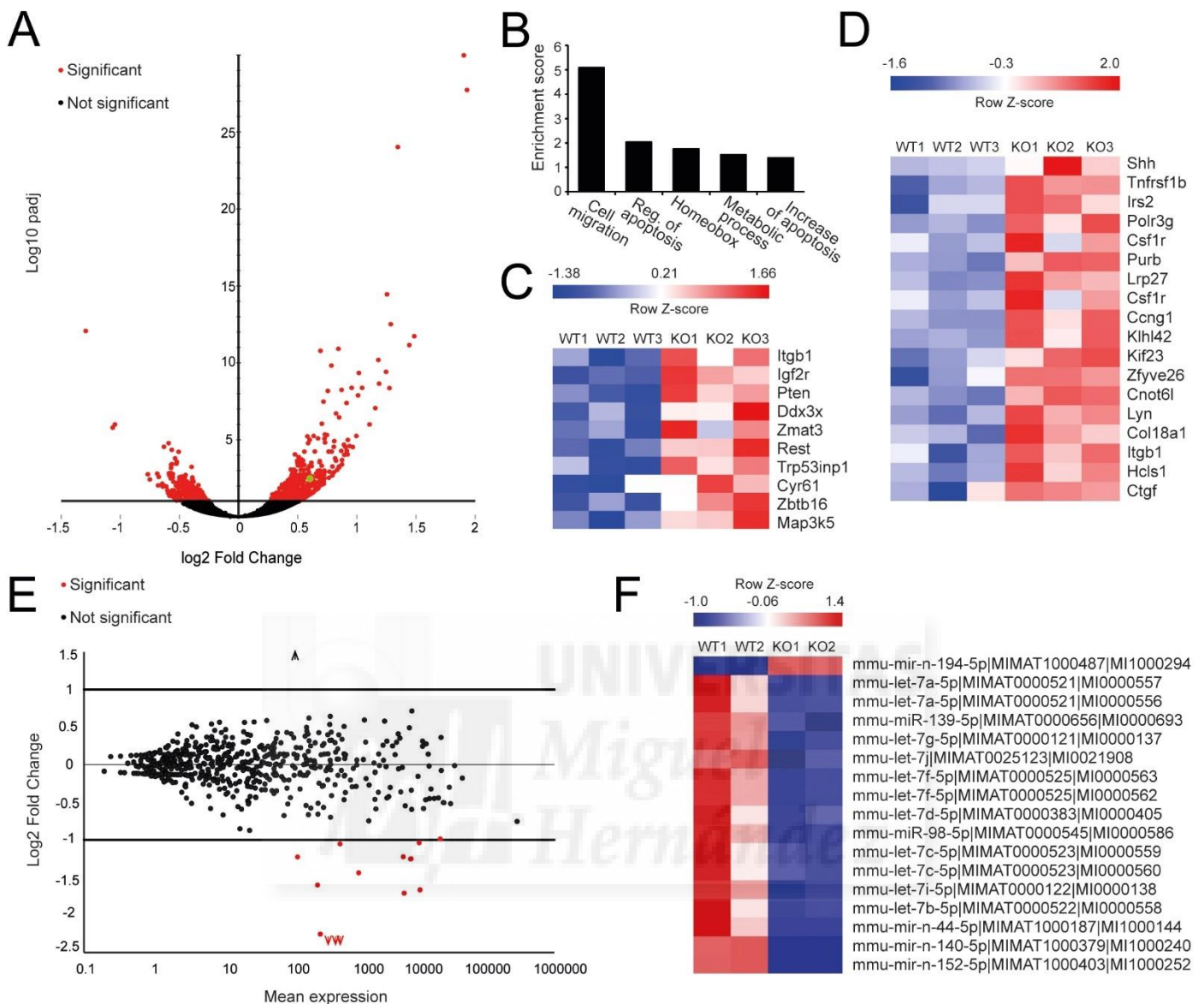


Figure 7. Coding and non-coding RNAs changed in *Dicer* KOs. (A) Volcano plot showing the log₂Fold Change vs between WT and *Dicer* KO OB. 230 genes were differentially expressed (red dots). Differentially expressed genes were determined by unequal variance Student's t-test followed by Benjamini-Hochberg correction ($p < 0.01$). (B) Barr graph of significantly enriched gene ontology terms associated with DEGs between WT animals and *Dicer* mutants. Heatmaps of genes related with p53 cascade (C) or proliferation (D) generated from a subset extracted from the list of differentially expressed genes (Table1). Columns represent individual arrays, while rows represent specific genes of interest. Z-score for a gene in a given sample represents its deviation from the mean expression of the gene across all samples (row) in terms of its standard variation, with red indicating upregulation and blue downregulation. (E) Differential expression of miRNAs among WT and *Dicer* KO OB. Seq-normalized mean expression (x axis; log₁₀ scale) and fold changes (y axis; log₂ values) of differentially expressed (red) or unchanged (black) miRNAs are indicated. Points out of the graph are indicated by a red arrow (*mmu-mir-n-140-5p*, log₂FoldChange=-6.9, mean expression= 541.625; *mmu-mir-n-152-5p*, log₂FoldChange=-6.9, mean expression= 541.95; *mmu-mir-n-44-5p*, log₂FoldChange=-5.5, mean expression= 398.35; *mmu-mir-n-194-5p*, log₂FoldChange=5.0, mean expression: 116.025). (F) Heatmap of miRNAs. Columns represent individual arrays, while rows represent specific miRNAs of interest. Z-score

for a miRNA in a given sample represents its deviation from the mean expression of the miRNA across all samples (row) in terms of its standard variation, with red indicating upregulation and blue downregulation.

RNA-Seq results for non-protein-coding genes showed a decrease of 13 mature miRNAs and a tendency to increase in one (Figure 7E, 7F). The vast majority of downregulated miRNAs (8 out of 13) were members of the *let-7* family (Roush and Slack 2008). This is an extensively studied family of miRNAs due to the fact that their expression is down-regulated in various cancers (Johnson, Grosshans et al. 2005). It has been previously described that members of *let-7* family could regulate in a loop manner p53 (Hau, Ceppi et al. 2012, Jian Liu 2016) and there are also in charge of regulating cell proliferation and tumorigenicity (Yu, Yao et al. 2007, Duldulao, Lee et al. 2011, Suh, Remillard et al. 2012, Wang, Cao et al. 2012). These two processes regulated by *let-7* family (cell proliferation and cell death) beautifully coincided with those altered in *Dicer* KO animals.

Surprisingly we found a new miRNA that exhibit a tendency of being upregulated: *mir-n-194-5p*, the mature sequence of which is: AGUGUGCUUGGAAUAAAA. Unfortunately, the number of reads of this miRNA was too low to perform the adjusted p value, so it is not statistically upregulated in *Dicer* KO animals. Moreover, we found another three novel miRNAs that were statistically downregulated in upon *Dicer* ablation: *mir-n-44-5p*, *mir-n-140-5p*; and *mir-n-152-5p*. (Methods Table 2; and Figure 8). The predicted secondary structure of the precursors of these novel miRNAs (Figure 8 A-D) was obtained using *RNAstructure* software (Reuter & Mathews, 2010). Surprisingly, some of them had a complexity higher-than-expected compared with the typical pre-miRNA structure. Nevertheless, some studies show that miRNA precursors sometimes have complex secondary structures, as for example multiple star duplexes or multiple hairpin loops (Rother and Meister 2011, Evers, Huttner et al. 2015). With the help of the online Software TargetScanCostume we were able to know the putative targets of these novel miRNAs (*Supplementary material, Tables 1-4*). Moreover, performing gene ontology analysis we found that these miRNAs target genes were related with metabolism control, DNA binding and organ grow (Figure 8E), indicating that their future study could be useful in order to understand how homeostasis is regulated at early stages of development.

Taken together, those findings indicate that miRNAs members of the *let-7* family together with the tree novel miRNAs: *mir-n-44-5p*, *mir-n-140-5p*, and *mir-n-152-5p* were highly expressed miRNAs in the rostral telencephalon at E11.5. Their dramatic reduction in *Dicer* KO embryos suggest that presumably they play an important role in rosette generation. Moreover, the discovery of a new miRNA that showed a tendency of being upregulated under *Dicer* ablation suggested that the non-canonical pathway of miRNA generation could be positively regulated under of loss of *Dicer* conditions.

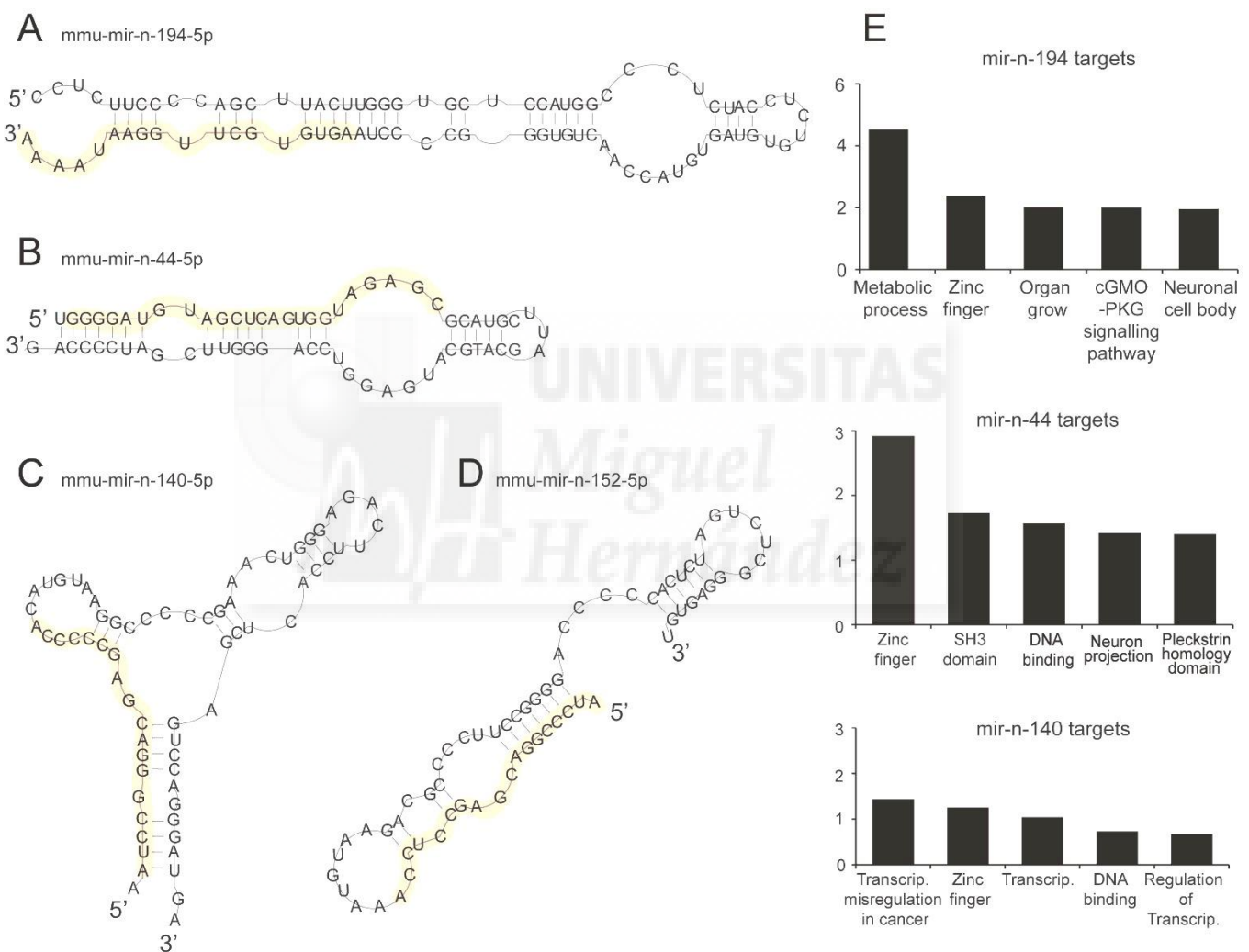
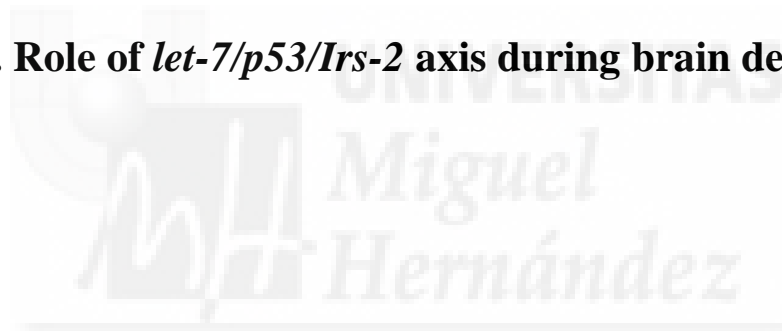


Figure 8. Novel miRNAs found in *Dicer* mutants at E11.5. Predicted secondary structure of miRNA-n-194-5p (A) *miRNA-n-44-5p* (B), miRNA-n-140-5p (C) and miRNA-n-152-5p (D) with the mature sequence labelled in orange. (E) Barr graph of significantly enriched gene ontology terms associated with putative target genes of each miRNA. The generation of the predicted secondary structure was performed using **RNAstructure** software (Reuter and Mathews 2010).

Part2. Role of *let-7/p53/Irs-2* axis during brain development



p53 is required for rosette formation in Dicer ablated embryos

One of the first observed phenotypes in *Dicer* KO embryos was a massive increase in cell death at early stages of development (Figure 5C, 5D). Accordingly, at E11.5 there was an increase in the transcription of genes related with the p53 cascade (Figure 7B, 7C). These results suggest that in *Dicer* ablated embryos could be an increase in p53, which is known to regulate *let-7* (Li, Jones et al. 2014, Subramanian, Francis et al. 2014), the miRNA family down-expressed in *Dicer* KOs. Interestingly, it has been suggested that *let-7* can also regulate p53 in a loop-manner (Hau, Ceppi et al. 2012, Jian Liu 2016). To test if the activated form of p53 is increased in *Dicer* KOs, we performed immunostaining for the activated form of p53: phospho-p53 (Siliciano, Canman et al. 1997) (Figure 9B), finding that there is a dramatic increase in the activated form after the loss of miRNAs. To further understand if cell death, particularly the one produced by an activation of *p53* cascade, was responsible of the OB reduction and the rosette formation in *Dicer* KO embryos, we eliminated functional *p53* in *Dicer* KO embryos (*p53;DicerKO*, Figure 9A). As expected, the analysis at E12.5 of the rostral telencephalon of *p53;DicerKO* embryos revealed a dramatic reduction in apoptosis compared with *Dicer* KOs (Figure 9C-9E'). This reduction in cell death was not equal in all double mutants, the 40% of the analysed embryos showed near absence of cell death as in WT embryos but there were a 60% in which the reduction in apoptotic events was partial. We next investigated whether in *Dicer* absent conditions, the reduction of the massive apoptosis could also suppress the phenotype of neuronal delocalization and apical junction disruptions observed in *Dicer* KO embryos at E12.5. In other words, if cell death *per se* was responsible of the early phenotypes that we found in *Dicer* mutants. In order to address that question we performed immunostaining for Tuj1 and Par3 in *p53;Dicer* KO embryos at E12.5 (Figure 9I and 9J), which confirmed that the neuronal delocalization was at least partially rescued and the apical junction belt was maintained, without visible disruptions.

Given the rescue of the early phenotype in *Dicer* KO animals with impaired *p53*, we studied the presence of rosettes at E17.5 in these animals. Surprisingly, we found that 80% of *p53;Dicer* KO animals (4 out of 5) didn't showed any rosette. These results suggested that, directly or indirectly, the activation of the *p53* cascade at early stages during development was necessary for the formation of rosettes and for the reduction of the OB in a niche without functional *Dicer*.

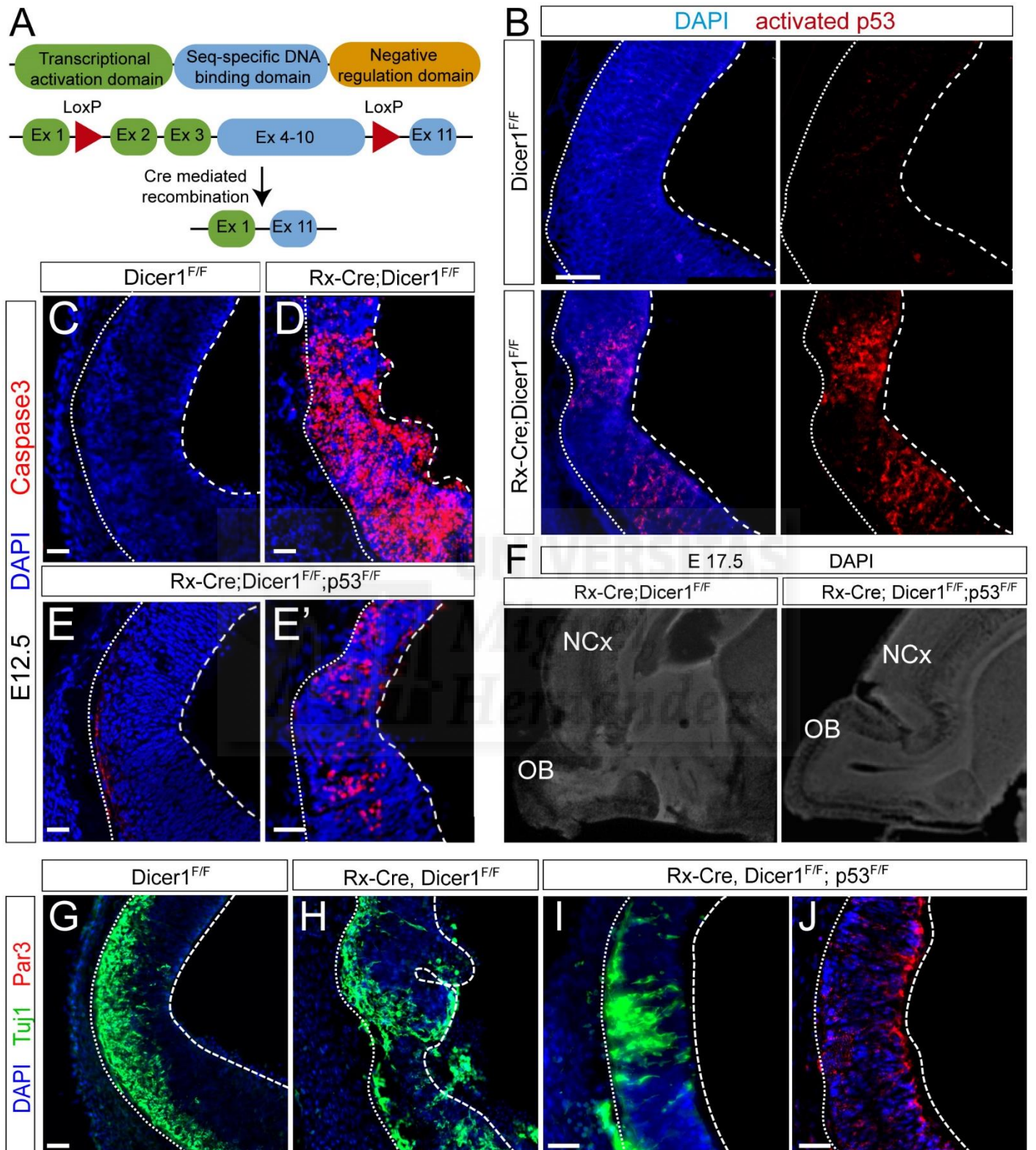


Figure 9. Loss of functional *p53* in *Dicer* KO animals impairs rosette formation. (A) Schematic representation of the *p53* gene with LoxP sites shown like red arrows and the Cre-mediated recombination resulting in the excision of Exons 2-10. (B) Sagittal cryosections showing the rostral telencephalon of WT and *Dicer* KO embryos immunostained for activated

p53. (C-E) High magnification images of the OB in control, *Dicer* KO and double mutant embryos at the indicated ages immunostained for activated Caspase3 (F) Sagittal sections of E17.5 *Dicer* KO (right) and *p53*; *Dicer* KO (left) embryos stained with DAPI (grey). (G-I) Sagittal sections of the pOB at E12.5 from WT (G), *Rx-Cre*; *Dicer*^{F/F} (H) and *Rx-Cre*; *Dicer*^{F/F}; *p*; *53*^{F/F} (I) sagittal sections with immunostaining for Tuj1 (green) and DAPI (blue). The line with stripes is indicating the ventricular surface and the dotted line indicates the basal membrane of the cortex. (J) Sagittal sections of the pOB at E12.5 from a *Rx-Cre*; *Dicer*^{F/F}; *p*; *53*^{F/F} embryo showing the apical junction complex protein Par3 (red) and DAPI (blue). Note the absence of neuronal heterotopias and Par3 disruptions in double mutant animals. Scale bars, 50µm (B), 500 µm (F), 25µm (C, D, E, G, H, I, J).

Overexpression of Irs-2 promotes rosette formation

Dicer KO embryos showed a dramatic increase in proliferation, as showed by the presence of rosettes and also by the increase in basal mitoses at early stages of development (Figure 5B), this was correlated with an increment in the expression of proliferative-promoting genes at E11.5 (Figure 7D). Notwithstanding, as previously shown, in the absence of activated p53 the phenotypes of neural heterotopias and rosette formation in *Dicer* KO embryos were rescued (Figure 9D-9E). Hence, we asked whether *p53* was acting directly or indirectly as a proliferation enhancer. This apparent contradiction has been previously reported, showing that an increase in apoptosis could drive proliferation and tumour formation under certain circumstances (Labi and Erlacher 2015).

To further elucidate if rosettes may be formed by an increase in proliferation due to the increased levels of proliferative genes, we decided to search for DEG in *Dicer* KO embryos that promote proliferation and are under the regulation of *let-7* (See target prediction in Methods). From these genes, we selected the ones that could be also regulated by stress signals like those released in a niche with an increase in apoptosis. We only found one gene fulfilling these features: *Insuline Receptor Substrate-2 (Irs-2)* (Udelhoven, Leaser et al. 2010)). We decided to study whether overexpression (OE) of *Irs-2* could recapitulate the *Dicer* KO phenotype. Using IUE (see Methods) we acutely overexpressed *Irs-2* in wild-type embryos (Figure 10H). We were able to follow the electroporated cells thanks to the coelectroporation with a GFP expressing plasmid. Two days after IUE with the *Irs-2* OE plasmid (E14.5), we observed the presence of neuronal heterotopias in the rostral telencephalon (n=7, Figure 10B). Moreover, we found that in the OE condition there were rosette-like structures with apical and basal mitosis and neurons surrounding the progenitor band (Figure 10E). Finally, the presence of apical

junction proteins in the rosette-like structures was analysed in order to determine if these structures could be generated from invaginations of the ventricle, as we postulated that occurs in *Dicer* KO animals. In full agreement with the phenotype observed upon ablation of functional *Dicer*, rosette-like structures found in the OE condition had Par3 proteins in their centre (Figure 10G, 10G'). These structures were also visible at E17.5 (five days after electroporation) in the white matter of some embryos (2 out of 5) (Figure 10F). These results suggested that increasing the proliferation by acute overexpression of *Irs-2* is sufficient to promote the formation of rosettes.

Given that *let-7* downregulates *Irs-2* (Zhu, Shyh-Chang et al. 2011, Gao, Wang et al. 2014), we wanted to elucidate if the acute loss of *let-7* in WT embryos could recapitulate the phenotype observed in *Irs-2* OE experiments. For this purpose, we designed a Tough Decoy for *let-7* (TuD *let-7*), which we validated as downregulating *let-7* expression (Figure 10H). We coelectroporated TuD *let-7* with GFP at E12.5 and analysed the electroporated brains two days after the surgery (Figure 10C). We found that a decrease in *let-7* also promotes the formation of hyperproliferative rosettes, recapitulating the phenotype that takes place in *Dicer* KO and in *Irs-2* OE embryos.

Finally, we wanted to investigate if the formation of rosette-like structures by overexpression of *Irs-2* could be rescued by increasing *let-7*. In order to address that question, we coelectroporated *Irs-2* together with a mix of mature *let-7* miRNAs (*let-7a-5p*, *let-7b-5p* and *let-7c-5p*) (Figure 10D) which were statistically downregulated in *Dicer* KO embryos. We observed that under this condition no rosettes were formed two days after electroporation.

Taking into account the results of this and the previous sections, we postulate that at early stages of brain development, the loss of functional *Dicer* produces a dramatic reduction in *let-7* expression, leading to the upregulation of both *p53* and *Irs-2*. The increase in *p53* under these conditions increases the repression of *let-7* (in a loop-manner (Jones and Lal 2012)) and promotes a massive increase in apoptotic events which leads to the liberation of stress signalling molecules possibly including metabolites and pro-inflammatory molecules. These effectors produce an additional increase in hyperproliferative genes including *Irs-2*. Thus, both the absence of *let-7*, an *Irs-2*

suppressor, and the increase in *Irs-2*, lead to an overexpression of this gene that finally promotes an increase in proliferation and rosette formation (Figure 10I).

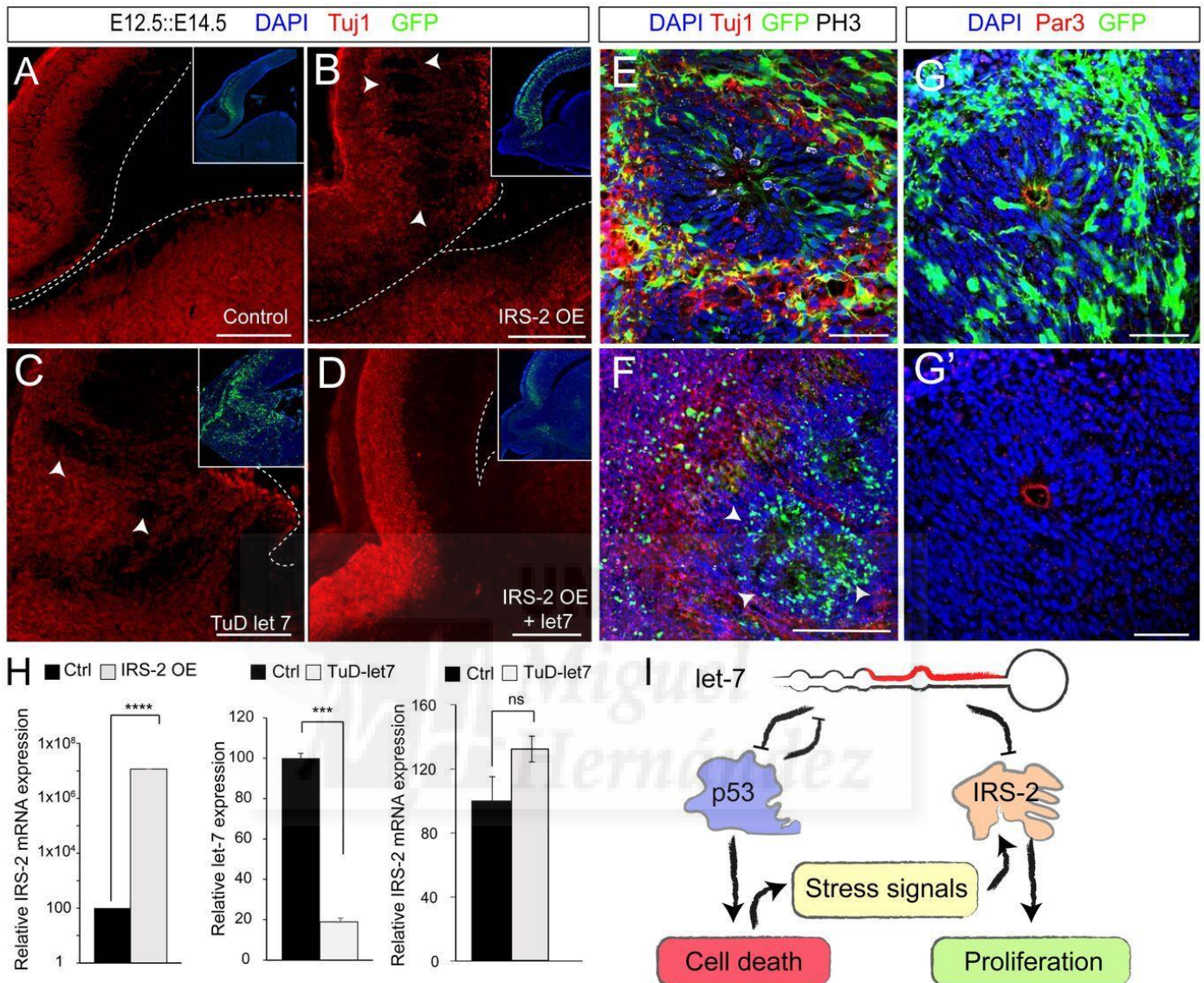


Figure 10. Overexpression of IRS-2 leads to rosette formation. Sagittal sections immunostained for Tuj1 (red) of WT mouse brains 2 days after electroporation at E12.5 with either *pCAG-IRES-GFP* (*GFP* or Control) (A) or *pCAG-IRES-IRS-2* coelectroporated with *GFP* (*IRS-2* OE) (B), Tough Decoy for *let7* (TuD-*let7*) coelectroporated with *GFP* (C) and *IRS-2* OE coelectroporated with *let7-a, b* and *c* (D), in the upper-right corner there are overviews of the electroporated brains immunostained with DAPI (blue) and GFP (green). The white line with stripes is indicating the ventricular surface. Note the presence of neurons close to the ventricle in the *IRS-2* OE and TuD-*let7* cases and the presence of several rosette like structures (white arrow heads). Zoom of a section electroporated with *IRS-2* OE two days after the electroporation at E12.4 (E) or 5 days after electroporation (F) immunostained for PH3 (white), Tuj1 (red), GFP (green) and DAPI (blue). (G, G') Zoom of a section electroporated with *IRS-2* OE two days after the electroporation at E12.4 immunostained for Par3 (red), GFP (green) and DAPI (blue). Note the presence of apical junction proteins in the centre of the rosette-like structures. (H) Functional validation with qPCR of the plasmids used in the electroporations. Left, increase of *IRS-2* after the cellular transfection with the *pCAG-IRES-IRS-2* plasmid (Expression of *IRES-2* mRNA:

GFP= 100%, *IRS-2*= 1,1x107%). Centre: Decrease of *let-7* mature miRNA after transfection with Tough Decoy for *let-7* (Expression of *let-7* miRNA: Scramble 100%, TuD-*let7*: 18.87%). Right, tendency of increase of *IRS-2* after transfection with Tough Decoy for *let-7* (Expression of *IRS-2* mRNA: Scramble 100%, TuD-*let7*: 132.06%). Data are shown as percentage \pm SEM from three different samples. t-test * $p < 0.05$, ** $p < 0.01$, *** $p < 0.005$, **** $p < 0.001$. (I) Model proposed for *let-7/p53/IRS-2* axis role during early stages of brain development. Scale bars, 200 μ m (A-D, F), 50 μ m (E, G).

Function of IRS-2 in iPSC-derived cerebral organoids

Cerebral organoids generated using derived iPSC cells and cultured in suspension are able to form complex brain-like structures (see Methods). These 3D structures have been used to model human brain development in health and disease (Lancaster, Renner et al. 2013, Camp, Badsha et al. 2015, Giandomenico and Lancaster 2017). In order to determine if *Irs-2* plays an important role controlling early human brain proliferation, we decided to produce iPSC-derived cerebral organoids and test *Irs-2* function on them. The maturation process of cerebral organoids is recapitulated in Figure 11 (A-D). Day 40 (D40, Figure 11E)) is equivalent to 40 wpc in human embryos (Kelava and Lancaster 2016), it is the day of organoid development that we choose in order to elucidate the role of *Irs-2* during early brain neurogenesis because is the one that correlates with E12.5 in mouse embryos (the age that we used in previous mouse electroporation assays (Figure 10). Moreover, day 40 organoids had a thick neuroepithelium (Figure 11E) and ventricular-like cavities that allow its genetic manipulation via electroporation (Figure 11F-11H).

We electroporated D40 cerebral organoids derived from iPSC from healthy donors with GFP (control) or with *Irs-2* overexpression plasmid and GFP (*Irs-2* OE) (Figure 11 I). We wanted to know if the acute overexpression of *Irs-2* could promote an increase in proliferation in cerebral organoids. To address that question, we performed immunostaining for Ki67, in the electroporated organoids (Figure 11I). We found no significant differences between control and *Irs-2* OE groups, although there was a clear tendency of increase in proliferative cells in the *Irs2*-OE cerebral organoids (Figure 11J). This result suggested that high levels of *Irs-2* could increase the proliferative potential of human brain progenitor cells, but this is not sufficient to promote the formation of rosettes in cerebral organoids.

Finally, we wondered if the local increase in *Irs-2* would lead to the formation of neuronal heterotopias in human organoids showed in *Dicer* KO embryos (Figure 6A) and

in WT electroporated embryos with an *Irs-2* OE plasmid. To examine whether neurons are located in aberrant ventricular positions we immunolabeled cyrosections of electroporated organoids for Tuj1 (a marker of newborn neurons) (Figure 11K). As previously shown, (Lancaster, Renner et al. 2013) we found that both in control and in *Irs-2* OE situations there were Tuj1 positive neurons located inside of the ventricular zone (Figure 11K) but these neurons are not forming groups nor heterotopias inside of the ventricle-like cavity. These observations suggest that in human cerebral organoids the local increase of *Irs-2* at D40 could lead to the increase in proliferation but this is not sufficient to generate structural malformations like neuronal heterotopias. This could be due to the intrinsic properties of this 3D model such as the capacity of the ventricular zone to expand, which allows the increase in proliferation without modifying the ventricular surface nor its cytoarchitecture. It is mandatory to point that the results shown in this last paragraph are preliminary results and we should increase the replicates to end with a solid result.



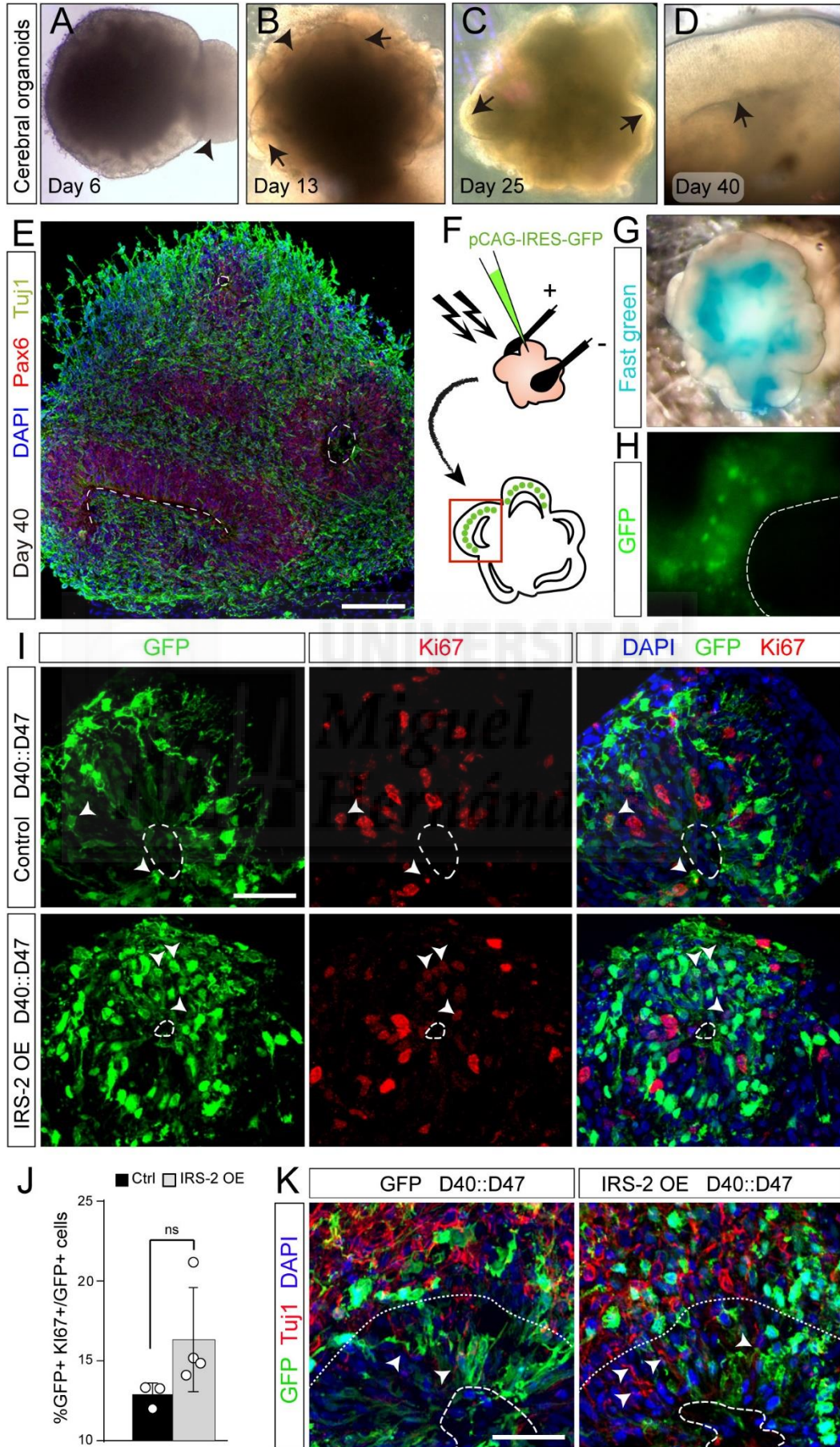
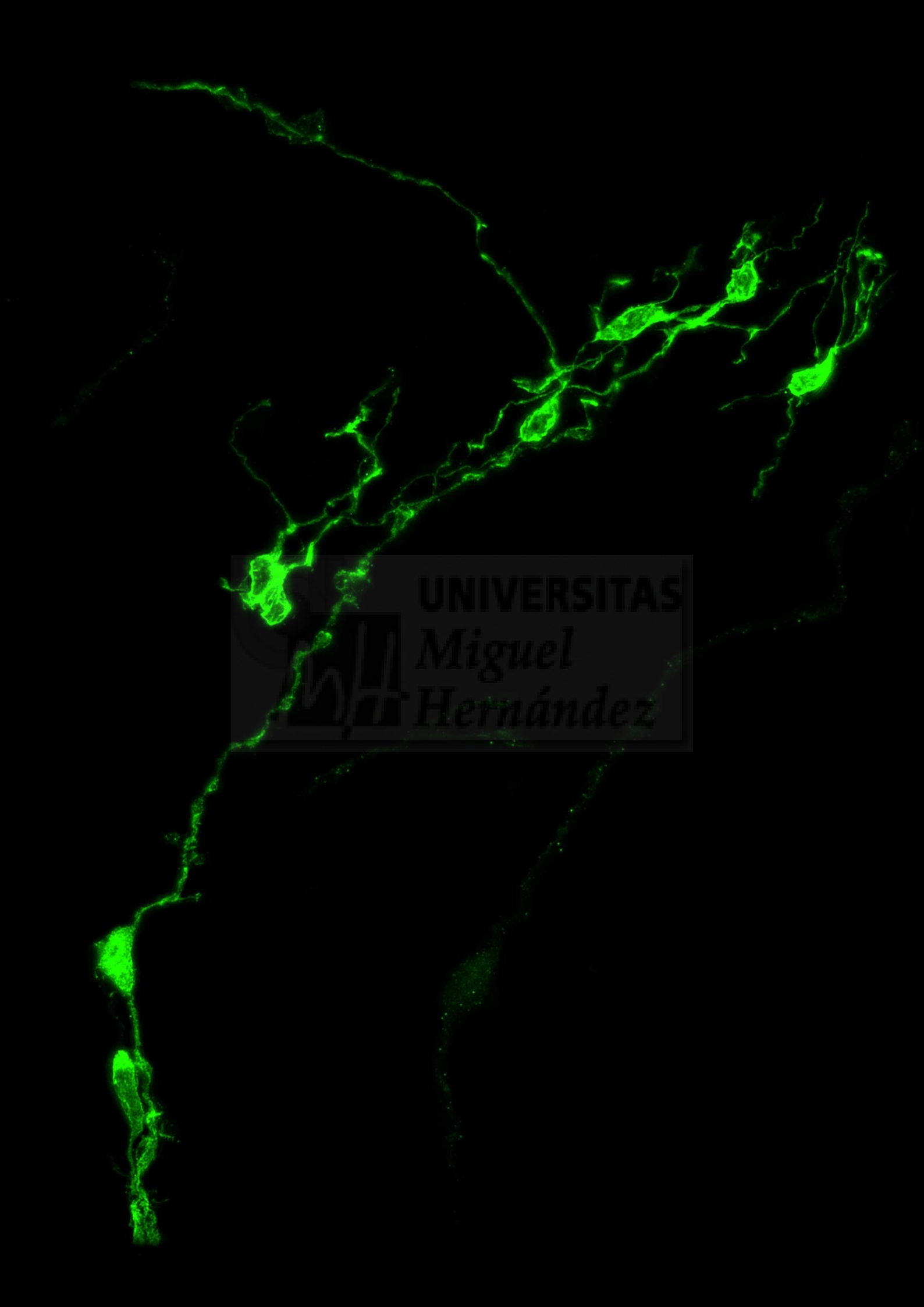
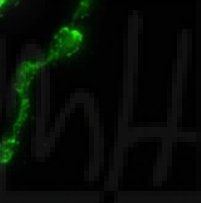


Figure 11. Effect of *Irs-2* OE in iPSCs derived cerebral organoids. (A-D) Example images of cerebral organoids in different stages. (A) Note small buds of ectodermal tissue that is not organized radially (black arrowhead). Neuroepithelium (black arrow) start being appreciated at day 13 (B) and its thickness increases with the age (C, D). Outgrowths and migrating cells are visible (black arrow) but they don't interfere with the organoid development. (E) Section of a complete cerebral organoid immunostained for Pax6 (red), Tuj1 (green) and DAPI (blue). Ventricule-like cavities (white dotted line) are surrounded by progenitor cells. (F) Schematic of electroporation technique. Plasmid DNA (for instance *pCAG-IRES-GFP*) was injected into ventricular-like cavities within the organoid and an electric pulse was applied to electroporate progenitor cells located in the ventricular line. (G) Fast green (blue) was used to follow the injected mix. Note that some ventricular cavities are connected. (H) One day post electroporation, at Day 40, green –electroporated– cells can be seen from the outside of the organoid. (I) Cryosections of cerebral organoids 4 days after electroporation with *pCAG-IRES-GFP* (Control, Ctrl. Top images) or *pCAG-IRES-Irs-2* coelectroporated with *pCAG-IRES-GFP* (*Irs-2* OE, bottom images). Sections were immunostained for GFP (green), Ki67 (red) and DAPI (blue). (J) The proportion of electroporated cells which were progenitors ((GFP+Ki67+)/totalGFP+) under each experimental condition was determined. (K) Cryosections of cerebral organoids 4 days after control electroporation (left) or *Irs-2* OE (right) showing immunostaining for Tuj1 (red) and GFP (green). In both cases neurons are present in the progenitor zone (white arrowheads). Data are shown as percentage \pm SM. $n \geq 3$. t-test * $p < 0.05$, ** $p < 0.01$, *** $p < 0.005$, **** $p < 0.001$. Scale bars, 100 μ m (E), 30 μ m (I, K).





 UNIVERSITAS
Miguel
Hernández



7. Discussion

“The number of different hypotheses erected to explain a given biological phenomenon is inversely proportional to the available knowledge”

Edington's Theory

Miguel

Hernández

7. Discussion

The discovery in 1993 of miRNAs as gene expression regulators opened the door to a large number of studies about their role during brain development. At early stages of CNS development, the program of progenitor cells changes allowing them to acquire different specific features. These changes promote that neuroepithelial cells sequentially generate apical and basal radial glia cells, intermediate progenitor cells and different types of neurons. miRNAs are molecules expressed specifically at certain time and in a particular spatial location. Thus, not all miRNAs are expressed in all tissues, and not all miRNAs that are expressed in one tissue do so at the same time. This makes the miRNA machinery suitable to control developmental processes in which cells must go through different maturation stages, modifying the transcriptome profile through the expression of different miRNAs. In this thesis I wanted to understand what the role of miRNAs during early stages of telencephalic development is, when NECs' transcriptional program undergoes sequential changes that allow the generation of new types of progenitors and, subsequently, different neuronal types populating the telencephalon.

Characterization of Dicer^{F/F}-Rx3Cre mice

To understand the role of miRNAs at the very beginning of neurogenesis, we ablated functional Dicer taking advantage of Cre-mediated recombination in a Rx3-Cre expressing mouse line. We used this Cre line due to the early Rx3 expression (from E7.5) in the whole telencephalon (Klimova, Lachova et al. 2013). Surprisingly, the expression of Td tomato after Cre recombination is not homogenous in all the Rx3 positive area, we found that it takes place at higher levels in the rostro-ventral part of the telencephalon (OB, Septum, BG and pOA) than in the caudal neocortex. A possible explanation is that the time when Rx3 is expressed (5 days in the rostro-ventral part and 2-3 days in the caudal part) is determinant for Cre expression levels and same as for the strength of the subsequent Cre-mediated recombination. These differences in the duration of Rx3 expression could be responsible for producing high recombination levels in the ventral and low in the dorsal telencephalon, explaining the different phenotypes obtained in these two areas. Nevertheless, the analyses of Dicer ablated embryonic cortex at E17.5 reveal that even a low level of recombination is enough to produce a reduction in miRNAs expression and a decrease in the thickness of the neocortex, in agreement with what was previously published (De Pietri Tonelli et al., 2008, Nowakowski et al., 2011).

Regarding the proliferative effects upon loss of miRNAs, we found that the ablation of functional Dicer doesn't produce major alterations in the number of apical mitoses (related to aRGCs) at any of the ages analysed except for E12.5, when there is a slight and transient reduction on them. This alteration in apical cells divisions is rapidly rectified, suggesting that the system is able to find a fast way to compensate and maintain the correct number of apical divisions. As for basal progenitors, we found a reduction in mitoses located in the SVZ, together with a decrease in Tbr2 positive cells, suggesting that in the absence of miRNAs the amount of IPCs is reduced compared to control conditions. This result comes into conflict with previous publications (Nowakowski et al., 2011), and could be explained due to the gradual expression of Tbr2. This marker is widely used to identify IPCs, but its expression is not restricted to them. In the process of an aRGC becoming an IPC, the RGC starts expressing Tbr2 before the intermediate progenitor is born. Likewise, when a neuron is produced from an IPC, it will express Tbr2 in a transient manner. To study the true population of IPCs, we should analyse Tbr2 positive cells negative for neuronal markers (as Tuj1) and for radial glia markers (Pax6).

In the mouse telencephalon, the vast majority of cell divisions taking place in the SVZ are those produced by IPCs. Accordingly, changes in basal mitoses indicate alterations in the population of IPCs. An alternative explanation for a decrease in the number of basal progenitors undergoing mitosis (basal PH3+ cells) would be a lower number of progenitors in M phase. This is not necessarily linked to a decrease in the amount of cycling progenitors, but to a longer cell cycle since the probability of finding a progenitor in M phase is lower. If this is the case, there will be a lower number of PH3+ cells without alteration in the number of cycling progenitors. Nevertheless, as we found a correlation between the number of cells undergoing mitosis and the number of Tbr2+ cells, we conclude that the amount of IPCs is altered in the absence of miRNAs. After a first period in which there is a decrease in IPCs, a second period is characterized by an increase in basal mitoses. This rebound effect may act as compensatory mechanism to maintain the number of basal progenitors, as if there was a feed-back signalling mechanism.

We hypothesize that this compensatory mechanism must exist also for apical progenitor cells because after a dramatic increase in cell death (and thus, of dying progenitors) the density of apical mitoses was maintained. This result suggests that the remaining apical progenitors are proliferating in a way that compensates the decrease in

their population. So, after a massive tissue injury, mechanisms of cellular communication promote the activation of proliferative genes in the remaining cells in order to maintain the homeostasis of the tissue.

It has been previously reported that the loss of functional Dicer during development produces an increase in cell death ((Swahari, Nakamura et al. 2016, Chmielarz, Konovalova et al. 2017)Cuellar et al., 2008; De Pietri Tonelli et al., 2008). In the work by De Pietri et al., they found an increased number of apoptotic cells in VZ and SVZ, but they didn't find any change in the thickness of these proliferative layers, concluding that apoptotic cells found in proliferative layers should be newborn neurons. In this thesis, we demonstrate that cell death in the rostral part of the telencephalon due to the loss of functional Dicer affects neurons as well as progenitors. The contradictory results could be explained by the time of the recombination. It is possible that if the peak of cell death takes place at later stages (for instance at E14.5, as in Di Pietri Tonelli et al. investigation) the population of progenitors have more mechanisms in order to prevent massive cell death, so this kind of cells could escape from the apoptotic fate. Another possible option could be that *Emx-Cre, Dicer^{F/F}* mice display also cell death in progenitors, but the loss of progenitor cells is compensated with a faster cell cycle, giving as a result the same number of mitotic cells.

The fact that in our model cell death stops at E13.5 could be due to two possible reasons. First, from E13.5 onwards, *let-7* is no longer necessary in order to control cell death levels, being this process regulated though other molecules. Second: at later stages of development, the system could be more robust and, with more redundant mechanisms allowing the maintenance of the homeostasis regardless of the *let-7* absence.

Rosette characterization and formation

The reduction in the perimeter of the OB upon Dicer ablation takes place maintaining the laminar structure of this area but it comes with a strong reduction in granule cell layer. Granule cells are interneurons that mediate the low-threshold perception of odorants and the odour discrimination. Hence, the olfactory phenotype expected after miRNA deprivation would be the impairment of the processes of perception and discrimination of odorants.

In the absence of functional *Dicer*, additionally to the reduction of the OB, embryos showed true rosettes (hyperproliferative cells surrounding an empty lumen). These rosettes are formed by proliferative progenitors, as demonstrated by cell cycle assays, this is important in order to corroborate their proliferative behaviour. Progenitors could be arrested in other phase such as, G1 which is the case of other mutants with increased density of progenitors (Doobin, Kemal et al. 2016). *Dicer* KO's rosettes are similar to those showed in Embryonal Tumours with Multi-layered Rosettes (ETMR; (Phillips, Tihan et al. 2015) and in the *Lgl1*^{-/-} mouse (Klezovitch et.al; 2003). ETMR were previously named as Embryonal Tumour with Abundant Neuropil and True Rosettes (ETANTR). They are characterized by been formed by undifferentiated neuroepithelial cells with abundant neuropil, showing high number of apoptotic cells and mitosis, which are later surrounded by neuronal cells (that are thought to be part of the neoplasia) (Phillips, Tihan et al. 2015). Rosettes found in *Lgl1*^{-/-} mouse show an increased progenitor domain, an increase in cell-cycle re-entry and apoptotic events and disrupted apical junction proteins (Klezovitch et.al; 2003). These results together with the ones showed in this thesis suggest that all these features could lead to rosette formation.

Interestingly, rosettes observed in *Dicer* ablated embryos are located in the septum, in the basal ganglia and in the rostral part of the cortex, suggesting that the mechanism whereby they are formed is not specific of a determined region but dependant of the strength of the recombination. Additionally, they don't lose their regional identity, suggesting that progenitors which start forming each rosette maintain their own molecular features although they are isolated of the ventricle.

Which are the cellular mechanisms leading to rosette formation?

The phenotypical differences showed between the neocortex and the ventral brain in *Dicer* ablated animals indicated that, during development, different processes (or with different intensity) were altered in each region. We found a massive increase in cell death taking place in the OB, the Stm and BG. Interestingly, the number of mitotic cells was not reduced in these areas, moreover there is an increase at E12.5. This could be explained like the compensated proliferation in mutant neocortex: remaining progenitors are proliferating in order to maintain the homeostasis of their population. Thus, inside of the areas were "healthy" or "not-dying" progenitors are located, should be a relative increase in proliferation.

Experiments in this thesis supported by previous studies (Klezovitch et.al; 2003) suggest that a suitable mechanism for true-rosette formation is the direct invagination from the ventricle, as it is shown by the apical junction belt labelling there are intrusions of the ventricular line inside of the tissue. But, how is promoted the generation of invaginations? It has been previously demonstrated that elevated rate of proliferation and vertically oriented cell divisions (self-amplifying divisions) can generate local stratification and invagination (Linde 1984). Presence of disruptions in the apical belt take place in areas where neuronal heterotopias are formed. It is possible that the increase in progenitor apoptosis lead to loss in apical junction proteins, which facilitates the intrusion of neurons in the lumen of the ventricle. We postulate that invaginations could be enhanced by presence of these neuronal heterotopias, as they act as physical barriers in the ventricle preventing its lateral expansion and promoting its *invaginative* grow. Following our model of rosette generation, all rosettes start their formation from an invagination. Thus, we propose that invagination is critical for their formation and preventing it could also prevent rosette generation.

We hypothesized that upon the ablation of functional *Dicer*, the formation of an invagination could be enhanced physically by the salt-and-pepper ventricular tension, which is produced by the presence of areas in the ventricular surface with low tension (due to the increase in apoptosis and loss of apical junction proteins) and areas with high tension (due to the increase in proliferation). Nevertheless, we suggest that rosettes could be virtually produced by any increase in the ventricular-surface tension. This is supported by results from Gil-Sanz et al. in which an increase in proliferation produced by *Mltt4* and *Cdh2* ablation increasing proliferation leads to the misallocation of progenitors and the formation of rosette-like structures formation (Gil-Sanz, Landeira et al. 2014).

Transcriptional consequences of Dicer ablation at early stages of development

The analysis of the RNAseq experiment revealed that, at E11.5 in *Dicer* ablated embryos, the most downexpressed miRNAs belong to *let-7* family. Surprisingly, we only found 13 statistically downregulated miRNAs in *Dicer* ablated animals, a possible explanation for having such a reduced number of downexpressed miRNAs after functional *Dicer* elimination is the presence of wild-type cells in the dissected tissue, which would “dilute” the amount of differentially expressed miRNAs, as a result we only found differences in

the most-changed miRNAs. This issue would be avoided performing FACS (fluorescence-activated cell sorting) assays in order to perform RNAseq analysis only in cells with Cre expression. As at early stages during development (from E7.5 to E11.5) the most demanded miRNAs are the ones from *let-7* family; another possible explanation is that their high consumption rate followed by the impossibility of renewal, could dramatically reduce the levels of expression of these miRNAs. Although we cannot demonstrate that *let-7* is the only family of miRNAs differentially expressed in *Dicer* KO embryos, we demonstrated that in the rostral part of the brain at E11.5, *let-7* family is the most reduced one upon *Dicer* ablation. In addition, we found four new miRNAs, three of them (*mir-n-140-5p*, *mir-n-152-5p* and *mir-n-44-5p*) were highly downregulated in our model. Their putative targets reveal their role controlling DNA transcription, metabolic balance and proliferation, suggesting that they could also play an important role in *Dicer* KO phenotype. Interestingly, we also found an upregulated novel miRNA: *mir-n-194-5p*; as previously indicated, there are different non-cannonical pathways that allow the generation of mature miRNAs without following the canonical steps, nevertheless only one miRNA has been previously described as *Dicer*-independent: miR-451, whose precursor has a free 3' OH end. The presence of a 3' OH end makes the precursor susceptible to be cleaved by Ago2, suggesting that other *Dicer*-independent miRNAs could exhibit the same feature. It would be interesting to study in detail the features of the *pre-mir-n-194-5p* in order to determine if it could be also processed by Ago2.

In order to transcriptionally understand rosette formation, we searched for protein-coding genes differentially expressed in the rostral telencephalon of *Dicer* ablated embryos compared to a control situation. As miRNAs negatively regulate gene expression, the major part of differentially expressed genes were upregulated in *Dicer* KO embryos. Among these genes we focused our attention on genes potentially regulated by *let-7* and related with two (technically) antagonist processes: *cell death* and *proliferation*.

As expected because of the massive cell death found in *Dicer* ablated embryos, genes related with p53 cascade were upregulated on them. After DNA damage or cellular stress p53 is activated, triggering cell cycle arrest (to repair damaged DNA) or, if the DNA is gravely damaged p53 can play its pro-apoptotic function eliminating injured cells and preventing the damaged DNA of been inherited to daughter cells. The activation of this pathway could be due to direct loss of p53 inhibitors or indirectly due to DNA damage produced by the absence of *Dicer*-dependant miRNAs. We addressed the importance of

p53 activation in rosette formation ablating p53 in *Dicer* KO embryos. The phenotype in these mutants is variable, we found embryos with and without rosettes. Nevertheless, the 75% of double mutants showed a total rescue of the phenotype. With the results showed in this thesis we can point that, in a scenario without functional *Dicer*, the activation of p53 cascade is necessary in the majority of the cases in order to promote rosette formation. This doesn't mean that an increase in cell death would necessarily produce rosettes in a healthy situation. *Dicer* ablated embryos lack an important mechanism of tissue homeostasis and we postulate that this condition makes the tissue more susceptible to the appearance of rosettes after an increase in cell death. Interestingly, it has been previously shown that p53 dramatically downregulates *let-7* expression (Jones and Lal 2012), which could partially explain the strong reduction in the *let-7* family of miRNAs in our model.

One interesting question raised from rosette formation is how hyperproliferative structures appear after massive cell death. To understand this process, we focus on DEG related with proliferation that are potentially regulated by stress factors (like the ones released in a niche with massive cell death) and by *let-7*. We only found one gene fulfilling these characteristics: *Insulin receptor substrate-2 (Irs-2)*. It has been previously demonstrated that an increase in oxidative stress raised the activity of *Irs-2* promoter as well as the expression of *Irs-2* protein, leading to the activation of the insulin-PI3K-mTOR signalling pathway and promoting cell proliferation (Zhu, Shyh-Chang et al. 2011). Thus, with the *let-7/p53/Irs-2* axis *cell death* and *proliferation* could be linked, which seems to have a coherent biological basis: should be a mechanism regulating the balance between cell death and proliferation in order to maintain the homeostasis of the tissue. After a damage in a tissue, a regenerative response takes place: dying cells activate macrophages, dendritic cells, neutrophils and tissue stem cells. These cells secrete mitogenic cytokines such as IL1, IL6 or TNF α , producing an expansion of undifferentiated precursors such as tissue stem cells. This process could produce an overgrowth if the tissue in which the compensatory regeneration takes place has regulatory imbalances has been previously described in the context of cancer. Thus, cell death could promote cell proliferation through different participants, in this thesis we revealed that one via involves the *let-7/p53/Irs-2* axis.

The relationship between an increase in *Irs-2* and an abnormal grow of the tissue has been previously found. Thus, *Irs-2* expression is upregulated in some human tumours when compared with normal tissue. The expression of *Irs-2* is increased in hepatocellular,

pancreatic, prostate cancer and malignant pleural mesothelioma (Mardilovich, Pankratz et al. 2009). In breast cancer, *Irs-2* is found to be implicated in metastasis, but not in growth and proliferation (Day, Pouligiannis et al. 2013). On the other hand, the most reduced family of miRNAs in *Dicer* KO embryos, *let-7*, is widely known for its role as tumour suppressor as they target multiple oncogenes and tumour-suppressor genes. These data suggest that the formation of true-rosettes in *Dicer* ablated embryos could share common mechanisms with abnormal growth in some cancer types.

Focussing in true-rosette tumours, it has been described that they are genetically characterized by having a genomic amplification involving a microRNA at 19q13.42 cluster (not related with *let-7*). Additionally, a molecular marker used in order to identify this tumour type is the expression of the Lin28A protein (Korshunov, Remke et al. 2010). Lin28A downregulates *let-7*, promoting an increase in *Irs-2* (Zhu, Shyh-Chang et al. 2011). This beautifully coincides with the results showed in this thesis, in which there is an increase in Lin28A coincident with a downexpression of *let-7* that promotes an overexpression of *Irs-2*, been this process sufficient in order to generate true-rosettes.

Interestingly, the elimination of functional *p53* is sufficient in order to prevent rosette formation in *Dicer* KO embryos. This suggests that in the *Dicer* KO context, *p53* is necessary to increase cell death in order to push the system and increase cell proliferation, maybe through the downregulation of *let-7* by this protein (future experiments are needed to check this hypothesis). This is not the case in a control situation, in which without an increase in apoptosis but with an acute decrease in *let-7* by IUE we are able to generate true rosettes. We hypothesize that the results obtained with IUE experiments show a stronger phenotype due to the extreme genetic modifications produced with this manipulation. When we overexpress *Irs-2*, we produce an increase of 5 orders of magnitude in *Irs-2* mRNA, and with the Tough Decoy we produce a decrease of 5 times in *let-7* mature miRNA. Although these two manipulations are much more acute than the ones produced in *Dicer* KO embryos, the rosette phenotype obtained is the same. This suggests that increasing directly or indirectly *Irs-2* above a threshold is sufficient to produce rosettes (*Irs-2* OE experiments). When the threshold is not reached (*p53*; *Dicer* KO embryos), alternative ways of increasing the levels of *Irs-2* (increasing cell death) could be necessary in order to produce these structures.

Increase of proliferation in iPSC-derived Cerebral Organoids

In this thesis, we successfully generated cerebral organoids from human iPSC using a modified protocol based in the one created by Lancaster et al. This system has been intensively studied in the past five years, since Madeline Lancaster published her work developing and characterizing cerebral organoids. We decided to use this model because of its uniqueness similarity to human embryonic brain development.

Analysis of cerebral organoids produced in our laboratory revealed morphological features that had been recently reported in this model, as progenitor zones with dorsal and ventral telencephalic regions and the presence of connections between different ventricle-like structures (Renner, Lancaster et al. 2017). One remarkable characteristic that we found in several organoids is the presence of an out-inside ventricular zone; thus, we found ventricular zones located in the surface of the organoid, with the apical side facing the culture media. The processes involved in the generation of out-inside VZ are unknown but they have some physical advantages for studying human progenitor's behaviour as the capability of growing without the collapse of the ventricle and the better accessibility of progenitors to nutrients and oxygen.

To elucidate if the mechanism by which *Irs-2* increases proliferation is maintained in human stem cells we decided to take advantage of cerebral organoid genetic manipulations. We performed organoid electroporation in order to acutely increase the amount of *Irs-2* in human neural progenitor cells. For that purpose, we fine tune the technique of cerebral organoids electroporation using classical round electrodes manually oriented, instead of the typical petri dish tissue electrode. Due to the longer cell cycle in human progenitor cells (takes 20 hours to complete one cycle) compared with mouse progenitors (4-7 hours), we decided to maintain electroporated organoids for seven days before their fixation and posterior analysis. Preliminary results indicate that an increase in *Irs-2* promotes an upward tendency in the amount of human progenitor cells. This result is not statistical significant, but the clear tendency indicates that additional experiments are necessary in order to have a solid result. Nevertheless, the proliferation could have increase without increasing the total number of progenitors; for example, if the total number or progenitors is not changed but there is a larger number of neurons produced. This could be tested performing cell-cycle exit assays. Another possible explanation for not-significant changes in proliferative experiments using cerebral organoids relies on the

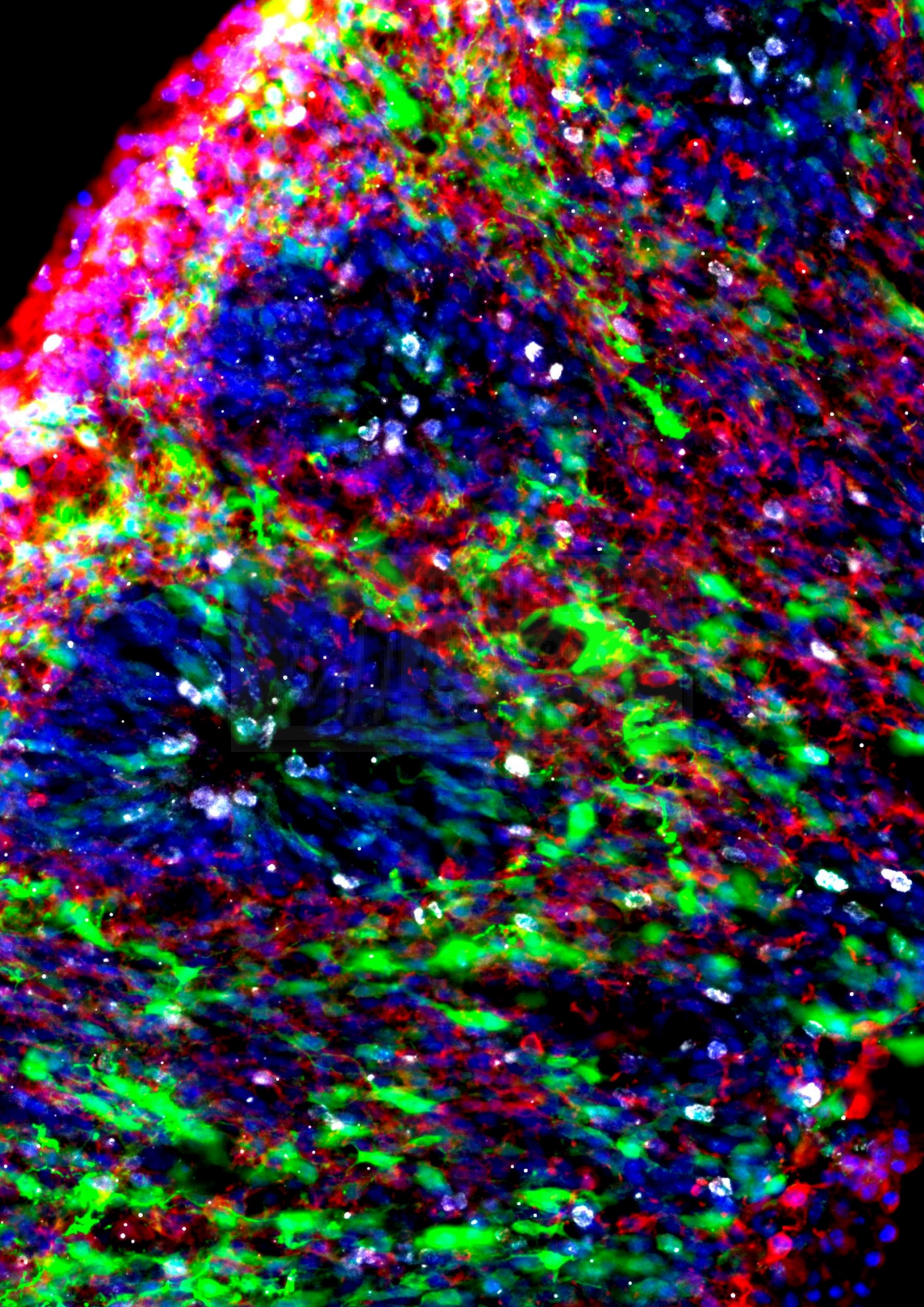
model itself: cerebral organoids are structures generated from iPSC grown in media with high levels of proliferative molecules, it is possible that the system is partially saturated in terms of proliferation. As we found neuronal delocalization in *Dicer* KO embryos as well as in *Irs-2* OE experiments, we wanted to elucidate if *Irs-2* OE promotes the presence of neuronal heterotopias in human tissue. Interestingly, the results obtained in this thesis revealed that upon the overexpression of *Irs-2* in cerebral organoids no neuronal heterotopias are formed, maybe due to the presence of a well-structured apical belt. Additionally, control and *Irs-2* OE cerebral organoids showed newborn neurons labelled with Tuj1 located in the ventricular zone. This is an indicative of neurons produced directly from aRGCs (direct neurogenesis) that we rarely find in the mouse Neocortex.

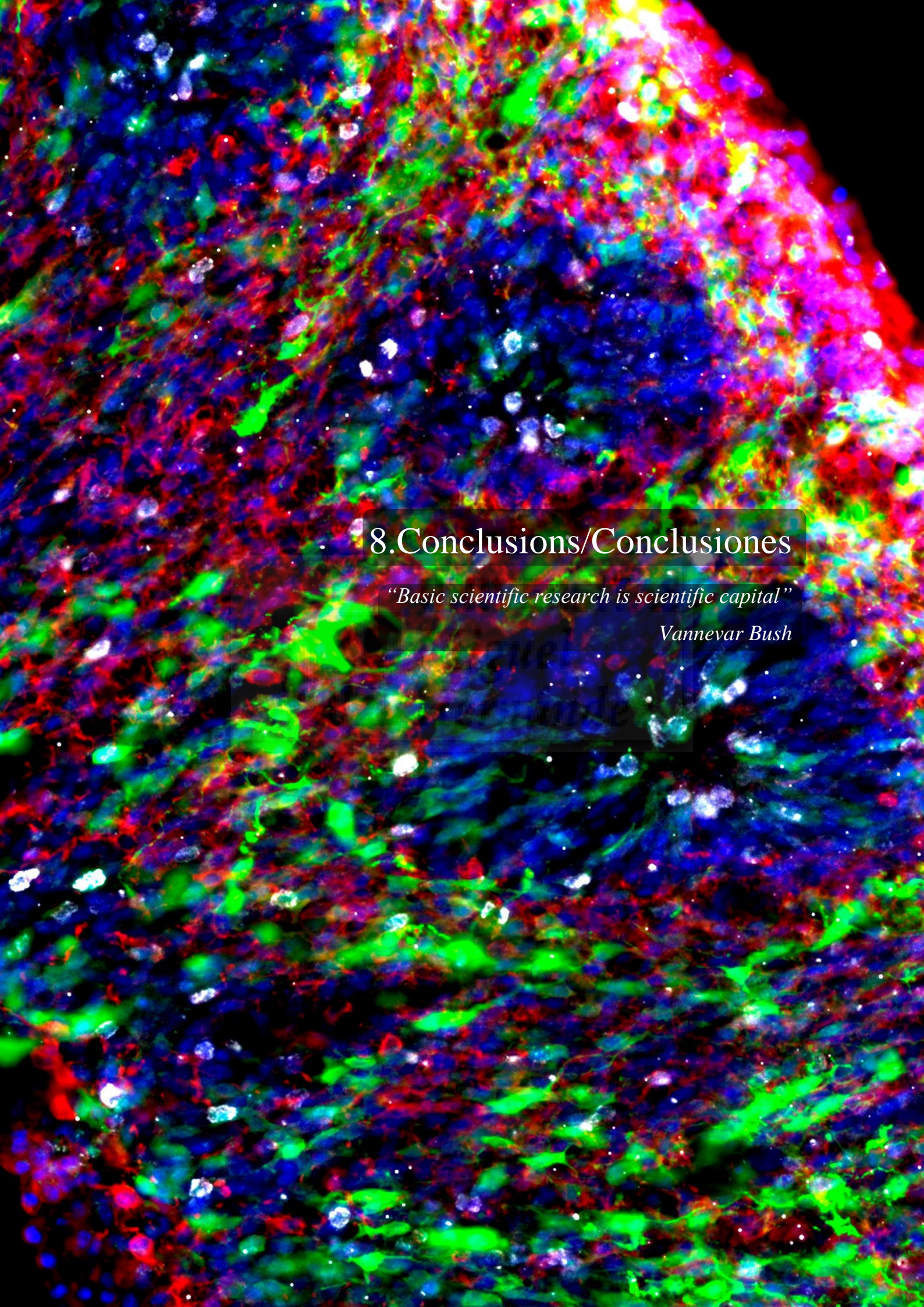
Finally, it is interesting to note that upon increase of *Irs-2* in human cerebral organoids no rosettes were found. If our hypothesis is true, the formation of rosettes is ligated to an increase in the ventricular tension produced by an increase in proliferation. Then, if the system has the capability of growing unlimitedly in the space, the ventricular tension will not increase. Thus, increasing acutely the proliferation would likely produce a larger ventricular zone instead of promoting the appearance of invaginations and true rosettes. As previously indicated, it is important to realize that cerebral organoids offer a huge advantage in order to understand certain human brain developmental processes such as: radial migration, interkinetic nuclear migration, types of migration, production of different neuron types... However, cerebral organoids have some important limitations that makes them not a good model to study processes in order to understand processes involving more complexes elements like neuronal connexions, cortical folding or progenitor's massive movements like the ones produced by rosette formation.

A final thought

In this thesis we started investigating the role of miRNA's machinery during brain development at a determinate stage. Then, we focused on the function of a miRNA family and their target genes. Finally, we found a set of molecules that work together in order to maintain alive the tissue under a critical situation. It is important to notice that one single molecule has rarely a unique biological function, the beautiful complexity of biological processes shouldn't be simplified in order to fit in our limited minds. In this thesis, we demonstrate the existence of one new via through which two antagonist processes -cell death and proliferation- are linked in the developing neurosystem. I hope that this small contribution could be useful for future researches.







8. Conclusions/Conclusiones

“Basic scientific research is scientific capital”

Vannevar Bush

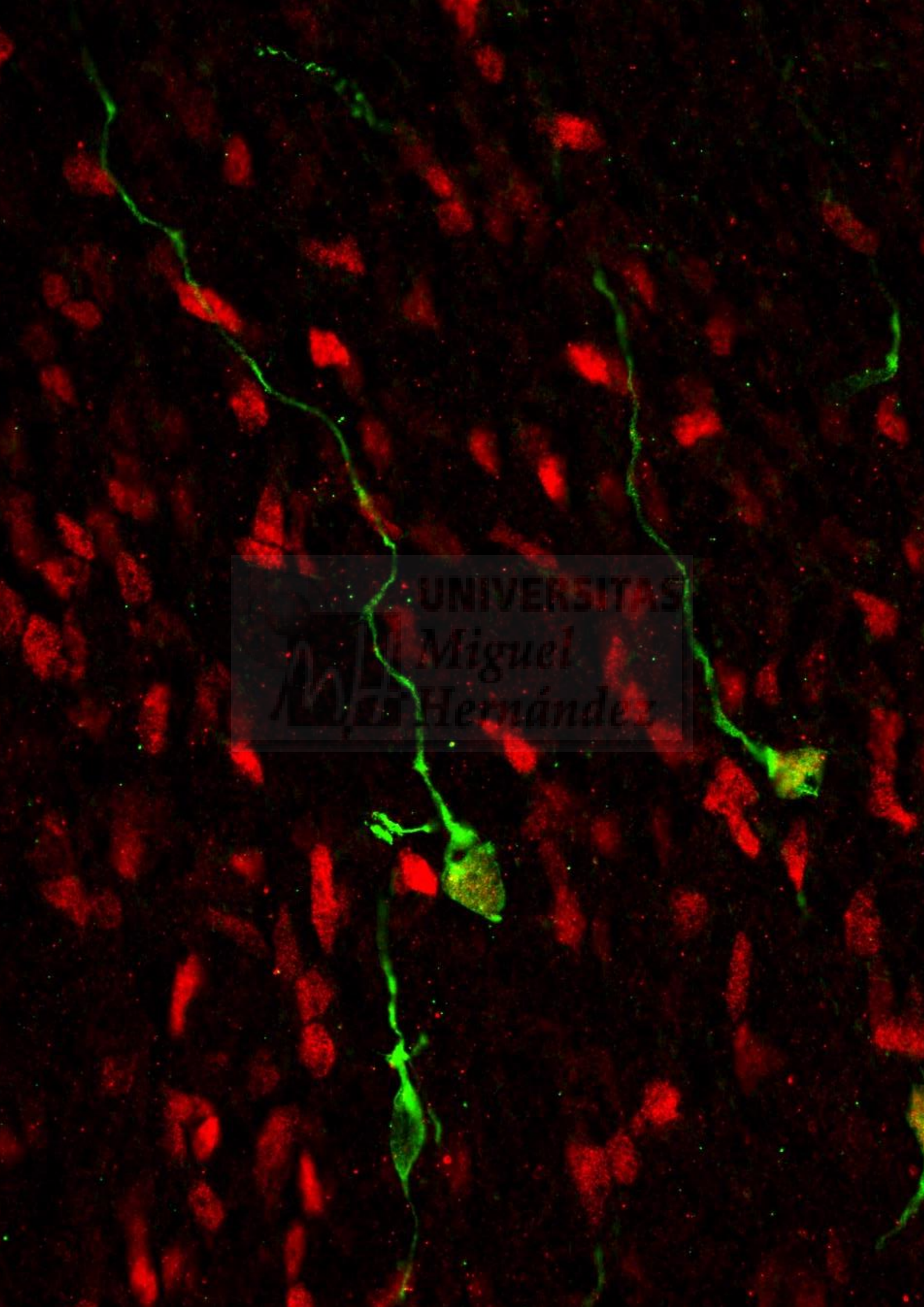
8. Conclusions/Conclusiones

1. The expression of TdTomato after Cre-recombination under the Rx3 promoter presents different intensities in different areas of the murine telencephalon, being it higher in the subpallium and in the rostral pallium than in the caudal pallium.
2. The elimination of functional Dicer at early stages of telencephalic development is sufficient to decrease the expression of mature miRNAs.
3. Rx-Cre; Dicer^{F/F} embryos show a reduction of the cerebral size accompanied by a thinning of the neuronal layers in the neocortex, as well as a reduction in the olfactory bulb.
4. The loss of Dicer at early stages of nervous system development promotes an increase in cell death, in proliferation, the appearance of neuronal heterotopias and ruptures of apical junctions. This is followed by the formation of true rosettes.
5. After the elimination of functional Dicer at E11.5 there is a dramatic loss of miRNAs from *let-7* family as well as three new miRNAs (*miRNA-n-44-5p*, *miRNA-n-140-5p* and *miRNA-n-152-5p*) in the rostral telencephalon.
6. At E11.5 in Dicer mutant embryos, there is an increase in genes involved in cell death (belonging to the *p53* cascade) and proliferation (*Irs-2*). These two processes and genes are regulated by *let-7* miRNAs.
7. The loss of functional *p53* protein in Dicer mutant embryos rescues the developmental defects leading to the formation of rosettes.
8. Decrease of *let-7* in wild-type embryos is sufficient to induce the formation of rosettes. OE of *Irs-2* phenocopies this defect, which is rescued by *let-7* OE.
9. Our experiments in cerebral organoids suggest that *Irs-2* is also involved in controlling the proliferation in human brain progenitor cells.

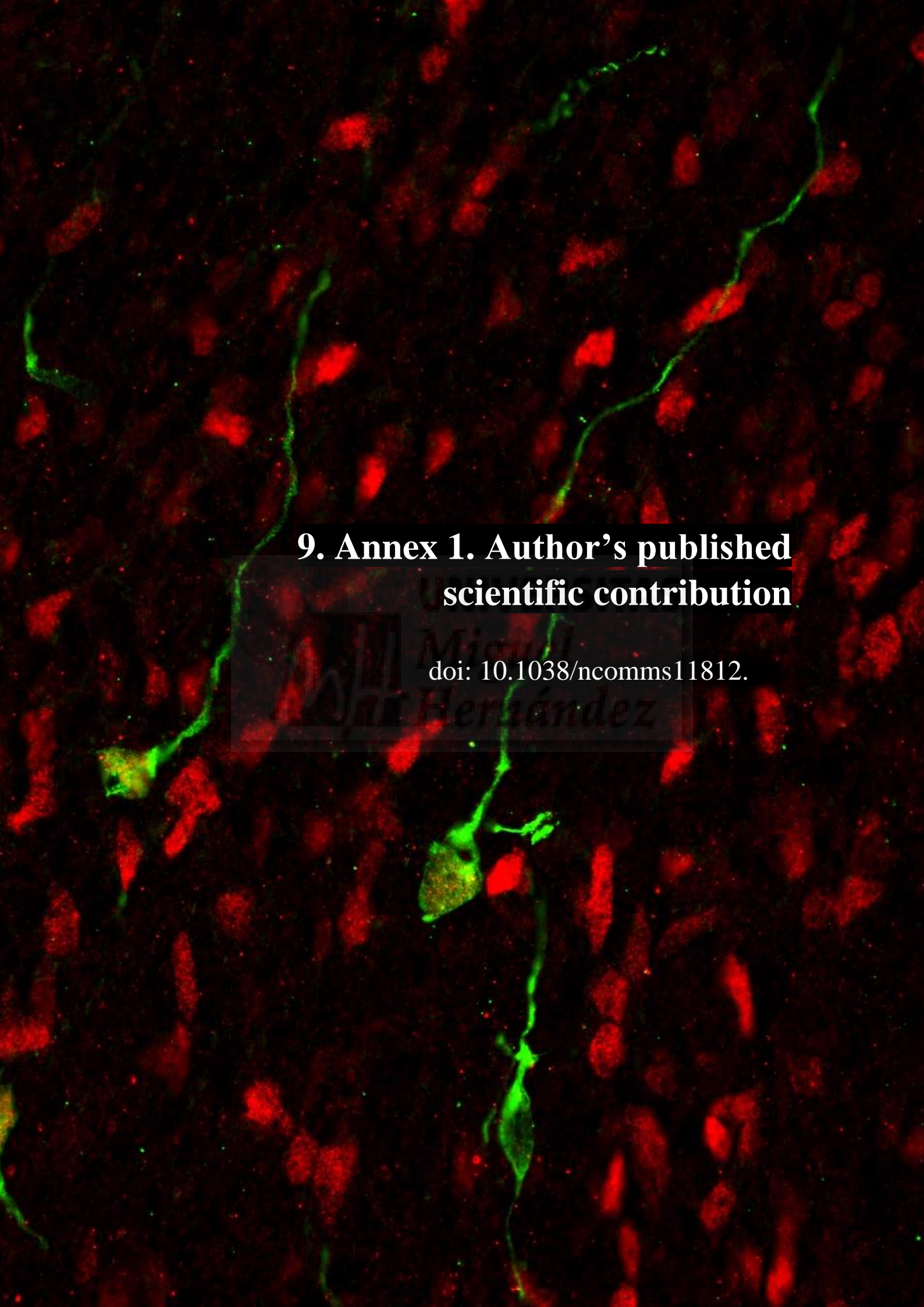
1. La expresión de TdTomato tras la recombinación mediada por Cre bajo el promotor de Rx3 presenta diferentes intensidades en diferentes áreas del telencéfalo murino. Siendo esta mayor en el subpalio y en el palio rostral que en el palio caudal.
2. La eliminación de Dicer funcional a estadios tempranos del desarrollo telencefálico es suficiente para producir una disminución en la expresión de miRNAs maduros.
3. Los embriones Rx; Dicer^{F/F} presentan una reducción del tamaño cerebral acompañada de un afinamiento de las capas neuronales en el neocortex así como una reducción en el tamaño del bulbo olfativo.
4. La pérdida de Dicer a estadios tempranos del desarrollo del sistema nervioso produce un aumento en muerte celular, y en proliferación, así como la aparición de heterotopias neuronales y rupturas de las uniones apicales. Esto es seguido por la formación de verdaderas rosetas.
5. Tras la eliminación de Dicer funcional a E11.5 se reducen dramáticamente miRNAs pertenecientes a la familia de *let-7*, además de tres nuevos miRNAs (miRNA-n-44-5p, miRNA-n-140-5p y miRNA-n-152-5p) en el telencéfalo rostral.
6. A E11.5 en embriones mutantes para Dicer hay un aumento en genes involucrados en muerte celular (pertenecientes a la cascada de *p53*) y en proliferación (*Irs-2*). Estos dos procesos y genes son regulados por miRNAs de la familia de *let-7*.
7. La pérdida de *p53* funcional en embriones mutantes para Dicer rescata los defectos del desarrollo que llevan a la aparición de rosetas.
8. La disminución de *let-7* en embriones silvestres es suficiente para inducir la formación de rosetas. La sobreexpresión de *Irs-2* fenocopia este defecto, el cual es rescatado por la sobreexpresión de *let-7*.

9. Nuestros experimentos en organoides cerebrales sugiere que Irs-2 también está involucrado en controlar la proliferación en células progenitoras cerebrales humanas.





UNIVERSITAS
*Miguel
Hernández*

A fluorescence microscopy image showing a dense population of neurons. The neurons are stained with two different fluorescent dyes. One set of neurons is stained red, appearing as bright red spots against a dark background. Another set of neurons is stained green, appearing as bright green spots. Some neurons show co-localization of the two dyes, appearing yellow or orange. The neurons have a characteristic morphology with cell bodies and extending processes.

**9. Annex 1. Author's published
scientific contribution**

doi: [10.1038/ncomms11812](https://doi.org/10.1038/ncomms11812).

Miguel
Ángel Hernández



ARTICLE

Received 1 Apr 2015 | Accepted 3 May 2016 | Published 6 Jun 2016

DOI: 10.1038/ncomms11812

OPEN

A restricted period for formation of outer subventricular zone defined by *Cdh1* and *Trnp1* levels

Maria Ángeles Martínez-Martínez¹, Camino De Juan Romero¹, Virginia Fernández¹, Adrián Cárdenas¹, Magdalena Götz^{2,3,4} & Víctor Borrell¹

The outer subventricular zone (OSVZ) is a germinal layer playing key roles in the development of the neocortex, with particular relevance in gyrencephalic species such as human and ferret, where it contains abundant basal radial glia cells (bRGCs) that promote cortical expansion. Here we identify a brief period in ferret embryonic development when apical RGCs generate a burst of bRGCs that become founders of the OSVZ. After this period, bRGCs in the OSVZ proliferate and self-renew exclusively locally, thereby forming a self-sustained lineage independent from the other germinal layers. The time window for the brief period of OSVZ bRGC production is delineated by the coincident downregulation of *Cdh1* and *Trnp1*, and their upregulation reduces bRGC production and prevents OSVZ seeding. This mechanism in cortical development may have key relevance in brain evolution and disease.

¹Instituto de Neurociencias, Consejo Superior de Investigaciones Científicas and Universidad Miguel Hernández, Sant Joan d'Alacant 03550, Spain.

²Helmholtz Center Munich, German Research Center for Environmental Health, Institute for Stem Cell Research, 85764 Neuherberg, Germany.

³Physiological Genomics, University of Munich, 80336 Munich, Germany. ⁴SYNERGY, Excellence Cluster of Systems, Neurology, Biomedical Center, 82152 Martinsried-Planegg, Germany. Correspondence and requests for materials should be addressed to V.B. (vborrell@umh.es).

A hallmark of neocortical development in gyrencephalic mammals is the formation of the outer subventricular zone (OSVZ)¹. This is a specialized germinal layer that emerges at mid-corticogenesis, contains vast numbers of progenitor cells and is crucial for the evolutionary expansion of the mammalian cerebral cortex in neuron number and surface area, thus promoting the emergence of gyrencephaly^{1–7}. To date, the mechanisms regulating the developmental emergence of the OSVZ remain largely unknown.

The OSVZ contains a variety of basal progenitor cells, namely, basal radial glial cells (bRGCs) and intermediate progenitor cells (IPCs)^{4,5,7–10}. IPCs are multipolar cells expressing the t-box transcription factor *Tbr2*, and are a major source of neocortical neurons in rodents^{11–16}. Basal RGCs resemble the apical RGCs (aRGCs) of the ventricular zone (VZ), including a radially extended basal process and expression of *Pax6*, but lack attachment to the apical adherens junction (AJ) belt^{4,8–10,17–19}. Basal RGCs are scarce in lissencephalic species^{17,18}, but very abundant in gyrencephalic mammals, where they are highly neurogenic and accumulate prominently in the OSVZ^{4,8–10,20}. Although lissencephalic mammals may develop a vestigial form of an OSVZ, it is in gyrencephalic species where this is largest, most complex and mitotically active^{1,4,8,10,21–23}.

In mouse, video microscopy studies of brain slices *in vitro* have revealed that IPCs and bRGCs have very poor self-renewing capacity, and their pool can only be maintained by the continuous production from aRGCs in the VZ^{13–16,18,24}. This process is finely regulated by the action of *Trnp1*, a DNA-binding protein that limits IPC and bRGC production^{7,25,26}. Similar *in vitro* analyses have shown that this process is much more complex in gyrencephalic species such as ferret, macaque and human, where IPCs and bRGCs in the OSVZ have been reported to proliferate and self-renew to some extent locally^{4,8,10,27}. However, it is not known when and where these cells first arise and if feeding into these progenitor pools continues throughout development.

Here we present the first *in vivo* analysis of progenitor cell lineage dynamics in ferret, a gyrencephalic carnivore, performed at multiple developmental stages and providing us with unprecedented insights into OSVZ formation and expansion in the intact embryo. Although phylogenetically distant from humans, cortical development in ferret shares many key features with humans and other primates, and uniquely allows *in vivo* and *in utero* manipulations. We find that the OSVZ is initiated during a brief period of embryonic development, when aRGCs undergo self-consuming divisions to massively produce bRGCs, which migrate past the inner subventricular zone (ISVZ) and become the founder cells of the OSVZ. After closure of this restricted period, aRGCs in VZ continue generating bRGCs, but only for the ISVZ, while progenitor cells in the OSVZ follow a completely independent lineage. The timing and duration of this restricted period depends on the dynamic regulation of *Cdh1* and *Trnp1* expression levels, when low expression of both genes is necessary to open this period, and high levels are sufficient to impair bRGC generation. Genetic abrogation of this restricted period reduces markedly seeding of bRGCs to the OSVZ and their abundance for the remaining cortical development, suggesting that its occurrence and modulation may have played an essential role in the evolutionary emergence and expansion of the OSVZ.

Results

Late OSVZ progenitor cells follow an independent lineage. To define the germinal layers generating OSVZ progenitor cells *in vivo*, we began by tracing the lineage of cortical progenitors. We injected *Gfp*-encoding retroviral vectors (*rv::Gfp*) into postnatal day 1 (P1) ferrets, stage equivalent to mouse embryonic

day (E) 15, rat E16 and 16 gestational weeks in human cerebral cortex, and analysed the lineage progression of infected progenitor cells at subsequent stages. We chose P1 because this is when OSVZ proliferation and bRGC abundance are maximal in this species^{4,20,28}. The lineage of VZ progenitors was selectively labelled by injecting *rv::Gfp* into the lateral telencephalic ventricle, thereby only transducing progenitor cells in contact with the ventricular surface, whereas the lineage of progenitors in ISVZ and OSVZ was labelled by local *rv::Gfp* injections into these layers (see Methods). Multiple cell populations were labelled across cortical layers regardless of the injection site, including cells with typical morphology of aRGCs, bRGCs, multipolar cells resembling IPCs (MP), bipolar cells resembling migrating neurons, differentiating neurons (DNs) and cells with star-like glial morphology (StC), which included cells in the astrocyte and oligodendrocyte lineages (Fig. 1a–f; Supplementary Figs 1 and 2). Analyses of marker expression with morphology confirmed the identity of aRGCs and bRGCs by their expression of *Ki67* and *Pax6*, and also showed that 24–34% of them expressed the T-box transcription factor *Tbr2*, as in primates⁸ (Fig. 1g–k).

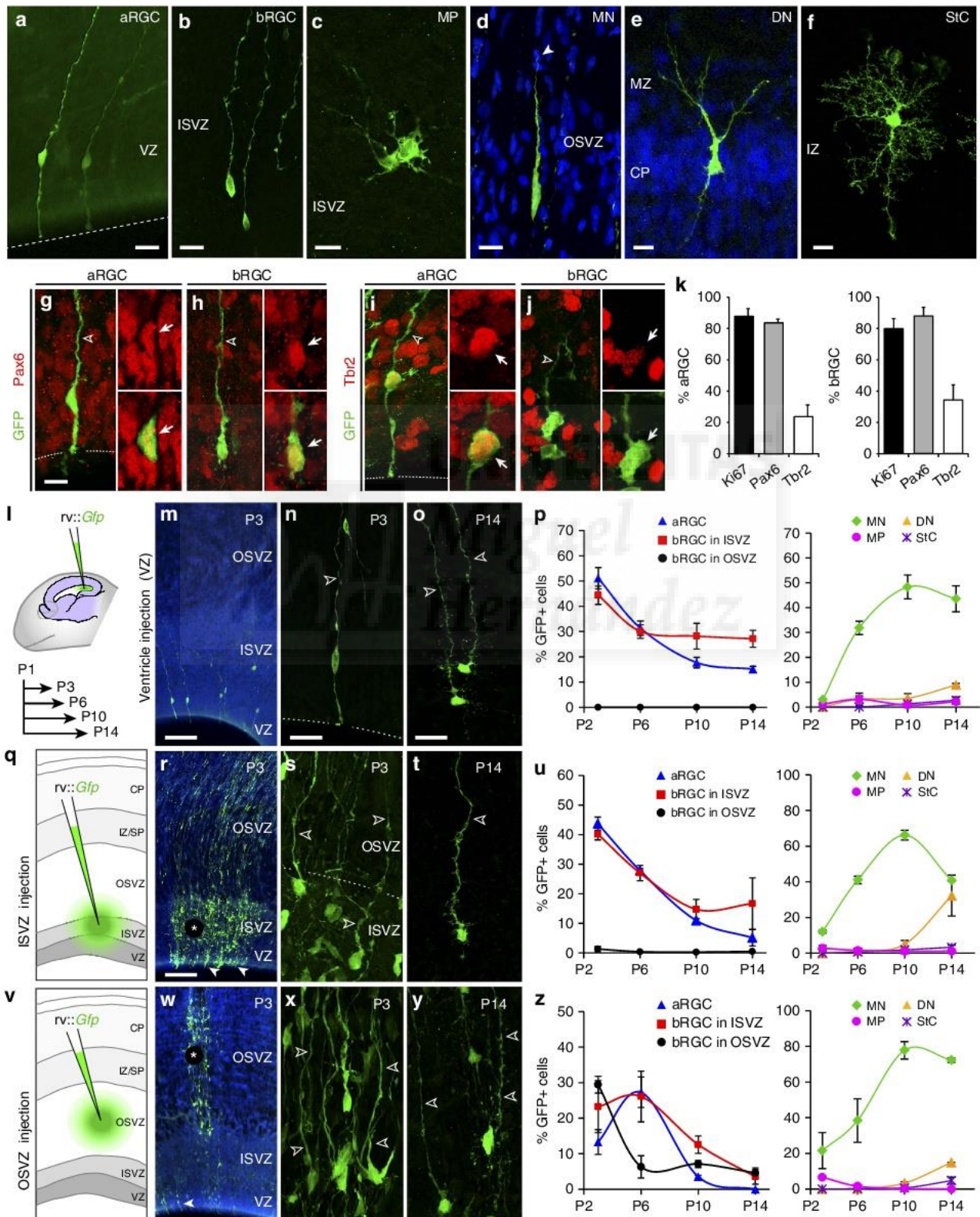
On infection of VZ progenitors with *rv::Gfp* at P1, by P3 we found that 50.6% of GFP+ cells were aRGCs and 45.3% bRGCs (Fig. 1l–n,p). The production of bRGCs from aRGCs was confirmed by two-photon video microscopy in slice cultures (Fig. 2a), in agreement with previous reports^{18,26,27,29}. Remarkably, the cell bodies of all bRGCs were found in ISVZ (hereon referred to as bRGCs in ISVZ) and none in OSVZ (hereon referred to as bRGCs in OSVZ; Fig. 1p). Because the OSVZ is further away from the VZ than ISVZ, we reasoned that 2 days of survival might be insufficient time for newly generated bRGCs to migrate from VZ to OSVZ. To test this, we next allowed longer survival periods after *rv::Gfp* injection. GFP labelling was traced for up to 2 weeks post injection, but the cell bodies of bRGCs continued absent from the OSVZ while very abundant in ISVZ (Figs 1o,p and 2b). These results provided the first demonstration *in vivo* that aRGCs are an abundant source of bRGCs in gyrencephalic species, but also that at late stages of cortical development these are solely destined to the ISVZ, without contributing to the OSVZ.

Next, we reasoned that if bRGCs in OSVZ were not produced directly from VZ, they might be generated indirectly via bRGCs in ISVZ. The above results seemed to rule out this possibility, as GFP+ bRGCs were not seen in OSVZ even long after they had been observed in ISVZ (Fig. 1o,p). An alternative possibility was that bRGCs in OSVZ were produced by other types of progenitor cells resident in ISVZ and/or not derived from the postnatal VZ. In such case, bRGCs in OSVZ would only be revealed by direct labelling of ISVZ progenitors. To test this, we injected *rv::Gfp* locally into the ISVZ of P1 ferrets (Fig. 1q,r). After 2 days of survival, abundant aRGCs and bRGCs were labelled in VZ and ISVZ, respectively, but were virtually absent in OSVZ (Fig. 1s,u). At longer survival times, bRGCs continued to represent the vast majority of GFP+ cells in ISVZ, but remained absent from OSVZ (Fig. 1t,u; Fig. 2b), demonstrating that bRGCs in OSVZ were not produced by progenitor cells in the postnatal ISVZ. Taken together, our results demonstrated that at peak stages of OSVZ expansion, VZ and ISVZ are abundant sources of bRGCs that will exclusively populate the ISVZ, but never contribute to the OSVZ.

Abundant generation of bRGCs in the postnatal OSVZ. To elucidate if bRGCs in the postnatal OSVZ were generated locally, we injected *rv::Gfp* into the OSVZ of P1 ferret kits (Fig. 1v,w). At P3, we found a majority of GFP+ cells in the OSVZ displaying bRGC morphology (Figs 1x,z and 2b), a proportion

that decreased by P6 to then remain similar until P14 (Figs 1y,z and 2b), demonstrating that OSVZ bRGCs are abundantly generated in the postnatal OSVZ. To investigate the dynamics of this bRGC production in OSVZ, we injected *rv::Gfp* at various stages and analysed after only 2 days of survival in each case. At P3 and P8, bRGCs represented 60–52% of cells born in OSVZ

(Fig. 2c), indicating their net increase (see Methods). Video microscopy in slice cultures demonstrated self-amplification of bRGCs, including *de novo* generation of a basal process (Fig. 2d) as in primates^{8,10}. Although OSVZ injections also labelled cells in ISVZ and VZ via their radial process (see Methods and Fig. 1w), our above analyses showed that these layers never generate OSVZ



bRGCs, and therefore these were being generated only locally by *rv::Gfp*-infected progenitors within the postnatal OSVZ.

At all these stages, IPCs (defined as the subset of MP cells that are Ki67+, Tbr2+) in ISVZ and OSVZ were a very small minority of cortical progenitors, as opposed to the mouse SVZ (Fig. 1p,u,z; Supplementary Fig. 3; Supplementary Note 1). Moreover, the few IPCs in OSVZ were not generated by VZ or ISVZ progenitors, but mainly locally within OSVZ similar to bRGCs (Supplementary Fig. 2). Taken together, our findings demonstrated that the OSVZ is a unique niche of progenitor cell production at postnatal stages, following a lineage independent from progenitors in VZ and ISVZ, and where the vast majority of progenitors are bRGCs that expand by self-amplification.

Embryonic initiation of OSVZ by founder bRGCs seeded from VZ.

In spite of our above findings, the key question of where and when OSVZ progenitors (mainly bRGCs) arise initially remained open. Given that all cortical cells derive from the early embryonic VZ at some point³⁰, we focused on earlier stages to determine the origin of OSVZ bRGCs. In ferret, the OSVZ is first distinguishable at E36 (equivalent to mouse E13), 6 days before birth (E42/P0; Fig. 3a), so we traced VZ progenitors with injections of *rv::Gfp* into the lateral telencephalic ventricle at E34 (equivalent to mouse E12.5) and E36 *in utero* (Fig. 3b). Two days after infection, numerous bRGCs expressed GFP in ISVZ, but none in OSVZ (Fig. 3c,d). Because 2 days of survival might be insufficient time for new bRGCs to migrate from VZ to OSVZ, we repeated the injections at E34, but now analysing at E38. Four gestational days after infection (E34–E38), 21.7% of bRGCs were in OSVZ (representing $8.0 \pm 1.8\%$ of all GFP+ cells; Fig. 3d). These results demonstrated that bRGCs in the postnatal OSVZ had been originally produced by aRGCs at embryonic stages, though not anymore at postnatal stages.

The lineage tracing between E34 and E38 potentially allowed for several rounds of cell division, so we could not distinguish if bRGCs in OSVZ had been generated in a single step directly by aRGCs in VZ at E34 or indirectly following a second round of division in ISVZ between E36 and E38. To distinguish between these possibilities, we injected *rv::Gfp* at E34, administered BrdU at E36.0 and E36.5 to label cells cycling between E36 and E37 (S-phase ≈ 12 h)^{20,31}, and analysed at E38 (Fig. 3e). BrdU administration was interrupted at E37 to avoid labelling bRGCs that might have reached the OSVZ early. Only 11.5% of all bRGCs in OSVZ contained BrdU (Fig. 3f–h), indicating that the majority had been directly generated by aRGCs in VZ before E36. In addition, *rv::Gfp* infection of VZ at E34 labelled some IPCs in OSVZ at E38 (MP, Ki67+; $0.46 \pm 0.37\%$ of GFP+ cells), unlike their null labelling at postnatal stages (Supplementary Fig. 2). Hence, aRGCs in the embryonic VZ produce bRGCs and IPCs

that migrate through the ISVZ *en route* to the OSVZ, a process not occurring after birth (E42) in the ferret cerebral cortex (Fig. 3i). Together, our results demonstrated that the OSVZ develops into two distinct phases: an early period of progenitor cell seeding from the VZ and a later period of self-amplification independent from other germinal layers.

A restricted period to massively produce OSVZ bRGCs from VZ.

To precisely define the embryonic period during which the VZ produces bRGCs (for any germinal layer), we monitored the developmental dynamics of bRGC generation from aRGCs with *rv::Gfp* injections *in utero* and 2-gestational day survivals (Fig. 4a). At all ages, virtually all cells born from VZ (GFP+) were aRGCs or bRGCs (Fig. 4b,c), but their proportions changed significantly along development. At E32 and E34, 47–56% of GFP+ cells were aRGCs, and only 29–34% bRGCs. Between E34 and E36, the production of bRGCs increased markedly to represent 66% of GFP+ cells at E36, paralleled by the self-consumption of aRGCs (24%; aRGCs are not regenerated on division, but produce two daughter cells different from the mother aRGC; see Methods; Fig. 4b,c). This situation lasted only 2 days, and by E38 and P1, the generation of bRGCs was down to 53–45% of GFP+ cells, respectively, and aRGCs were back up to 47–51% (Fig. 4b,c).

Given the short-survival time of these lineage experiments, and that the originally infected cells were aRGCs, we interpreted changes in the percentage of GFP+ aRGCs as changes in cell-fate decisions at the population level: self-amplification (>50% of GFP+ cells are aRGCs), self-renewal (50%) or consumption (<50% are aRGCs). Cell-fate decisions by aRGCs co-vary with their angle of mitotic cleavage plane, where vertical cleavage planes (60–90° to the VZ surface) occur in symmetric self-amplifying divisions and horizontal cleavage planes (0–30° to VZ surface) occur in asymmetric divisions generating bRGCs^{17,25,29,32,33}. In agreement with this notion, we found that the proportion of horizontal mitotic cleavage planes in VZ peaked transiently at E34, following a temporal dynamics parallel to the depletion of aRGCs and the production of bRGCs, which are maximal for VZ progenitors infected at E34 (Fig. 4d–f; Supplementary Fig. 4). In summary, bRGCs are generated by aRGCs following self-consuming divisions with a burst between E34 and E36.

Unfortunately, these lineage tracings across embryonic development were done with only 2 days of survival, which is too short to determine if the bRGCs generated were destined to OSVZ or not (Fig. 3d). To investigate whether the embryonic production of OSVZ bRGCs from the VZ was narrowly restricted to the burst period between E34 and E36 (Fig. 4c), or it continued at later stages, we infected VZ progenitors *in utero* with *rv::Gfp* at

Figure 1 | Postnatal VZ and ISVZ do not generate bRGCs for the OSVZ. (a–f) Examples of GFP+ cells after injection of *rv::Gfp* into VZ (lateral ventricle), ISVZ or OSVZ at P1, with stereotyped morphologies: apical radial glia cells (aRGCs), basal radial glia cells (bRGCs), multipolar cells (MP), migrating neuron (MN), differentiating neuron (DN) and star-like cells (StCs). DNs typically had the cell soma in the cortical plate (CP) and a single apical dendrite branching in the marginal zone (MZ). IZ, intermediate zone. (g–k) GFP+ aRGCs in VZ (g,i) and bRGCs in ISVZ (h,j) at P6 after ventricular injection of *rv::Gfp* at P1, showing expression of Pax6 (g,h) and Tbr2 (i,j) in both populations. (k) Abundance of aRGCs and bRGCs expressing Ki67, Pax6 or Tbr2 (aRGCs, $n=57$ cells, Ki67; 82 cells, Pax6; 61 cells, Tbr2; 3 animals; and bRGCs, $n=72$ cells, Ki67; 59 cells, Pax6; 31 cells, Tbr2; 3 animals). (l–u) P1 ferrets were injected with *rv::Gfp* into the lateral telencephalic ventricle to infect VZ (l–p) or injected locally into ISVZ (q–u), and analysed at various subsequent stages (p,u). Data refer to GFP+ cells across the cortical thickness. Cell lineages from these layers contained aRGCs in VZ (n) and abundant bRGCs in ISVZ throughout development (o,t; open arrowheads indicate the basal process), but null presence in OSVZ ($n=962$ – $5,544$ cells per group; Supplementary Table 1). (v–z) Ferrets were injected with *rv::Gfp* locally into OSVZ at P1 and analysed at later stages (z). GFP+ bRGCs were abundant in OSVZ at all survival times (x,y), demonstrating local bRGC production ($n=420$ – $3,742$ cells per group; Supplementary Table 1). The relative abundance of GFP+ aRGCs and bRGCs decreased rapidly from P3 to P6 regardless of the injection site, due to the progressive accumulation of GFP+ migrating neurons (MNs; p,u,z). Images in r and w show clusters of GFP+ cells at the injection site (asterisks), and cells retrogradely labelled in VZ (solid arrowheads). Values are mean \pm s.e.m. in k,p,u and z. Scale bars, 20 μ m (a–f); 10 μ m (g–j); 100 μ m (m–y) low magnifications, 20 μ m details.

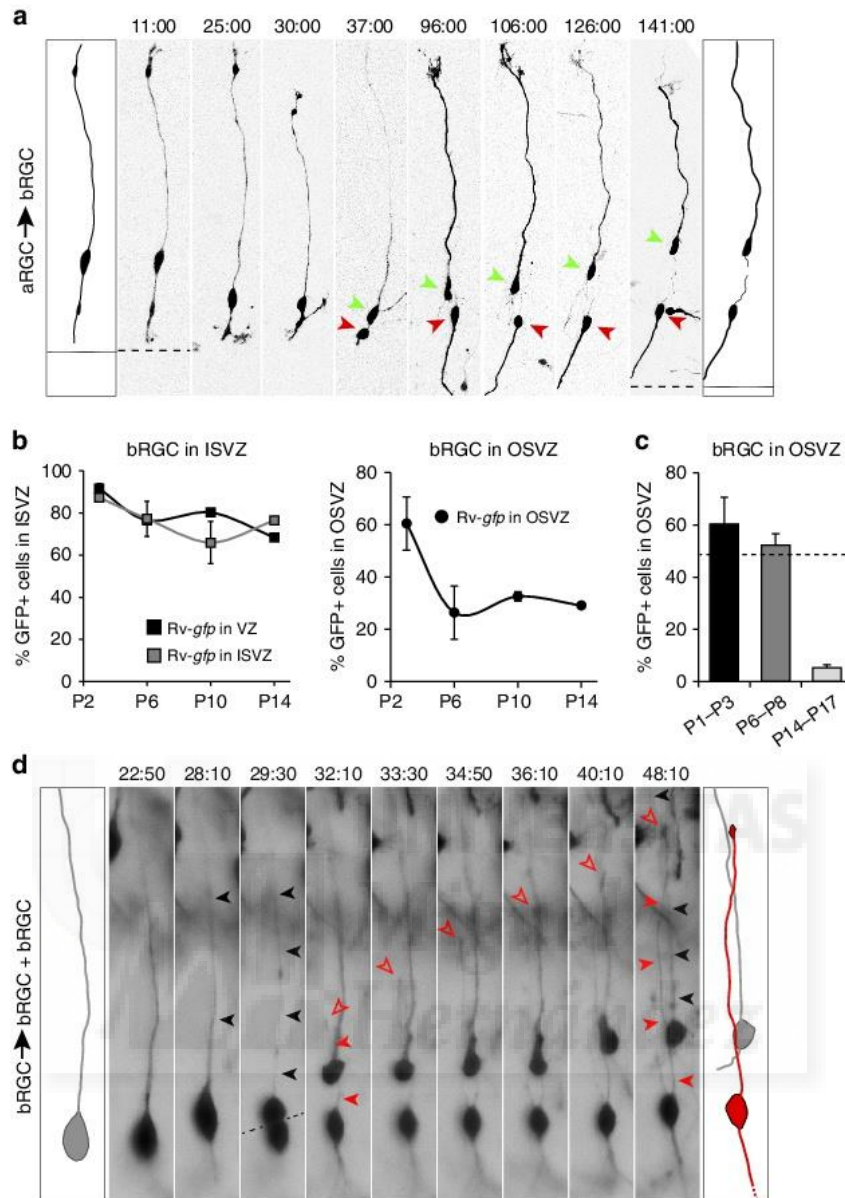


Figure 2 | Postnatal aRGCs generate ISVZ bRGCs, while OSVZ bRGCs are generated by self-amplification. (a) Time-lapse imaging frames of an aRGC dividing apically, between 30 and 37 h of imaging time, to generate a bRGC (green arrowhead) retaining the basal process. The apical cell (red arrowhead) retained the apical process. (b) Abundance of GFP + bRGCs located in ISVZ after VZ and ISVZ infections at P1 or in OSVZ after OSVZ injections at P1, and analysed at the indicated ages (mean values + s.e.m.; $n = 420$ -5,544 cells, 2-5 animals per group; Supplementary Table 1). (c) Abundance of GFP + bRGCs in OSVZ at the indicated postnatal stages after injections of *rv::Gfp* in OSVZ and 2-3 days of survival. Data are mean \pm s.e.m. ($n = 420$ cells, 3 animals, P1-P3; 1,288 cells, 4 animals, P6-P8; 819 cells, 2 animals, P14-P17); dashed line indicates 50%. (d) Time-lapse imaging frames of a bRGC in OSVZ with a basal process (black arrowheads), undergoing a near-horizontal division at $t = 29:30$ hours (dashed line) to generate two bRGCs. The basal daughter cell (top) retained the maternal basal process, whereas the apical daughter (bottom) grew a new basal process (solid red arrowheads) tipped with a small growth cone (red open arrowheads).

various stages and allowed 7-8 days of survival in each case, providing sufficient time for labelled cells to migrate and reach the OSVZ. We observed most OSVZ bRGCs in pups infected at E34, very few when infections were done at E36 and E38, and none in P1 injections (Fig. 4g,h). These experiments thus allowed us to identify and delineate the period of OSVZ bRGC production/seeding from the VZ with a prominent peak at E34 and very limited contributions at E36 and E38. As no OSVZ bRGCs are generated any longer at P1, their production is strikingly restricted to a rather brief period of cortical development (E34-P0), with a burst or maximum peak between E34 and E36.

***Cdh1* and *Trmp1* restrict the period for OSVZ generation.** To identify candidate genes regulating the dynamics of bRGC production by aRGCs, we searched for differential gene expression in VZ between three key stages: E30, E34 and P1. Using a ferret-specific microarray^{34,35}, we identified 1,852 differentially expressed genes (DEGs) between at least two stages (false discovery rate < 0.05 , fold change > 2 ; Fig. 5a). Only 59 DEGs were found between E30 and E34 (27 upregulated and 32 downregulated), whereas 1,822 genes changed between E34 and P1 (871 upregulated and 951 downregulated). Because the production of bRGCs increased in the early period (E30-E34), but then decreased in the late period (E34-P1; Fig. 4c), we

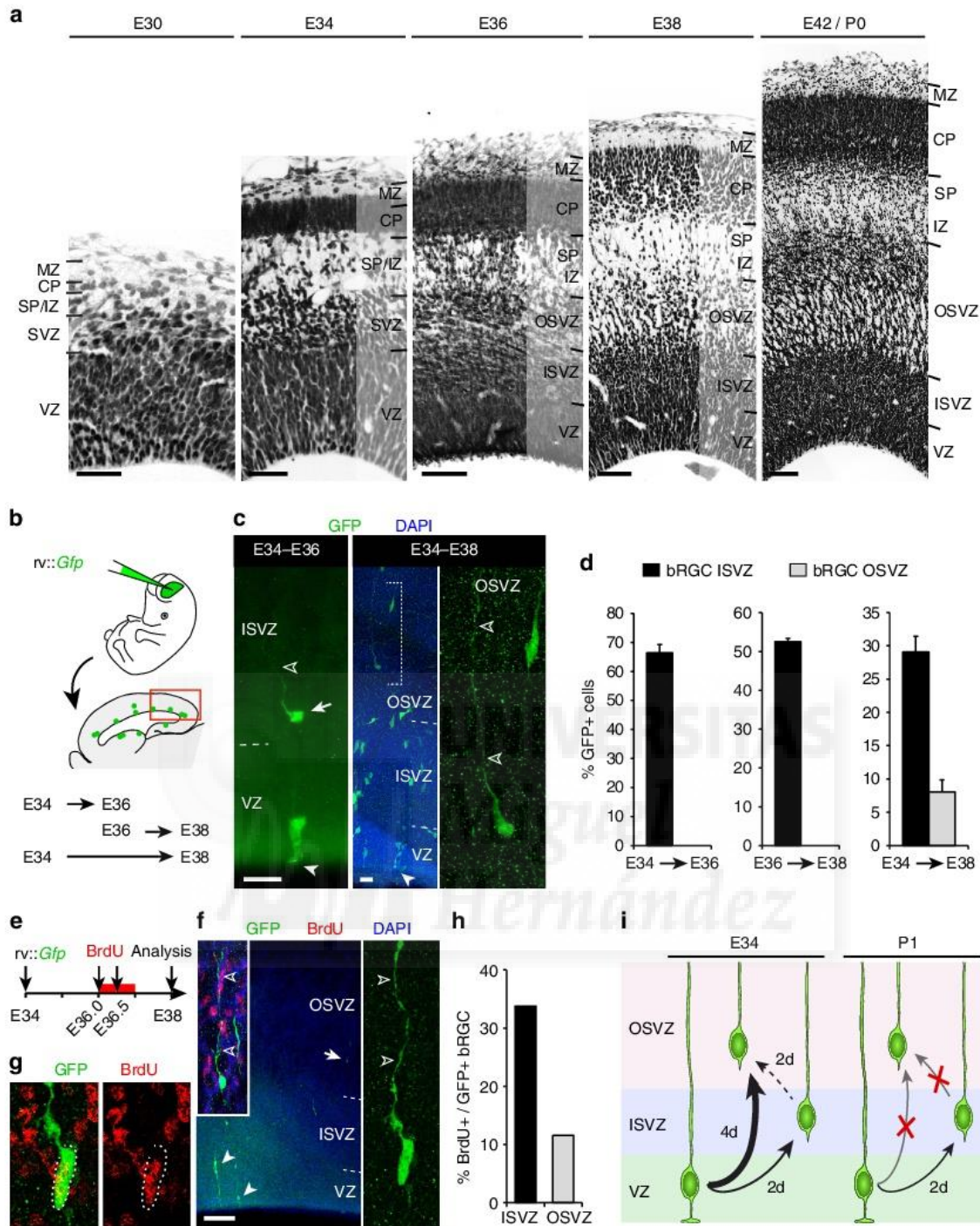


Figure 3 | Embryonic aRGCs generate directly bRGCs for the OSVZ. (a) Nissl stains of the ferret embryonic neocortex illustrate the developmental progression of germinal layers and the first histological recognition of OSVZ between E34 and E36. (b-d) Ferret embryos received a ventricular injection of *rv::Gfp* at E34 or E36, and developed *in utero* until E36 or E38. GFP + bRGCs were found in OSVZ after 4 days of survival (E34-E38, detail), but only in ISVZ after 2 days (E34-36, arrow; $n = 931$ cells, 8 embryos; E36-38, $n = 104$ cells, 2 embryos; E34-38, $n = 1,830$ cells, 7 embryos; mean values + s.e.m.). (e-h) VZ progenitors were labelled with *rv::Gfp* at E34, BrdU was administered 2 days later and were analysed at E38 (f,g). Arrow in f points at the bRGC magnified in inset. Very few GFP + bRGCs in OSVZ contained BrdU (f, right; f,g; $n = 229$ cells, 5 embryos), indicating that most were directly generated from VZ. In c and f, solid arrowheads indicate aRGCs and open arrowheads indicate basal process of bRGCs. (i) At E34, aRGCs generate bRGCs that reach the ISVZ 2 days later (E36) and OSVZ 4 days later (E38). Few bRGCs in OSVZ are generated between E36 and E38 (likely from ISVZ), the majority being generated between E34 and E36 directly from VZ. Postnatally, aRGCs generate bRGCs for the ISVZ, but neither generates bRGCs for the OSVZ. Scale bar, 30 μm (E30 and E34; a), 100 μm (E36; a), 150 μm (E38; a), 200 μm (E42/P0; a), 25 μm (c); 150 μm (f).

discarded DEGs whose expression levels changed in the same direction in both periods (first up- then again upregulated or first down- then again downregulated). Following the same reasoning, from the remaining DEGs we selected those whose expression

levels changed in opposite directions between early and late phases (first up- then downregulated or down- then upregulated). Only one gene followed this 'peak' profile of expression, which encodes a synaptic protein (Sv2b) that is not expressed in mouse

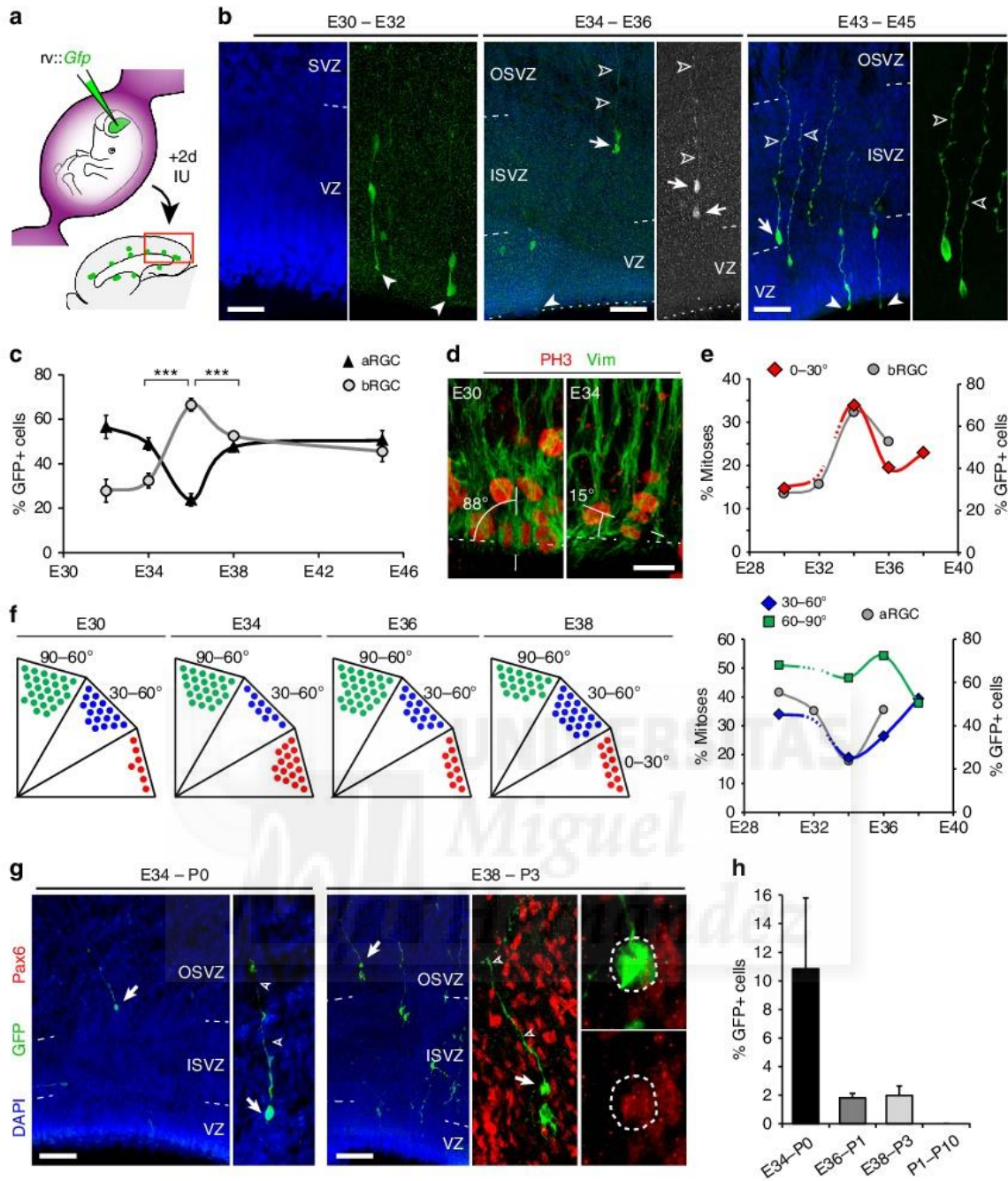


Figure 4 | Transient peak of bRGC production from aRGCs at the onset of OSVZ. (a-c) Tracing of bRGC production from aRGCs along development. Ferret embryos aged E30, E32, E34, E36 and E43/P1 kits received an intraventricular injection of *rv::Gfp* and were analysed 2 days later. (b) GFP labelling in embryos injected as indicated; solid arrowheads indicate ventricular end feet of aRGCs, arrows indicate bRGCs and open arrowheads indicate basal process. (c) Abundance of GFP + aRGCs and bRGCs at the indicated ages. Production of bRGCs peaked at E36, when aRGCs self-consumed (< 50%); ****P* < 0.001, χ^2 -test; *n* = 170 cells, E32; 304 cells, E34; 931 cells, E36; 104 cells, E38; 1,094 cells, E45/P3; 2-8 embryos per group; mean values \pm s.e.m. (d-f) Analysis of cleavage orientation plane of VZ mitoses with respect to ventricular surface (dashed lines; *n* = 91 cells, E30; 90 cells, E34; 124 cells, E36; 69 cells, E38; 2-8 embryos per group). Each dot in f represents 2% of mitoses. Data in e show that developmental variations in horizontal (0-30°, red) and oblique (30-60°, blue) cleavage planes were paralleled by bRGC and aRGC production, respectively, after *rv::Gfp* infection of VZ at those ages (grey curves). (g,h) Long-term GFP labelling of bRGCs in OSVZ (arrows) after intraventricular injection of *rv::Gfp* and analysis at the indicated ages. High magnifications show details of these bRGCs in OSVZ exhibiting a long basal process (open arrowheads) and expressing Pax6 (single confocal plane). (h) Abundance of GFP + cells corresponding to bRGCs in OSVZ at the indicated ages (E34-P0, *n* = 513 cells, 2 kits; E36-P1, *n* = 958 cells, 3 kits; E38-P3, *n* = 906 cells, 3 kits; P1-P10, *n* = 1,499 cells, 5 kits; mean values \pm s.e.m.). Note that embryonic VZ progenitors generate bRGCs that populate the postnatal OSVZ, in contrast to postnatal VZ progenitors that do not. Scale bar, 40 μ m (E32; b); 75 μ m (E36 and E45; b); 15 μ m (d); 100 μ m (g).

cortical progenitors (www.genepaint.org), and has no known function in cell proliferation, cell fate or delamination³⁶. At this point, we considered that the early phase (E30-E34) and late

phase (E34-P1) might be regulated by different genes, so we distinguished between genes changing only in the early phase ('early-change' profile) or the late phase ('late-change' profile);

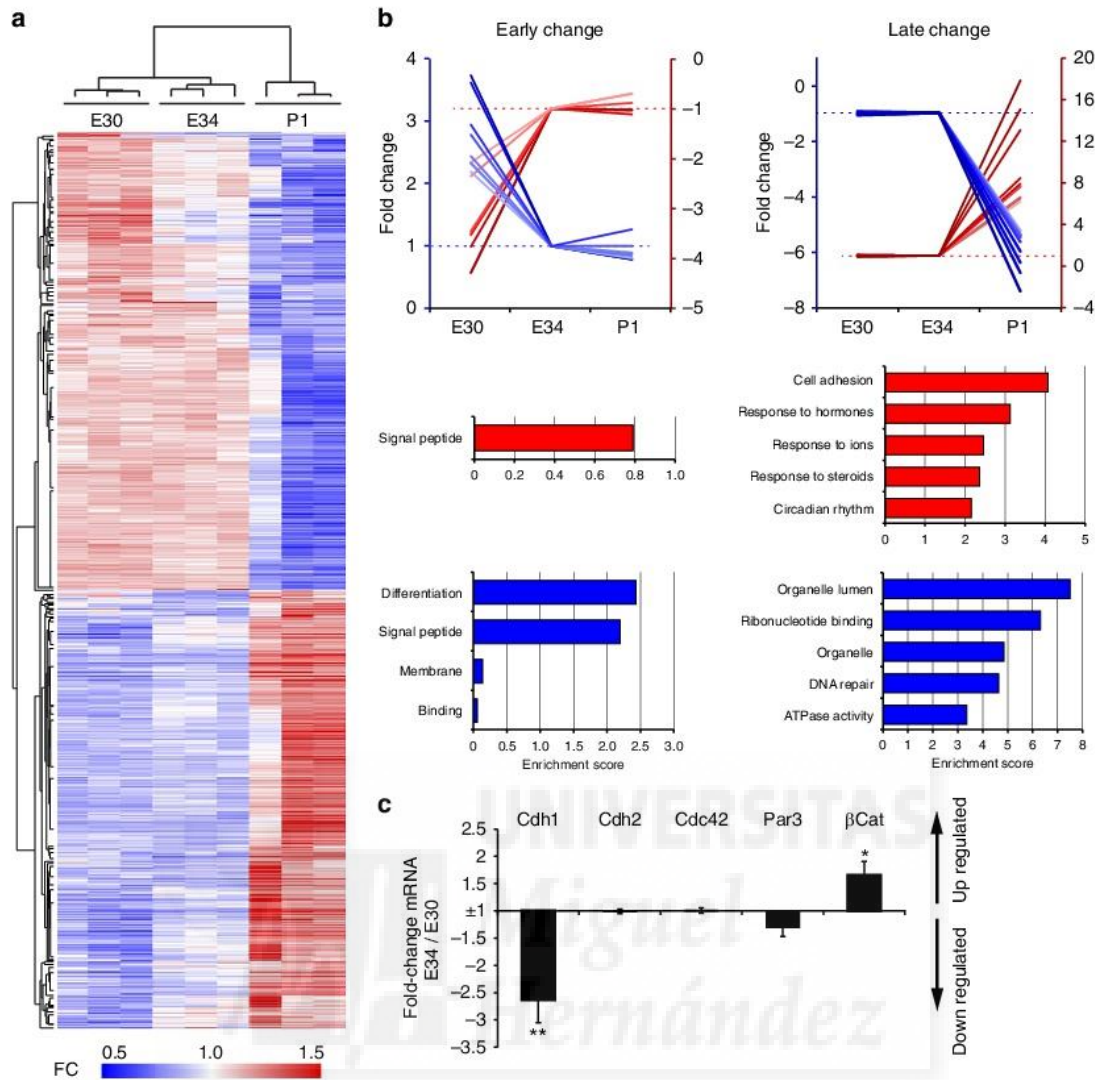


Figure 5 | Differential gene expression in VZ across developmental stages. (a) Heatmap of unsupervised hierarchical clustering of gene probes differentially expressed in VZ between E30, E34 and P1 (FC, fold change), and dendrogram of similarity between samples. Each lane is a biological replica. The vast majority of probes were differentially expressed between E34 and P1, but not between embryonic stages. (b) Examples of developmental expression profiles of differentially expressed genes, and for each profile the functional gene annotation terms as analysed and clustered using DAVID. The five clusters with the highest enrichment scores for up- and downregulated genes are shown. The vast majority of DEGs (FC > 2, $P < 0.05$) had 'late-change' profile (increase, red axis; decrease, blue axis; only 10 genes with highest FC in each axis are plotted), whereas much fewer had 'early' change profiles (41 probes). Red axes are for data represented in red, and blue axes for data in blue. (c) Quantitative RT-PCR data for candidate gene expression levels in VZ, expressed as FC between E34 and E30 (mean values \pm s.e.m.). Negative values indicate lower expression at E34 and positive values indicate higher expression at E34. *Cdh1* expression decreased > 2.5-fold between these two ages, whereas β Cat increased 1.6-fold and other apical complex protein genes remained unchanged. * $P < 0.05$, ** $P < 0.01$, t -test.

Fig. 5b; Supplementary Tables 2 and 3). Some of the early genes are related to axonal navigation (Slit and EphA5), whereas others are implicated in human diseases (LYPD1 and FAM167A). Late genes also include human disease genes such as BATF2 (acute stress disorder), GJB6 (sensorineural deafness and a variety of skin disorders) or APOE (lipoproteinemias), as well as a variety of biological functions such as cell adhesion (NDNF and THBS1), ribonucleotide binding (NABP1 and MSH3) or interaction with various organelles (FKBP4 and MARS2).

Unfortunately, functional gene annotation analysis of these gene sets showed that none of the 'early' DEGs were associated to biological processes related to BRGC production, such as mitotic spindle orientation or cell delamination from the apical junction belt^{7,19,37} (Fig. 5b; Supplementary Fig. 5), and hence were not

mechanistically promising. As microarray analysis always includes many false negatives due to the stringent statistical criteria, we scrutinized the array for AJ-related genes and found a trend of regulation for *Cdh1*. Therefore, we re-screened our samples by qRT-PCR to analyse AJ-related genes³⁰. Among our tested candidates, *Cadherin1* (*Cdh1*) was the only gene with significantly lower messenger RNA levels in VZ at E34 compared with E30 (Fig. 5c). Low *Cdh1* levels are known to promote cell detachment from the VZ in the embryonic cerebral cortex^{37–39}, so our data were consistent with the potential involvement of *Cdh1* in regulating BRGC generation from aRGCs in VZ between E30 and E34 (Fig. 6a–c). To test this hypothesis, we first performed *in utero* electroporation to express a dominant-negative *Cdh1* at E30 (DN-*Cdh1*, as described in ref. 40; Fig. 6d).

Of note, due to the high density of GFP+ cells in SVZ on electroporation (Fig. 6e), bRGCs could not be identified by morphology, unlike with *rv::Gfp*; hence, aRGCs and bRGCs were identified here as GFP+ cells expressing Pax6+ in VZ and SVZ, respectively. Overexpression of *DN-Cdh1* caused a 2.5-fold increase in GFP+ bRGC abundance and a significant decrease in GFP+ aRGCs by E32 (Fig. 6e,f). Because only a proportion of aRGCs were electroporated, this decrease in GFP+ aRGCs did not cause a general depletion of the VZ. Conversely, electroporation to overexpress *Cdh1* at E34 was sufficient to abrogate the massive bRGC production normally occurring between E34 and E36, down to 33% of control embryos (Fig. 6f). Thus, reduced *Cdh1* function is instrumental for the burst production of bRGCs destined for the OSVZ.

Cdh1 loss may promote bRGC formation and delamination by disruption of AJ integrity, but also by inducing changes in mitotic cleavage plane orientation, from vertical to oblique or horizontal⁴¹, as observed between E30 and E34 (Fig. 4e,f). To test this possibility, we compared the orientation of mitotic cleavage planes between control and cells expressing *DN-Cdh1* between E30 and E32. Similar to the endogenous reduction in cleavage angles between E30 and E34, we found that loss of *Cdh1* function led to a switch from vertical to smaller angles (Fig. 6g,h).

However, these changes did not perfectly phenocopy those observed between E32 and E34 in normal development (Fig. 4e), indicating that this process may be co-regulated by additional factors. These results demonstrated that the developmental loss of *Cdh1* leading to increased bRGC production may act both on the switch in mitotic cleavage plane orientation and loss of cell adhesion.

Regarding 'late' DEGs that might be responsible for the decrease in bRGC production between E34 and P1, Gene ontology analysis highlighted the terms cell adhesion, response to hormones, ions and steroids, organelle lumen, ribonucleotide binding and DNA repair (Fig. 5b). This list of 'late' genes included *Trnp1*, which was expressed twofold more at P1 than at E34 (Supplementary Table 3; Supplementary Fig. 5; Supplementary Note 1). *Trnp1* is a protein previously involved in bRGC generation, but only in mouse (without OSVZ), where acute downregulation of *Trnp1* causes overproduction of bRGCs²⁵. Thus, our expression data suggested that low levels of endogenous *Trnp1* in ferret VZ at E34 may favour massive bRGC production for the OSVZ, while higher *Trnp1* levels at birth may close this period (Fig. 7a-c). To test the potential involvement of *Trnp1* in regulating bRGC production for the OSVZ, we first used retroviruses to overexpress *Trnp1* in the VZ of E34 embryos and

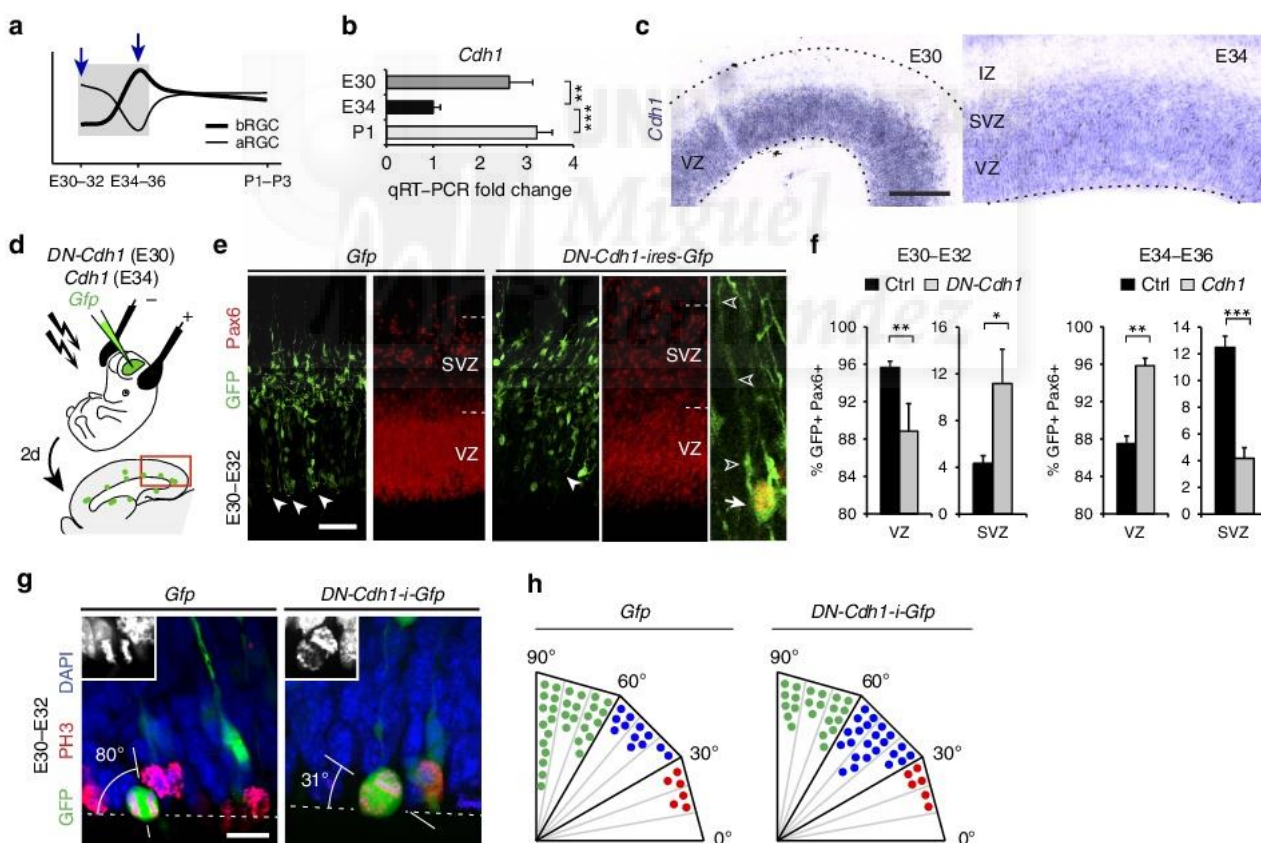


Figure 6 | Onset of the restricted period for bRGC production and OSVZ generation depends on developmental variations of *Cdh1* expression. (a) Schematic of the early period of bRGC generation from aRGCs. (b,c) Candidate gene screening by qRT-PCR revealed *Cdh1* as differentially expressed in VZ between E30, E34 and P1 (b; mean values + s.e.m., ** $P < 0.01$, *** $P < 0.001$, unpaired *t*-test), also shown by ISH (c). (d-f) *In utero* electroporation of *DN-Cdh1* from E30 to E32 increased bRGC production (GFP+ /Pax6+ cells in SVZ) and decreased aRGCs, whereas overexpression of *Cdh1* from E34 to E36 had the opposite effect. In these experiments, GFP+ cells in SVZ were at high density, making unreliable the identification of bRGCs by morphology. Instead, bRGCs were identified as Pax6+ /GFP+ cells with the cell body in SVZ, and aRGCs as Pax6+ /GFP+ cells with the cell body in VZ and a distinct apical process. Numbers of cells and embryos analysed are indicated in Supplementary Table 4; * $P < 0.05$, ** $P < 0.01$, *** $P < 0.001$, χ^2 -test. (g,h) Analysis of cleavage orientation plane of VZ mitoses with respect to ventricular surface (dashed lines) in *Gfp*- and *DN-Cdh1-i-Gfp*-overexpressing cells ($n = 103$ cells, Ctrl; 51 cells, *DN-Cdh1*; 2 embryos per group). Insets are details of each mitosis under 4,6-diamidino-2-phenylindole (DAPI) stain. Each dot in h represents 2% of mitoses. Scale bar, 150 μm (c); 75 μm (e); 15 μm (g).

analysed the cellular output at E36 (Fig. 7d). The abundance of GFP+ bRGCs was reduced to nearly half in *Trnp1*-overexpressing embryos compared with control embryos expressing GFP alone, and this was concomitant with a twofold increase in aRGC abundance (Fig. 7e,f). This demonstrated that low levels of endogenous *Trnp1* expression are important for bRGC production between E34 and E36. To define if this decrease in bRGC generation indeed affects seeding of the OSVZ, we again overexpressed *Trnp1* in VZ cells at E34, but now followed by long-term survival until E42/P0 (Fig. 7g). The OSVZ of *Trnp1*-overexpressing ferrets was nearly devoid of GFP+ bRGCs (these only represented 0.9% of GFP+ cells), concomitant with a relative increase in aRGCs, but remarkably with no relative alteration of ISVZ (Fig. 7h,i). This demonstrated that in our previous short-survival experiments, many bRGCs observed in ISVZ were *en route* to the OSVZ. Also, that E34–E42/P0 is a period essential for the generation of bRGCs that will seed and found the OSVZ, with a peak of bRGC production between E34 and E36, before this layer becomes independent from VZ at P1.

Finally, we performed the converse manipulation, overexpressing a dominant-negative *Trnp1* in VZ progenitors between P1 and P3 (*Trnp1*-GFP fusion protein, as described in ref. 25), to test whether the high endogenous levels of *Trnp1* expression at P1 might be responsible for the significant decrease in bRGC generation and closure of the restricted period (Fig. 7d).

Compared with GFP-injected controls, expression of DN-*Trnp1* increased significantly the production of bRGCs, while reducing aRGCs (Fig. 7f). Together, our results demonstrated that the dynamic temporal regulation of *Cdh1* and *Trnp1* expression is necessary and sufficient to control the variations in bRGC generation from aRGCs during cortical development. High expression of *Cdh1* and *Trnp1* is sufficient to limit bRGC generation before and after the restricted period, respectively, whereas low expression of both genes simultaneously is necessary for the massive self-consumption of aRGCs to produce bRGCs, and thus for the restricted period of OSVZ generation.

Discussion

Our study identifies a completely novel mechanism involved in cortical development, whereby the formation of a germinal layer (OSVZ) depends on the seeding of founder progenitor cells during a restricted period. We show that the OSVZ first emerges by the accumulation of large amounts of bRGCs generated directly by apical progenitors in the VZ. This seeding of progenitor cells from VZ to OSVZ is only transient, and eventually the OSVZ lineage becomes completely independent from the other germinal layers and thereon relies on the self-amplification of its progenitor cells for further expansion to its remarkable size at subsequent stages (Fig. 8). These are highly

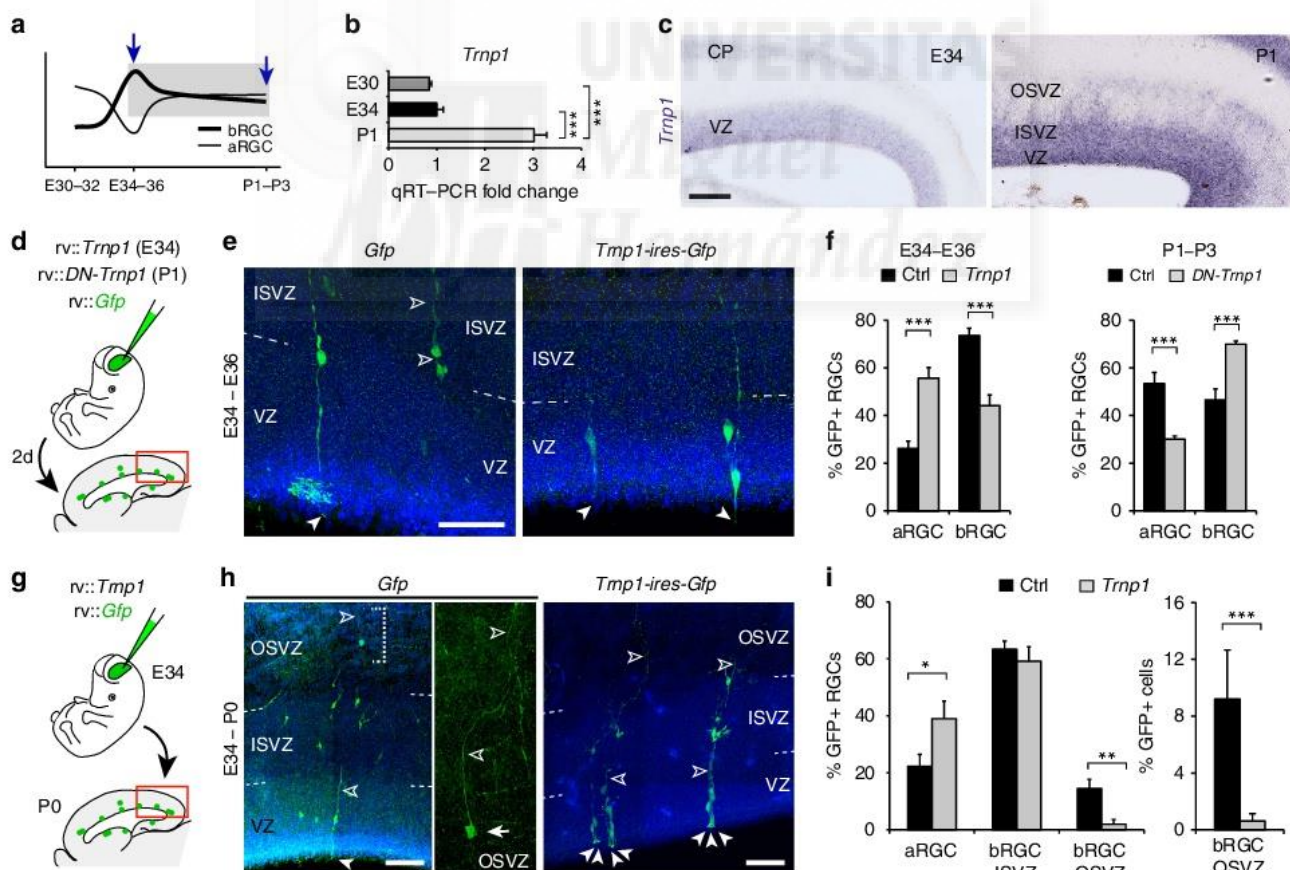


Figure 7 | Closure of the restricted period for bRGC production and OSVZ generation depends on developmental variations of *Trnp1* expression. (a–c) Validation by qRT-PCR and ISH of differential expression of *Trnp1* between E34 and P1 (later period of bRGC generation from aRGC; mean values + s.e.m., $^{***}P < 0.001$, unpaired *t*-test). (d–f) Overexpression of *Trnp1* by retroviral delivery from E34 to E36 decreased bRGC production and increased aRGC abundance, whereas expression of dominant-negative (DN) *Trnp1* from P1 to P3 had the opposite effect (mean values + s.e.m., $^{***}P < 0.001$, χ^2 -test). (g–i) Sustained overexpression of *Trnp1* from E34 to P0 by retroviral delivery markedly blocked bRGC production for the OSVZ. Measures are relative to GFP+ RGCs, or all GFP+ cells in lineage (mean values + s.e.m., $^{*}P < 0.05$, $^{**}P < 0.01$, $^{***}P < 0.001$, χ^2 -test). In all panels, solid arrowheads indicate apical end feet of aRGCs and open arrowheads indicate basal fibres of bRGCs. Scale bar, 150 μm (c); 75 μm (e,h).

unexpected findings, extending the complexity of the mechanisms that regulate cortical development and expansion^{3,42,43}. We find that the period for bRGC seeding of the OSVZ depends on the combined temporal regulation of *Cdh1* and *Trnp1* expression in VZ (Fig. 8). These two genes were previously studied in mouse and shown to play key roles in the balance between self-renewal and delamination of aRGCs in the VZ^{25,40,44}. Here we provide the first demonstration of a functional relationship between *Cdh1* and *Trnp1*, and of their endogenous regulation to dynamically modulate bRGC production in the developing embryo. Importantly, we show that abrogation of bRGC production by maintaining elevated *Trnp1* levels from E34 onward resulted in a severe reduction of OSVZ cell lineages in the long term (E42/P0). Therefore, given that this period of production of bRGC for the OSVZ is very brief (with a maximum peak between E34 and E36 and very limited contributions at E36 and E38), its timing is under tight genetic control, and the abrogation of bRGC production during this embryonic period results in their virtual absence in the postnatal OSVZ, this may be considered a critical period for the formation of the OSVZ. Given the relevance of the OSVZ in the development of gyrencephaly^{2,3,7,45}, the temporally dynamic regulation of endogenous *Trnp1* and *Cdh1* expression during embryogenesis might have evolved as a mechanism generating cortical phenotypic diversity in mammals.

Previous video microscopy analyses of slice cultures from embryonic human and non-human primate cerebral cortex revealed a wide variety of progenitor cell types in the OSVZ and other germinal layers, and some of their complex lineage relationships^{8,10,29}. However, the developmental origin of the OSVZ during gestation was never identified primarily due to the lack of appropriate *in vivo* models where this can be addressed. Likewise, the types of neurons generated by VZ, ISVZ and OSVZ cannot be studied in slice cultures due to survival time limitations, but only *in vivo*. One previous report in the early postnatal ferret demonstrated that the lineages of both VZ and OSVZ are neurogenic, producing layer 2/3 pyramidal neurons with no reported differences⁴. Here we use also the ferret to define the cellular substrates for the developmental origin and expansion of the OSVZ *in vivo*. The process we have identified in ferret is completely different than in the mouse cerebral cortex, where basal progenitors rarely self-renew and the SVZ is formed by transient populations of progenitor cells that are continuously seeded by the VZ and self-consumed shortly after^{13–16,24}. Even in the mouse lateral ganglionic eminence, where the SVZ is largest and progenitors frequently self-amplify, there is continuous seeding from aRGCs²⁶. Importantly, although rodents and primates are closer in phylogeny than with carnivores such as

the ferret⁴⁶, many of the typical features of OSVZ and bRGCs in ferret are strikingly similar to human and macaque, but different from mouse (that is, self-amplification, relative abundance of bRGCs and IPCs). Hence, we speculate that a similar critical period for the formation of the OSVZ, and its subsequent independent lineage, may also occur in human and other primates. Given that seeding of the OSVZ occurs only during a brief and transient period (E34–P0), the rate of self-amplification of its constituent progenitor cells becomes a major factor for its expansion and size. This notion is consistent with the dynamics of bRGC proliferation in the OSVZ observed in non-human primates, where this layer undergoes a massive increase in the size during a period of rapid bRGC self-amplification⁸. Intriguingly, the ISVZ seems to share features with the mouse SVZ, as it continuously receives bRGCs from the VZ while maintaining some self-renewing capacity. Expansive cell lineages are frequent in the mouse lateral ganglionic eminence (LGE)²⁶, suggesting the evolutionary co-option of this strategy in forebrain development⁴².

One major difference between aRGCs and bRGCs is their epithelial nature, where aRGCs are anchored to the ventricular surface by AJs, while bRGCs are not. Thus, the generation of bRGCs from aRGCs may be favoured by oblique and horizontal mitotic cleavage planes, combined with an active loss of AJs, leading to the apical detachment of daughter cells^{17,25–27,29}. Orientation of mitotic spindle is molecularly regulated by a protein complex including mInsc, LGN, Par3, aPKC and also *Cdh1*, the blockade of which favours oblique or horizontal cleavage planes and results in an excess of daughter cells delaminating from the ventricular surface^{33,41,47,48}. Accordingly, we find that the onset of the restricted period with a massive generation of bRGCs from aRGCs is bookmarked by a significant decrease in *Cdh1* expression and a shift in mitotic cleavage plane orientation, and we have demonstrated a causal relationship between these three events. However, the combined frequency of divisions with oblique or horizontal cleavage planes that we have observed at the critical period (E34: 50%) can only explain the delamination from VZ of 25% of daughter cells, but not 70% as we observed by lineage tracing (Fig. 4). The delamination of additional cells may require the loss of apical anchoring, which occurs on the loss of AJ proteins, their links to the cytoplasm such as α - and β -catenin or regulators of the F-actin belt linking AJs such as RhoA^{30,49}. Among these factors, *Cdh1* is a crucial component of AJs previously implicated in regulating apical cell delamination (though not bRGC production), and here we show that the loss of *Cdh1* leads to the loss of aRGCs and increased bRGC production. Hence, our present findings point at *Cdh1* as

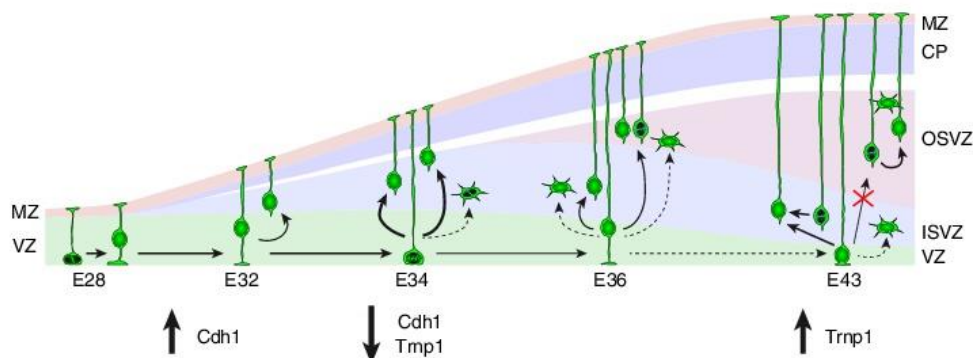


Figure 8 | Model of developmental formation of OSVZ. During an early developmental period aRGCs self-renew, sustained by high levels of *Cdh1*. Between E34 and E36, a decrease in *Cdh1* expression combined with low *Trnp1* levels open the critical period for OSVZ formation, driving aRGCs into self-consuming divisions and generating bRGCs massively. These early bRGCs become founder cells of the OSVZ. After birth (E42/P0), a rise in *Trnp1* levels blocks the production of bRGCs to the OSVZ and closes this critical period. From this point onward, the OSVZ follows a lineage independent from VZ and ISVZ, sustained by bRGC self-amplification, while VZ continues to seed bRGCs to ISVZ.

key in the production of bRGCs from aRGCs by regulating both mitotic cleavage plane orientation and delamination from the AJ belt. Repression of cadherins and cell delamination from VZ is promoted by the Snail family of transcription factors, and also by Robo receptor signalling^{37,38,50}. Unfortunately, current detection methods are insufficient to reveal differences in membrane-bound Cdh1 between individual aRGCs primed for delamination versus not. Finally, closure of the period of massive bRGC production at E36 is marked by an increase in *Trnp1* expression, which favours vertical cleavage planes and has been shown to repress bRGC production in mouse²⁵.

Our results demonstrate that the combined regulation of endogenous *Cdh1* and *Trnp1* levels is necessary and sufficient to control the abundance of VZ cell depletion and bRGC seeding, and thus it defines the time window for our newly identified critical period of OSVZ formation. Our *Cdh1* and *Trnp1* downregulation experiments demonstrate that aRGCs have the intrinsic potential to generate OSVZ bRGCs before and after the critical period, so the onset and duration of this period could be easily modified in phylogeny or disease by changing the temporal expression of these genes. Given the relevance of the OSVZ in cortical expansion and folding^{2,3,7}, the evolution of mechanisms controlling the precise temporal regulation of critical period genes seems key to generate the extraordinary diversity of cortical phenotypes across mammals^{42,51}.

Critical periods are unique windows of opportunity during development, but also periods of high vulnerability to disease^{52,53}. Given the central role of the OSVZ in cortical development from ferrets to monkeys and humans, including neurogenesis and surface area expansion^{4,6,8,10}, the critical period of OSVZ seeding is a time of susceptibility to cortical disease, where subtle or acute defects may have magnified long-term consequences. Indeed, acute abrogation of cell proliferation in ferret embryos at the onset of this critical period leads to reduced OSVZ and lissencephaly⁵⁴. In humans, brain malformations due to acute insults in fetal development are rarely traced, but defects in VZ integrity, progenitor proliferation and precise gene expression regulation are emerging as critical in malformations of cortical development^{55–58}. Our identification of the critical period for OSVZ formation in ferret brings a novel perspective to fundamental mechanisms of cortical development, and this may help to better frame the mechanistic effect of mutations perturbing cerebral cortex development in humans.

Methods

Animals. Pigmented ferrets (*Mustela putorius furo*) were obtained from Marshall Bioresources (North Rose, NY) and isoquimen (Barcelona, Spain), and kept on a 16:8-h light:dark cycle at the Animal Facilities of the Universidad Miguel Hernández. Wild-type mice were maintained in an Institute for Cancer Research; Harlan Inc. (ICR) background. The day of vaginal plug was considered as embryonic day (E) 0.5. All animals were treated according to Spanish and EU regulations, and experimental protocols were approved by the Universidad Miguel Hernández Institutional Animal Care and Use Committee (IACUC).

Constructs. For retroviral delivery, constructs encoding *Gfp* alone, *Trnp1-Gfp* fusion protein (*Trnp1-DN*) or a bicistronic cassette encoding *Trnp1-IRES-Gfp*²⁵ were subcloned into a murine moloney leukemia virus (MMLV) retroviral-packaging vector downstream of the CAG promoter (generous gift of F.H. Gage). For electroporation, constructs encoding *Gfp*, *E-Cadherin* (Addgene #28009) or *DN-Cdh1* ref. 40) were subcloned into a pCAG promoter-containing vector. All plasmids were produced under endotoxin-free conditions (QIAGEN EndoFree Plasmid Maxi kit).

Virus injections and electroporation. High-titre MMLV-based VSVG-pseudotyped retrovirus (5×10^7 – 5×10^8 p.f.u. ml⁻¹) encoding *Gfp*, *Trnp1-ires-Gfp* or *Trnp1-Gfp* under the CAG promoter were prepared by transient transfection of HEK293 cells, concentrated by ultracentrifugation and viral titre estimated by clonal infection of HEK cell cultures⁵⁹. High-titre replication-incompetent adenovirus (9.3×10^{11} v.p. ml⁻¹) encoding *Gfp* under the CMV promoter were

obtained from QBioGene (Irvine, CA). Viral solutions were injected using pulled glass micropipettes. For postnatal injections, ferret kits were deeply anaesthetized and maintained with 1.5% isoflurane during surgery, and injections were aimed at the telencephalic lateral ventricle, ISVZ or OSVZ by means of stereotaxic coordinates: lateral ventricle: antero-posterior (AP) = -0.5 mm, latero-medial (LM) = 2.0 mm, dorso-ventral (DV) = 2.0 mm, with an AP inclination of 22.5°; ISVZ: AP = -1.3 mm, LM = 2.0 mm, DV = 2.0 mm, with an AP inclination of 22.5°; OSVZ: AP = -1.3 mm, LM = 1.6 mm, DV = 2 mm, with an AP inclination of 45°. These injections were very accurate, as confirmed *a posteriori* with short-survival animals where the bulk of GFP-labelled cells indicated the tip of the injection pipette (for ISVZ and OSVZ injections), and sparse cell labelling in VZ across the entire cortex indicated that the virus had been injected in the lateral telencephalic ventricle (Fig. 1). We only found 2 out of 11 animals where injections aimed at ISVZ actually labelled a sparse number of VZ cells, and thus had occurred in the ventricular cavity. On injection in ISVZ and OSVZ, aRGCs cells in VZ and bRGCs in ISVZ were also labelled immediately below the injection site, infected retrogradely via their basal process.

For *in utero* injections in both ferret and mouse, timed-pregnant females were deeply anaesthetized and maintained in 2% isoflurane during surgery. The abdominal cavity was open, the uterine horns exposed and retrovirus solutions were pressure injected into the telencephalic lateral ventricle of embryos through the uterine wall.

For electroporation, DNA plasmids encoded *Gfp*, *E-Cadherin* (*Cdh1*) or *DN-Cdh1*, under the CAG promoter. *In utero* and postnatal electroporation of ferret embryos and kits were performed as described^{60,61}. After the appropriate survival period, postnatal kits or pregnant females were overdosed with sodium pentobarbital (Nembutal), and further processed for immunohistochemistry or *in situ* hybridization (ISH).

Immunohistochemistry and ISH. For histological analysis, embryos were obtained by caesarean section of timed-pregnant females on deep anaesthesia with sodium pentobarbital, and perfused transcardially with 4% paraformaldehyde; postnatal ferrets were deeply anaesthetized with sodium pentobarbital before transcardiac perfusion with paraformaldehyde. After perfusion, brains were extracted and sectioned. For immunohistochemistry, brain sections were incubated with primary antibodies overnight (anti-GFP, 1:1,000, Aves Labs; anti-Pax6 1:500, Millipore; anti-Tbr2 1:200, Abcam; anti-PhVim, 1:1,000, Abcam; anti-PH3, 1:1,000, Upstate; anti-Ki67, 1:200, Novocastra; anti-BrdU, 1:200, Abcam; anti-GFAP, 1:1,000, Dako; anti-Olig2, 1:100, IBL), followed by appropriate fluorescently conjugated secondary antibodies (1:200, Jackson), and counterstained with 4,6-diamidino-2-phenylindole (Sigma). For anti-BrdU staining, sections were pretreated with 2N HCl for 30 min. For ISH, sense and anti-sense complementary RNA probes were synthesized and labelled with digoxigenin (Roche Diagnostics) according to the manufacturer's instructions. ISH was performed as described previously⁴. Ferret-specific ISH probes were cloned using the following primers: *Trnp1*, forward: 5'-TCTGGACTCTGGATTGAGC-3', reverse: 5'-TGCCCGTGTGTCTATCTGAG-3'; *Cdh1*, forward: 5'-CGGAGCTGAGTTTCTGGTC-3', reverse: 5'-GAGGCTGTGGATTCTTCFG-3'. These ferret-specific primers were designed based on the same ferret-specific sequences as in the microarray. PCR was performed using Go Taq Flexi DNA polymerase (Promega), and the resulting amplicons were purified with Wizard SV Gel and PCR Clean-Up System (Promega) and cloned into pGEM-T Easy Vector System I.

Slice culture and time-lapse imaging. Ferret brain slices were prepared and maintained in culture as described previously⁶². To image aRGC behaviours, P1 ferrets were injected with rv:*Gfp*, and their brains obtained for slicing at P6. To image the behaviour of bRGCs in OSVZ, slices were prepared from unmanipulated P18 ferrets, and 1 h later, slices received various injections of Ad-GFP (3–6 nl per injection site, 2–8 injection sites per slice) in the cortical plate. One day after slice preparation, slices containing fluorescent cells were selected for time-lapse imaging. Images were obtained either under fluorescence optics (Filter 41017, EX449-489/EM500-548; Chroma, Rockingham, VT, USA) through an air immersion $\times 20$ lens in an inverted epifluorescence microscope or under two-photon optics ($\times 40$) through a water immersion $\times 20$ lens in a Leica SP2 inverted microscope, both equipped with an incubation chamber: 5% CO₂, 37 °C. Frames were obtained intermittently during 49–142 h in culture. Digital images were acquired, contrast-enhanced and analysed with Metamorph (Microbrightfield) or Imaris software (Bitplane).

Microarray and qRT-PCR. For RNA extraction, P1 ferret kits were deeply anaesthetized, and timed-pregnant ferret females were deeply anaesthetized and their living embryos were obtained by caesarean section. Subjects were then decapitated, their brains dissected and blocked in ice-cold ACSF (140 mM NaCl, 5 mM KCl, 1 mM MgCl₂, 24 mM D-glucose, 10 mM HEPES, 1 mM CaCl₂, pH 7.2), and tissue blocks containing the occipital cortex were vibrotome-cut in 300- μ m-thick slices. Living cortical slices were further microdissected with microsurgical tools in ice-cold ACSF to isolate the VZ from the caudal pole of the cerebral cortex. Germinal layers were identified in living slices under the dissection scope, where the VZ was the most opaque layer on the apical side of the cortex. Tissue pieces were fresh-frozen in Trizol for RNA extraction, with a post-mortem interval of <1 h.

Total RNA was extracted using RNeasy Mini kit (Quiagen), followed by treatment with RNase-Free DNase Set (Quiagen). RNA quality was confirmed using the RNA 6000 Nano kit on the Agilent Bioanalyzer platform, and then 200 ng of total RNA was labelled using the one-colour labelling kit from Agilent Technologies according to the manufacturer's protocol. Labelled complementary RNA was then hybridized for 16 h on a custom-made microarray containing 43,692 ferret-specific probes covering 17,386 genes⁶³. Microarray slides were scanned on an Agilent High-Resolution C Scanner, and the raw image files were processed by the Agilent feature extraction software. Raw data files were normalized using quantile normalization in Partek Genomics Suite. Statistical analysis of microarray data was done in Multiexperiment Viewer⁶⁴. To identify genes with significantly different expression levels, we used analysis of variance comparisons between samples, using *P*-values based on 500 permutations and Bonferroni false discovery correction, as in Ayoub *et al.*⁶⁵. Functional gene annotation analysis was performed using the web-based DAVID v6.7 software (<http://david.abcc.ncifcrf.gov>)⁶⁶. The microarray data from this publication have been submitted to the GEO database (<http://www.ncbi.nlm.nih.gov/geo/>) and assigned the identifier GSE63203.

For qRT-PCR, primers for ferret gene homologues were designed based on the same ferret-specific sequences. Template complementary DNA was generated using Maxima First Strand cDNA Synthesis kit for quantitative real-time PCR (qRT-PCR; Thermo Fisher). Quantitative RT-PCR was performed using the Step One Plus sequence detection system and the SYBR Green method (Applied Biosystems), with each point examined in triplicate. Transcript levels were calculated using the comparative Ct method normalized using actin. Primers used were: Trnp1, forward: 5'-TTGGTCTGAGAAATCCCTGC-3', reverse: 5'-CGCTGTGCTCTATCTGAGGAAG-3'; Cdh1, forward: 5'-TGCCCAGAAAACGAGAAAGG-3', reverse: 5'-ACAAATACACCAACCGGAGG-3'; actin, primers as in ref. 67. In each experimental group, we analysed two to three samples, each consisting of a pool of two to three embryos/kits. Reactions were performed in triplicate per independent sample. Data were statistically analysed with SPSS software using *t*-test.

Cell count measurements. Cell types were identified according to the following criteria: aRGC, cell with the soma located within the VZ, a single apical process contacting the ventricular surface and a very long radially oriented basal process, expressing Pax6 and Ki67; bRGC, cell with the soma located outside the VZ, with a very long radially oriented basal process, without an apical process anchored to the ventricular AJ belt, expressing Pax6 and Ki67; MP, cell with multiple short processes extended from the cell soma and without obvious polarity; IPC, MP cell expressing Ki67 and Tbr2; migrating neuron, cell with clear apical-basal polarity extending a relatively thin basal process much shorter than that of RGCs, and a much shorter and thinner apical process; DN, cell with a single basally-directed process highly branched at a distance from the cell body, frequently located at the top of the cortical plate; StC, multipolar cell with several very highly branched and short processes extending from the cell soma. In electroporation experiments, identification of GFP+ cell identity in SVZ based on morphology was unreliable due to their high density. In those experiments, aRGCs were defined as Pax6+/GFP+ cells with the cell body in VZ and a distinct apical process, while bRGCs were identified as Pax6+/GFP+ cells with the cell body in SVZ. The angle of mitotic cleavage plane was measured using PH3 stains and considering only cells at telophase. Angles were measured with respect to the general trajectory of the radial fibre scaffold, or with respect to the ventricular surface^{20,27}. Cleavage planes were considered horizontal if they occurred at 60–90° with respect to radial fibres or 0–30° with respect to the ventricular surface.

Double-labelling analyses. Quantification of cell co-staining was performed by confocal microscopy (Leica) through a ×40 lens and ×2–4 zoom. Images were acquired from cells in four sections per subject, two to three subjects per condition and age. Images were analysed using Imaris software (Bitplane) and Canvas X software.

Progenitor self-amplification. To determine whether the population of RGCs increased or not, we profited from a unique property of retroviruses: the GFP reporter gene they encode is randomly integrated into one of the two daughter cells after division of the originally infected cell. Thus, if a bRGC infected with our retrovirus generates two bRGCs, one will always observe one GFP+ bRGC; but if it divides to generate one bRGC+ one neuron, there is a random chance of observing the bRGC or the neuron (50–50%). This unique property of retroviruses has been utilized previously by other labs^{13,68,69}. Taken to the population level, in a homogeneous pool of symmetric amplificative divisions where each progenitor cell generates two progenitors like itself, 100% of GFP+ cells will be progenitors; in a homogeneous population of asymmetric divisions, where each progenitor divides to generate one progenitor like itself plus a different cell, 50% of labelled cells will be progenitors and 50% will be of another type; in a homogeneous population of symmetric self-consuming divisions, where progenitors divide to generate two cells different than the mother, 0% of labelled cells will be like the mother progenitor. Therefore, if after one cell division we observed that >50% of GFP+ cells were bRGCs, like in our P1–P3 and P6–P8 experiments, this means that the population

of bRGCs was expanding (there was a net production). Unfortunately, it is not possible to know with precision which kinds of divisions occurred, but one can conclude an increase in this cell type at the population level.

Statistical analysis. Statistical analysis was performed using either unpaired *t*-test (two-tailed distribution) or χ^2 -test. For analysis of microarray data, we performed one-way analysis of variance followed by Bonferroni's test for multiple comparisons and Duncan's test for subset homogeneity. All values represent mean values \pm s.e.m. Normality and equality of variance were formally tested with SPSS Statistics software.

Data availability. The microarray data that support the findings of this study have been deposited in the GEO database (<http://www.ncbi.nlm.nih.gov/geo/>) and assigned the identifier GSE63203. All other relevant data are available from the authors.

References

- Smart, I. H., Dehay, C., Giroud, P., Berland, M. & Kennedy, H. Unique morphological features of the proliferative zones and postmitotic compartments of the neural epithelium giving rise to striate and extrastriate cortex in the monkey. *Cereb. Cortex* **12**, 37–53 (2002).
- Borrell, V. & Reillo, I. Emerging roles of neural stem cells in cerebral cortex development and evolution. *Dev. Neurobiol.* **72**, 955–971 (2012).
- Lui, J. H., Hansen, D. V. & Kriegstein, A. R. Development and evolution of the human neocortex. *Cell* **146**, 18–36 (2011).
- Reillo, I., de Juan Romero, C., Garcia-Cabezas, M. A. & Borrell, V. A role for intermediate radial glia in the tangential expansion of the mammalian cerebral cortex. *Cereb. Cortex* **21**, 1674–1694 (2011).
- Bayatti, N. *et al.* A molecular neuroanatomical study of the developing human neocortex from 8 to 17 postconceptional weeks revealing the early differentiation of the subplate and subventricular zone. *Cereb. Cortex* **18**, 1536–1548 (2008).
- Nonaka-Kinoshita, M. *et al.* Regulation of cerebral cortex size and folding by expansion of basal progenitors. *EMBO J.* **32**, 1817–1828 (2013).
- Borrell, V. & Gotz, M. Role of radial glial cells in cerebral cortex folding. *Curr. Opin. Neurobiol.* **27**, 39–46 (2014).
- Betizeau, M. *et al.* Precursor diversity and complexity of lineage relationships in the outer subventricular zone of the primate. *Neuron* **80**, 442–457 (2013).
- Fietz, S. A. *et al.* OSVZ progenitors of human and ferret neocortex are epithelial-like and expand by integrin signaling. *Nat. Neurosci.* **13**, 690–699 (2010).
- Hansen, D. V., Lui, J. H., Parker, P. R. & Kriegstein, A. R. Neurogenic radial glia in the outer subventricular zone of human neocortex. *Nature* **464**, 554–561 (2010).
- Kowalczyk, T. *et al.* Intermediate neuronal progenitors (basal progenitors) produce pyramidal-projection neurons for all layers of cerebral cortex. *Cereb. Cortex* **19**, 2439–2450 (2009).
- Englund, C. *et al.* Pax6, Tbr2, and Tbr1 are expressed sequentially by radial glia, intermediate progenitor cells, and postmitotic neurons in developing neocortex. *J. Neurosci.* **25**, 247–251 (2005).
- Noctor, S. C., Martinez-Cerdeno, V., Ivic, L. & Kriegstein, A. R. Cortical neurons arise in symmetric and asymmetric division zones and migrate through specific phases. *Nat. Neurosci.* **7**, 136–144 (2004).
- Haubensak, W., Attardo, A., Denk, W. & Huttner, W. B. Neurons arise in the basal neuroepithelium of the early mammalian telencephalon: a major site of neurogenesis. *Proc. Natl Acad. Sci. USA* **101**, 3196–3201 (2004).
- Miyata, T. *et al.* Asymmetric production of surface-dividing and non-surface-dividing cortical progenitor cells. *Development* **131**, 3133–3145 (2004).
- Attardo, A., Calegari, F., Haubensak, W., Wilsch-Brauninger, M. & Huttner, W. B. Live imaging at the onset of cortical neurogenesis reveals differential appearance of the neuronal phenotype in apical versus basal progenitor progeny. *PLoS ONE* **3**, e2388 (2008).
- Shitamukai, A., Konno, D. & Matsuzaki, F. Oblique radial glial divisions in the developing mouse neocortex induce self-renewing progenitors outside the germinal zone that resemble primate outer subventricular zone progenitors. *J. Neurosci.* **31**, 3683–3695 (2011).
- Wang, X., Tsai, J. W., Lamonica, B. & Kriegstein, A. R. A new subtype of progenitor cell in the mouse embryonic neocortex. *Nat. Neurosci.* **14**, 555–561 (2011).
- Taverna, E., Gotz, M. & Huttner, W. B. The cell biology of neurogenesis: toward an understanding of the development and evolution of the neocortex. *Annu. Rev. Cell Dev. Biol.* **30**, 465–502 (2014).
- Reillo, I. & Borrell, V. Germinal zones in the developing cerebral cortex of ferret: ontogeny, cell cycle kinetics, and diversity of progenitors. *Cereb. Cortex* **22**, 2039–2054 (2012).

21. Garcia-Moreno, F., Vasistha, N. A., Trevia, N., Bourne, J. A. & Molnar, Z. Compartmentalization of cerebral cortical germinal zones in a lissencephalic primate and gyrencephalic rodent. *Cereb. Cortex* **22**, 482–492 (2012).
22. Kelava, I. *et al.* Abundant occurrence of basal radial glia in the subventricular zone of embryonic neocortex of a lissencephalic primate, the common marmoset *Callithrix jacchus*. *Cereb. Cortex* **22**, 469–481 (2012).
23. Martinez-Cerdeno, V. *et al.* Comparative analysis of the subventricular zone in rat, ferret and macaque: evidence for an outer subventricular zone in rodents. *PLoS One* **7**, e30178 (2012).
24. Noctor, S. C., Martinez-Cerdeno, V. & Kriegstein, A. R. Distinct behaviors of neural stem and progenitor cells underlie cortical neurogenesis. *J. Comp. Neurol.* **508**, 28–44 (2008).
25. Stahl, R. *et al.* Trnp1 regulates expansion and folding of the mammalian cerebral cortex by control of radial glial fate. *Cell* **153**, 535–549 (2013).
26. Pilz, G. A. *et al.* Amplification of progenitors in the mammalian telencephalon includes a new radial glial cell type. *Nat. Commun.* **4**, 2125 (2013).
27. Gertz, C. C., Lui, J. H., LaMonica, B. E., Wang, X. & Kriegstein, A. R. Diverse behaviors of outer radial glia in developing ferret and human cortex. *J. Neurosci.* **34**, 2559–2570 (2014).
28. Jackson, C. A., Peduzzi, J. D. & Hickey, T. L. Visual cortex development in the ferret. I. Genesis and migration of visual cortical neurons. *J. Neurosci.* **9**, 1242–1253 (1989).
29. LaMonica, B. E., Lui, J. H., Hansen, D. V. & Kriegstein, A. R. Mitotic spindle orientation predicts outer radial glial cell generation in human neocortex. *Nat. Commun.* **4**, 1665 (2013).
30. Gotz, M. & Huttner, W. B. The cell biology of neurogenesis. *Nat. Rev. Mol. Cell Biol.* **6**, 777–788 (2005).
31. Turrero Garcia, M., Chang, Y., Arai, Y. & Huttner, W. B. S-phase duration is the main target of cell cycle regulation in neural progenitors of developing ferret neocortex. *J. Comp. Neurol.* **524**, 456–470 (2015).
32. Xie, Y., Juschke, C., Esk, C., Hirotsune, S. & Knoblich, J. A. The phosphatase PP4c controls spindle orientation to maintain proliferative symmetric divisions in the developing neocortex. *Neuron* **79**, 254–265 (2013).
33. Postiglione, M. P. *et al.* Mouse inescuteable induces apical-basal spindle orientation to facilitate intermediate progenitor generation in the developing neocortex. *Neuron* **72**, 269–284 (2011).
34. Bruder, C. E. *et al.* Transcriptome sequencing and development of an expression microarray platform for the domestic ferret. *BMC Genomics* **11**, 251 (2010).
35. de Juan Romero, C., Bruder, C., Tomasello, U., Sanz-Anquela, J. M. & Borrell, V. Discrete domains of gene expression in germinal layers distinguish the development of gyrencephaly. *EMBO J.* **34**, 1859–1874 (2015).
36. Janz, R., Goda, Y., Geppert, M., Missler, M. & Sudhof, T. C. SV2A and SV2B function as redundant Ca²⁺ regulators in neurotransmitter release. *Neuron* **24**, 1003–1016 (1999).
37. Itoh, Y. *et al.* Scratch regulates neuronal migration onset via an epithelial-mesenchymal transition-like mechanism. *Nat. Neurosci.* **16**, 416–425 (2013).
38. Borrell, V. *et al.* Slit/Robo signaling modulates the proliferation of central nervous system progenitors. *Neuron* **76**, 338–352 (2012).
39. Hatakeyama, J. *et al.* Cadherin-based adhesions in the apical endfoot are required for active Notch signaling to control neurogenesis in vertebrates. *Development* **141**, 1671–1682 (2014).
40. Noles, S. R. & Chenn, A. Cadherin inhibition of beta-catenin signaling regulates the proliferation and differentiation of neural precursor cells. *Mol. Cell. Neurosci.* **35**, 549–558 (2007).
41. Le Borgne, R., Bellaiche, Y. & Schweisguth, F. Drosophila E-cadherin regulates the orientation of asymmetric cell division in the sensory organ lineage. *Curr. Biol.* **12**, 95–104 (2002).
42. Borrell, V. & Calegari, F. Mechanisms of brain evolution: Regulation of neural progenitor cell diversity and cell cycle length. *Neurosci. Res.* **86**, 14–24 (2014).
43. Rakic, P. Evolution of the neocortex: a perspective from developmental biology. *Nat. Rev. Neurosci.* **10**, 724–735 (2009).
44. Rasin, M. R. *et al.* Numb and Numb1 are required for maintenance of cadherin-based adhesion and polarity of neural progenitors. *Nat. Neurosci.* **10**, 819–827 (2007).
45. Sun, T. & Hevner, R. F. Growth and folding of the mammalian cerebral cortex: from molecules to malformations. *Nat. Rev. Neurosci.* **15**, 217–232 (2014).
46. Bininda-Emonds, O. R. *et al.* The delayed rise of present-day mammals. *Nature* **446**, 507–512 (2007).
47. Morin, X., Jaouen, F. & Durbec, P. Control of planar divisions by the G-protein regulator LGN maintains progenitors in the chick neuroepithelium. *Nat. Neurosci.* **10**, 1440–1448 (2007).
48. Inaba, M., Yuan, H., Salzman, V., Fuller, M. T. & Yamashita, Y. M. E-cadherin is required for centrosome and spindle orientation in *Drosophila* male germline stem cells. *PLoS ONE* **5**, e12473 (2010).
49. Cappelletti, S. *et al.* A radial glia-specific role of RhoA in double cortex formation. *Neuron* **73**, 911–924 (2012).
50. Wong, G. K., Baudet, M. L., Norden, C., Leung, L. & Harris, W. A. Slit1b-Robo3 signaling and N-cadherin regulate apical process retraction in developing retinal ganglion cells. *J. Neurosci.* **32**, 223–228 (2012).
51. Welker, W. in *Cerebral Cortex* (eds Peters A. & Jones E.G.) (Plenum Press, 1990).
52. LeBlanc, J. J. & Fagiolini, M. Autism: a "critical period" disorder? *Neural. Plast.* **2011**, 921680 (2011).
53. Levelt, C. N. & Hubener, M. Critical-period plasticity in the visual cortex. *Annu. Rev. Neurosci.* **35**, 309–330 (2012).
54. Poluch, S. & Juliano, S. L. Fine-tuning of neurogenesis is essential for the evolutionary expansion of the cerebral cortex. *Cereb. Cortex* **25**, 346–364 (2013).
55. Kielar, M. *et al.* Mutations in Eml1 lead to ectopic progenitors and neuronal heterotopia in mouse and human. *Nat. Neurosci.* **17**, 923–933 (2014).
56. Bae, B. I. *et al.* Evolutionarily dynamic alternative splicing of GPR56 regulates regional cerebral patterning. *Science* **343**, 764–768 (2014).
57. Cappelletti, S. *et al.* Mutations in genes encoding the cadherin receptor-ligand pair DCHS1 and FAT4 disrupt cerebral cortical development. *Nat. Genet.* **45**, 1300–1308 (2013).
58. Barkovich, A. J., Guerrini, R., Kuzniecky, R. I., Jackson, G. D. & Dobyns, W. B. A developmental and genetic classification for malformations of cortical development: update 2012. *Brain* **135**, 1348–1369 (2012).
59. Tashiro, A., Zhao, C. & Gage, F. H. Retrovirus-mediated single-cell gene knockout technique in adult newborn neurons *in vivo*. *Nat. Protoc.* **1**, 3049–3055 (2006).
60. Borrell, V. *In vivo* gene delivery to the postnatal ferret cerebral cortex by DNA electroporation. *J. Neurosci. Methods* **186**, 186–195 (2010).
61. Kawasaki, H., Toda, T. & Tanno, K. *In vivo* genetic manipulation of cortical progenitors in gyrencephalic carnivores using *in utero* electroporation. *Biol. Open* **2**, 95–100 (2013).
62. Borrell, V., Kaspar, B. K., Gage, F. H. & Callaway, E. M. *In vivo* evidence for radial migration of neurons by long-distance somal translocation in the developing ferret visual cortex. *Cereb. Cortex* **16**, 1571–1583 (2006).
63. Camp, J. V. *et al.* De-novo transcriptome sequencing of a normalized cDNA pool from influenza infected ferrets. *PLoS One* **7**, e37104 (2012).
64. Saeed, A. I. *et al.* TM4: a free, open-source system for microarray data management and analysis. *Biotechniques* **34**, 374–378 (2003).
65. Ayoub, A. E. *et al.* Transcriptional programs in transient embryonic zones of the cerebral cortex defined by high-resolution mRNA sequencing. *Proc. Natl Acad. Sci. USA* **108**, 14950–14955 (2011).
66. Dennis, Jr. G. *et al.* DAVID: Database for Annotation, Visualization, and Integrated Discovery. *Genome Biol.* **4**, P3 (2003).
67. Fang, Y. *et al.* Molecular characterization of *in vivo* adjuvant activity in ferrets vaccinated against influenza virus. *J. Virol.* **84**, 8369–8388 (2010).
68. Brown, K. N. *et al.* Clonal production and organization of inhibitory interneurons in the neocortex. *Science* **334**, 480–486 (2011).
69. Ciceri, G. *et al.* Lineage-specific laminar organization of cortical GABAergic interneurons. *Nat. Neurosci.* **16**, 1199–1210 (2013).

Acknowledgements

We thank E. Picó, Y. Torregrosa and G. Exposito for technical support, Y. Miralles for assistance in surgeries, F.H. Gage for retroviral vectors and help with video microscopy, I. Fariñas for DN-Cdh1 plasmids and the viral vector facility of the SFB 870 funded by the German Research Foundation for vector production. The Spanish Ministry of Economy and Competitiveness (MINECO) provided support to M.A.M.-M. (Consolider fellowship), A.C. and V.F. (FPI fellowships), and in part to C.D.J.R. (Juan de la Cierva contract). The research leading to a part of these results received funding from the European Union Seventh Framework Programme FP7/2007–2013 under the project DESIRE (grant agreement no. 602531), European Research Council (309633) and MINECO (SAF2009-07367, BFU2012-33473 and CSD2007-00023) to V.B. and European Research Council grant (340793) to M.G. The Instituto de Neurociencias is a "Centre of Excellence Severo Ochoa".

Author contributions

M.A.M.-M. and V.B. conceived and designed the study; M.A.M.-M., A.C. and V.F. performed cell lineage analyses and video microscopy; M.A.M.-M. and C.D.J.R. obtained samples for microarray analysis; C.D.J.R. analysed microarray data, and performed GO analyses and qPCR experiments; M.G. and V.B. provided expertise, reagents and tools; V.B. supervised the work and wrote the manuscript; all the authors discussed the results and commented on the manuscript.

Additional information

Supplementary Information accompanies this paper at <http://www.nature.com/naturecommunications>

Competing financial interests: The authors declare no competing financial interests.

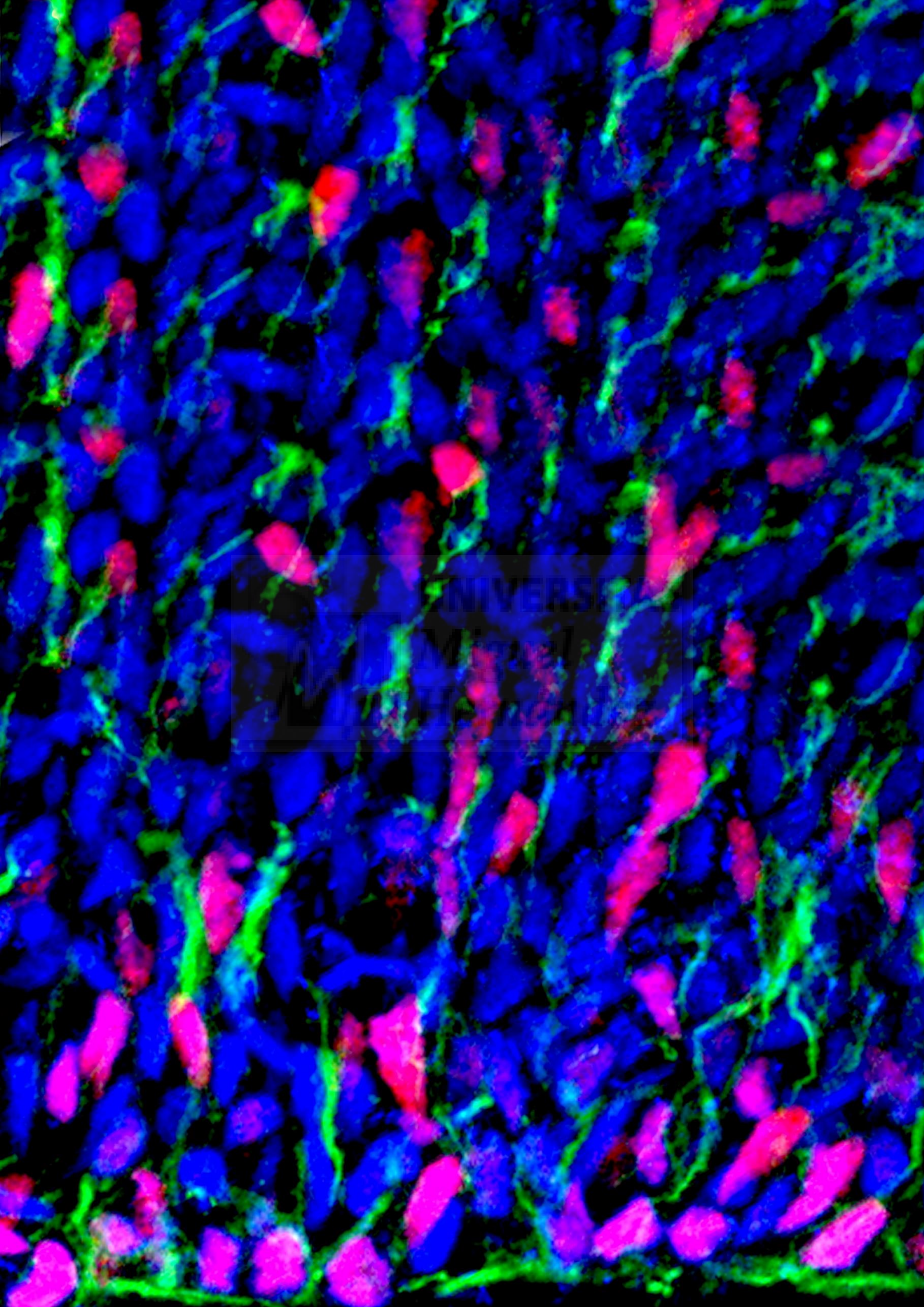
Reprints and permission information is available online at <http://npg.nature.com/reprintsandpermissions/>

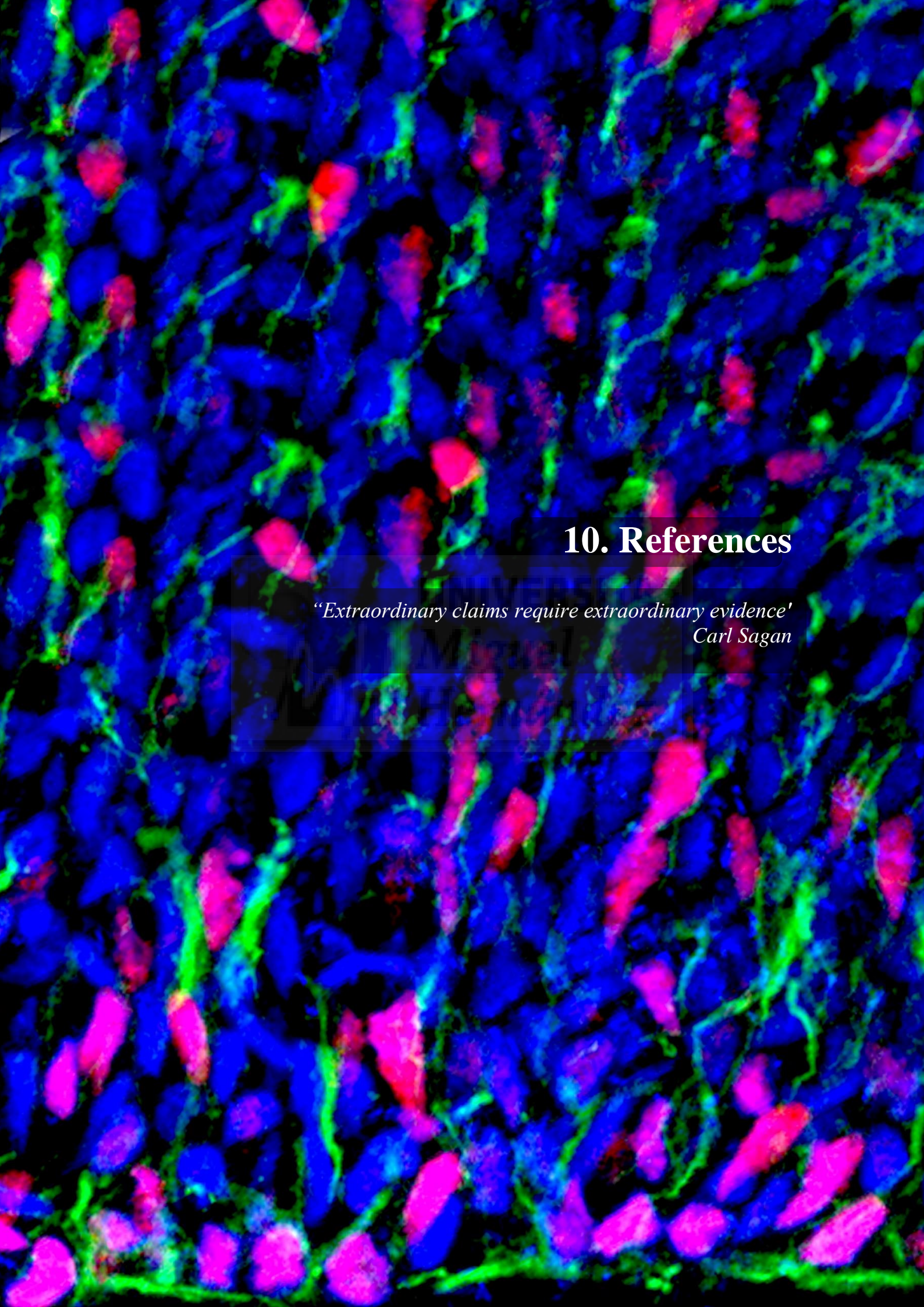
How to cite this article: Martínez-Martínez, M. A. *et al.* A restricted period for formation of outer subventricular zone defined by *Cdh1* and *Trnp1* levels. *Nat. Commun.* 7:11812 doi: 10.1038/ncomms11812 (2016).



This work is licensed under a Creative Commons Attribution 4.0 International License. The images or other third party material in this article are included in the article's Creative Commons license, unless indicated otherwise in the credit line; if the material is not included under the Creative Commons license, users will need to obtain permission from the license holder to reproduce the material. To view a copy of this license, visit <http://creativecommons.org/licenses/by/4.0/>







10. References

"Extraordinary claims require extraordinary evidence"
Carl Sagan



10. References

- Andersen, R. K., K. Hammer, H. Hager, J. N. Christensen, M. Ludvigsen, B. Honore, M. B. Thomsen and M. Madsen (2015). "Melanoma tumors frequently acquire LRP2/megalin expression, which modulates melanoma cell proliferation and survival rates." *Pigment Cell Melanoma Res* **28**(3): 267-280.
- Anderson, S. A., O. Marin, C. Horn, K. Jennings and J. L. Rubenstein (2001). "Distinct cortical migrations from the medial and lateral ganglionic eminences." *Development* **128**(3): 353-363.
- Arber, C. and M. Li (2013). "Cortical interneurons from human pluripotent stem cells: prospects for neurological and psychiatric disease." *Frontiers in Cellular Neuroscience* **7**(10).
- Aslam, A., S. Mittal, F. Koch, J. C. Andrau and G. S. Winkler (2009). "The Ccr4–Not Deadenylase Subunits CNOT7 and CNOT8 Have Overlapping Roles and Modulate Cell Proliferation." *Mol Biol Cell* **20**(17): 3840-3850.
- Babiarz, J. E., R. Hsu, C. Melton, M. Thomas, E. M. Ullian and R. Blelloch (2011). "A role for noncanonical microRNAs in the mammalian brain revealed by phenotypic differences in Dgcr8 versus Dicer1 knockouts and small RNA sequencing." *Rna* **17**(8): 1489-1501.
- Bak, R. O., A. K. Hollensen and J. G. Mikkelsen (2013). "Managing MicroRNAs with Vector-Encoded Decoy-Type Inhibitors." *Mol Ther* **21**(8): 1478-1485.
- Barh, D., R. Malhotra, B. Ravi and P. Sindhurani (2010). "MicroRNA let-7: an emerging next-generation cancer therapeutic." *Curr Oncol* **17**(1): 70-80.
- Baskerville, S. and D. P. Bartel (2005). "Microarray profiling of microRNAs reveals frequent coexpression with neighboring miRNAs and host genes." *Rna* **11**(3): 241-247.
- Bayraktar, O. A. and C. Q. Doe (2013). "Combinatorial temporal patterning in progenitors expands neural diversity." *Nature* **498**(7455): 449-455.
- Behm-Ansmant, I., J. Rehwinkel and E. Izaurralde (2006). "MicroRNAs silence gene expression by repressing protein expression and/or by promoting mRNA decay." *Cold Spring Harb Symp Quant Biol* **71**: 523-530.
- Berezikov, E., W. J. Chung, J. Willis, E. Cuppen and E. C. Lai (2007). "Mammalian Mirtron Genes." *Mol Cell* **28**(2): 328-336.
- Bernstein, E., S. Y. Kim, M. A. Carmell, E. P. Murchison, H. Alcorn, M. Z. Li, A. A. Mills, S. J. Elledge, K. V. Anderson and G. J. Hannon (2003). "Dicer is essential for mouse development." *Nat Genet* **35**(3): 215-217.
- Bersani, C., L. Xu, A. Vilborg, W. Lui and K. G. Wiman (2014). "Wig-1 regulates cell cycle arrest and cell death through the p53 targets FAS and 14-3-3 σ ." *Oncogene* **33**(35): 4407-4417.
- Bian, S., T. L. Xu and T. Sun (2013). "Tuning the cell fate of neurons and glia by microRNAs." *Curr Opin Neurobiol* **23**(6): 928-934.
- Borchert, G. M., W. Lanier and B. L. Davidson (2006). "RNA polymerase III transcribes human microRNAs." *Nat Struct Mol Biol* **13**(12): 1097-1101.

- Borrell, V. and F. Calegari (2014). "Mechanisms of brain evolution: regulation of neural progenitor cell diversity and cell cycle length." *Neurosci Res* **86**: 14-24.
- Borrell, V., A. Cardenas, G. Ciceri, J. Galceran, N. Flames, R. Pla, S. Nobrega-Pereira, C. Garcia-Frigola, S. Peregrin, Z. Zhao, L. Ma, M. Tessier-Lavigne and O. Marin (2012). "Slit/Robo signaling modulates the proliferation of central nervous system progenitors." *Neuron* **76**(2): 338-352.
- Borrell, V. and M. Gotz (2014). "Role of radial glial cells in cerebral cortex folding." *Curr Opin Neurobiol* **27C**: 39-46.
- Boyerinas, B., S. M. Park, A. Hau, A. E. Murmann and M. E. Peter (2010). "The role of let-7 in cell differentiation and cancer." *Endocr Relat Cancer* **17**(1): F19-36.
- Boyerinas, B., S. M. Park, N. Shomron, M. M. Hedegaard, J. Vinther, J. S. Andersen, C. Feig, J. Xu, C. B. Burge and M. E. Peter (2008). "Identification of let-7-regulated oncofetal genes." *Cancer Res* **68**(8): 2587-2591.
- Brown, K. N., S. Chen, Z. Han, C.-H. Lu, X. Tan, X.-J. Zhang, L. Ding, A. Lopez-Cruz, D. Saur, S. A. Anderson, K. Huang and S.-H. Shi (2011). "Clonal Production and Organization of Inhibitory Interneurons in the Neocortex." *Science* **334**(6055): 480-486.
- Bulfone, A., S. Martinez, V. Marigo, M. Campanella, A. Basile, N. Quaderi, C. Gattuso, J. L. R. Rubenstein and A. Ballabio (1999). "Expression pattern of the Tbr2 (Eomesodermin) gene during mouse and chick brain development." *Mechanisms of Development* **84**(1): 133-138.
- Butt, S. J., M. Fuccillo, S. Nery, S. Noctor, A. Kriegstein, J. G. Corbin and G. Fishell (2005). "The temporal and spatial origins of cortical interneurons predict their physiological subtype." *Neuron* **48**(4): 591-604.
- Cai, X., C. H. Hagedorn and B. R. Cullen (2004). "Human microRNAs are processed from capped, polyadenylated transcripts that can also function as mRNAs." *Rna* **10**(12): 1957-1966.
- Calin, G. A., C. D. Dumitru, M. Shimizu, R. Bichi, S. Zupo, E. Noch, H. Aldler, S. Rattan, M. Keating, K. Rai, L. Rassenti, T. Kipps, M. Negrini, F. Bullrich and C. M. Croce (2002). "Frequent deletions and down-regulation of micro- RNA genes miR15 and miR16 at 13q14 in chronic lymphocytic leukemia." *Proc Natl Acad Sci U S A* **99**(24): 15524-15529.
- Camp, J. G., F. Badsha, M. Florio, S. Kanton, T. Gerber, M. Wilsch-Brauninger, E. Lewitus, A. Sykes, W. Hevers, M. Lancaster, J. A. Knoblich, R. Lachmann, S. Paabo, W. B. Huttner and B. Treutlein (2015). "Human cerebral organoids recapitulate gene expression programs of fetal neocortex development." *Proc Natl Acad Sci U S A* **112**(51): 15672-15677.
- Cao, D. D., L. Li and W. Y. Chan (2016). "MicroRNAs: Key Regulators in the Central Nervous System and Their Implication in Neurological Diseases." *Int J Mol Sci* **17**(6).
- Castro, D. S., D. Skowronska-Krawczyk, O. Armant, I. J. Donaldson, C. Parras, C. Hunt, J. A. Critchley, L. Nguyen, A. Gossler, B. Gottgens, J. M. Matter and F. Guillemot (2006). "Proneural bHLH and Brn proteins coregulate a neurogenic program through cooperative binding to a conserved DNA motif." *Dev Cell* **11**(6): 831-844.

- Catalanotto, C., C. Cogoni and G. Zardo (2016). "MicroRNA in Control of Gene Expression: An Overview of Nuclear Functions." *Int J Mol Sci* **17**(10).
- Cazalla, D., T. Yario and J. A. Steitz (2010). "Down-regulation of a host microRNA by a Herpesvirus saimiri noncoding RNA." *Science* **328**(5985): 1563-1566.
- Cesana, M., D. Cacchiarelli, I. Legnini, T. Santini, O. Sthandier, M. Chinappi, A. Tramontano and I. Bozzoni (2011). "A long noncoding RNA controls muscle differentiation by functioning as a competing endogenous RNA." *Cell* **147**(2): 358-369.
- Cheloufi, S., C. O. Dos Santos, M. M. W. Chong and G. J. Hannon (2010). "A dicer-independent miRNA biogenesis pathway that requires Ago catalysis." *Nature* **465**(7298): 584-589.
- Chen, Y., D. Y. Gao and L. Huang (2015). "In vivo delivery of miRNAs for cancer therapy: Challenges and strategies." *Adv Drug Deliv Rev* **81**: 128-141.
- Cheng, Y., I. Jutooru, G. Chadalapaka, J. C. Corton and S. Safe (2015). "The long non-coding RNA HOTTIP enhances pancreatic cancer cell proliferation, survival and migration." *Oncotarget* **6**(13): 10840-10852.
- Chenn, A. and C. A. Walsh (2002). "Regulation of cerebral cortical size by control of cell cycle exit in neural precursors." *Science* **297**(5580): 365-369.
- Chmielarz, P., J. Konovalova, S. S. Najam, H. Alter, T. P. Piepponen, H. Erfle, K. C. Sonntag, G. Schütz, I. A. Vinnikov and A. Domanskyi (2017). "Dicer and microRNAs protect adult dopamine neurons." *Cell Death & Disease* **8**: e2813.
- Christopher, A. F., R. P. Kaur, G. Kaur, A. Kaur, V. Gupta and P. Bansal (2016). "MicroRNA therapeutics: Discovering novel targets and developing specific therapy." *Perspect Clin Res* **7**(2): 68-74.
- Cocas, L. A., P. A. Georgala, J. M. Mangin, J. M. Clegg, N. Kessar, T. F. Haydar, V. Gallo, D. J. Price and J. G. Corbin (2011). "Pax6 is required at the telencephalic pallial-subpallial boundary for the generation of neuronal diversity in the post-natal limbic system." *J Neurosci* **31**(14): 5313-5324.
- Costa, M. R., G. Wen, A. Lepier, T. Schroeder and M. Gotz (2008). "Par-complex proteins promote proliferative progenitor divisions in the developing mouse cerebral cortex." *Development* **135**(1): 11-22.
- Cowland, J. B., C. Hother and K. Gronbaek (2007). "MicroRNAs and cancer." *APMIS* **115**.
- Davis, T. H., T. L. Cuellar, S. M. Koch, A. J. Barker, B. D. Harfe, M. T. McManus and E. M. Ullian (2008). "Conditional Loss of Dicer Disrupts Cellular and Tissue Morphogenesis in the Cortex and Hippocampus." *J Neurosci* **28**(17): 4322-4330.
- Day, E., G. Poulgiannis, F. McCaughan, S. Mulholland, M. J. Arends, A. E. K. Ibrahim and P. H. Dear (2013). "IRS2 is a candidate driver oncogene on 13q34 in colorectal cancer." *Int J Exp Pathol* **94**(3): 203-211.
- de Juan Romero, C., C. Bruder, U. Tomasello, J. M. Sanz-Anquela and V. Borrell (2015). "Discrete domains of gene expression in germinal layers distinguish the development of gyrencephaly." *Embo j* **34**(14): 1859-1874.
- De Pietri Tonelli, D., J. N. Pulvers, C. Haffner, E. P. Murchison, G. J. Hannon and W. B. Huttner (2008). "miRNAs are essential for survival and differentiation of newborn

- neurons but not for expansion of neural progenitors during early neurogenesis in the mouse embryonic neocortex." *Development* **135**(23): 3911-3921.
- DeFelipe, J. (2011). "The Evolution of the Brain, the Human Nature of Cortical Circuits, and Intellectual Creativity." *Front Neuroanat* **5**.
- Deng, S., G. A. Calin, C. M. Croce, G. Coukos and L. Zhang (2008). "Mechanisms of microRNA deregulation in human cancer." *Cell Cycle* **7**(17): 2643-2646.
- Desai, A. R. and S. K. McConnell (2000). "Progressive restriction in fate potential by neural progenitors during cerebral cortical development." *Development* **127**(13): 2863-2872.
- Dhanoa, B. S., T. Cogliati, A. G. Satish, E. A. Bruford and J. S. Friedman (2013). "Update on the Kelch-like (KLHL) gene family." *Hum Genomics* **7**(1): 13.
- Dimou, L. and M. Gotz (2014). "Glial cells as progenitors and stem cells: new roles in the healthy and diseased brain." *Physiol Rev* **94**(3): 709-737.
- Doench, J. G. and P. A. Sharp (2004). "Specificity of microRNA target selection in translational repression." *Genes Dev* **18**(5): 504-511.
- Doyle, M., L. Badertscher, L. Jaskiewicz, S. Güttinger, S. Jurado, T. Hugenschmidt, U. Kutay and W. Filipowicz (2013). "The double-stranded RNA binding domain of human Dicer functions as a nuclear localization signal." *Rna* **19**(9): 1238-1252.
- Du, Z., J. K. Lee, R. Tjhen, R. M. Stroud and T. L. James (2008). "Structural and biochemical insights into the dicing mechanism of mouse Dicer: a conserved lysine is critical for dsRNA cleavage." *Proc Natl Acad Sci U S A* **105**(7): 2391-2396.
- Duldulao, M. P. N., W. Lee, M. Le, Z. Chen, W. Li, J. Kim and J. Garcia-Aguilar (2011). "Let-7 microRNA regulates p53 and K-ras in colorectal cancer cells." *Journal of the American College of Surgeons* **213**(3): S25.
- Durston, A. J., J. P. Timmermans, W. J. Hage, H. F. Hendriks, N. J. de Vries, M. Heideveld and P. D. Nieuwkoop (1989). "Retinoic acid causes an anteroposterior transformation in the developing central nervous system." *Nature* **340**(6229): 140-144.
- Dweep, H. and N. Gretz (2015). "miRWalk2.0: a comprehensive atlas of microRNA-target interactions." *Nature Methods* **12**: 697.
- Easow, G., A. A. Teleman and S. M. Cohen (2007). "Isolation of microRNA targets by miRNP immunopurification." *Rna* **13**(8): 1198-1204.
- Ebert, M. S. and P. A. Sharp (2010). "Emerging Roles for Natural MicroRNA Sponges." *Curr Biol* **20**(19): R858-861.
- Eisenstat, D. D., J. K. Liu, M. Mione, W. Zhong, G. Yu, S. A. Anderson, I. Ghattas, L. Puelles and J. L. Rubenstein (1999). "DLX-1, DLX-2, and DLX-5 expression define distinct stages of basal forebrain differentiation." *J Comp Neurol* **414**(2): 217-237.
- Elias, L. A., D. D. Wang and A. R. Kriegstein (2007). "Gap junction adhesion is necessary for radial migration in the neocortex." *Nature* **448**(7156): 901-907.
- Englund, C., A. Fink, C. Lau, D. Pham, R. A. Daza, A. Bulfone, T. Kowalczyk and R. F. Hevner (2005). "Pax6, Tbr2, and Tbr1 are expressed sequentially by radial glia, intermediate progenitor cells, and postmitotic neurons in developing neocortex." *J Neurosci* **25**(1): 247-251.

- Erickson, S. L., F. J. de Sauvage, K. Kikly, K. Carver-Moore, S. Pitts-Meek, N. Gillett, K. C. Sheehan, R. D. Schreiber, D. V. Goeddel and M. W. Moore (1994). "Decreased sensitivity to tumour-necrosis factor but normal T-cell development in TNF receptor-2-deficient mice." *Nature* **372**(6506): 560-563.
- Ertürk, A., K. Becker, N. Jährling, C. P. Mauch, C. D. Hojer, J. G. Egen, F. Hellal, F. Bradke, M. Sheng and H.-U. Dodt (2012). "Three-dimensional imaging of solvent-cleared organs using 3DISCO." *Nat. Protocols* **7**(11): 1983-1995.
- Espinosa, J. S. and L. Luo (2008). "Timing Neurogenesis and Differentiation: Insights from Quantitative Clonal Analyses of Cerebellar Granule Cells." *J Neurosci* **28**(10): 2301-2312.
- Esquela-Kerscher, A. and F. J. Slack (2006). "Oncomirs - microRNAs with a role in cancer." *Nat Rev Cancer* **6**(4): 259-269.
- Eulalio, A., E. Huntzinger, T. Nishihara, J. Rehwinkel, M. Fauser and E. Izaurralde (2009). "Deadenylation is a widespread effect of miRNA regulation." *Rna* **15**(1): 21-32.
- Evers, M., M. Huttner, A. Dueck, G. Meister and J. C. Engelmann (2015). "miRA: adaptable novel miRNA identification in plants using small RNA sequencing data." *BMC Bioinformatics* **16**.
- Eystathioy, T., E. K. Chan, S. A. Tenenbaum, J. D. Keene, K. Griffith and M. J. Fritzler (2002). "A phosphorylated cytoplasmic autoantigen, GW182, associates with a unique population of human mRNAs within novel cytoplasmic speckles." *Mol Biol Cell* **13**(4): 1338-1351.
- Fabian, M. R., N. Sonenberg and W. Filipowicz (2010). "Regulation of mRNA translation and stability by microRNAs." *Annu Rev Biochem* **79**: 351-379.
- Fernández, V., C. Llinares-Benadero and V. Borrell (2016). "Cerebral cortex expansion and folding: what have we learned?" *The EMBO Journal* **35**(10): 1021-1044.
- Fiore, R., G. Siegel and G. Schratt (2008). "MicroRNA function in neuronal development, plasticity and disease." *Biochimica et Biophysica Acta (BBA) - Gene Regulatory Mechanisms* **1779**(8): 471-478.
- Fogarty, M., M. Grist, D. Gelman, O. Marin, V. Pachnis and N. Kessaris (2007). "Spatial genetic patterning of the embryonic neuroepithelium generates GABAergic interneuron diversity in the adult cortex." *J Neurosci* **27**(41): 10935-10946.
- Franco-Zorrilla, J. M., A. Valli, M. Todesco, I. Mateos, M. I. Puga, I. Rubio-Somoza, A. Leyva, D. Weigel, J. A. Garcia and J. Paz-Ares (2007). "Target mimicry provides a new mechanism for regulation of microRNA activity." *Nat Genet* **39**(8): 1033-1037.
- Franks, T. M. and J. Lykke-Andersen (2008). "The control of mRNA decapping and P-body formation." *Mol Cell* **32**(5): 605-615.
- Freeman, D. J., A. G. Li, G. Wei, H.-H. Li, N. Kertesz, R. Lesche, A. D. Whale, H. Martinez-Diaz, N. Rozengurt, R. D. Cardiff, X. Liu and H. Wu (2003). "PTEN tumor suppressor regulates p53 protein levels and activity through phosphatase-dependent and -independent mechanisms." *Cancer Cell* **3**(2): 117-130.
- Gaiano, N., J. S. Nye and G. Fishell (2000). "Radial glial identity is promoted by Notch1 signaling in the murine forebrain." *Neuron* **26**(2): 395-404.

- Gao, L., X. Wang, X. Wang, L. Zhang, C. Qiang, S. Chang, W. Ren, S. Li, Y. Yang, D. Tong, C. Chen, Z. Li, T. Song, K. Zhi and C. Huang (2014). "IGF-1R, a target of let-7b, mediates crosstalk between IRS-2/Akt and MAPK pathways to promote proliferation of oral squamous cell carcinoma." *Oncotarget* **5**(9): 2562-2574.
- Gao, P., P. Postiglione M, G. Krieger T, L. Hernandez, C. Wang, Z. Han, C. Streicher, E. Papusheva, R. Insolera, K. Chugh, O. Kodish, K. Huang, D. Simons B, L. Luo, S. Hippenmeyer and S. H. Shi (2014). "Deterministic Progenitor Behavior and Unitary Production of Neurons in the Neocortex." *Cell* **159**(4): 775-788.
- Giandomenico, S. L. and M. A. Lancaster (2017). "Probing human brain evolution and development in organoids." *Current Opinion in Cell Biology* **44**(Supplement C): 36-43.
- Gil-Sanz, C., B. Landeira, C. Ramos, M. R. Costa and U. Müller (2014). "Proliferative Defects and Formation of a Double Cortex in Mice Lacking Mltt4 and Cdh2 in the Dorsal Telencephalon." *The Journal of Neuroscience* **34**(32): 10475-10487.
- Giraldez, A. J., R. M. Cinalli, M. E. Glasner, A. J. Enright, J. M. Thomson, S. Baskerville, S. M. Hammond, D. P. Bartel and A. F. Schier (2005). "MicroRNAs regulate brain morphogenesis in zebrafish." *Science* **308**(5723): 833-838.
- Gordon Betts, P. D., Eddie Johnson, Jody E. Johnson, Oksana Korol, Dean H. Kruse, Brandon Poe. (2017). "Anatomy & Physiology." Retrieved February 26, 2016.
- Gorski, J. A., T. Talley, M. Qiu, L. Puelles, J. L. R. Rubenstein and K. R. Jones (2002). "Cortical Excitatory Neurons and Glia, But Not GABAergic Neurons, Are Produced in the Emx1-Expressing Lineage." *The Journal of Neuroscience* **22**(15): 6309-6314.
- Gotz, M. and W. B. Huttner (2005). "The Cell Biology Of Neurogenesis." *Nat Rev Mol Cell Biol* **6**(10): 777-788.
- Gritli-Linde, A., M. Bei, R. Maas, X. M. Zhang, A. Linde and A. P. McMahon (2002). "Shh signaling within the dental epithelium is necessary for cell proliferation, growth and polarization." *Development* **129**(23): 5323-5337.
- Gross, R. E., M. F. Mehler, P. C. Mabie, Z. Zang, L. Santschi and J. A. Kessler (1996). "Bone morphogenetic proteins promote astroglial lineage commitment by mammalian subventricular zone progenitor cells." *Neuron* **17**(4): 595-606.
- Grove, E. A., B. P. Williams, D. Q. Li, M. Hajihosseini, A. Friedrich and J. Price (1993). "Multiple restricted lineages in the embryonic rat cerebral cortex." *Development* **117**(2): 553-561.
- Gu, S., L. Jin, F. Zhang, P. Sarnow and M. A. Kay (2009). "The biological basis for microRNA target restriction to the 3' untranslated region in mammalian mRNAs." *Nat Struct Mol Biol* **16**(2): 144-150.
- Guo, H., N. T. Ingolia, J. S. Weissman and D. P. Bartel (2010). "Mammalian microRNAs predominantly act to decrease target mRNA levels." *Nature* **466**(7308): 835-840.
- Gurtan, A. M., V. Lu, A. Bhutkar and P. A. Sharp (2012). "In vivo structure–function analysis of human Dicer reveals directional processing of precursor miRNAs." *Rna* **18**(6): 1116-1122.
- Ha, M. and V. N. Kim (2014). "Regulation of microRNA biogenesis." *Nat Rev Mol Cell Biol* **15**(8): 509-524.

- Habif, G., M. F. Grasset, S. Kieffer-Jaquinod, L. Kuhn, G. Mouchiroud and S. Gobert-Gosse (2013). "Phosphoproteome analyses reveal specific implications of Hcls1, p21-activated kinase 1 and Ezrin in proliferation of a myeloid progenitor cell line downstream of wild-type and ITD mutant Fms-like tyrosine kinase 3 receptors." *J Proteomics* **78**: 231-244.
- Hagan, J. P., E. Piskounova and R. I. Gregory (2009). "Lin28 recruits the TUTase Zcchc11 to inhibit let-7 maturation in mouse embryonic stem cells." *Nat Struct Mol Biol* **16**(10): 1021-1025.
- Han, J., Y. Lee, K. H. Yeom, J. W. Nam, I. Heo, J. K. Rhee, S. Y. Sohn, Y. Cho, B. T. Zhang and V. N. Kim (2006). "Molecular basis for the recognition of primary microRNAs by the Drosha-DGCR8 complex." *Cell* **125**(5): 887-901.
- Hansen, D. V., J. H. Lui, P. R. Parker and A. R. Kriegstein (2010). "Neurogenic radial glia in the outer subventricular zone of human neocortex." *Nature* **464**(7288): 554-561.
- Haraguchi, T., Y. Ozaki and H. Iba (2009). "Vectors expressing efficient RNA decoys achieve the long-term suppression of specific microRNA activity in mammalian cells." *Nucleic Acids Res* **37**(6): e43.
- Harfe, B. D., M. T. McManus, J. H. Mansfield, E. Hornstein and C. J. Tabin (2005). "The RNaseIII enzyme Dicer is required for morphogenesis but not patterning of the vertebrate limb." *Proc Natl Acad Sci U S A* **102**(31): 10898-10903.
- Harrison-Uy, S. J., J. A. Siegenthaler, A. Faedo, J. L. Rubenstein and S. J. Pleasure (2013). "CoupTFI interacts with retinoic acid signaling during cortical development." *PLoS One* **8**(3): e58219.
- Hau, A., P. Ceppi and M. E. Peter (2012). "CD95 Is Part of a Let-7/p53/miR-34 Regulatory Network." *PLOS ONE* **7**(11): e49636.
- Havens, M. A., A. A. Reich, D. M. Duelli and M. L. Hastings (2012). "Biogenesis of mammalian microRNAs by a non-canonical processing pathway." *Nucleic Acids Res* **40**(10): 4626-4640.
- He, L. and G. J. Hannon (2004). "MicroRNAs: small RNAs with a big role in gene regulation." *Nat Rev Genet* **5**(7): 522-531.
- He, L., J. M. Thomson, M. T. Hemann, E. Hernando-Monge, D. Mu, S. Goodson, S. Powers, C. Cordon-Cardo, S. W. Lowe, G. J. Hannon and S. M. Hammond (2005). "A microRNA polycistron as a potential human oncogene." *Nature* **435**(7043): 828-833.
- Hébert, J. M. and G. Fishell (2008). "The genetics of early telencephalon patterning: some assembly required." *Nat Rev Neurosci* **9**(9): 678-685.
- Heimberg, A. M., L. F. Sempere, V. N. Moy, P. C. Donoghue and K. J. Peterson (2008). "MicroRNAs and the advent of vertebrate morphological complexity." *Proc Natl Acad Sci U S A* **105**(8): 2946-2950.
- Henke, J. I., D. Goergen, J. Zheng, Y. Song, C. G. Schuttler, C. Fehr, C. Junemann and M. Niepmann (2008). "microRNA-122 stimulates translation of hepatitis C virus RNA." *Embo j* **27**(24): 3300-3310.

- Heo, I., C. Joo, Y. K. Kim, M. Ha, M. J. Yoon, J. Cho, K. H. Yeom, J. Han and V. N. Kim (2009). "TUT4 in concert with Lin28 suppresses microRNA biogenesis through pre-microRNA uridylation." *Cell* **138**(4): 696-708.
- Herculano-Houzel, S., P. R. Manger and J. H. Kaas (2014). "Brain scaling in mammalian evolution as a consequence of concerted and mosaic changes in numbers of neurons and average neuronal cell size." *Front Neuroanat* **8**: 77.
- Hirabayashi, Y., Y. Itoh, H. Tabata, K. Nakajima, T. Akiyama, N. Masuyama and Y. Gotoh (2004). "The Wnt/beta-catenin pathway directs neuronal differentiation of cortical neural precursor cells." *Development* **131**(12): 2791-2801.
- Hornstein, E., J. H. Mansfield, S. Yekta, J. K. Hu, B. D. Harfe, M. T. McManus, S. Baskerville, D. P. Bartel and C. J. Tabin (2005). "The microRNA miR-196 acts upstream of Hoxb8 and Shh in limb development." *Nature* **438**(7068): 671-674.
- Huang, C. J., P. N. N. Nguyen, K. B. Choo, S. Sugii, K. Wee, S. K. Cheong and T. Kamarul (2014). "Frequent Co-Expression of miRNA-5p and -3p Species and Cross-Targeting in Induced Pluripotent Stem Cells." *Int J Med Sci* **11**(8): 824-833.
- Humphreys, D. T., B. J. Westman, D. I. Martin and T. Preiss (2005). "MicroRNAs control translation initiation by inhibiting eukaryotic initiation factor 4E/cap and poly(A) tail function." *Proc Natl Acad Sci U S A* **102**(47): 16961-16966.
- Hutvagner, G. and P. D. Zamore (2002). "A microRNA in a multiple-turnover RNAi enzyme complex." *Science* **297**(5589): 2056-2060.
- Iwamoto, K. S. (2002). "The p53 and M6P/IGF2r genes of Thorotrast- and atomic bomb-induced liver cancers: a glimpse into the mechanisms of radiation carcinogenesis." *International Congress Series* **1236**(Supplement C): 195-200.
- Jakymiw, A., K. M. Pauley, S. Li, K. Ikeda, S. Lian, T. Eystathioy, M. Satoh, M. J. Fritzler and E. K. Chan (2007). "The role of GW/P-bodies in RNA processing and silencing." *J Cell Sci* **120**(Pt 8): 1317-1323.
- Ji, M., E. Rao, H. Ramachandrareddy, Y. Shen, C. Jiang, J. Chen, Y. Hu, A. Rizzino, W. C. Chan, K. Fu and T. W. McKeithan (2011). "The miR-17-92 MicroRNA Cluster Is Regulated by Multiple Mechanisms in B-Cell Malignancies." *Am J Pathol* **179**(4): 1645-1656.
- Jian Liu, N. D., Huangzhen Wang, Xin Wang, Peili Wang, Jia Zhang, Gang Li, Jing Zhang, Sida Qin, Chongwen Xu, Shou-Ching Tang, Xin Sun, Boxiang Zhang, Dapeng Liu and Hong Ren (2016). "P53 Sensitizes Breast Cancer Stem Cells to Let-7 miRNAs Induced Repression." *Int J Cancer Clin Res* **3**(2): 3:047.
- Johnson, S. M., H. Grosshans, J. Shingara, M. Byrom, R. Jarvis, A. Cheng, E. Labourier, K. L. Reinert, D. Brown and F. J. Slack (2005). "RAS Is Regulated by the let-7 MicroRNA Family." *Cell* **120**(5): 635-647.
- Jones, M. F. and A. Lal (2012). "MicroRNAs, wild-type and mutant p53: More questions than answers." *RNA Biol* **9**(6): 781-791.
- Kaas, J. H. (2016). *Evolution of Nervous Systems*, Elsevier Science.
- Kanellopoulou, C., S. A. Muljo, A. L. Kung, S. Ganesan, R. Drapkin, T. Jenuwein, D. M. Livingston and K. Rajewsky (2005). "Dicer-deficient mouse embryonic stem cells are defective in differentiation and centromeric silencing." *Genes Dev* **19**(4): 489-501.

- Karreth, F. A., Y. Tay, D. Perna, U. Ala, S. M. Tan, A. G. Rust, G. DeNicola, K. A. Webster, D. Weiss, P. A. Perez-Mancera, M. Krauthammer, R. Halaban, P. Provero, D. J. Adams, D. A. Tuveson and P. P. Pandolfi (2011). "In vivo identification of tumor-suppressive PTEN ceRNAs in an oncogenic BRAF-induced mouse model of melanoma." *Cell* **147**(2): 382-395.
- Kawase-Koga, Y., G. Otaegi and T. Sun (2009). "Different timings of Dicer deletion affect neurogenesis and gliogenesis in the developing mouse central nervous system." *Dev Dyn* **238**(11): 2800-2812.
- Kelava, I. and M. A. Lancaster (2016). "Dishing out mini-brains: Current progress and future prospects in brain organoid research." *Dev Biol* **420**(2): 199-209.
- Kim, Y. K., B. Kim and V. N. Kim (2016). "Re-evaluation of the roles of DROSHA, Exportin 5, and DICER in microRNA biogenesis." *Proc Natl Acad Sci U S A* **113**(13): E1881-1889.
- Kingsbury, M. A., S. K. Rehen, J. J. Contos, C. M. Higgins and J. Chun (2003). "Non-proliferative effects of lysophosphatidic acid enhance cortical growth and folding." *Nat Neurosci* **6**(12): 1292-1299.
- Klimova, L., J. Lachova, O. Machon, R. Sedlacek and Z. Kozmik (2013). "Generation of mRx-Cre Transgenic Mouse Line for Efficient Conditional Gene Deletion in Early Retinal Progenitors." *PLoS One* **8**(5).
- Kloosterman, W. P., E. Wienholds, E. de Bruijn, S. Kauppinen and R. H. Plasterk (2006). "In situ detection of miRNAs in animal embryos using LNA-modified oligonucleotide probes." *Nat Methods* **3**(1): 27-29.
- Kowalczyk, T., A. Pontious, C. Englund, R. A. Daza, F. Bedogni, R. Hodge, A. Attardo, C. Bell, W. B. Huttner and R. F. Hevner (2009). "Intermediate neuronal progenitors (basal progenitors) produce pyramidal-projection neurons for all layers of cerebral cortex." *Cereb Cortex* **19**(10): 2439-2450.
- Kumar, M. S., J. Lu, K. L. Mercer, T. R. Golub and T. Jacks (2007). "Impaired microRNA processing enhances cellular transformation and tumorigenesis." *Nat Genet* **39**(5): 673-677.
- Labi, V. and M. Erlacher (2015). "How cell death shapes cancer." *Cell Death Dis* **6**(3): e1675-.
- Lai, E. C. (2015). "Two decades of miRNA biology: lessons and challenges." *Rna* **21**(4): 675-677.
- Lancaster, M. A., M. Renner, C.-A. Martin, D. Wenzel, L. S. Bicknell, M. E. Hurles, T. Homfray, J. M. Penninger, A. P. Jackson and J. A. Knoblich (2013). "Cerebral organoids model human brain development and microcephaly." *Nature* **501**(7467): 373-379.
- Lange, C., W. B. Huttner and F. Calegari (2009). "Cdk4/cyclinD1 overexpression in neural stem cells shortens G1, delays neurogenesis, and promotes the generation and expansion of basal progenitors." *Cell Stem Cell* **5**(3): 320-331.
- Laudato, S., N. Patil, M. L. Abba, J. H. Leupold, A. Benner, T. Gaiser, A. Marx and H. Allgayer (2017). "P53-induced miR-30e-5p inhibits colorectal cancer invasion and metastasis by targeting ITGA6 and ITGB1." *International Journal of Cancer* **141**(9): 1879-1890.

- Lee, H., S. Han, C. S. Kwon and D. Lee (2016). "Biogenesis and regulation of the let-7 miRNAs and their functional implications." *Protein Cell* **7**(2): 100-113.
- Lee, Y., C. Ahn, J. Han, H. Choi, J. Kim, J. Yim, J. Lee, P. Provost, O. Radmark, S. Kim and V. N. Kim (2003). "The nuclear RNase III Drosha initiates microRNA processing." *Nature* **425**(6956): 415-419.
- Lee, Y., K. Jeon, J. T. Lee, S. Kim and V. N. Kim (2002). "MicroRNA maturation: stepwise processing and subcellular localization." *Embo j* **21**(17): 4663-4670.
- Lee, Y., M. Kim, J. Han, K. H. Yeom, S. Lee, S. H. Baek and V. N. Kim (2004). "MicroRNA genes are transcribed by RNA polymerase II." *Embo j* **23**(20): 4051-4060.
- Lehtinen, M. K. and C. A. Walsh (2011). "Neurogenesis at the brain-cerebrospinal fluid interface." *Annu Rev Cell Dev Biol* **27**: 653-679.
- Lewis, B. P., C. B. Burge and D. P. Bartel (2005). "Conserved seed pairing, often flanked by adenosines, indicates that thousands of human genes are microRNA targets." *Cell* **120**(1): 15-20.
- Li, Q., S. Bian, J. Hong, Y. Kawase-Koga, E. Zhu, Y. Zheng, L. Yang and T. Sun (2011). "Timing specific requirement of microRNA function is essential for embryonic and postnatal hippocampal development." *PLoS One* **6**(10): e26000.
- Li, W., C. A. Cogswell and J. J. LoTurco (1998). "Neuronal differentiation of precursors in the neocortical ventricular zone is triggered by BMP." *J Neurosci* **18**(21): 8853-8862.
- Li, X. L., M. F. Jones, M. Subramanian and A. Lal (2014). "Mutant p53 exerts oncogenic effects through microRNAs and their target gene networks." *FEBS Letters* **588**(16): 2610-2615.
- Li, Y. and K. V. Kowdley (2012). "MicroRNAs in Common Human Diseases." *Genomics, Proteomics & Bioinformatics* **10**(5): 246-253.
- Li, Y. and K. V. Kowdley (2012). "MicroRNAs in common human diseases." *Genomics Proteomics Bioinformatics* **10**(5): 246-253.
- Li, Z. and T. M. Rana (2014). "Therapeutic targeting of microRNAs: current status and future challenges." *Nat Rev Drug Discov* **13**(8): 622-638.
- Lim, L. P., N. C. Lau, P. Garrett-Engele, A. Grimson, J. M. Schelter, J. Castle, D. P. Bartel, P. S. Linsley and J. M. Johnson (2005). "Microarray analysis shows that some microRNAs downregulate large numbers of target mRNAs." *Nature* **433**(7027): 769-773.
- Linde, A. (1984). *Dentin and dentinogenesis*, CRC Press.
- Liu, F., X. Gao, H. Yu, D. Yuan, J. Zhang, Y. He and L. Yue (2013). "Effects of expression of exogenous cyclin G1 on proliferation of human endometrial carcinoma cells." *Chin J Physiol* **56**(2): 83-89.
- Luzzati, F. (2015). "A hypothesis for the evolution of the upper layers of the neocortex through co-option of the olfactory cortex developmental program." *Front Neurosci* **9**.
- Mabie, P. C., M. F. Mehler and J. A. Kessler (1999). "Multiple roles of bone morphogenetic protein signaling in the regulation of cortical cell number and phenotype." *J Neurosci* **19**(16): 7077-7088.

- MacFarlane, L. A. and P. R. Murphy (2010). "MicroRNA: Biogenesis, Function and Role in Cancer." *Curr Genomics* **11**(7): 537-561.
- Machon, O., C. J. van den Bout, M. Backman, R. Kemler and S. Krauss (2003). "Role of beta-catenin in the developing cortical and hippocampal neuroepithelium." *Neuroscience* **122**(1): 129-143.
- Madisen, L., T. A. Zwingman, S. M. Sunkin, S. W. Oh, H. A. Zariwala, H. Gu, L. L. Ng, R. D. Palmiter, M. J. Hawrylycz, A. R. Jones, E. S. Lein and H. Zeng (2010). "A robust and high-throughput Cre reporting and characterization system for the whole mouse brain." *Nat Neurosci* **13**(1): 133-140.
- Magalhães, A. C. D. (2016). On The Mechanisms Of Neural Development In The Ventral Telencephalon. Doctoral Program Brain & Mind (B&M), University of Helsinki
- Mairet-Coello, G., A. Tury and E. DiCicco-Bloom (2009). "Insulin-like growth factor-1 promotes G(1)/S cell cycle progression through bidirectional regulation of cyclins and cyclin-dependent kinase inhibitors via the phosphatidylinositol 3-kinase/Akt pathway in developing rat cerebral cortex." *J Neurosci* **29**(3): 775-788.
- Malatesta, P., M. A. Hack, E. Hartfuss, H. Kettenmann, W. Klinkert, F. Kirchhoff and M. Gotz (2003). "Neuronal or glial progeny: regional differences in radial glia fate." *Neuron* **37**(5): 751-764.
- Malatesta, P., E. Hartfuss and M. Gotz (2000). "Isolation of radial glial cells by fluorescent-activated cell sorting reveals a neuronal lineage." *Development* **127**(24): 5253-5263.
- Mardilovich, K., S. L. Pankratz and L. M. Shaw (2009). "Expression and function of the insulin receptor substrate proteins in cancer." *Cell Commun Signal* **7**: 14.
- Marin, O. (2013). "Cellular and molecular mechanisms controlling the migration of neocortical interneurons." *Eur J Neurosci* **38**(1): 2019-2029.
- Marin, O. and J. L. Rubenstein (2001). "A long, remarkable journey: tangential migration in the telencephalon." *Nat Rev Neurosci* **2**(11): 780-790.
- Martinez-Martinez, M. A., C. De Juan Romero, V. Fernandez, A. Cardenas, M. Gotz and V. Borrell (2016). "A restricted period for formation of outer subventricular zone defined by Cdh1 and Trnp1 levels." *Nat Commun* **7**: 11812.
- Martynoga, B., D. Drechsel and F. Guillemot (2012). "Molecular control of neurogenesis: a view from the mammalian cerebral cortex." *Cold Spring Harb Perspect Biol* **4**(10).
- Masuda, K., T. Toda, Y. Shinmyo, H. Ebisu, Y. Hoshiba, M. Wakimoto, Y. Ichikawa and H. Kawasaki (2015). "Pathophysiological analyses of cortical malformation using gyrencephalic mammals." *Sci Rep* **5**: 15370.
- McConnell, S. K. (1988). "Fates of visual cortical neurons in the ferret after isochronic and heterochronic transplantation." *J Neurosci* **8**(3): 945-974.
- Medina, L., A. Abellan, A. Vicario and E. Desfilis (2014). "Evolutionary and developmental contributions for understanding the organization of the basal ganglia." *Brain Behav Evol* **83**(2): 112-125.
- Megraw, M., V. Baev, V. Rusinov, S. T. Jensen, K. Kalantidis and A. G. Hatzigeorgiou (2006). "MicroRNA promoter element discovery in Arabidopsis." *Rna* **12**(9): 1612-1619.

- Mercier, P.-L., M. Bachvarova, M. Plante, J. Gregoire, M.-C. Renaud, K. Ghani, B. Têtu, I. Bairati and D. Bachvarov (2011). "Characterization of DOK1, a candidate tumor suppressor gene, in epithelial ovarian cancer." *Molecular Oncology* **5**(5): 438-453.
- Mizutani, K., K. Yoon, L. Dang, A. Tokunaga and N. Gaiano (2007). "Differential Notch signalling distinguishes neural stem cells from intermediate progenitors." *Nature* **449**(7160): 351-355.
- Mogilyansky, E. and I. Rigoutsos (2013). "The miR-17/92 cluster: a comprehensive update on its genomics, genetics, functions and increasingly important and numerous roles in health and disease." *Cell Death Differ* **20**(12): 1603-1614.
- Montiel, J. F. and F. Aboitiz (2015). "Pallial patterning and the origin of the isocortex." *Front Neurosci* **9**.
- Moreno, N. and A. González (2011). "The Non-Evaginated Secondary Prosencephalon of Vertebrates." *Front Neuroanat* **5**.
- Moss, E. G. (2007). "Heterochronic genes and the nature of developmental time." *Curr Biol* **17**(11): R425-434.
- Mott, J. L., S. Kobayashi, S. F. Bronk and G. J. Gores (2007). "mir-29 regulates Mcl-1 protein expression and apoptosis." *Oncogene* **26**(42): 6133-6140.
- Munji, R. N., Y. Choe, G. Li, J. A. Siegenthaler and S. J. Pleasure (2011). "Wnt signaling regulates neuronal differentiation of cortical intermediate progenitors." *J Neurosci* **31**(5): 1676-1687.
- Murchison, E. P., J. F. Partridge, O. H. Tam, S. Cheloufi and G. J. Hannon (2005). "Characterization of Dicer-deficient murine embryonic stem cells." *Proc Natl Acad Sci U S A* **102**(34): 12135-12140.
- Nechiporuk, T., J. McGann, K. Mullendorff, J. Hsieh, W. Wurst, T. Floss and G. Mandel (2016). "The REST remodeling complex protects genomic integrity during embryonic neurogenesis." *eLife* **5**.
- Noctor, S. C., A. C. Flint, T. A. Weissman, R. S. Dammerman and A. R. Kriegstein (2001). "Neurons derived from radial glial cells establish radial units in neocortex." *Nature* **409**(6821): 714-720.
- Noctor, S. C., V. Martinez-Cerdeno, L. Ivic and A. R. Kriegstein (2004). "Cortical neurons arise in symmetric and asymmetric division zones and migrate through specific phases." *Nat Neurosci* **7**(2): 136-144.
- Nonaka-Kinoshita, M., I. Reillo, B. Artegiani, M. A. Martinez-Martinez, M. Nelson, V. Borrell and F. Calegari (2013). "Regulation of cerebral cortex size and folding by expansion of basal progenitors." *Embo j* **32**(13): 1817-1828.
- Nottrott, S., M. J. Simard and J. D. Richter (2006). "Human let-7a miRNA blocks protein production on actively translating polyribosomes." *Nat Struct Mol Biol* **13**(12): 1108-1114.
- Nowakowski, T. J., K. S. Mysiak, T. Pratt and D. J. Price (2011). "Functional dicer is necessary for appropriate specification of radial glia during early development of mouse telencephalon." *PLoS One* **6**(8): e23013.
- O'Carroll, D. and A. Schaefer (2013). "General principals of miRNA biogenesis and regulation in the brain." *Neuropsychopharmacology* **38**(1): 39-54.

- O'Laughlin-Bunner, B., N. Radosevic, M. L. Taylor, Shivakrupa, C. DeBerry, D. D. Metcalfe, M. Zhou, C. Lowell and D. Linnekin (2001). "Lyn is required for normal stem cell factor-induced proliferation and chemotaxis of primary hematopoietic cells." *Blood* **98**(2): 343-350.
- O'Leary, D. D. and D. Borngasser (2006). "Cortical ventricular zone progenitors and their progeny maintain spatial relationships and radial patterning during preplate development indicating an early protomap." *Cereb Cortex* **16 Suppl 1**: i46-56.
- Okamura, K., J. W. Hagen, H. Duan, D. M. Tyler and E. C. Lai (2007). "The Mirtron Pathway Generates microRNA-Class Regulatory RNAs in Drosophila." *Cell* **130**(1): 89-100.
- Okamura, S., H. Arakawa, T. Tanaka, H. Nakanishi, C. C. Ng, Y. Taya, M. Monden and Y. Nakamura (2001). "p53DINP1, a p53-inducible gene, regulates p53-dependent apoptosis." *Mol Cell* **8**(1): 85-94.
- Olmos-Alonso, A., S. T. Schettters, S. Sri, K. Askew, R. Mancuso, M. Vargas-Caballero, C. Holscher, V. H. Perry and D. Gomez-Nicola (2016). "Pharmacological targeting of CSF1R inhibits microglial proliferation and prevents the progression of Alzheimer's-like pathology." *Brain* **139**(Pt 3): 891-907.
- Palmero, E. I., S. G. P. de Campos, M. Campos, N. C. N. de Souza, I. D. C. Guerreiro, A. L. Carvalho and M. M. C. Marques (2011). "Mechanisms and role of microRNA deregulation in cancer onset and progression." *Genet Mol Biol* **34**(3): 363-370.
- Park, C. Y., Y. S. Choi and M. T. McManus (2010). "Analysis of microRNA knockouts in mice." *Hum Mol Genet* **19**(R2): R169-175.
- Pasquinelli, A. E. (2012). "MicroRNAs and their targets: recognition, regulation and an emerging reciprocal relationship." *Nat Rev Genet* **13**(4): 271-282.
- Peuhu, E., S. I. Salomaa, N. De Franceschi, C. S. Potter, J. P. Sundberg and J. Pouwels (2017). "Integrin beta 1 inhibition alleviates the chronic hyperproliferative dermatitis phenotype of SHARPIN-deficient mice." **12**(10): e0186628.
- Phillips, J., T. Tihan and G. Fuller (2015). "Practical molecular pathology and histopathology of embryonal tumors." *Surg Pathol Clin* **8**(1): 73-88.
- Phoenix, T. N. and S. Temple (2010). "Spred1, a negative regulator of Ras-MAPK-ERK, is enriched in CNS germinal zones, dampens NSC proliferation, and maintains ventricular zone structure." *Genes Dev* **24**(1): 45-56.
- Pilz, G.-A., A. Shitamukai, I. Reillo, E. Pacary, J. Schwausch, R. Stahl, J. Ninkovic, H. J. Snippert, H. Clevers, L. Godinho, F. Guillemot, V. Borrell, F. Matsuzaki and M. Götz (2013). "Amplification of progenitors in the mammalian telencephalon includes a new radial glial cell type." **4**: 2125.
- Poliseno, L., L. Salmena, L. Riccardi, A. Fornari, M. S. Song, R. M. Hobbs, P. Sportoletti, S. Varmeh, A. Egia, G. Fedele, L. Rameh, M. Loda and P. P. Pandolfi (2010). "Identification of the miR-106b~25 microRNA cluster as a proto-oncogenic PTEN-targeting intron that cooperates with its host gene MCM7 in transformation." *Sci Signal* **3**(117): ra29.
- Pollen, A. A., T. J. Nowakowski, J. Shuga, X. Wang, A. A. Leyrat, J. H. Lui, N. Li, L. Szpankowski, B. Fowler, P. Chen, N. Ramalingam, G. Sun, M. Thu, M. Norris, R. Lebofsky, D. Toppani, D. W. Kemp, 2nd, M. Wong, B. Clerkson, B. N. Jones, S.

- Wu, L. Knutsson, B. Alvarado, J. Wang, L. S. Weaver, A. P. May, R. C. Jones, M. A. Unger, A. R. Kriegstein and J. A. West (2014). "Low-coverage single-cell mRNA sequencing reveals cellular heterogeneity and activated signaling pathways in developing cerebral cortex." *Nat Biotechnol* **32**(10): 1053-1058.
- Pópulo, H., J. M. Lopes and P. Soares (2012). "The mTOR Signalling Pathway in Human Cancer." *Int J Mol Sci* **13**(2): 1886-1918.
- Postiglione, M. P., C. Juschke, Y. Xie, G. A. Haas, C. Charalambous and J. A. Knoblich (2011). "Mouse invertebrate induces apical-basal spindle orientation to facilitate intermediate progenitor generation in the developing neocortex." *Neuron* **72**(2): 269-284.
- Puelles, L., M. Harrison, G. Paxinos and C. Watson (2013). "A developmental ontology for the mammalian brain based on the prosomeric model." *Trends Neurosci* **36**(10): 570-578.
- Raballo, R., J. Rhee, R. Lyn-Cook, J. F. Leckman, M. L. Schwartz and F. M. Vaccarino (2000). "Basic fibroblast growth factor (Fgf2) is necessary for cell proliferation and neurogenesis in the developing cerebral cortex." *J Neurosci* **20**(13): 5012-5023.
- Radhakrishnan, B. and A. Alwin Prem Anand (2016). "Role of miRNA-9 in Brain Development." *J Exp Neurosci* **10**: 101-120.
- Rakic, P. (1972). "Mode of cell migration to the superficial layers of fetal monkey neocortex." *J Comp Neurol* **145**(1): 61-83.
- Rakic, P. (1995). "A small step for the cell, a giant leap for mankind: a hypothesis of neocortical expansion during evolution." *Trends Neurosci* **18**(9): 383-388.
- Rakic, P., L. J. Stensas, E. P. Sayre and R. L. Sidman (1974). "Computer-aided three-dimensional reconstruction and quantitative analysis of cells from serial electron microscopic montages of foetal monkey brain." *Nature* **250**(5461): 31-34.
- Rana, T. M. (2007). "Illuminating the silence: understanding the structure and function of small RNAs." **8**: 23.
- Rash, B. G., H. D. Lim, J. J. Breunig and F. M. Vaccarino (2011). "FGF signaling expands embryonic cortical surface area by regulating Notch-dependent neurogenesis." *J Neurosci* **31**(43): 15604-15617.
- Raver-Shapira, N., E. Marciano, E. Meiri, Y. Spector, N. Rosenfeld, N. Moskovits, Z. Bentwich and M. Oren (2007). "Transcriptional activation of miR-34a contributes to p53-mediated apoptosis." *Mol Cell* **26**(5): 731-743.
- Reddy, K. B. (2015). "MicroRNA (miRNA) in cancer." *Cancer Cell Int* **15**.
- Rehwinkel, J., I. Letunic, J. Raes, P. Bork and E. Izaurralde (2005). "Nonsense-mediated mRNA decay factors act in concert to regulate common mRNA targets." *Rna* **11**(10): 1530-1544.
- Reillo, I., C. de Juan Romero, M. A. Garcia-Cabezas and V. Borrell (2011). "A role for intermediate radial glia in the tangential expansion of the mammalian cerebral cortex." *Cereb Cortex* **21**(7): 1674-1694.
- Reinhart, B. J., F. J. Slack, M. Basson, A. E. Pasquinelli, J. C. Bettinger, A. E. Rougvie, H. R. Horvitz and G. Ruvkun (2000). "The 21-nucleotide let-7 RNA regulates developmental timing in *Caenorhabditis elegans*." *Nature* **403**(6772): 901-906.

- Renner, M., M. A. Lancaster, S. Bian, H. Choi, T. Ku, A. Peer, K. Chung and J. A. Knoblich (2017). "Self-organized developmental patterning and differentiation in cerebral organoids." *Embo j* **36**(10): 1316-1329.
- Reuter, J. S. and D. H. Mathews (2010). "RNAstructure: software for RNA secondary structure prediction and analysis." *BMC Bioinformatics* **11**: 129.
- Ribes, V., F. Stutzmann, L. Bianchetti, F. Guillemot, P. Dolle and I. Le Roux (2008). "Combinatorial signalling controls Neurogenin2 expression at the onset of spinal neurogenesis." *Dev Biol* **321**(2): 470-481.
- Rother, S. and G. Meister (2011). "Small RNAs derived from longer non-coding RNAs." *Biochimie* **93**(11): 1905-1915.
- Roush, S. and F. J. Slack (2008). "The let-7 family of microRNAs." *Trends in Cell Biology* **18**(10): 505-516.
- Rupaimoole, R., G. A. Calin, G. Lopez-Berestein and A. K. Sood (2016). "MicroRNA deregulation in cancer cells and the tumor microenvironment." *Cancer Discov* **6**(3): 235-246.
- Rybak, A., H. Fuchs, L. Smirnova, C. Brandt, E. E. Pohl, R. Nitsch and F. G. Wulczyn (2008). "A feedback loop comprising lin-28 and let-7 controls pre-let-7 maturation during neural stem-cell commitment." *Nat Cell Biol* **10**(8): 987-993.
- Saito, Y., H. Saito, G. Liang and J. M. Friedman (2014). "Epigenetic Alterations and MicroRNA Misexpression in Cancer and Autoimmune Diseases: a Critical Review." *Clin Rev Allergy Immunol* **47**(2): 128-135.
- Sandmann, T. and S. M. Cohen (2007). "Identification of Novel Drosophila melanogaster MicroRNAs." *PLoS One* **2**(11).
- Saugier-Veber, P., F. Marguet, F. Lecoquierre, H. Adle-Biassette, F. Guimiot, S. Cipriani, S. Patrier, M. Brasseur-Daudruy, A. Goldenberg, V. Layet, Y. Capri, M. Gérard, T. Frébourg and A. Laquerrière (2017). "Hydrocephalus due to multiple ependymal malformations is caused by mutations in the MPDZ gene." *Acta Neuropathol Commun* **5**.
- Schanen, B. C. and X. Li (2011). "Transcriptional regulation of mammalian miRNA genes." *Genomics* **97**(1): 1-6.
- Schier, A. F. and A. J. Giraldez (2006). "MicroRNA function and mechanism: insights from zebra fish." *Cold Spring Harb Symp Quant Biol* **71**: 195-203.
- Selbach, M., B. Schwanhauser, N. Thierfelder, Z. Fang, R. Khanin and N. Rajewsky (2008). "Widespread changes in protein synthesis induced by microRNAs." *Nature* **455**(7209): 58-63.
- SF, G. (2000). Differentiation of the Neural Tube. *Developmental Biology*. S. Associates.
- Shell, S., S. M. Park, A. R. Radjabi, R. Schickel, E. O. Kistner, D. A. Jewell, C. Feig, E. Lengyel and M. E. Peter (2007). "Let-7 expression defines two differentiation stages of cancer." *Proc Natl Acad Sci U S A* **104**(27): 11400-11405.
- Shields, J. D., M. S. Emmett, D. B. Dunn, K. D. Joory, L. M. Sage, H. Rigby, P. S. Mortimer, A. Orlando, J. R. Levick and D. O. Bates (2007). "Chemokine-mediated migration of melanoma cells towards lymphatics: a mechanism contributing to metastasis." *Oncogene* **26**.

- Shimo, T., T. Nakanishi, T. Nishida, M. Asano, M. Kanyama, T. Kuboki, T. Tamatani, K. Tezuka, M. Takemura, T. Matsumura and M. Takigawa (1999). "Connective tissue growth factor induces the proliferation, migration, and tube formation of vascular endothelial cells in vitro, and angiogenesis in vivo." *J Biochem* **126**(1): 137-145.
- Shitamukai, A., D. Konno and F. Matsuzaki (2011). "Oblique radial glial divisions in the developing mouse neocortex induce self-renewing progenitors outside the germinal zone that resemble primate outer subventricular zone progenitors." *J Neurosci* **31**(10): 3683-3695.
- Siegenthaler, J. A., A. M. Ashique, K. Zarbalis, K. P. Patterson, J. H. Hecht, M. A. Kane, A. E. Folias, Y. Choe, S. R. May, T. Kume, J. L. Napoli, A. S. Peterson and S. J. Pleasure (2009). "Retinoic acid from the meninges regulates cortical neuron generation." *Cell* **139**(3): 597-609.
- Siliciano, J. D., C. E. Canman, Y. Taya, K. Sakaguchi, E. Appella and M. B. Kastan (1997). "DNA damage induces phosphorylation of the amino terminus of p53." *Genes Dev* **11**(24): 3471-3481.
- Sipola, A., L. Seppinen, T. Pihlajaniemi and J. Tuukkanen (2009). "Endostatin affects osteoblast behavior in vitro, but collagen XVIII/endostatin is not essential for skeletal development in vivo." *Calcif Tissue Int* **85**(5): 412-420.
- Stamateris, R. E., R. B. Sharma, Y. Kong, P. Ebrahimpour, D. Panday, P. Ranganath, B. Zou, H. Levitt, N. A. Parambil, C. P. O'Donnell, A. Garcia-Ocana and L. C. Alonso (2016). "Glucose Induces Mouse beta-Cell Proliferation via IRS2, MTOR, and Cyclin D2 but Not the Insulin Receptor." *Diabetes* **65**(4): 981-995.
- Stappert, L., B. Roese-Koerner and O. Brustle (2015). "The role of microRNAs in human neural stem cells, neuronal differentiation and subtype specification." *Cell Tissue Res* **359**(1): 47-64.
- Stenman, J., H. Toresson and K. Campbell (2003). "Identification of two distinct progenitor populations in the lateral ganglionic eminence: implications for striatal and olfactory bulb neurogenesis." *J Neurosci* **23**(1): 167-174.
- Stenvang, J., A. Petri, M. Lindow, S. Obad and S. Kauppinen (2012). "Inhibition of microRNA function by anti-miR oligonucleotides." *Silence* **3**: 1.
- Storm, E. E., S. Garel, U. Borello, J. M. Hebert, S. Martinez, S. K. McConnell, G. R. Martin and J. L. Rubenstein (2006). "Dose-dependent functions of Fgf8 in regulating telencephalic patterning centers." *Development* **133**(9): 1831-1844.
- Subramanian, M., P. Francis, S. Bilke, X. L. Li, T. Hara, X. Lu, M. F. Jones, R. L. Walker, Y. Zhu, M. Pineda, C. Lee, L. Varanasi, Y. Yang, L. A. Martinez, J. Luo, S. Ambs, S. Sharma, L. M. Wakefield, P. S. Meltzer and A. Lal (2014). "A mutant p53/let-7i-axis-regulated gene network drives cell migration, invasion and metastasis." *Oncogene* **34**: 1094.
- Sugahara, F., S.-i. Aota, S. Kuraku, Y. Murakami, Y. Takio-Ogawa, S. Hirano and S. Kuratani (2011). "Involvement of Hedgehog and FGF signalling in the lamprey telencephalon: evolution of regionalization and dorsoventral patterning of the vertebrate forebrain." *Development* **138**(6): 1217-1226.

- Suh, E. J., M. Y. Remillard, A. Legesse-Miller, E. L. Johnson, J. M. S. Lemons, T. R. Chapman, J. J. Forman, M. Kojima, E. S. Silberman and H. A. Collier (2012). "A microRNA network regulates proliferative timing and extracellular matrix synthesis during cellular quiescence in fibroblasts." *Genome Biol* **13**(12): R121.
- Sun, M., T. Zhou, E. Jonasch and R. S. Jope (2013). "DDX3 regulates DNA damage-induced apoptosis and p53 stabilization." *Biochim Biophys Acta* **1833**(6): 1489-1497.
- Suzuki, H., R. Maruyama, E. Yamamoto and M. Kai (2013). "Epigenetic alteration and microRNA dysregulation in cancer." *Front Genet* **4**.
- Swahari, V., A. Nakamura, J. Baran-Gale, I. Garcia, A. J. Crowther, R. Sons, T. R. Gershon, S. Hammond, P. Sethupathy and M. Deshmukh (2016). "Essential Function of Dicer in Resolving DNA Damage in the Rapidly Dividing Cells of the Developing and Malignant Cerebellum." *Cell Reports* **14**(2): 216-224.
- Swindell, E. C., T. J. Bailey, F. Loosli, C. Liu, F. Amaya-Manzanares, K. A. Mahon, J. Wittbrodt and M. Jamrich (2006). "Rx-Cre, a tool for inactivation of gene expression in the developing retina." *Genesis* **44**(8): 361-363.
- Takahashi, S., N. Fusaki, S. Ohta, Y. Iwahori, Y. Iizuka, K. Inagawa, Y. Kawakami, K. Yoshida and M. Toda (2012). "Downregulation of KIF23 suppresses glioma proliferation." *J Neurooncol* **106**(3): 519-529.
- Taverna, E., M. Gotz and W. B. Huttner (2014). "The cell biology of neurogenesis: toward an understanding of the development and evolution of the neocortex." *Annu Rev Cell Dev Biol* **30**: 465-502.
- Thomson, D. W. and M. E. Dinger (2016). "Endogenous microRNA sponges: evidence and controversy." **17**: 272.
- Tsuruzoe, K., R. Emkey, K. M. Kriauciunas, K. Ueki and C. R. Kahn (2001). "Insulin receptor substrate 3 (IRS-3) and IRS-4 impair IRS-1- and IRS-2-mediated signaling." *Mol Cell Biol* **21**(1): 26-38.
- Turrero García, M., Y. J. Chang, Y. Arai and W. B. Huttner (2016). "S-phase duration is the main target of cell cycle regulation in neural progenitors of developing ferret neocortex." *J Comp Neurol* **524**(3): 456-470.
- Udelhoven, M., U. Leiser, S. Freude, M. M. Hettich, M. Laudes, J. Schnitker, W. Krone and M. Schubert (2010). "Identification of a region in the human IRS2 promoter essential for stress induced transcription depending on SP1, NFI binding and ERK activation in HepG2 cells." *J Mol Endocrinol* **44**(2): 99-113.
- Urbach R, T. G. (2000-2013). "Dorsoventral Patterning of the Brain: A Comparative Approach." from <https://www.ncbi.nlm.nih.gov/books/NBK6006/>.
- van Rooij, E., L. B. Sutherland, X. Qi, J. A. Richardson, J. Hill and E. N. Olson (2007). "Control of stress-dependent cardiac growth and gene expression by a microRNA." *Science* **316**(5824): 575-579.
- Vasudevan, S., Y. Tong and J. A. Steitz (2007). "Switching from repression to activation: microRNAs can up-regulate translation." *Science* **318**(5858): 1931-1934.
- Viswanathan, S. R., G. Q. Daley and R. I. Gregory (2008). "Selective blockade of microRNA processing by Lin28." *Science* **320**(5872): 97-100.

- Viswanathan, S. R., J. T. Powers, W. Einhorn, Y. Hoshida, T. L. Ng, S. Toffanin, M. O'Sullivan, J. Lu, L. A. Phillips, V. L. Lockhart, S. P. Shah, P. S. Tanwar, C. H. Mermel, R. Beroukhim, M. Azam, J. Teixeira, M. Meyerson, T. P. Hughes, J. M. Llovet, J. Radich, C. G. Mullighan, T. R. Golub, P. H. Sorensen and G. Q. Daley (2009). "Lin28 promotes transformation and is associated with advanced human malignancies." *Nat Genet* **41**(7): 843-848.
- Viti, J., A. Gulacsi and L. Lillien (2003). "Wnt regulation of progenitor maturation in the cortex depends on Shh or fibroblast growth factor 2." *J Neurosci* **23**(13): 5919-5927.
- Waclaw, R. R., L. A. Ehrman and A. Pierani (2010). "Developmental origin of the neuronal subtypes that comprise the amygdalar fear circuit in the mouse." **30**(20): 6944-6953.
- Waclaw, R. R., B. Wang, Z. Pei, L. A. Ehrman and K. Campbell (2009). "Distinct temporal requirements for the homeobox gene Gsx2 in specifying striatal and olfactory bulb neuronal fates." *Neuron* **63**(4): 451-465.
- Wang, X., L. Cao, Y. Wang, X. Wang, N. Liu and Y. You (2012). "Regulation of let-7 and its target oncogenes (Review)." *Oncol Lett* **3**(5): 955-960.
- Wang, X., J. W. Tsai, B. LaMonica and A. R. Kriegstein (2011). "A new subtype of progenitor cell in the mouse embryonic neocortex." *Nat Neurosci* **14**(5): 555-561.
- Wang, Y., X. Li and H. Hu (2011). "Transcriptional regulation of co-expressed microRNA target genes." *Genomics* **98**(6): 445-452.
- Westholm, J. O. and E. C. Lai (2011). "Mirtrons: microRNA biogenesis via splicing." *Biochimie* **93**(11): 1897-1904.
- Wonders, C. P. and S. A. Anderson (2006). "The origin and specification of cortical interneurons." *Nat Rev Neurosci* **7**(9): 687-696.
- Wong, R. C.-B., S. Pollan, H. Fong, A. Ibrahim, E. L. Smith, M. Ho, A. L. Laslett and P. J. Donovan (2011). "A Novel Role for an RNA Polymerase III Subunit POLR3G in Regulating Pluripotency in Human Embryonic Stem Cells." *STEM CELLS* **29**(10): 1517-1527.
- Woodhead, G. J., C. A. Mutch, E. C. Olson and A. Chenn (2006). "Cell-autonomous beta-catenin signaling regulates cortical precursor proliferation." *J Neurosci* **26**(48): 12620-12630.
- Xie, Y., C. Juschke, C. Esk, S. Hirotsune and J. A. Knoblich (2013). "The phosphatase PP4c controls spindle orientation to maintain proliferative symmetric divisions in the developing neocortex." *Neuron* **79**(2): 254-265.
- Yang, J. S. and E. C. Lai (2010). "Dicer-independent, Ago2-mediated microRNA biogenesis in vertebrates." *Cell Cycle* **9**(22): 4455-4460.
- Yekta, S., I. H. Shih and D. P. Bartel (2004). "MicroRNA-directed cleavage of HOXB8 mRNA." *Science* **304**(5670): 594-596.
- Yoo, J., R. J. Hajjar and D. Jeong (2017). "Generation of Efficient miRNA Inhibitors Using Tough Decoy Constructs." *Methods Mol Biol* **1521**: 41-53.
- Yu, F., H. Yao, P. Zhu, X. Zhang, Q. Pan, C. Gong, Y. Huang, X. Hu, F. Su, J. Lieberman and E. Song (2007). "let-7 regulates self renewal and tumorigenicity of breast cancer cells." *Cell* **131**.

- Yun, K., S. Potter and J. L. Rubenstein (2001). "Gsh2 and Pax6 play complementary roles in dorsoventral patterning of the mammalian telencephalon." Development **128**(2): 193-205.
- Yung, S. Y., S. Gokhan, J. Jurcsak, A. E. Molero, J. J. Abrajano and M. F. Mehler (2002). "Differential modulation of BMP signaling promotes the elaboration of cerebral cortical GABAergic neurons or oligodendrocytes from a common sonic hedgehog-responsive ventral forebrain progenitor species." Proc Natl Acad Sci U S A **99**(25): 16273-16278.
- Zhang, B., X. Pan, G. P. Cobb and T. A. Anderson (2007). "microRNAs as oncogenes and tumor suppressors." Dev Biol **302**.
- Zhang, C., X. Ge, Q. Liu, M. Jiang, M. W. Li and H. Li (2015). "MicroRNA-mediated non-cell-autonomous regulation of cortical radial glial transformation revealed by a Dicer1 knockout mouse model." Glia **63**(5): 860-876.
- Zhang, L., J. Huang, N. Yang, J. Greshock, M. S. Megraw, A. Giannakakis, S. Liang, T. L. Naylor, A. Barchetti, M. R. Ward, G. Yao, A. Medina, A. O'Brien-Jenkins, D. Katsaros, A. Hatzigeorgiou, P. A. Gimotty, B. L. Weber and G. Coukos (2006). "microRNAs exhibit high frequency genomic alterations in human cancer." Proc Natl Acad Sci U S A **103**(24): 9136-9141.
- Zhang, Z., Y. W. Qin, G. Brewer and Q. Jing (2012). "MicroRNA degradation and turnover: regulating the regulators." Wiley Interdiscip Rev RNA **3**(4): 593-600.
- Zhu, H., N. Shyh-Chang, A. V. Segrè, G. Shinoda, S. P. Shah, W. S. Einhorn, A. Takeuchi, J. M. Engreitz, J. P. Hagan, M. G. Kharas, A. Urbach, J. E. Thornton, R. Triboulet, R. I. Gregory, D. Altshuler and G. Q. Daley (2011). "The Lin28/let-7 axis regulates glucose metabolism." Cell **147**(1): 81-94.